The Henryk Niewodniczański Institute of Nuclear Physics
Polish Academy of Sciences
Kraków, Poland

Report on Research Activities 2017-2020

The Henryk Niewodniczański Institute of Nuclear Physics
Polish Academy of Sciences

Radzikowskiego 152
31-342 Kraków, Poland

http://www.ifj.edu.pl

Phone: +48-12 66 28 200
Fax: +48-12 66 28 458
e-mail: dyrektor@ifj.edu.pl

Report on Research Activities 2017-2020

ISSN: 1425-3763 *(printed version)*
ISSN: 2544-5162 *(electronic version)*

May 2021

Contents

Foreword

The Henryk Niewodniczański Institute of Nuclear Physics Polish Academy of Sciences (IFJ PAN) belongs to the topmost research centers in Poland – our Institute proudly holds the highest A+ grade in the nation-wide categorization of research institutions.

In the period 2017-2020, the IFJ PAN's scientific activities continued with vigor in both fundamental and application research. Studies concerning basic research were carried out at the Division of Particle Physics and Astrophysics, the Division of Nuclear Physics and Strong Interactions, the Division of Condensed Matter Physics and at the Division of Theoretical Physics. In turn, the works related to scientific applications were conducted at the Division of Interdisciplinary Research, the Division of Applications of Physics and at the Cyclotron Centre Bronowice (CCB).

In the area of basic research, the driving force for the IFJ PAN is the desire to unravel the nature of the matter constituents and the interactions between them on the smallest possible scale, to understand the fundamental properties of physical objects made of these constituents, and, ultimately, to determine the emergent complex structures of different forms of matter. The IFJ PAN is strictly following this path by being involved in the most advanced international research projects carried out at large research infrastructures spread out around the globe, such as CERN (Geneve), ILL (Grenoble) or GANIL (Caen), to name but a few. Engineers at IFJ PAN are world's renowned specialists who contribute with great success to the construction of new research infrastructures, like recently to the E-XFEL (Hamburg), and now to the ESS (Lund) and ITER (Cadarache).

Research at IFJ PAN related to applications is also very ambitious and versatile. It encompasses, in particular, a large variety of techniques originating from nuclear physics, particle physics and solid state physics, which were harnessed to studies in biology, medicine, dosimetry, environmental protection, but also to such "remote" topics as linguistics, the behavior of financial markets or preservation of the cultural heritage.

History has shown that fundamental research, by generating knowledge verified in experiment, can enrich our understanding of the Universe, creating at the same time new avenues for technological development, which have a very beneficial impact on the society. The Cyclotron Centre Bronowice at IFJ PAN is particularly spectacular demonstration of this strong connection between basic research and applications. It is a state-of-the-art proton therapy center and a research laboratory, operating two proton cyclotrons: 230 MeV Proteus C-235 and 60 MeV AIC-144. The whole-body treatment is performed on two rotating gantries with Pencil Scanning Beam, while the treatment of eye cancer takes place in a dedicated room. The number of treated patients is constantly growing. The other pillar of the CCB activity, that is basic science research, encompasses experiments in nuclear physics, medical physics, dosimetry, microdosimetry, radiobiology and materials engineering.

The IFJ PAN is also actively engaged in education of graduate students. Following a new law on higher education and science introduced in 2018, an interinstitutional, interdisciplinary doctoral school was created to train PhD students in the domain of physics, chemistry, medical sciences and materials engineering under auspices of IFJ PAN: the Krakow School of Interdisciplinary PhD Studies (KISD).

One has to stress that the impressive list of achievements that are presented in this Research Report is the fruit of the competence and commitment of the IFJ PAN's Staff, the Scientific Council as well as the Board of Directors. We wish to express our deepest gratitude to all these contributors and, especially, to Prof. Marek Jeżabek, who, in August

2020, after 16 years, ended his term of the IFJ PAN Director General.

We invite the Reader of the IFJ PAN Report 2017–2020 to learn about the research achievements of our Institute. We are convinced, that they demonstrate a wide spectrum of scientific works as well as the author's enthusiasm, which all contribute to the high scientific level of our Institute on the international forum.

❖

1. Division of Particle and Astroparticle Physics

The research activities of the Division of Particle and Astroparticle Physics are focused on two areas: one of them are studies of fundamental constituents of matter and forces governing particle interactions, and the other is astrophysics, through studies of cosmic rays as well as gamma and neutrino astronomy. The research teams of our Division participate in many leading scientific projects conducted by large international collaborations. These include particle physics projects, such as the ATLAS and LHCb experiments at the CERN Large Hadron Collider, the Belle II e^+e^- experiment at KEKB in Japan as well as the T2K neutrino experiment at the JPARC facility in Japan. In addition, our astroparticle physics projects include the Pierre Auger cosmic ray observatory, the H.E.S.S., HAWC and CTA gamma ray observatories as well as the Baikal-GVD neutrino project. We are involved in all phases of these projects: from the initial design, optimization and construction of the detector systems, preparation of research programs, active participation in data analyses, to maintaining and upgrading the detectors. Thus our activities are fully in line with current project requirements.

During the past four years some organizational changes have occurred in our Division to adjust better to the evolving engagement of our groups in research projects. Thus, the Department of Cosmic Ray Research and the Department of Neutrino and Dark Matter Studies were merged into a new Department of Cosmic Ray Research and Neutrino Studies. The Department of Linear Colliders was closed, while a new Department of Diffractive Processes was created. Finally, the Department for Leptonic Interactions was renamed the Belle II Experiment Department. The research profiles of the six departments of the Division are outlined below.

❖

Direct searches for physics phenomena from beyond the Standard Model (BSM) are the principal activities of the **ATLAS Experiment Department**. The Higgs boson postulated in the Standard Model (SM) was discovered in 2012 by the ATLAS and CMS experiments at the Large Hadron Collider (LHC). However, theories that go beyond the SM typically require an extended Higgs sector implying the existence of additional scalar bosons. The decay chains of these bosons often contain heavy fermions (*t*-, *b*-quarks and leptons) as indicators of BSM phenomena. The processes with such particles are examined in detail by the ATLAS Experiment Department. In particular, searches for heavy neutral and charged Higgs bosons are performed with a pair of leptons or *b*-quarks and a lepton in the final state, respectively. Another interesting BSM process studied is the production of pairs of SM Higgs bosons. Such events may suggest the existence of an exotic object, such as graviton, which would decay into a Higgs boson pair and enhance the production rate over the very small rate predicted by the SM.

The Department has been involved in the ATLAS experiment for over two decades by taking part in the detector design and construction as well as physics analysis of proton-proton (pp) and heavy ion collisions. Currently, the group plays a leading role in the Inner Tracker system designed to measure trajectories of charged particles, especially in the Transition Radiation Tracker that provides data vital for the vast majority of physics analyses conducted by the ATLAS collaboration. The scientific program of the LHC contains a series of upgrades aiming at collecting an integrated luminosity of 3000 fb^{-1} using pp collisions. The extensive improvements to the accelerator will increase its performance and bring the accelerator to the so-called High-Luminosity LHC phase (HL-LHC). The HL-LHC will provide an unprecedented instantaneous luminosity of 7.5×10^{34} cm^{-2} s^{-1} and the average number of about 200 inelastic pp interactions per beam crossing. Looking into the future, the group takes part in the design and construction of a new all-silicon tracker for the upgraded ATLAS detector at the HL-LHC, with a focus on radiation-tolerant and magnetic-field-tolerant electronics equipment to be

installed inside the ATLAS detector to provide power for future silicon strip sensors.

The **Department of Diffractive Processes** was created in January 2020 to consolidate a group of physicists working on issues known under the common name of forward physics. The employees of the Department take part in the STAR experiment at RHIC and in the ATLAS Roman Pot (ARP) system consisting of the ATLAS Forward Proton (AFP) and Absolute Luminosity For ATLAS (ALFA) detectors. These detectors enable a precise measurement of protons scattered at very small angles. Three groups of phenomena are studied. One of them is the elastic proton-proton scattering (STAR, ALFA), which requires special settings of the accelerator. Another group covers diffractive processes (STAR, AFP), in which the main emphasis is put on the properties of the ensemble of particles produced in an interaction. The third domain concentrates on very rare phenomena of two-photon interactions leading to the exclusive production of particle and anti-particle pairs (AFP). The staff of the Department have also worked on the technical side of the measurements, including testing, installation and alignment of the apparatus, detector control as well as trigger and data acquisition systems.

The physicists of the **LHCb Experiment Department** are involved in various physics analyses, development of software and hardware construction in the LHCb experiment (Large Hadron Collider beauty experiment), which is one of the large high-energy physics experiments collecting data at the Large Hadron Collider. The main goal of the LHCb experiment is to measure precisely the breaking of symmetry between matter and antimatter observed in the Universe, and to search for new physics phenomena in rare decays of hadrons containing heavy quarks. The indirect approach taken by LHCb is complementary to the direct search for new physics by the general purpose detectors of the ATLAS and CMS experiments. This approach has enormous potential to provide the first evidence for new physics as it allows one to probe processes at energies beyond the LHC center-of-mass energy. The analysis of the data collected in Run-1 and Run-2 phases of the LHC showed a few intriguing anomalies with respect to SM predictions. In order to collect more data with higher luminosity at the LHCb beam crossing point, the detector undergoes a major transformation to cope with these new demanding conditions in the LHC Run-3 phase.

The **Belle II Experiment Department** has continued its work on data delivered by the Belle experiment and its successor, Belle II, at the upgraded super-B-factory. The primary motivation of these experiments are studies of CP violation in heavy flavor systems. The B-factories are e^+e^- asymmetric colliders, allowing the resonant production of $\Upsilon(4s)$, the $b\bar{b}$ quarks bound state, which decays into a coherent pair of B mesons. The resonant production provides an efficient and clean source of mesons containing the b quark. This environment offers a unique opportunity to study B decays into final states with undetectable particles, such as multiple neutrinos or new exotic states of matter. This allows us to search for processes violating lepton universality, including leptons which are hard to access at hadronic colliders.

The Belle experiment finished data taking in 2009. The data collected by the detector allowed the collaboration to publish around 70 scientific papers over the last 4 years, with valuable scientific results. The Belle II experiment successfully started taking data in 2018 and is currently the only next-generation B-factory in operation. At present, it is also the world's highest-luminosity machine with further substantial increase in prospect. The target dataset of 50 ab^{-1} will surpass the previously accumulated statistics from B-factories by a factor of 50. The Belle II collaboration has already started publishing scientific papers, currently concentrating mostly on a search for exotic particles in the low-mass region, providing competing limits for low-mass supersymmetry particles.

The scientists of the **Department of Cosmic Ray Research and Neutrino Studies** participate in several projects. One of them is the Pierre Auger Observatory to study ultra-high energy cosmic rays (UHECR), i.e. particles with energies exceeding the LHC beam energy by several orders of magnitude. These are the highest-energy particles known to exist in Nature, yet their origin is still unclear. Explaining the nature of UHECR and identifying their sources are the main goals of the Observatory. The data accumulated so far enabled the determination of the UHECR spectrum and confirmation of its suppression at highest energies, but more precise data are needed for explaining the cause of this suppression and the UHECR composition. To meet this objective, a large-scale upgrade of the Observatory, known as AugerPrime, is under way. IFJ PAN actively contributes to this effort of the Pierre Auger Collaboration.

The Department is also involved in neutrino research. The Tokai-to-Kamioka experiment (T2K) is focused on

studies of neutrino oscillations, precise measurements of neutrino mixing parameters, and measurements of cross sections of various final states of neutrino interactions. The Department is also engaged in the ND280 detector upgrade of the T2K experiment. Furthermore, our scientists participate in the development of the Baikal Gigaton Volume Detector (Baikal-GVD). The detector is a deep underwater neutrino telescope, now under construction, designed for detailed studies of the flux of high-energy cosmic neutrinos and for searching for their sources as well as dark matter candidates and other exotic particles.

Our group continues its involvement in the Cosmic Ray Extremely Distributed Observatory (CREDO), which is mostly a "citizen science" and outreach project, but it also has a fundamental astrophysics objective of looking for correlations of cosmic rays arriving at Earth.

The group in the **Department of Gamma-Ray Astrophysics** performs research in the field of theoretical and observational high-energy astrophysics, with the main interest in astronomical phenomena and objects that are sources of high-energy particles and electromagnetic radiation in the ultraviolet, X-ray, and gamma-ray energy ranges. Such objects include remnants of supernova explosions, pulsars and pulsar wind nebulae, active galactic nuclei, and gamma-ray bursts. Theoretical studies concern the microphysics of particle acceleration processes in cosmic plasmas. In these studies advanced ab-initio numerical methods of simulating astrophysical plasmas are employed with the use of supercomputers of high computational power. Observational projects of high-energy gamma ray astronomy use ground-based facilities, such as the High Energy Stereoscopic System (H.E.S.S.) and the High-Altitude Water Cherenkov Observatory (HAWC). The main scientific topic our team investigates concerns the physics of blazars and the search for Galactic sources of high-energy cosmic rays. The team is also involved in the construction of scientific equipment for the next-generation ground-based gamma-ray observatory, the Cherenkov Telescope Array (CTA).

Selected Research Highlights of the Division of Particle and Astroparticle Physics

The ATLAS group of IFJ PAN was actively involved in **searches for beyond-the-Standard-Model (BSM) Higgs bosons**. Various non-minimal Higgs scenarios, such as Two-Higgs-Doublet Models (2HDM) or models containing Higgs triplets, predict the existence of heavy neutral pseudoscalar (A) and scalar (H) states as well as charged Higgs bosons, $H^{\pm}$, in addition to the 125 GeV light scalar (h) already discovered. The BSM Higgs bosons could additionally manifest themselves through a substantially increased cross-section for b pair production, still not observed at the LHC.

Four complementary analyses were performed to find evidence for an extended Higgs sector or exclude ever larger regions of parameter space available to the BSM scenarios.

A model independent search for $H^{\pm}$ in its decay to a lepton and a neutrino with an additional top quark in the final state was carried out with 36.1 fb^{-1} of proton-proton collision data at $\sqrt{s}$=13 TeV. The analysis incorporated both leptonic and hadronic decay modes of the top quark and exploited the mass range of Higgs from about 90 GeV to 2 TeV [JHEP 09 (2018) 139] [EurekAlert].

The probability of H/A decay into a $^{+}$ $^{-}$ pair can be enhanced relative to other decay modes in 2HDMs of type II, such as the Minimal Supersymmetric SM (MSSM). A search for such decays was performed using the full Run 2 data (139 fb^{-1}) over the mass range 0.2–2.5 TeV, with H/A produced either via the gluon fusion or in association with a b-quark and at least one -lepton decaying into final states with hadrons [Phys. Rev. Lett. 125 (2020) 051801].

Another analysis focused on heavy neutral Higgs bosons produced in association with one or two b-quarks and decaying into b-quark pairs. This search is sensitive to the type II and flipped scenarios of the 2HDM. The search was performed in the mass range 450–1400 GeV using 27.8 fb^{-1} of $\sqrt{s}$ = 13 TeV proton-proton collision data [Phys. Rev. D 102, 032004 (2020)].

The obtained upper limits on the production cross section were used for the combined exclusion of the hMSSM model parameters presented in Fig. 1.1.

Searches and a combination of results for Higgs boson pairs decaying into the $b\bar{b}b\bar{b}$, $b\bar{b}W^{+}W^{-}$, $b\bar{b}$ $^{+}$ $^{-}$, $W^{+}W^{-}W^{+}W^{-}$, $b\bar{b}$ and $W^{+}W^{-}$ final states, using up to 36.1fb^{-1} of $\sqrt{s}$ = 13 TeV data were performed [Phys. Lett. B 800 (2020) 135103]. The resulting upper limit on the non-resonant gluon fusion production cross-section as a function of Higgs self-coupling modifier is shown in Fig. 1.2.

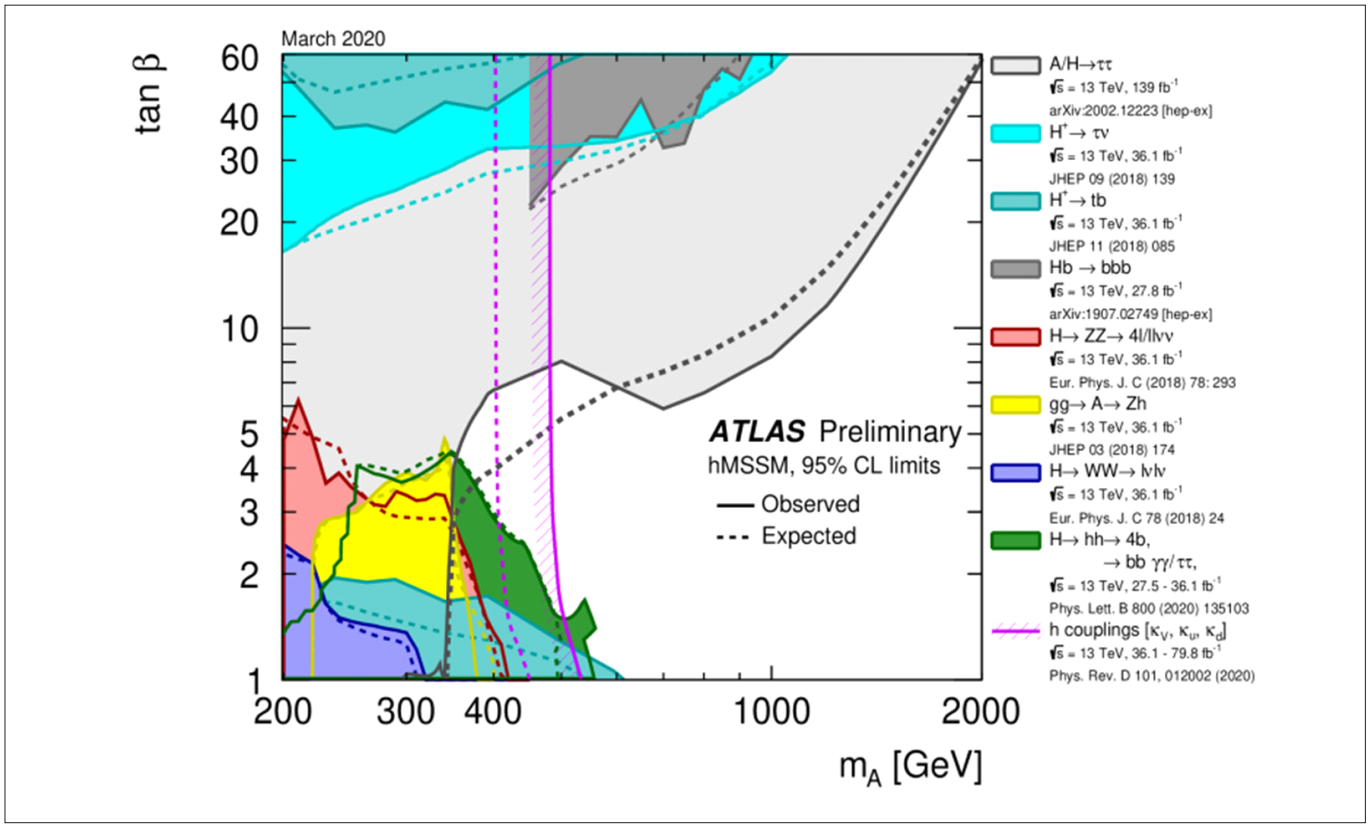

Fig. 1.1: Regions of the [m_A, tan] plane excluded in the hMSSM model via direct searches for heavy Higgs bosons and fits to the measured rates of observed Higgs boson production and decays. Limits are quoted at 95% CL and are indicated for the data (solid lines) and the expectation for the SM Higgs sector (dashed lines). The light shaded or hashed regions indicate the observed exclusions. [ATL-PHYS-PUB-2020-006]

All the presented analyses show no evidence for an extended Higgs sector, providing significantly improved limits compared to earlier results. This translates into reduced parameter space available to BSM scenarios.

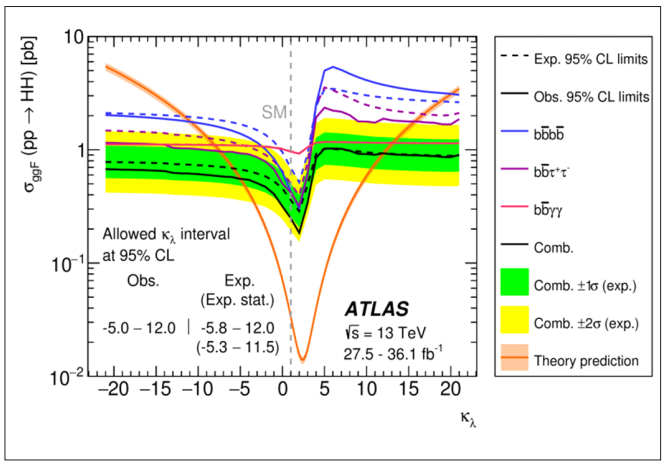

Fig. 1.2. 95% CL upper limit on the cross-section for non-resonant production of SM HH via gluon fusion as a function of . The observed (expected) limits are shown as solid (dashed) lines. In the $b\bar{b}$ $b\bar{b}$ final state, the observed and expected limits coincide. The ±1 and ±2 bands are only shown for the combined expected limit. The theoretical prediction of the cross-section as a function of is also shown. [Phys. Lett. B 800 (2020) 135103]

The LHC as a **heavy-ion collider recreates the state of matter similar to that present in the early universe**, the so-called **quark-gluon plasma (QGP)**. The ATLAS experiment, with its unique capabilities including large acceptance and extremely fast trigger,

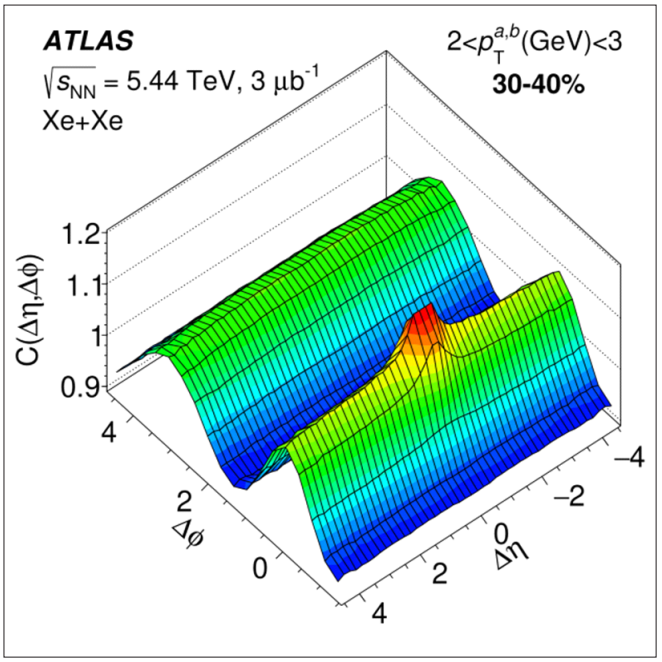

Fig.1.3: Two-dimensional correlation function, C(,), in 5.44 TeV Xe+Xe collisions (Phys. Rev. C 101 (2020) 024906).

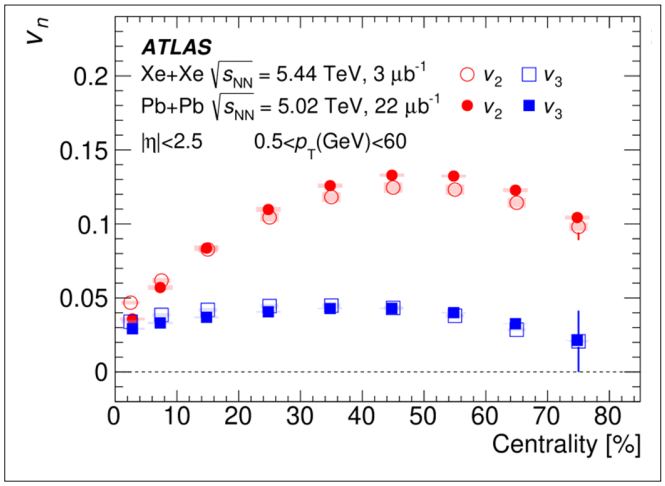

Fig. 1.4: Azimuthal flow harmonics v_n in the 5.44 TeV Xe + Xe and 5.02 Pb+Pb collisions, as a function of collision centrality (Phys.Rev.C 101(2020)024906, Eur.Phys.J.C78 (2018) 997).

continues the study of the physics properties of QGP in ultra-relativistic nuclear collisions at the LHC. One of the most important tools used by the ATLAS Group at IFJ PAN to study the properties of the unusual QGP state is the measurement of the azimuthal anisotropy of produced particles. Recently, **significant azimuthal anisotropy of charged hadrons** was observed in 5.44 TeV Xe+Xe (Fig.1.3) and 5.02 TeV Pb+Pb collisions. The measured azimuthal flow harmonics (Fig. 1.4) provide convincing arguments that the hot and dense medium created in these collisions behaves like an almost perfect fluid. The comparison of the Xe+Xe and Pb+Pb results provides constraints on the magnitude of fluctuations of the initial interaction zone, possible signs of the colliding nuclei deformation or the role of viscous effects in QGP.

P.A.M. Dirac predicted the existence of the anti-matter partner to the electron – the positron. The annihilation of the two can lead to the creation of two photons. The Quantum Mechanics predicts also a reverse process of creating a particle-anti-particle pair, in particular the lepton-anti-lepton pair. In 2020, the ATLAS Collaboration published the **observation and measurement of forward proton scattering in association with lepton pairs produced via the photon fusion mechanism** [Phys. Rev. Lett. 125 (2020) 261801]. In this measurement, the beam protons served as a source of the colliding photons. In the photon-photon interaction, an e^+e^- or a $^+$ $^-$ pair was created and the protons were scattered at very small angles. The pair was measured in the ATLAS central detector, while the scattered (forward) proton was measured in the ATLAS Forward Proton (AFP) spectrometer placed about 210 m away from the interaction point. The construction, installation and preparation of the physics program of AFP were to a large extent performed by IFJ PAN physicists. Theoretical predictions of photon fusion processes have significant uncertainties due to modeling of strong interactions of the scattered protons. Such interactions suppress the cross-section by soft-survival probability factors, quantifying the probability that a proton emerges intact from the interaction. These factors are poorly constrained at high invariant masses, important for new physics searches. The proton tagging suppresses the backgrounds to the investigated processes. The AFP includes Si-pixel detectors positioned about 2 mm away from the proton beam. If the relative energy loss of the scattered proton (=1–E_p/E_{beam}, where E_p (E_{beam}) is the scattered proton (beam) energy) is within 2-12%, then the proton is deflected into the AFP apparatus by the accelerator magnetic field. In this measurement, the ATLAS Collaboration data collected in 2017 were used. A sample of 53 e^+e^- and 123 $^+$ $^-$ pairs associated with an intact proton registered in the AFP was carefully selected, requiring also that the mass of the pair be outside the (80 GeV, 110 GeV) interval to reject the background due to Z^0 decays. A match of the relative energy losses calculated from the lepton pair, $_{ll}$, and the AFP measurements, $_{AFP}$ was also required. The $_{AFP}$ – $_{ll}$ distribution is shown in Fig. 1.5.

The expected background due to accidentally matching forward protons amounts to about 20 events. The statistical significance of this result exceeds 9 standard deviations for

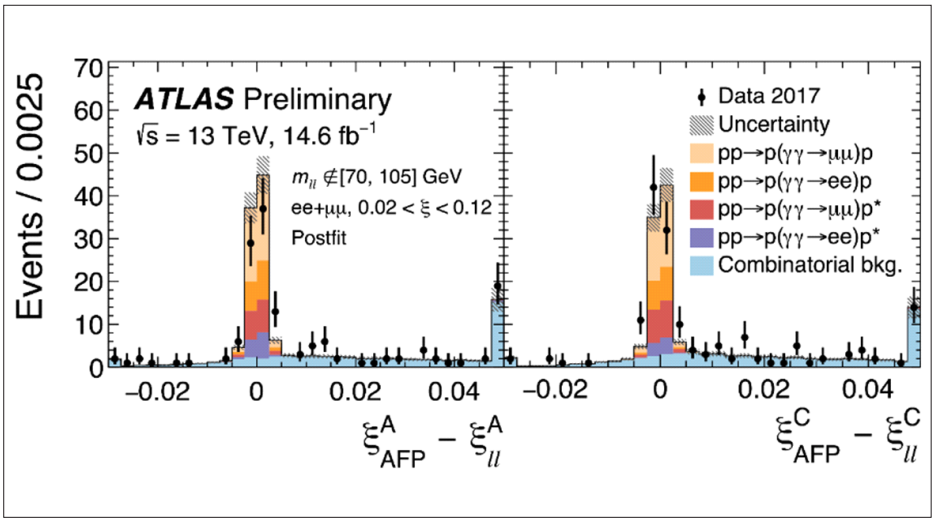

Fig. 1.5: The distribution of $_{AFP}$ – $_{ll}$ calculated using the AFP located at both sides (A, C) of the ATLAS detector from 2017 data. Contribution of various processes and the background are also shown.

each considered channel. The measurement yielded the observed cross sections of:

$_{e+e-+p}$ = 11.0 2.6(stat.) 1.2(syst.) 0.3(lumi)fb

and

$_{+\ -+p}$ = 7.2 1.6(stat.) 0.9(syst.) 0.2(lumi)fb.

These values are overestimated by the QED predictions by about 30%-40%, and introducing the survival factor considerably improves the agreement. The obtained results prove that the AFP performs well in high-luminosity data taking and show a successful application of the proton tagging technique. These measurements deliver important tests of the photon interactions. Such tests are especially significant since these interactions can be modified by hypothetical new particles, whose existence is predicted by certain theories.

The program of the LHCb experiment is focused on searching for physics beyond the Standard Model with an approach that is complementary to that used by the ATLAS and CMS experiments. The IFJ PAN group contributed to studies based on data collected since the start of the LHC collider. Flavor physics offers a rich spectrum of various measurements sensitive to physics beyond the SM. The best method to search for such New Physics effects is to measure precisely processes that are predicted to be very rare or are forbidden in the SM. The influence of hypothetical new heavy particles can give an additional contribution from New Physics effects and can show a significant difference between experimental measurements and the prediction of the SM.

These studies yielded a number of interesting measurements and a few of them appeared not to be fully compatible with the predictions of the Standard Model. One of the best known anomalies concerns a distortion in **angular distribution in the final state of the beauty meson decay** B_s K* $^{+}$ $^{-}$ observed in Run 1 data. The statistical significance

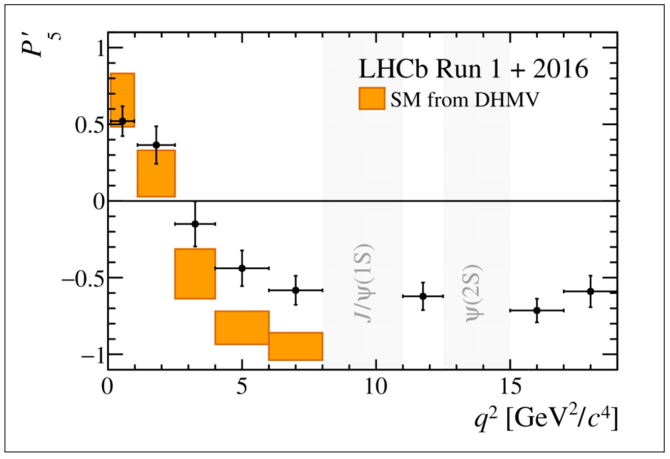

Fig. 1.6: The distribution of P'_5 variable for B_s K* $^{+}$ $^{-}$.

of the difference between the measured and predicted distribution of P'_5 (a special variable related to angular distribution constructed to minimize uncertainty of the theoretical prediction) was below the discovery threshold. To confirm the observed effect, a part of the data collected in Run 2 was analyzed and a combined distribution is presented in Fig. 1.6 [Phys. Rev. Lett. 125 (2020) 011802]. The result indicates that this anomaly is still present. The final conclusion on this intriguing anomaly will be made after adding data collected in 2017-2018 and, possibly, new data samples expected from future LHC runs.

The $_c$ p $^{+}$ $^{-}$ process is an example of a flavor-changing neutral-current decay, highly suppressed within the SM. The branching fraction for nonresonant contribution (nonresonant in contrast to decays via intermediate particles like meson, i.e. $_c$ p followed by the $^{+}$ $^{-}$) is expected to be of the order of 10^{-9} in the SM but can be enhanced by New Physics effects. The search for the $_c$ p $^{+}$ $^{-}$ decay was performed [Phys. Rev.

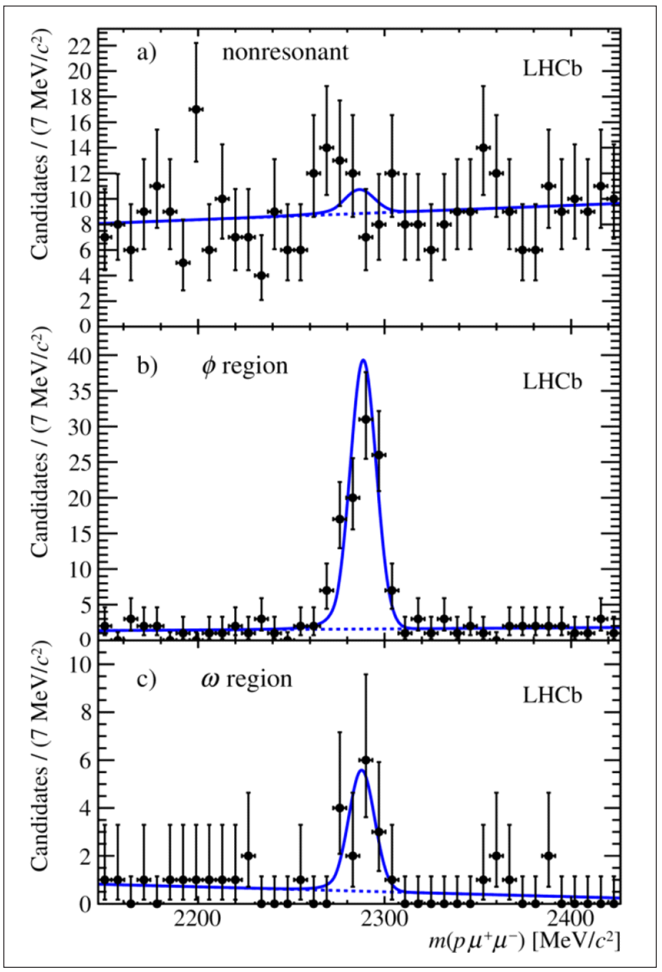

Fig 1.7: Mass distribution of selected p $^{+}$ $^{-}$ final state candidates in the three regions of the dimuon ($^{+}$ $^{-}$) invariant mass:
a) nonresonant $_c$ p $^{+}$ $^{-}$ decay,
b) −meson region: $_c$ p followed by the $^{+}$ $^{-}$ decay,
c) −meson region: $_c$ p followed by the $^{+}$ $^{-}$ decay.

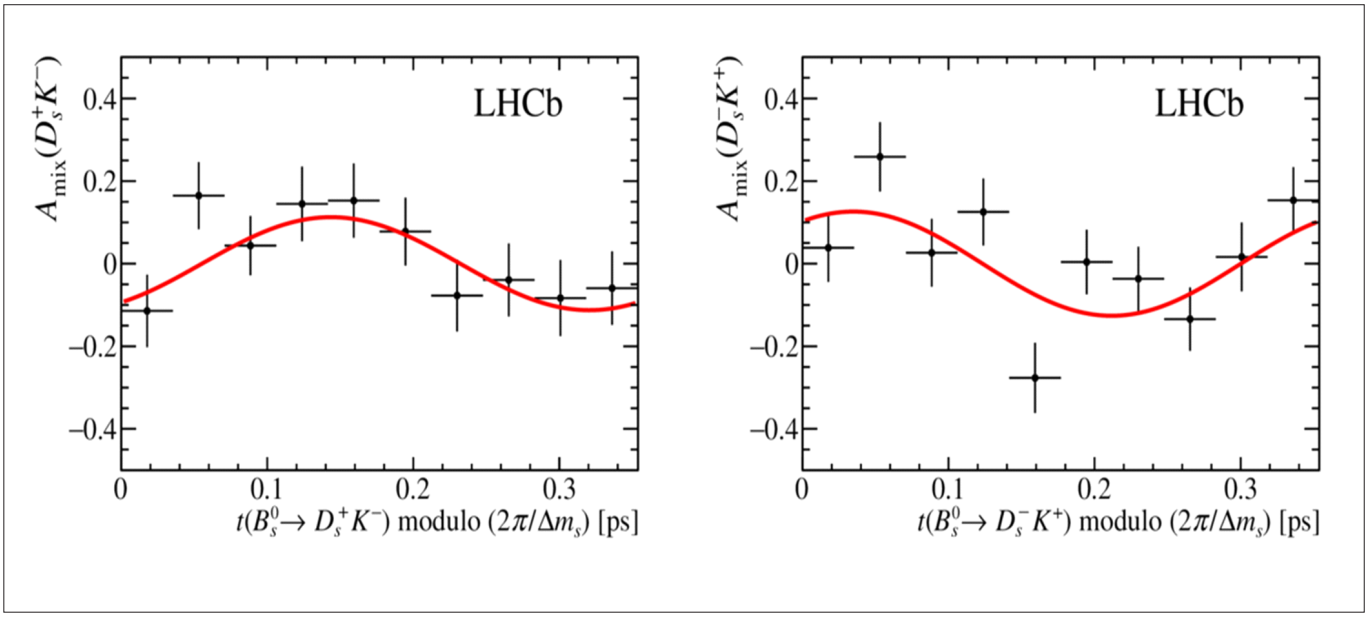

Fig.1.8: The asymmetries of the $D_S K$ and $D_S K$ final states.

D 97, 091101] using the $_c$ p decay for normalization. The result of the analysis conducted in three regions of $^+$ $^-$ invariant mass: a) nonresonant being the probe for New Physics, b) -meson region used for normalization and c) -meson region where the new decay mode was discovered. The reconstructed mass of $_c$ p $^+$ $^-$ for the three regions of $^+$ $^-$ subsystem invariant mass is presented in Fig 1.7.

No signal was seen in the nonresonant distribution where New Physics could enhance the branching fraction. Therefore an upper limit of the decay branching fraction BF($_c$ p $^+$ $^-$) < 7.7(9.6)x10^{-8} at 90%(95%) was set. **This determination improved the existing limit by a factor of about 100**. In the region a new decay mode $_c$ p with significance corresponding to 5 was observed [EurekAlert].

The LHCb experiment continues analyzing the properties of the **asymmetry between matter and antimatter in heavy hadron decays** needed to explain the matter dominance observed in the Universe. In particular, the collaboration is leading the field in the measurement of the Cabibbo-Kobayashi-Maskawa (CKM) angle which can be estimated from charmed decays of beauty mesons. The majority of these determinations are provided by the charged B mesons using the time-integrated methods by simply comparing the numbers of B^+ and B^- decays without looking at the time difference between the creation and decay of the B meson. The analysis of B_S^0 $D_S^{\mp}K$ decays [JHEP 03 (2018) 059] gives a unique opportunity to obtain the CKM angle in the system from time-dependent decay rates. The B_S^0 $D_S^{\mp}K$ decays are benchmark modes of the Standard Model, i.e. no contributions from the physics beyond it are expected. A comparison with respect to decays sensitive to New Physics establishes a powerful test of the SM. The analysis performed uses data recorded by the LHCb detector at the center-of-mass energy of 7 an 8 TeV. The decay-time-dependent asymmetries for the final states $D_S K$ and $D_S K$ are shown in Fig. 1.8. The evidence of this matter-antimatter asymmetry is determined at the level of 3.8 . Future updates with new data are not expected to be dominated by systematic uncertainty, and a predicted increase in statistics should lead to the first observation (with conventional 5 of statistical significance) of asymmetry in these decays.

The Belle II collaboration, using data collected during 2018 with a specialized trigger at the SuperKEKB collider, searched for a new vector boson Z'. Particles of this type occur in several extensions of the Standard Model (SM). Of special interest is the L-L model, in which Z' couples to the SM only through the 2nd and 3rd generation leptons, with the coupling constant g' . The model is potentially able to address important issues in particle physics, including the (g-2) anomaly. Searches for an invisibly decaying Z' boson in the process e^+e^- $^+$ $^-Z'$ and of a lepton-flavor-violating Z' in e^+e^- e $\mp Z'$ were performed for the first time. No significant excess of events was found, and 90% credibility level upper limits were set on the coupling constant g' (Fig. 1.9). The study shows that, with the full dataset, Belle II will be sensitive to the 10^{-3}-10^{-4} g' region that could explain the muon anomalous magnetic moment.

The report on this study [Phys. Rev. Lett. 125, 161806 (2020)] constitutes the first published physics results from Belle II.

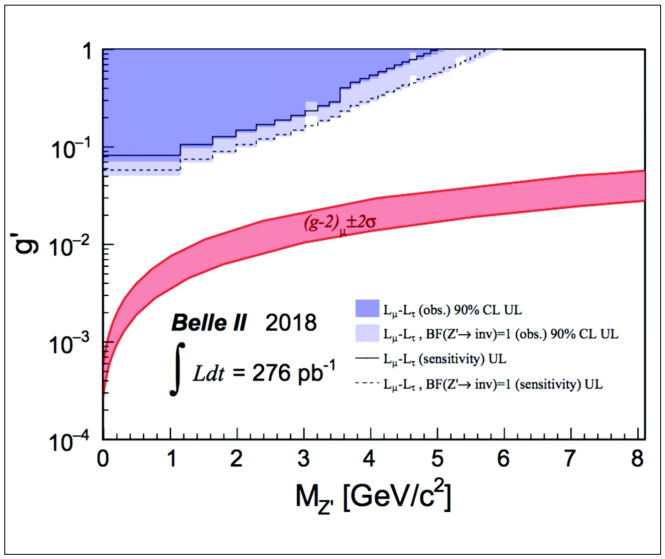

Fig. 1.9: 90% C.L. upper limits on coupling constant g'. The dark blue filled areas show the exclusion regions for g' at 90% C.L., assuming the L –L predicted branching fraction BF for Z' invisible; light blue areas are for BF(Z' invisible)=1 . The solid and dashed lines are the expected sensitivities in the two hypotheses. The red band shows the region that could explain the muon anomalous magnetic moment (g−2) ±2 .

B-meson decays involving a lepton are expected to be sensitive probes for physics beyond the Standard Model (SM). Indeed, the measured branching fractions of the decays B D(*) exceed the SM predictions by up to 3.5 standard deviations, hinting at the violation of lepton flavor universality. The Belle collaboration, after the first observation of exclusive semitauonic B decays in 2007, continued extensive studies of these processes with newly developed analysis techniques. Of special importance is the measurement of the branching fraction ratios R(D(*))= BF(B->D(*))/BF(B->D(*)l) (l=e,) with the tag-side B meson reconstructed in a semileptonic decay mode [Phys. Rev. Lett. 124, 161803 (2020)]. The measured values of R(D)= 0.307 ± 0.037 ± 0.016 and R(D*) = 0.283 ± 0.018 ± 0.014, where the first uncertainties are statistical and the second ones are systematic, represent the most precise measurements of these observables performed to date (Fig. 1.10). The results agree within 1.2 with the SM and reduce the overall tension between the SM and the world average of the data to 3.1 , but at the same time support the earlier observations of larger than expected values of R(D(*)).

Breaking the space-charge symmetry CP is one of the three conditions necessary to explain the dominance of matter over antimatter present in the Universe [A. D. Sakharov]. However, the measured amount of CP symmetry breaking in the quark interaction is too small to explain this dominance. For leptons, the dominance of matter could result from the mechanism called leptogenesis [M. Fukugita, T. Yanagida], but breaking of the CP symmetry has not been convincingly observed because suitable measurements require very demanding experiments. The T2K experiment published results that provide the **best constraint so far on the parameter describing the breaking of a symmetry between matter and antimatter in neutrino oscillations**, indicating a substantial violation of this symmetry [Nature 580, 339 (2000)]. This parameter, called CP phase, can range from -180 to 180 , and CP symmetry would be conserved for 0° or ± 180 °. T2K uses muon

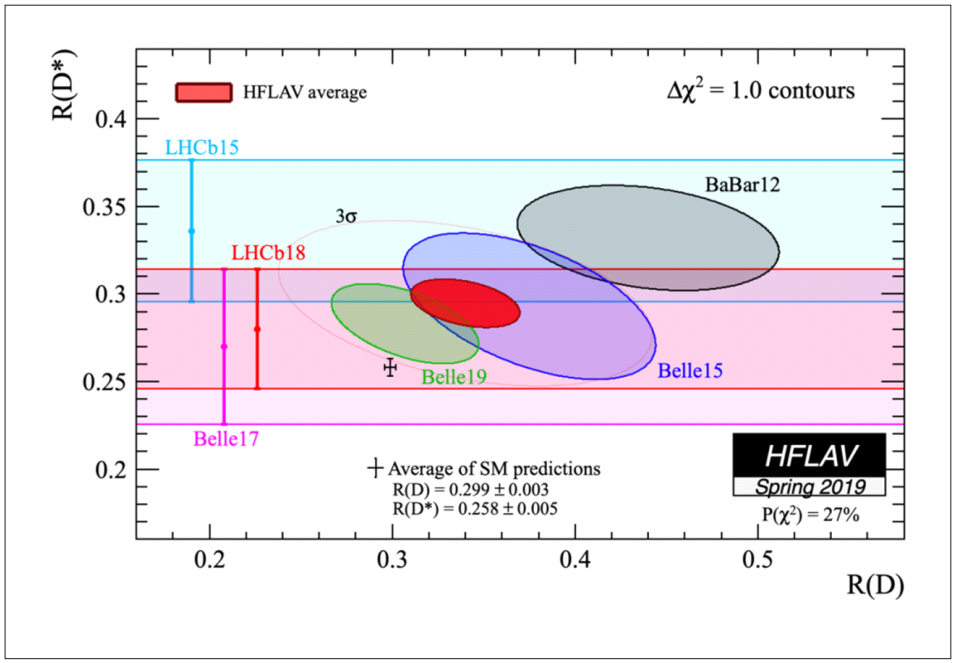

Fig. 1.10: Heavy Flavor Averaging Group (HFLAV) average of all measurements of R(D) and R(D*), updated with the latest result of the Belle collaboration. The light green area represents the new Belle results. The results agree within 1.2 with the SM. The blue area marks the previous independent Belle results, while the gray ellipse is the BaBar's measurement. Additional measurements of only R(D(*)) performed by LHCb and Belle are marked as bars on the left. The world average, the red area, disagrees with the SM prediction by 3.1 . This plot is retrieved from the HFLAV website.

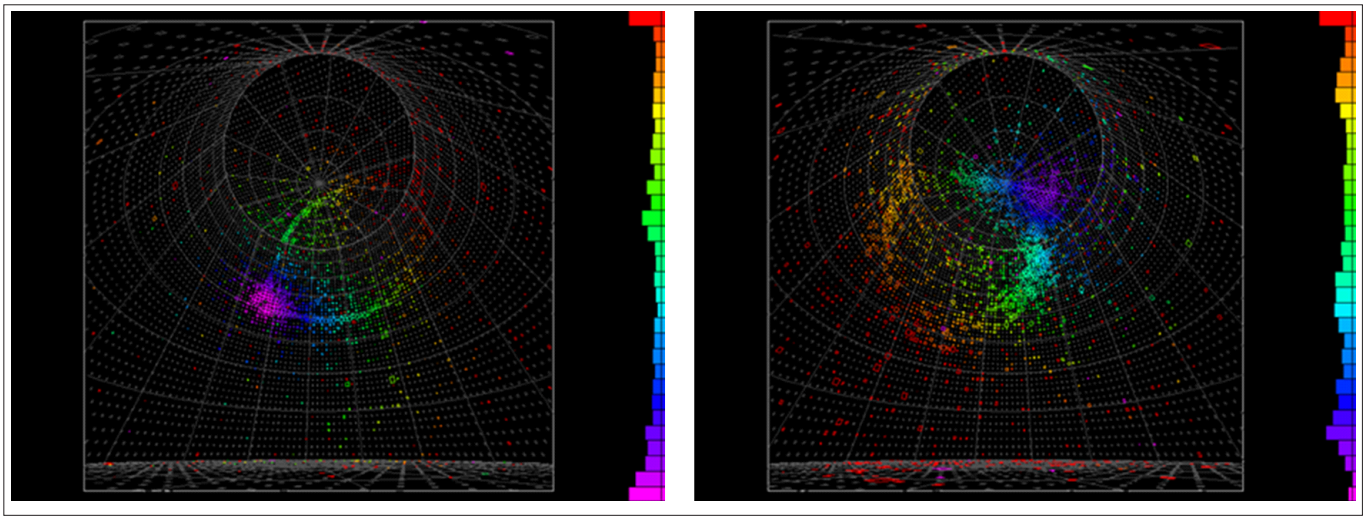

Fig.1.11: T2K neutrino beam interaction events: electron neutrino (left) and electron anti−neutrino (right) candidates observed in the Super−Kamiokande detector [©T2K experiment]

neutrino and anti-neutrino beams produced at J-PARC (Japan Proton Accelerator Research Complex) in Tokai, Japan. Neutrino interactions are studied in two detectors: near ND280+INGRID at J-PARC and far Super-Kamiokande, located 295 km from the place where the neutrino beam is produced. A small number of muon neutrinos and antineutrinos oscillate along a distance of 295 km into electron neutrinos and antineutrinos, respectively. The electrons/positrons formed as a result of the interaction of electron neutrinos/antineutrinos are detected in the Super-Kamiokande detector thanks to the registration of the characteristic "fuzzy" rings of Cherenkov radiation (Fig. 1.11). The analysis of the data collected by the T2K experiment for the neutrino (anti-neutrino) beam corresponding to 1.49 x 10^{21} (1.64 x 10^{21}) protons on target indicates a greater probability of neutrino oscillation than that of anti-neutrino oscillation. The range of $_{CP}$ values from -2° to 165° was excluded at the 3 confidence level (99.7%). This result is the strongest limitation on $_{CP}$ so far. The values of 0° and 180° are rejected at the 95% confidence level [T2K Coll.] and the strong CP symmetry breaking in neutrino oscillations seems to be favored. The second phase of the T2K experiment with the upgraded ND280 detector (high involvement of IFJ PAN) and the increased intensity of the neutrino beam will enhance the sensitivity of the CP symmetry breaking measurement. The next-generation Hyper-Kamiokande experiment with a far detector nearly ten times more sensitive than Super-Kamiokande will enable measuring $_{CP}$ with an accuracy of at least 5 required in particle physics to accept the result as a discovery.

Nature highlighted the T2K d_{CP} measurement as one of their top ten results published in 2020 [https://www.nature.com/articles/d41586-020-03514-8] **in all fields, including papers related to COVID-19.**

The GAMBIT Collaboration performed an analysis of various experimental data, searching for the existence of right-handed neutrinos introduced in extensions of the Standard Model (SM). Up to now, neutrino oscillations are the only direct evidence for the existence of physics beyond Standard Model. The discovery of such right-handed neutrinos can answer a few fundamental questions. The neutrinos can explain the non-zero mass of SM neutrinos and the phenomenon of their oscillations. They are also good candidates for the constituents of mysterious dark matter which is detected indirectly in

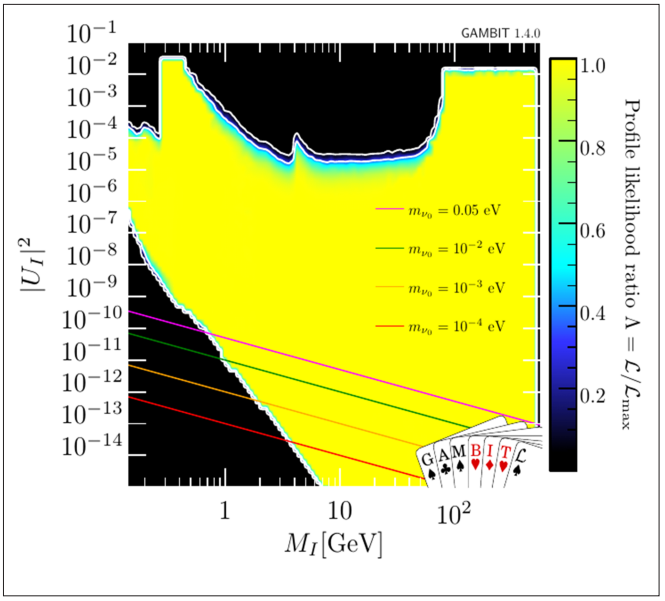

Fig. 1.12. Profile log−likelihood ratio with 1 and 2 confidence intervals (white contours) for the mass M_I of one right−handed neutrino and its total coupling $|U_I|^2$. Colored lines mark the lower limit on the coupling for fixed values of the lightest left−handed neutrino mass m $_0$.

astrophysical observations. In particular its existence is needed to explain the observed motion of stars in galaxies.

Right-handed neutrinos, if they exist, are different from other SM particles: they do not "feel" the fundamental forces of nature except gravity, which has also earned them the name "sterile neutrinos". This characteristic not only makes it extremely difficult to detect them, but also implies that the symmetries of the SM permit them to have an additional mass term, known as Majorana mass, which causes them to be their own antiparticles, a property that would be unique with respect to the so far known particles.

The result of a statistical combination of experimental results and cosmological constraints [Eur.Phys.J.C 80 (2020) 6, 569] is shown in Fig. 1.12 in the form of the profile log-likelihood ratio (quantity related to the compatibility between the theory prediction and experimental measurements) for values of the mass M_I of any right-handed neutrino in the range [0.06, 500] GeV and its total coupling $|U_I|^2$ to left-handed neutrinos in the range [10^{-15}, 10^{-1}]. As can be seen, the available parameter space is still large and spans 12 orders of magnitude in coupling strength [EurekAlert].

The Pierre Auger Observatory presented the **evidence of a large-scale anisotropy in the arrival directions of cosmic rays** above 8 EeV [Science 357 (2017) 1266]. The distribution of arrival directions of the cosmic rays is an important observable, which is expected to provide valuable information needed to understand their origin. Being charged particles, cosmic rays are significantly deflected by the magnetic fields present in the Universe. Only at the highest energies are the deflections expected to get small enough so that it should be possible to observe localized flux excesses associated with individual sources. On the other hand, as the energies decrease and the deflections become large, the propagation eventually becomes diffusive and it is likely that only large-scale patterns, such as a dipolar flux modulation, may be detectable.

The three-dimensional dipole was obtained by combining first-harmonic Fourier analyses in right ascension and azimuth. The analyses were performed using data collected over a period of more than 12 years. The anisotropy, detected at more than a 5.2 level of significance, can be described by a dipole with an amplitude of 6.5(+1.3/-0.9)% toward right ascension =100°±10° and declination =-24°(+12°/-13°). The dipolar pattern, with the highest excess pointing far from the Galactic center, is clearly seen in the flux map in Fig. 1.13. This result indicates an extragalactic origin of these ultrahigh-energy particles, and was included in the "Physics World Top Ten Breakthroughs of 2017".

Further analysis was later performed with a larger dataset [ApJ 891 (2020) 142]. It covered a wider energy range, down to about 0.03 EeV, in which the equatorial dipole component was studied. Combined with the results of other experiments (IceCube/IceTop, KASCADE-Grande), the analysis revealed a trend of increasing amplitudes with increasing energies, with values going from 0.1% at PeV energies to about 1% at EeV energies, and reaching about 10% at 30 EeV. The most significant modulation appears at energies above 8 EeV, with an equatorial dipole amplitude of 6.0(+1.0/-0.9)%, which has a significance of 6 . Below 8 EeV, none of the amplitudes obtained was significant and 99% CL upper bounds at the level of 1-3% were set. Regarding the phases determined in the different energy bins, a transition between the values lying close to the right ascension of the Galactic center, which is around -94°, towards the values in a nearly opposite direction (the phase of the maximum modulation is at 98° ± 9°) was observed to take place around a few EeV. **All this suggests that these dipolar anisotropies have a transition from a predominantly Galactic origin to an**

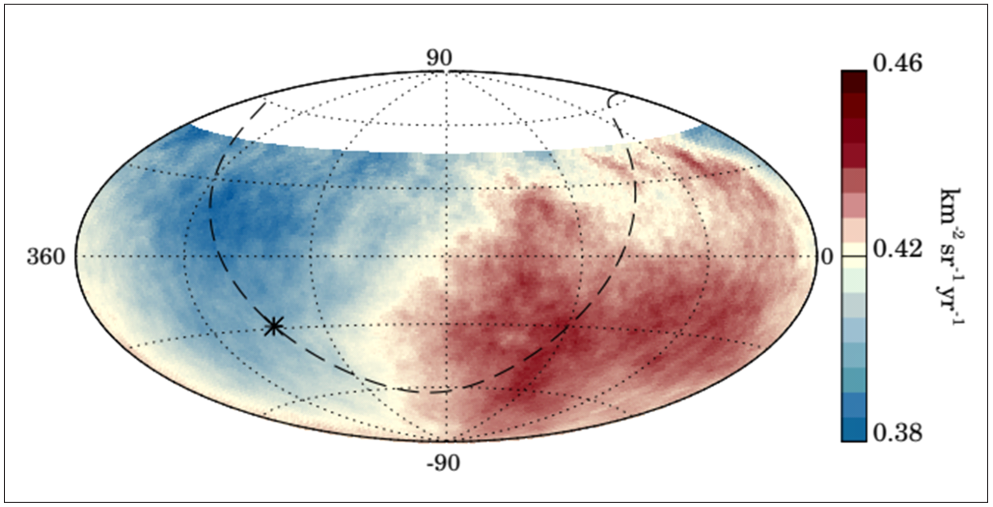

Fig. 1.13: Sky map in equatorial coordinates, showing the cosmic-ray flux above 8 EeV smoothed with a 45° top-hat function. The Galactic center is marked with the asterisk; the Galactic plane is marked with the dashed line. [Science 357 (2017) 1266].

extragalactic one somewhere in the range between 1 EeV and a few EeV.

More data as well as analyses exploiting the discrimination between the different cosmic-ray mass components that will become feasible with the upgrade of the Pierre Auger Observatory will be crucial to understand in depth the origin of the cosmic rays at these energies, and to learn how their anisotropies are produced.

Recently, the Pierre Auger Collaboration presented **the most precise measurement of the cosmic-ray energy spectrum at ultra-high energies** using the events recorded over more than 14 years by the Surface Detector. The data set consists of 215,030 events with zenith angles below 60° and energies larger than 2.5 10^{18} eV. The energy spectrum plays a key role in understanding cosmic rays and its measurement is particularly challenging given the rapid fall off of the flux with energy. The energy spectrum of ultra-high energy cosmic-rays was determined with very high statistics, so a new spectral feature, a break in the power law at about 1.3 10^{19} eV, was identified. The results were reported in two publications [Phys. Rev. Lett. 125, 121106 (2020) and Phys. Rev. D 102, 062005 (2020)] of the Pierre Auger Collaboration and are illustrated in Fig. 1.14, which shows a possible interpretation of the observed flux and composition data of ultra-high energy cosmic-rays in a scenario with sources that inject particles with a mass composition that changes with energy. The example shown represents a particular class of models, in which the acceleration of particles depends only on their rigidity (energy divided by charge). The abundance of nuclear elements appears to be dominated by intermediate-mass nuclei that are released from the sources with a very hard energy spectrum, and this spectrum is modified by extragalactic propagation effects. In such a scenario, the new feature in the spectrum would naturally occur because of the change of the composition in the energy range of the new spectral break. This measurement supports also a hypothesis that the suppression of the cosmic ray flux seen around 4 10^{19} eV is a manifestation of an upper-limit of the efficiency of the cosmic ray accelerators, rather than the Greisen-Zatsepin-Kuzmin (GZK) cut-off, predicted more than 50 years ago as a result of particle energy losses en route to Earth due to the pion photo-production on the cosmic microwave background.

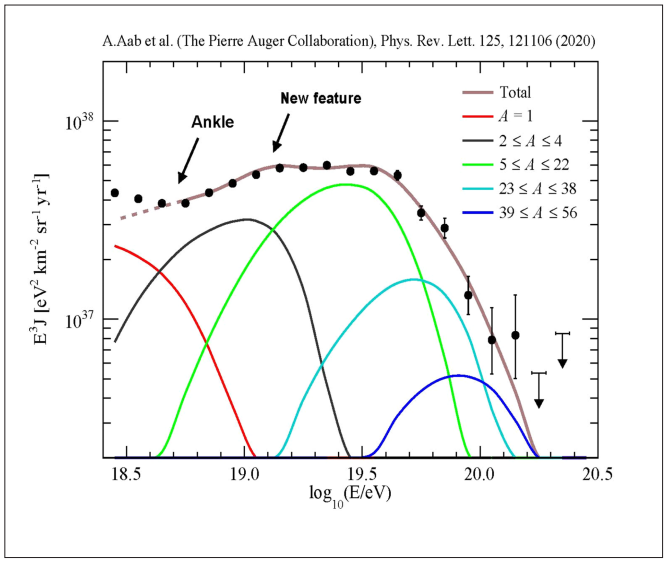

Fig.1.14: All-particle flux of the highest energy cosmic rays as measured by the Pierre Auger Observatory, scaled by E^3. The data are compared with a representative model scenario for sources, illustrating the correlation between the energy of the new spectral feature and the energy-dependent mass composition of the particles. Plot adapted from Phys. Rev. D 102, 062005 (2020).

The Pierre Auger Observatory is currently undergoing a large-scale upgrade by adding scintillation detectors and radio antennas on top of the existing water-Cherenkov detector stations. This will allow the scientists to obtain more information about the ultra-high energy cosmic-ray mass composition, extending it to the highest energies where a possible presence of light-mass nuclei could open a new window to composition-sensitive searches for sources and studies of cosmic magnetic fields.

The H.E.S.S. (High Energy Stereoscopic System) observatory for the first time succeeded in the **detection of a gamma-ray burst (GRB) at very-high photon energies** of 100-400 GeV. This discovery was made in 2018 with a 28-m telescope of the H.E.S.S. array - the largest Cherenkov telescope in the world. GRBs are flashes of gamma rays of extragalactic origin that result from cosmic explosions. They comprise seconds-to-minutes-long bright prompt emission at MeV energy range, followed by an afterglow which lasts from days to months and occurs mostly in the optical and X-ray spectral regions. Surprisingly, the GRB 180720B was detected deep in the afterglow phase – ten hours after the end of the prompt emission (see Fig. 1.15). This demonstrates that particles can be accelerated to very-high energies in GRBs, most likely at shock waves generated when the exploded matter collides with the circumburst medium. This also shows that energetic particles still exist or are produced a long time after the explosion. Responsible for gamma radiation are most likely ultrarelativistic electrons that scatter their own synchrotron photons, giving them a boost to very high energies. The groundbreaking detection of GRB 180720B offers new insight into the nature of cosmic gamma ray bursts. It also revolutionizes the methods for future searches for GRBs with Cherenkov telescopes.

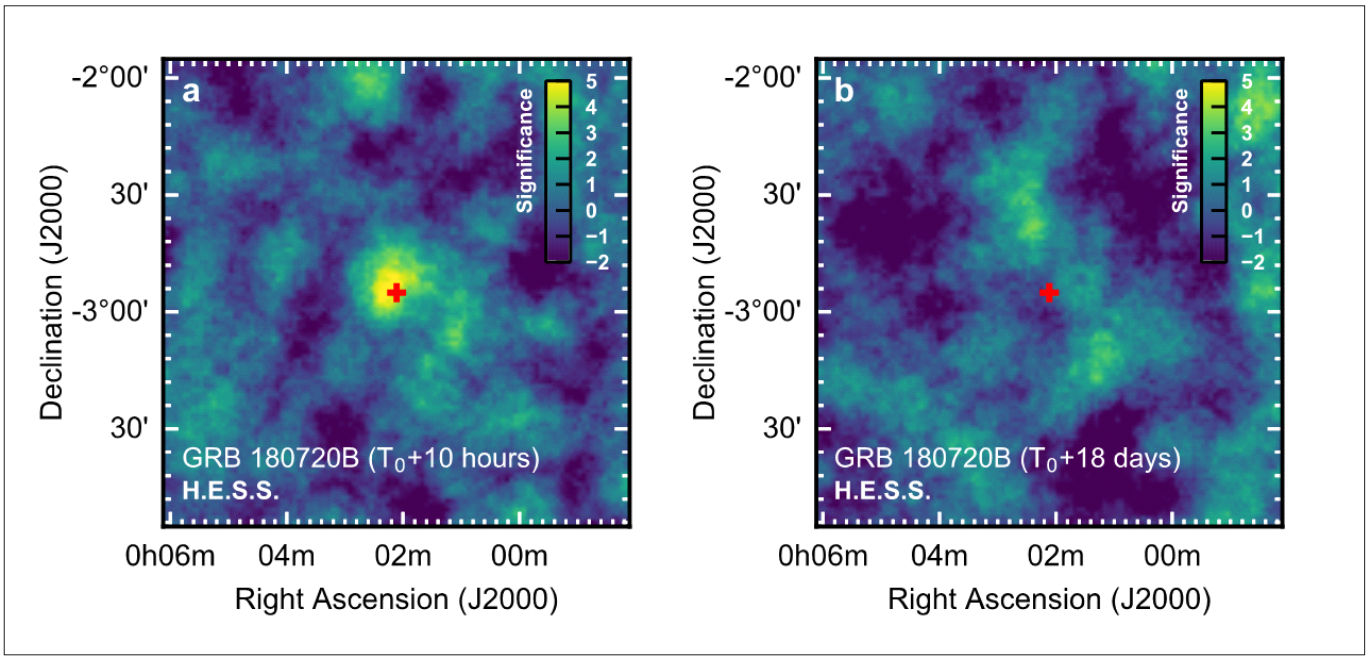

Fig. 1.15: Image of GRB 180720B taken by the large H.E.S.S. telescope in very−high−energy gamma light, 10 to 12 hours after the burst. The red cross indicates the position of the optical afterglow of the GRB (a). The same region of the sky as observed 18 to 24 days after the burst shows that gamma−ray flux significantly decreased (b) [Nature 575 (2019) 464].

Many years of observations of the galactic microquasar SS 433, carried out in the High-Altitude Water Cherenkov Gamma-Ray Observatory (HAWC), resulted in the **detection of ultra-high energy (UHE) gamma rays, for the first time in the history of microquasar studies.** The measured photon energies are at least 25 TeV. Microquasars are binary systems in which a supergiant star accretes its matter onto a compact object, either a black hole or neutron star. The accretion of the matter produces collimated plasma outflows – jets – in both directions along the axis of rotation of the object. Microquasars are therefore a scale version of quasars – active galactic nuclei hosting supermassive black holes and powerful jets, which are sources of extremely intense and highly variable electromagnetic radiation, covering almost the entire spectrum, from radio waves to high-energy gamma rays. They were recently identified as sources of high-energy neutrinos (see text below on "Multimessenger observations…") and are also believed to produce the highest-energy cosmic rays. As quasars are very distant objects, their VHE emission is not spatially resolved. The proximity of SS 433 and the orientation of its jets perpendicular to the line of sight offer a unique opportunity to study the sites and mechanisms responsible for the production of UHE gamma radiation. Observations reveal that TeV emission is not localized close to the compact object but in the places on both ends of jets, where they break off, colliding with the matter ejected by the supernova that formed the compact star (Fig. 1.16). Multi-wavelength modeling of SS 433 indicates that UHE photons are produced by highly energetic electrons interacting with photons from the cosmic microwave background through inverse-Compton scattering. The maximum electron energy is about 1 PeV. Such highly energetic electrons are probably accelerated in the jets and near the UHE gamma-ray emission regions, which presents a challenge to current acceleration models [EurekAlert].

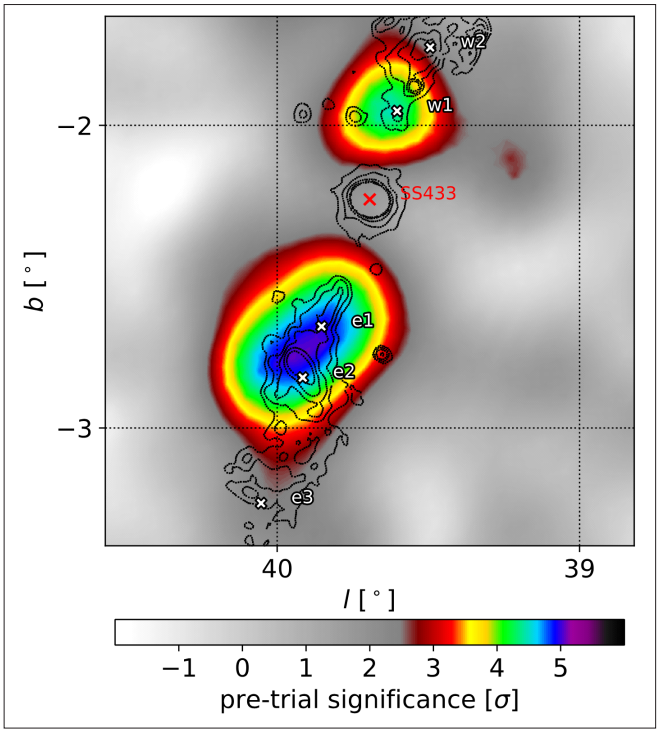

Fig. 1.16: UHE gamma−ray image of SS 433 (color scale) overlaid on the contours of X−ray emission (black lines). The location of the central binary is marked with the red cross [Nature 562 (2018) 82].

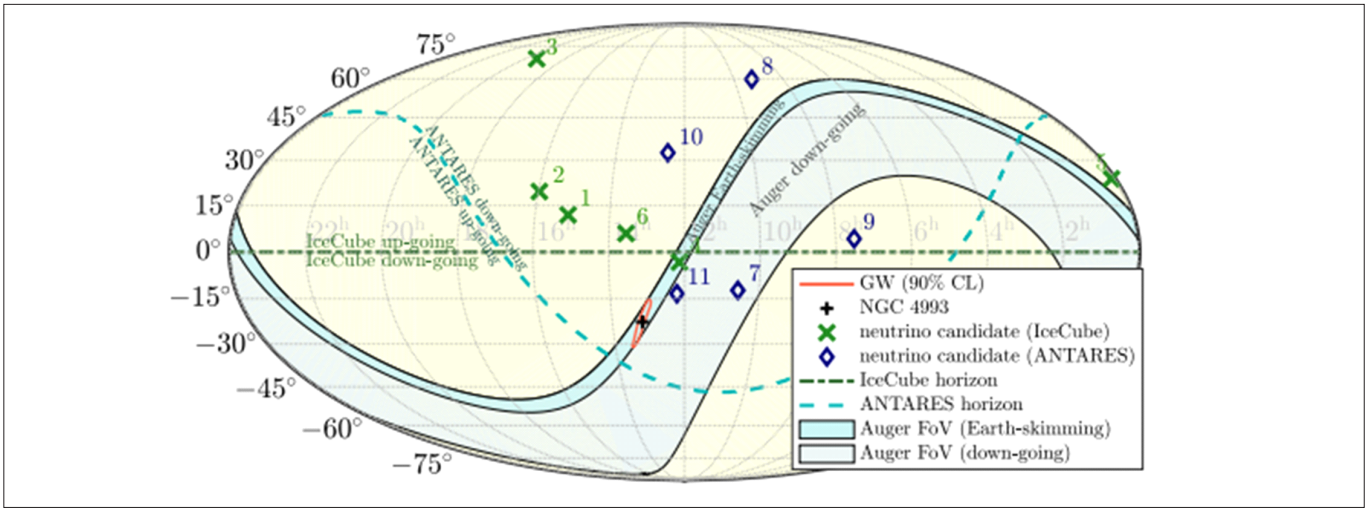

Fig. 1.17 : Localizations and sensitive sky areas at the time of the GW event in equatorial coordinates: GW 90% credible−level localization (red contour), direction of NGC4993 (black plus symbol), the lines represent horizons for Antares and IceCube, the bands are Auger's fields of view for Earth−skimming (darker blue) and down−going (lighter blue) directions. The zenith angle of the source at the time of the merger was 73.8° for Antares, 66.6° for IceCube, and 91.9° for Auger [source: ApJL 850 (2017) L35].

A joint publication [ApJL 848 (2017) L12] authored by more than 3000 scientists, including the H.E.S.S., HAWC and Pierre Auger Collaborations, reports the **first multi-messenger observation of a gravitational wave event**. On August 17, 2017 the LIGO and Virgo collaboration recorded a gravitational wave originating from a binary neutron star merger. Within 1.7 seconds, this event was followed by a gamma ray burst, recorded by the Fermi and INTEGRAL satellites. Numerous broadband observations followed, from radio to X-rays. These observations made it possible for the first time to pinpoint the source location of a gravitational wave event. The source was found to be in the galaxy NGC 4993 (at a distance of about 40 Mpc). According to model predictions, such a system may also accelerate cosmic rays to extreme energies, and thus emit photons and neutrinos up to GeV to EeV energies. For the H.E.S.S. and HAWC instrument, observations of the interesting part of the sky became possible only several hours after the event was recorded. These observations, which were repeated on the following nights, revealed no significant gamma-ray emissions in the energy range of several hundred GeV and higher. The search for neutrino emission from this collision of two neutron stars was conducted by the Pierre Auger, ANTARES, and IceCube collaborations. The Pierre Auger Observatory provides the best neutrino sensitivity in the EeV range: extensive air showers, produced either by interactions of downward-going neutrinos in the atmosphere or by decays of tau leptons originating from tau neutrino interactions in the Earth's crust, can be efficiently identified above the background of the more numerous cosmic rays. Remarkably, at the time of the merger the source could be seen from an ideal viewing angle for a search for Earth-skimming neutrinos by the Pierre Auger Observatory (Fig. 1.17). For IceCube and ANTARES, the direction to the source was in that part of the sky where the detectors are less sensitive, but still capable of making significant observations. The first study concentrated on a time window within ±500 seconds, and yielded no associated neutrino events. Later, the search was expanded to include a possible emission of high-energy neutrinos up to 14 days after the merger, suggested by theoretical predictions, and also to search for lower energy neutrinos associated with the merger remnant and ejected material. These follow-up studies did not find any significant emission either. The lack of the neutrino emission from the event is in good agreement with the observation of a GRB from a high viewing angle, i.e. with the outflow jet not pointing towards Earth. With a growing network of gravitational-wave detectors, it is expected that many more binary neutron star mergers will be discovered in the near future, expanding the capability to study these sources also through high-energy neutrinos.

Multimessenger observations of a flaring blazar coincident with high energy neutrinos were done by IceCube [Science 361 (2018) 146]. Neutrinos are tracers of cosmic-ray acceleration: electrically neutral and traveling at nearly the speed of light, they can escape even the densest environments and may be traced back to their source. High-energy neutrinos are expected to be produced in blazars: intense extragalactic radio, optical, x-ray, and, in some cases, -ray sources characterized by relativistic jets of plasma pointing close to our line of sight. Blazars are among the most powerful objects in the Universe and

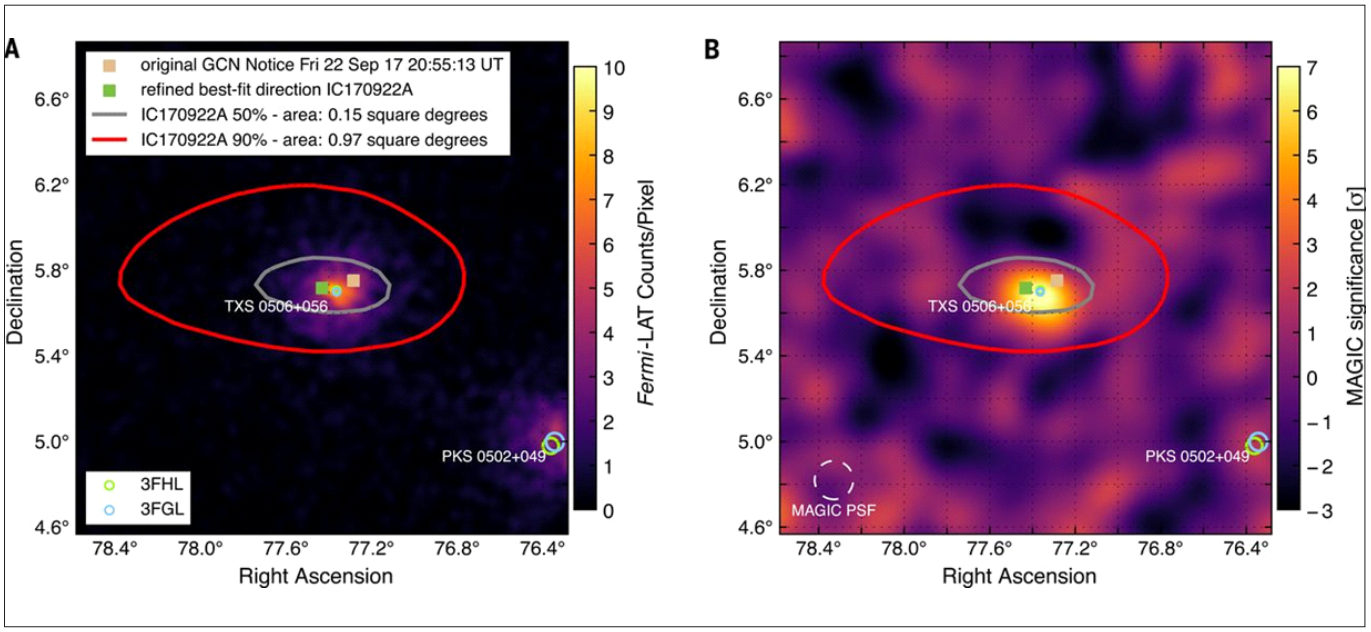

Fig. 1.18. Fermi−LAT (**left**) and MAGIC observations (**right**) of IceCube−170922A's location. [Figures taken from IceCube Collaboration et al. [Science 361 (2018) 146].

are widely speculated to be sources of high-energy cosmic rays.

On September 22, 2017 the IceCube observatory detected a high-energy neutrino: IceCube-170922A, see Fig. 1.18 (left). The detection of a single neutrino, like dozens of neutrino detections IceCube had previously observed, made it impossible to identify its source because of insufficient accuracy in determining the particle's direction of arrival. Therefore, soon after the neutrino was detected, observations of the selected area of the sky began with astronomical telescopes that record different types of electromagnetic radiation. Four hours after the IceCube team sent out the information, observations in the high energy gamma-ray range began, first by the H.E.S.S. Observatory in Namibia, and after 12 hours by the VERITAS Observatory located in Arizona (USA). The next day, the observations were continued by the MAGIC observatory in the Canary Islands, Spain. The first observations gave only an upper limit on the brightness of gamma rays from a possible neutrino source. Later, MAGIC observed this area of the sky for a total of 13 more hours, from September 24 to October 4, 2017. During these observations, a shining object appeared, the galaxy TXS 0506+56, which was identified as a possible source of both gamma rays and high-energy neutrinos from space, see Fig. 1.18 (right). These observations, also made with a number of other radio to high-energy gamma-ray instruments (including HAWC in Mexico), indicate that the source of the recorded neutrino could be the galaxy TXS 0506+056.

The detection of gamma rays in coincidence with neutrinos fascinates scientists because the emission of such gamma rays must be related to the acceleration of protons/nuclei to high energies, which are components of cosmic rays. The origin of cosmic rays has puzzled scientists since their discovery over 100 years ago. The observation of gamma rays and neutrinos from blazars is the first direct evidence for the existence of proton gas in these space objects. In addition, it is another success of the newly developing multimessenger astronomy, which combines observations not only in different ranges of the electromagnetic spectrum, but also of incoming particles – neutrinos and cosmic rays – and gravitational waves.

Particle acceleration processes at planetary and astrophysical shock waves were also studied theoretically with state-of-the-art large-scale and high-resolution **2D particle-in-cell simulations**. Numerical experiments were performed on supercomputers. The conditions for efficient electron pre-acceleration and heating and also magnetic field amplification at perpendicular high-Mach-number non-relativistic shocks were analyzed and the results were published in 6 papers in 2017-2021. The electrons were initially energized by interacting with electrostatic Buneman waves in the shock foot. The subsequent acceleration occurred through magnetic reconnection and stochastic scattering in the highly turbulent shock ramp and overshoot [Astrophys. J. 847 (2017) 71; 878 (2019) 5; 885 (2019) 10]. The magnetic fields were amplified in the shock transition owing to the ion-ion two-stream Weibel instability, whose evolution generates turbulence and creates conditions for magnetic reconnection (Fig. 1.19). The tangled magnetic field lines enabled electron heating by the

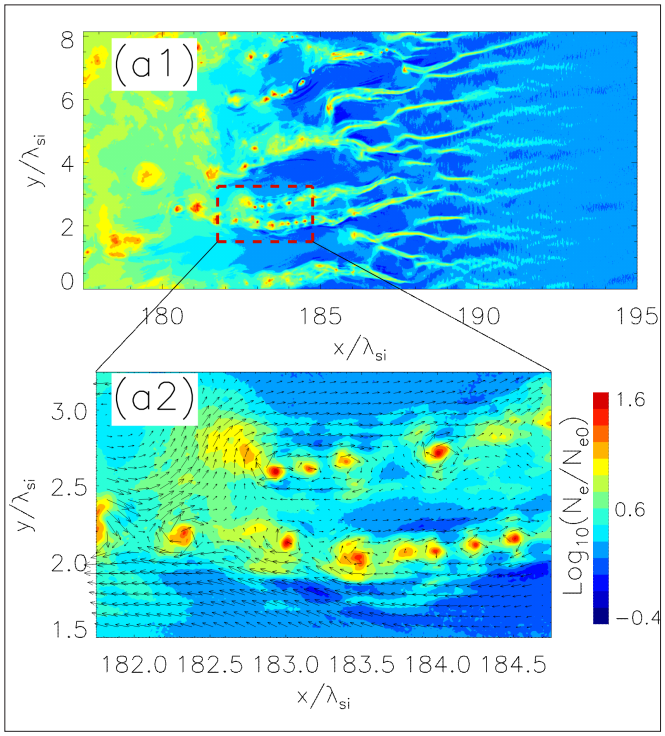

Fig. 1.19: Simulated structure of a perpendicular non−relativistic high Mach number shock (left). Filaments in electron density created because of the Weibel instability (top panel) trigger spontaneous turbulent magnetic reconnection forming X−points and magnetic islands (bottom panel) [Reproduced with permission from Bohdan et al. Astrophys. J. 893 (2020) 6 (AAS)].

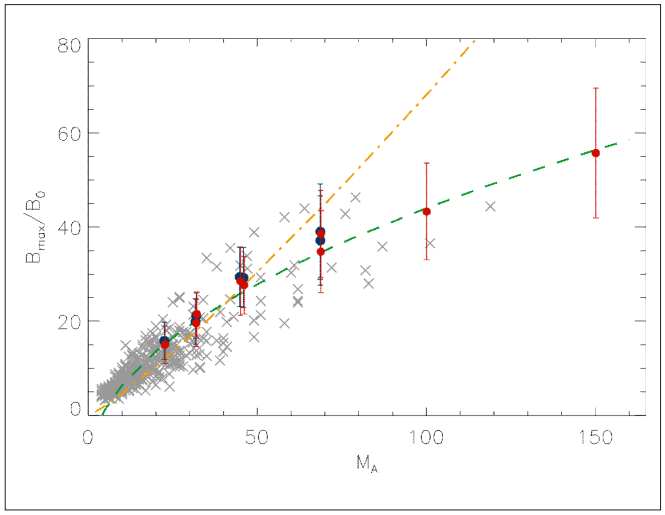

Fig. 1. 20. Magnetic field strength in function of the shock Alfvénic Mach number, M_A, measured by the Cassini spacecraft at Saturn's bow shock crossings (gray crosses) and PIC simulation data (blue and red dots, right). The yellow dash−dotted line shows prediction of an earlier modeling and the green dashed line is the dependence found in our PIC simulations. [Reproduced with permission from Bohdan et al. Phys. Rev. Lett. 126 (2021) 095101 (APS)].

shock potential. The derived model of electron heating predicted a proton-to-electron temperature ratio in the shock downstream, which is consistent with the observed values at supernova remnant shocks and in-situ measurements of the Saturn's bow shock done by the Cassini spacecraft [Astrophys. J. 904 (2020) 12]. The Weibel-instability-mediated magnetic field amplification is also fully consistent with in-situ data (Fig. 1.20).

A prototype single-mirror small-size **(SST-1M) telescope registered its first light** on August 31, 2017, while performing test observations of the extragalactic quasar 1ES 1959+650. The recorded flashes of the Cherenkov light were generated by gamma rays (Fig. 1.21) and cosmic rays. This internationally significant achievement was preceded by a five-year construction phase of individual components of the instrument, including the mechanical structure of the telescope and its innovative camera.

The SST-1M project is run by a consortium of Polish, Swiss, and Czech institutions. In Poland the project is led by IFJ PAN, where the mechanical structure of the telescope with the drive and control system was designed at the Division of Scientific Equipment and Infrastructure Construction in collaboration with the Department of Gamma-ray Astrophysics. The SST-1M (Fig. 1.22) has a 4 m diameter

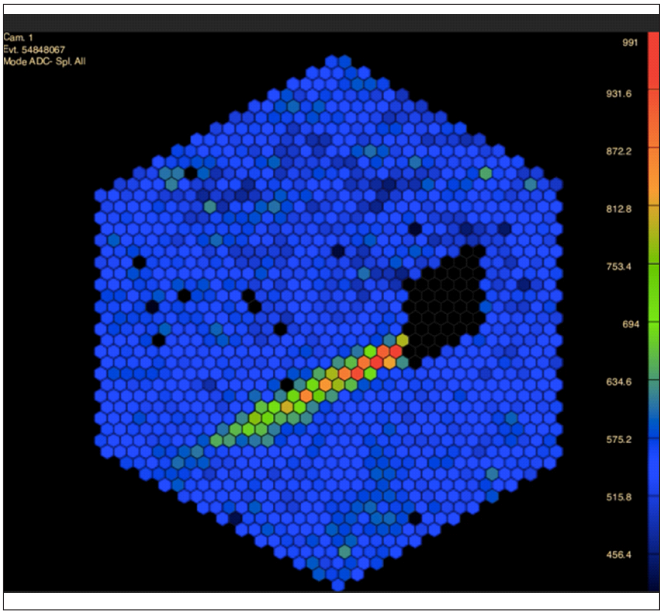

Fig.1.21. One of the first images of air showers induced by a possible gamma photon recorded by the SST−1M telescope .

dish composed of 18 mirror facets and the focal length of 5.6 m. The camera has a 9° field-of-view that enables surveying large portions of the sky with an angular resolution of 0.24°. The SST-1M was proposed for the small-size telescope array of the Cherenkov Telescope Array (CTA) observatory to cover the high end of CTA's energy range, between about 1 and 300 TeV. Since 2017 the SST-1M prototype has been modernized and the second telescope structure built. Both telescopes will soon be installed at the

Fig. 1.22. The SST−1M imaging atmospheric Cherenkov telescope equipped with mirrors and the Cherenkov camera. The telescope is installed at the test site in IFJ PAN.

Within the scientific task concerning the **study of correlations of cosmic rays on a global scale**, IFJ PAN initiated the establishment of an international cooperation of scientific and educational institutions and commercial partners under the name of the Cosmic Ray Extremely Distributed Observatory (CREDO), currently consisting of 42 entities from 19 countries on five continents [Symmetry 2020, 12(11), 1835]. Complementary to the intense program of forming the broad international collaboration, the global aspects of the CREDO mission (Fig. 1.23) require taking actions in the area of public engagement and citizen science, being a part of the adopted scientific methodology, as explained in [PoS (Asterics2019) 2019, 034]. The main component of these activities is the CREDO Detector mobile application [Symmetry 2020, 12(11), 1802], designed and prototyped at IFJ PAN in 2018. The application enables a detection of secondary cosmic radiation using mobile devices, and it currently operates on more than 7,000 devices located in approx. 150 countries around the world, providing data (approx. 10 million detections to date) which are both the subject of scientific analysis [Appl. Sci. 2021, 11(3), 1185] and the goal of educational and social activity. The latter includes e.g., the international competition "Particle Hunters"" organized by IFJ PAN since 2018. The competition is a team effort dedicated to detection of secondary cosmic radiation particles and local radioactivity using smartphones equipped with the CREDO Detector application. The main societal aim of the competition is to awaken in participants, mostly children and adolescents, the need to

Ondrejov Observatory in the Czech Republic, completed with the cameras and the optical systems to enable scientific observations with a mini-array of two telescopes.

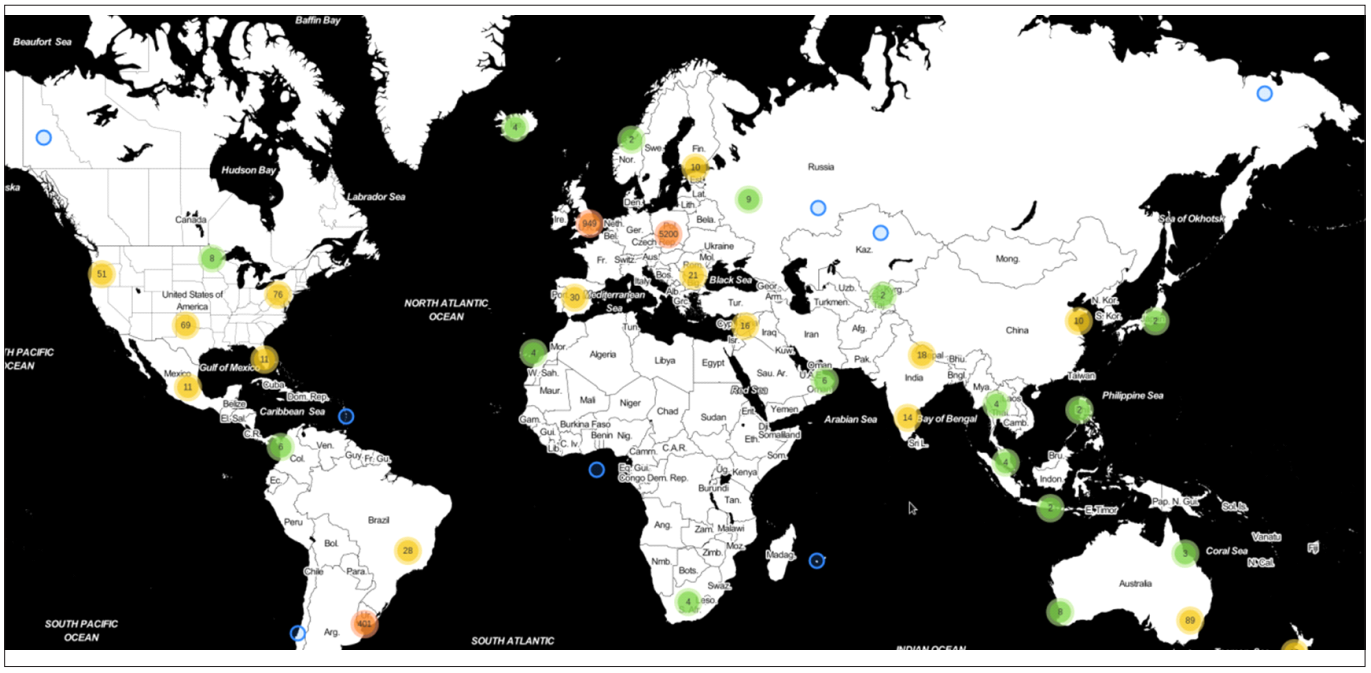

Fig. 1.23. The geographical distribution of the CREDO Detector mobile application users at the end of 2020. [Source: the CREDO Collaboration].

co-create science, and to enable them to participate actively and directly in top-class scientific research. The growing database and the enthusiasm of young participants further stimulate and empower the core scientific research being undertaken within CREDO, which is reflected e.g. in the continuous growth of the Collaboration, including acquiring valuable partners who operate other detectors of various types and collect data independently. [EurekAlert]

The Speakapp application (https://speakapp.link/), a conferencing tool based on modern html5 technology and developed at IFJ PAN, was used as an emergency conferencing system during the first phase of the Covid-19 pandemic. The Krakow high energy physics seminars, some lectures at the Jagiellonian University and online teaching in several high schools were conducted using Speakapp. The application has become a primary conferencing tool within the Belle II collaboration and in several smaller scientific collaborations.

In response to the Covid-19 pandemic, Szymon Bacher (a PhD student at IFJ PAN) started a grassroots project aimed at providing an open source, easy to replicate **non-invasive ventilator**, VentilAid. The project was started together with the Urbicum company, Szymon's partner during the design and production of a magnetic field measurement robot for Belle II and the Fussed Deposition Modeling (FDM) 3D printer controller, reported in previous years. The current design of the BiLevel Positive Airway Pressure (Bi-PAP) ventilator, based on a centrifugal turbine, was already validated on artificial lungs and dummies in collaboration with several medical institutions, including the Laerdal Medical company. The documentation of the first two (bellows-based) revisions was published in springtime 2020, while the third (turbine-based) revision publication is being prepared, to be ready in 2021. The extensive use of 3D printing and multi-variable control loop resulted in a design which is very simple to replicate. Despite the device's simplicity (Fig. 1.24), during its tests conducted at Laerdal's facility on an artificial lung used to simulate symptoms of acute respiratory distress syndrome (ARDS), chronic obstructive pulmonary disease (COPD), and asthma, the air pressures provided by the ventilator were well within normalized ranges.

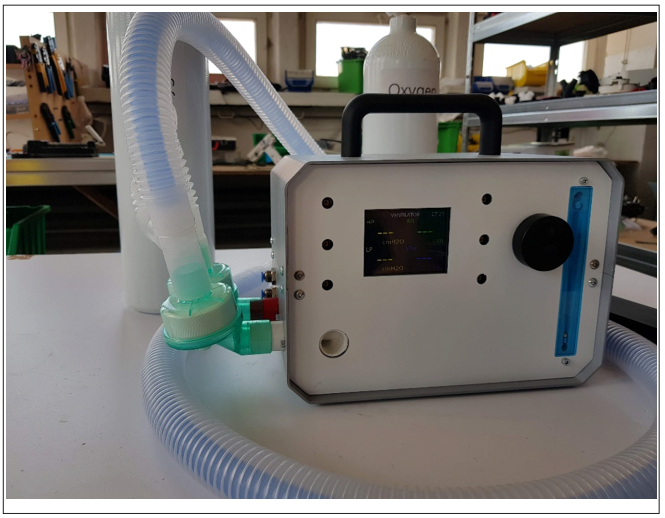

Fig. 1.24. VentilAid prototype as tested in Laerdal facility, including (inside the sheet metal casing) several novel parts: 3d printed pneumatic exhaust chock, 3d printed turbine and very fast regulation system. Here it is shown fitted with standard medical filters and concentric breathing system (coaxial hose feeding breathing mixture to a patient's mask).

❖

2. Division of Nuclear Physics and Strong Interactions

Nuclear physics is one of the most fundamental fields of science that seeks answers to the central questions about our Universe, i.e. its origin, evolution, and, especially, the creation and properties of its basic constituents – atomic nuclei of various elements. The ultimate goal of nuclear physics is to fully understand the basic properties of nuclei, from protons and neutrons up to very complex systems, by taking into account the underlying quark and gluon degrees of freedom, the features of strong-interactions, and mechanisms of nuclear reactions.

Nuclei are also a unique laboratory for a variety of investigations which deal with fundamental problems in physics. In many cases, these investigations are complementary to the research in particle physics. Currently, extensive experimental and theoretical efforts are being made around the world to solve the Big Questions of nuclear physics, which are:

> How is mass generated in QCD and what are the static and dynamical properties of hadrons?
>
> How does a strong force between nucleons emerge from the underlying quark-gluon structure?
>
> How does the complexity of nuclear structure arise from the interaction between nucleons?
>
> What are the limits of nuclear stability?
>
> How and where in the universe are the chemical elements produced?
>
> What are the properties of nuclei and strong-interacting matter as encountered shortly after the Big Bang, in catastrophic cosmic events, and in compact stellar objects?

At our Institute, research in experimental and theoretical nuclear physics is carried out at the **Division of Nuclear Physics and Strong Interactions**. The Division is actively involved in pursuing all the curiosity-driven quests to answer the aforementioned Big Questions. In particular, we contribute to the advancing of sophisticated theoretical models, to the development of the state-of-the-art detectors and experimental techniques, and, especially, to proposing and conducting top-level experiments both in the world and in Europe, including national laboratories (in Krakow and Warsaw). It is worth mentioning that over the last few years an ambitious program of fundamental research in nuclear physics with the use of a medical proton cyclotron has been initiated and implemented at the Cyclotron Centre Bronowice (CCB) at IFJ PAN.

All of these efforts are pursued within the framework of extensive international collaborations, many of which are located around Large Scale Facilities in Europe, such as GSI/FAIR (Darmstadt, Germany), GANIL/SPIRAL2 (Caen, France), LNL/SPES (Legnaro, Italy), or IPN/IJCLab (Orsay, France). A number of projects have also been located at other world-leading laboratories, such as CERN (experiments ALICE, NA61/SHINE, ISOLDE), ILL (Grenoble, France), ANL (Argonne, USA), RNCP (Osaka, Japan) or RIKEN (Wako, Tokyo, Japan), IFIN-HH and ELI (Bucharest, Romania). In most of these projects, the research and technical staff of our Division plays a key role.

The Division's last but not least important mission is to train next generations of nuclear scientists, which is accomplished by offering internships as well as master and Ph.D. degree programs in nuclear physics.

The scientific interests of the **Division of Nuclear Physics and Strong Interactions** consist of **four nuclear physics pillars**, studied in **four Departments**:

> Theoretical studies addressing a broad variety of issues in nuclear physics are carried out mainly in the **Department of the Theory of Strong Interactions and Many Body Systems**;
>
> Investigations in the field of nuclear structure are the main topic of the **Department of the Structure of Atomic Nucleus**;
>
> The studies concerning nuclear reactions, properties of processes involving hadrons and also basic

symmetries are carried out in the **Department of Nuclear Reactions and Hadron Processes**;

The investigations of the physics of strongly interacting matter at extreme energies and densities are pursued in the **Department of the Ultrarelativistic Nuclear Physics and Hadron Interactions**.

A brief description of the work and main results obtained in the four Departments of our Division is given in the section below, while some highlights of the achievements of our Divisions are described in more detail in the last part of this chapter.

The main activities of the **Department of the Theory of Strong Interactions and Many Body Systems** are focused on different theoretical aspects of strong interactions. Our activity can be classified into a number of different categories, such as the perturbative QCD processes with characteristic large scales, processes of inclusive production of hadrons, and single and pair meson production at low and high energies. Another subject of our interest is ultraperipheral production of leptons, hadrons and photons, heavy quarks and mesons, associated production of leptons and neutrinos, as well as production of quarkonia. In addition to that, we focus our studies on the initial conditions for quark-gluon plasma. The evolution of the so-called spectator systems, associated with the electromagnetic effects on charge particles in heavy ion collisions, is one of our expertise. Last but not least, within our main interests are theoretical aspects of light nuclei, concerning both the structure and reaction mechanism.

Our activities are strongly related to activities of experimental groups working in these areas. We explain the existing measurements as well as make predictions for future experiments and very often suggest new experiments. We closely collaborate with the ATLAS, CMS, ALICE and LHCb groups at the LHC, with the STAR and PHENIX experiments at RHIC, and with experiments related to e^+e^- collisions such as Belle or heavy ion experiments at SPS and GANIL.

We proposed a new subject to study: light-by-light scattering, not yet possible with lasers, in ultraperipheral collisions. Inspired by us, the ATLAS and CMS collaborations presented their first experimental results. We showed that the ALICE and LHCb experiments could make further progress in this field. We proved that the ultraperipheral reactions can be used to study the anomalous magnetic moment of leptons better than in other processes. Also, we developed a formalism for semi-central production of dilepton pairs using the so-called Wigner functions.

In recent years our group has also been working on the development of the so-called tensor pomeron approach and showed that it is consistent with existing experimental data. Several exclusive reactions were studied. We proposed different tests of the tensor pomeron model. Our approach is valid both for production of resonances ($q\bar{q}$ states, glueballs) and for di-meson continuum, i.e. it is much more consistent than other approaches in the literature.

We developed the formalism of single and double parton scattering in the context of charmed quark-antiquark production. Next we used the formalism of fragmentation functions to generate charmed mesons. We are also able to perform semileptonic decays of charmed mesons. This makes a link to high-energy neutrino production, what is relevant e.g. for the measurements of the IceCube apparatus or future experiments such as SHiP or FASER. Our calculations describe well both single D meson production and correlations between pairs of charmed mesons. We showed that the double-parton scattering may be responsible for the last year's observation of the $T_{4c}(6900)$ tetraquark.

We discussed in detail initial conditions for quark-gluon plasma at SPS energies and verified our prediction in studies of electromagnetic effects, such as the so-called Coulombic dip and/or directed flow. We also carefully studied the evolution of the associated spectator systems as a function of impact parameter using different nuclear models for calculating their excitation energy.

The activities of the **Department of the Structure of Atomic Nucleus** concern a wide range of current problems in nuclear physics. Breakthrough results on the structure of light neutron-rich nuclei, for example ^{16}C and ^{20}O, gave us a better understanding of the nature of nuclear forces, especially the role of the three body interactions. In the same A~20 mass region were also examined the properties of highly excited resonances emerged from exotic nucleonic configurations. Investigations of nuclides in the neighbourhood of the double magic cores of: ^{40}Ca, ^{78}Ni, ^{100}Sn, ^{132}Sn and ^{208}Pb provided new information on excitation of nucleons across the magic shells, especially in respect of a competition between single-particle and collective degrees of freedom, such as rotation. Special attention was paid to studies of long-lived shape isomers in neutron rich Ni and Y isotopes where shape coexistence and shape transitions occur. High spin isomeric states in heavier A~150 nuclei were a subject of extensive research as well. The focus was also put/placed on tracking the development of nuclear deformation in fast rotating nuclei, in particular in the transitional A~60 mass nuclei and in highly

deformed A~130 mass nuclei. Very active research line was devoted to studies of collective excitations associated with the so-called Pygmy and Giant Resonances in unstable neutron- and proton-rich nuclei such as ^{64}Fe and ^{80}Zr respectively, but also in stable ^{208}Pb. Of particular importance was the initiated search for a link between collective vibrations related to Giant Dipole Resonances occurring in hot compound nucleus and rotational bands built on isomers in a cold deformed evaporation residue, for example in the case of ^{188}Pt.

Nuclides from various regions of the nuclear chart mentioned above were examined by means of in-beam gamma ray and particle spectroscopy. Several approaches, such as Coulomb excitation, multinucleon transfer, fusion-evaporation or fission, were used to produce the nuclei of interest in their excited states. These nuclear reactions were induced either by stable and radioactive ion beams delivered by large accelerator systems operational at international laboratories such as GANIL, LNL, GSI, IFIN-HH or, especially fission products, by cold neutrons from the nuclear reactor at ILL and fast neutrons available at IPN. The experiments were performed using the most advanced detection systems combining the state-of-the-art gamma ray spectrometers, such as AGATA and PARIS, cooperating with various particle and ion detectors or mass separators. In addition, experiments conducted at CCB confirmed the competitiveness of the nuclear structure studies with the use of high-quality proton beams provided by the IBA PROTEUS 235 medical cyclotron.

At the same time, the department conducted research and development work on detection systems. One should mention here a contribution to the continuous progression in building the aforementioned multidetector array PARIS - the gamma-ray bolometer based on $LaBr_3$ scintillators (this initiative is coordinated by IFJ PAN scientists) and AGATA gamma-ray tracking high resolution spectrometer made of HPGe semiconductors. These systems will be accompanied by various ancillary detectors; some of them, e.g. ion and charged particle detectors, were constructed and tested in the department.

Particular effort was put into the setup of an experimental facility at CCB. This facility incorporates a set of gamma-ray and particle detectors (respectively PARIS, HECTOR and KRATTA) working in the coincidence mode. Besides being used in scientific experiments, the CCB proton beam was suitable for testing various detectors dedicated to large international projects, for example CALIFA for the R3B@NUSTAR/FAIR experiment and FAZIA for the SPIRAL2 and SPES experiments.

Research areas within the **Department of Nuclear Reactions and Hadron Processes** concentrate around four main topics: experimental study of few nucleon system dynamics, tests of the time reversal symmetry with a neutron as a laboratory, study of strangeness production and transport in hot nuclear matter, and investigation of nuclear matter equation of state with a focus on the symmetry energy.

The main motivation for the studies of few nucleon systems is the search for three-nucleon force which appears as the last unexplored part of nuclear dynamics, with the potential to contribute to many open questions in nuclear physics and astrophysics. The activities of our group in this field began with experiments performed at KVI, Groningen and FZ Juelich; however, the commissioning of a new proton cyclotron at CCB and installation of the BINA detector in its new experimental hall allowed us to continue the experimental program in Krakow. This continuation is gaining in importance as the results of succeeding analysis of rich sets of collected data, when compared with different state-of-the-art theoretical approaches, expose significant divergences, calling for farther experimental verification. New methods of data analysis are developed to extend the study to unexplored regions of breakup reaction phase-space and to crosscheck the obtained results. New experimental programs are proposed to enlarge the set of three nucleon force sensitive observables available for the study.

The search for Time Reversal Violation is one of the main motivations behind the nEDM experiment, as well as behind countless theoretical and experimental efforts tackling the problem of matter-antimatter asymmetry of the universe. It also plays a key role in the BRAND experiment, which has been under development/conducted at our Institute over the last three years. An innovative experimental principle assuming simultaneous measurement of extremely low energy protons and transverse component of electron polarization will enable precise measurements of eleven correlation coefficients in neutron decay, out of which five have never been attempted before. The first experimental run performed with a cold neutron beam in 2020 at ILL, Grenoble, showed a very good operation of the tracker detector for low energy electrons and promising results of feasibility tests of the detector for very low energy protons from neutron decay.

First results of the SPiRIT experiment at RIKEN performed with the use of the triggering detector, designed and built at our Institute, were obtained for central Sn+Sn collisions at 270 MeV/nucleon. They provide strong bonds on

the pion production mechanism and its link to the symmetry energy, revealing discrepancies and shortcomings of current models of the transport of pions through a dense nuclear matter. Charge distributions of large fragments in nuclear multifragmentation were expected to play a role of the order parameter indicating liquid-gas transition in finite systems. The coexistence of the signatures of first- and second-order phase transitions was observed in the experimental cumulant distributions of the intermediate-mass fragments in spectator fragmentation following ^{107,124}Sn+Sn and ^{124}La+Sn collisions at 600 MeV/nucleon, suggesting that this role of large fragment charge distributions is not restricted to the percolation transition but also applies to the liquid-vapor transition described with statistical multifragmentation models.

Study of hadronic interactions in a dense and hot nuclear environment is also the subject of the HADES collaboration. Of particular interest for physicists of our Department was the production of charged-pions in heavy ion collisions and of the -hyperon in elementary collisions pp, followed by its decay in a cascade process at 3.5 - 4.5 GeV. Efficient detection of this resonance will be facilitated by the upgraded version of the detector system. Better understanding of production mechanisms of this resonance was what lay behind a dedicated study of elementary scattering of negative pions on proton target at pion beam momenta ranging from 0.656 to 0.8 GeV/c.

Research areas within the **Department of the Ultrarelativistic Nuclear Physics and Hadron Interactions** are focused on nuclear matter at the extremely high temperature and pressure.

Since 1992 we have been members, and one of the founders, of the ALICE experiment at CERN LHC. We participated in all stages of the experiment: the design of the main ALICE tracker – the TPC, the development of the calibration procedure of this detector, the development of the simulation and reconstruction code. Since 2019 we have been involved in the upgrade of the TPC, participating mainly in tests of the modernized detector, in which classic multiwired readout chambers were replaced by GEM detectors. We also actively participate in data analysis. Our main fields of interest are: forward-backward correlations, electromagnetic probe, namely gammas and neutral mesons, hard probes – jets and nuclear modification factor. We are responsible for the Quality Assurance algorithms at the level of the entire experiment. In 2018, we joined the FIT Collaboration, which is involved in preparation of the fast trigger system for the RUN3.

In 2016 our Department joined the NA61/SHINE fixed target experiment at the CERN SPS facility. NA61/SHINE is a multi-purpose detector aimed at studying strongly interacting matter, in particular the properties of its deconfinement into the quark-gluon plasma and the position of its critical point (CP). The detector also provides reference measurements for neutrino and cosmic ray physics. To this program, we added a completely novel contribution, which is the study of electromagnetic phenomena as a new source of information on the space-time evolution of the created system. A dedicated scientific team was formed specially for this purpose. The team was additionally responsible for the coordination of the Critical Point Task Force and software development in the NA61/SHINE collaboration, as well as for the calibration of the detector response and optimization of its particle identification capabilities. Selected highlights on collisions of protons and nuclei in the energy range of 9-17 GeV are presented in the chapter below.

Selected Research Highlights of the Division of Nuclear Physics and Strong Interactions

Near threshold collectivization of shell model states due to the coupling to the nearby particle emission was investigated within the Shell Model Embedded in the Continuum (SMEC) [Phys. Rev. C 97 (2018) 044303; Phys. Rev. C 97 (2018) 054318; Phys. Rev. C 100 (2019) 064305]. Continuum induced mixing of SM eigenstates can be studied by calculating the continuum-coupling correlation energy: $E_{corr}(E) = \ _j | W_{Q0Q0}(E) | \ _j$, for the SMEC eigenstate Yj , i.e. the expectation value of the continuum coupling term in the SMEC eigenstate $_j$. $W_{Q0Q0}(E) = H_{Q0Q1}G^{(+)}(E)H_{Q1Q0}$ is the energy-dependent continuum coupling term between the orthogonal subspaces Q_0 and Q_1 containing 0 and 1 particle in the scattering continuum, respectively.

As an example, Fig. 2.1 shows the continuum coupling correlation energy for ^{9}Li nucleus as a function of proton energy. When coherent couplings to all open neutron-decay channels are included, the optimal energy for collectivization shifts down to Ep – 0.24 MeV, coinciding exactly with

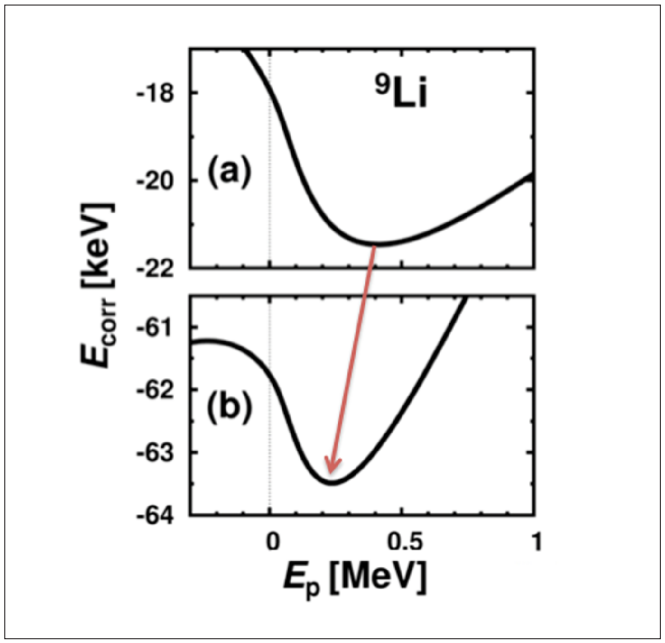

Fig. 2.1. The continuum−coupling correlation energy as a function of proton energy E_p for: (a) $J^\pi = 1/2^+$; T = 3/2 SM states with an excitation energy $E^* < 15$ MeV coupled in s−wave to the (lowest) one−proton decay channel and (b) with the additional coupling to all one−neutron decay channels.

the position of the physical near-threshold resonance in ^{9}Li [Phys. Rev. C 97 (2018) 044303].

The mysterious beta-delayed proton emission of the neutron halo ^{11}Be was explained within the SMEC, suggesting the existence of resonance, carrying the characteristics of a nearby proton-decay threshold [Phys. Rev. Lett. 124 (2020), 042504]. One of the most puzzling phenomena in nuclear physics is clustering. Such structures include a two-neutron halo of the ^{11}Li ground state or the famous Hoyle state in ^{12}C. Near threshold narrow resonances are fundamental for the nuclear synthesis in stars. Fig. 2.2 illustrates the situation in the case of ^{11}Be, where its neutron halo ground state decays into a resonance state in ^{11}B just above the proton emission threshold. Analysis within SMEC prefers the total angular momentum and parity of this state to be $^1/_2{}^+$, because of the substantial collectivization of the wave function. This state resembles many features of a nearby proton emission channel. Finally, maximum correlation energy for this state lies 142 keV above the threshold and is in rough agreement with experimental suggestions. What is more, the proximity of proton and tritium emission thresholds in ^{11}B suggests that this resonance could also contain an admixture of the configuration of tritium cluster channel. Another narrow resonance in ^{11}B lies just above neutron emission threshold lying a little bit higher. This $5/2^+$ state is responsible for huge neutron capture cross-section of ^{10}B. SMEC calculations also predict such a state, which strongly couples with l = 2 partial wave to the neutron + ^{10}B(3^+) channel. The emergence of collective proton (neutron) resonance around the proton (neutron) emission threshold comes from the l = 0 (l = 2) coupling to the proton (neutron) scattering space.

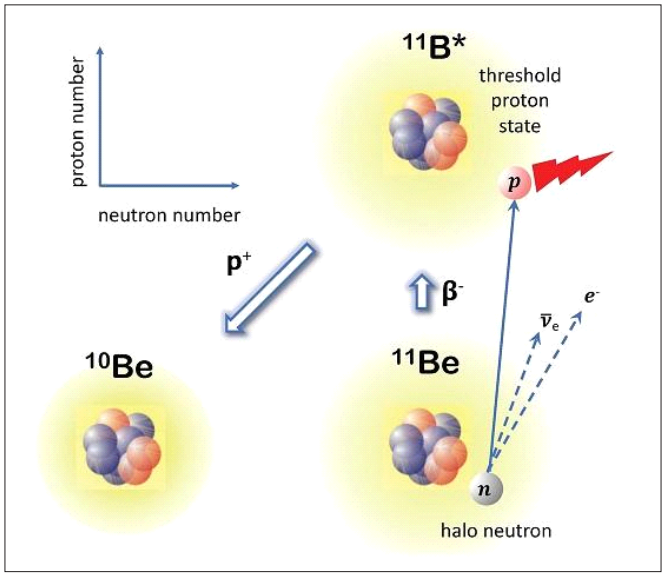

Fig 2.2. The −delayed proton emission of ^{11}Be. The neutron halo ground state of ^{11}Be undergoes decay to an excited state of ^{11}B, which lies just above the proton decay threshold. This state decays into ^{10}Be nucleus emitting proton [EurekAlert!]

A recent detection of ultra-high energy neutrino events with deposited energies up to a few PeV by the IceCube Observatory sets the beginning of neutrino astronomy. It is mandatory to know that the flux of atmospheric neutrino produced in cosmic-ray interactions with nuclei in Earth's atmosphere at different energies with high precision is an unavoidable background for cosmic neutrino studies.

The available data indicate that the neutrino flux observed in the experiment is dominated at low energies (E $< 10^5$ GeV) by atmospheric neutrinos that arise from the decay of light mesons (pions and kaons), denoted as the conventional atmospheric neutrino flux. On the other hand, the data for higher energies (E $> 10^7$ GeV) are most probably associated with cosmic neutrinos. In the intermediate energy range (10^5 GeV < E $< 10^7$ GeV) it is expected that the prompt atmospheric neutrino flux associated with the decay of heavy flavored hadrons, composed of heavy quarks, becomes important.

A detailed mapping of the dominant kinematical domains contributing to the prompt atmospheric neutrino flux at high neutrino energies was performed by studying its sensitivity to the cuts on several kinematical variables crucial for charm production in cosmic ray

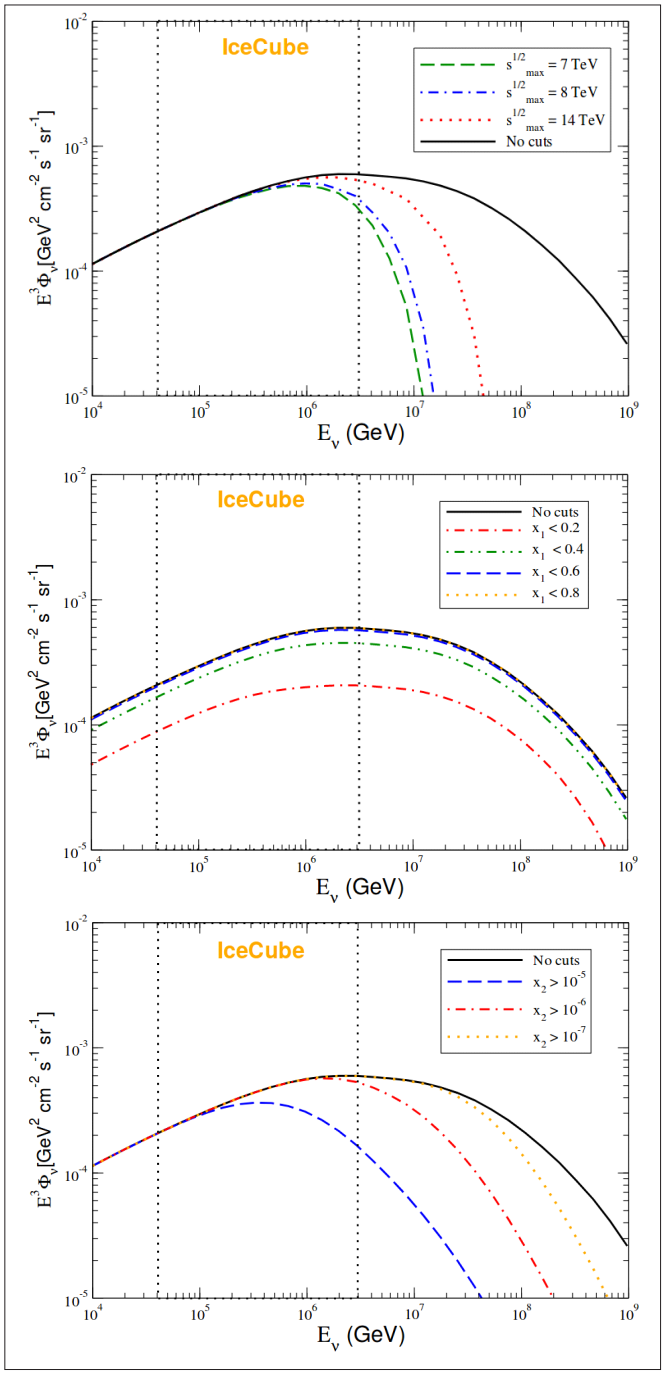

Fig. 2.3. Impact of different cuts on the maximal center-of-mass pp-collision energy (top), on the longitudinal momentum fractions in the target (middle) and on the longitudinal momentum fractions in the projectile(bottom) on the prompt neutrino flux. Reprinted figure with permission from: Victor P. Goncalves, Rafał Maciuła, Roman Pasechnik and Antoni Szczurek, Phys. Rev. D 96, 094026 (2017). Copyright 2017 by the American Physical Society. https://doi.org/10.1103/PhysRevD.96.094026

scattering in the atmosphere [Phys. Rev. D96 (2017) 9, 094026]. This includes the maximal center-of-mass energy for proton-proton scattering, the longitudinal momentum fractions of partons in the projectile (cosmic ray) and target (nucleus of the atmosphere), the Feynman x_F variable and the transverse momentum of charm quark/antiquark (cf. Fig. 2.3). It was found that the production of neutrinos is particularly sensitive to the center-of-mass energies larger than the ones at the LHC and to the longitudinal momentum fractions in the projectile $10^{-8} < x < 10^{-5}$. Clearly, these are regions where one does not control the parton, in particular gluon, densities. Also, the characteristic theoretical uncertainties in the charm production cross section coming from its QCD modelling were analyzed. The precision data on the prompt atmospheric neutrino flux can efficiently constrain the mechanism of heavy quark production and underlying QCD dynamics in kinematical ranges beyond the reach of the current collider measurements.

Explicit calculations of the contribution of the pp pp $^+$ $^-$, pp p $^+$ $^-$ and pp $^+$ $^-$ processes to exact kinematically 2 4 calculation were performed. The resonance contributions constitute about 15% of the conventional pp pp $^+$ $^-$ cross section and lead to an enhancement of the measured cross-sections for exclusive $^+$ $^-$ production in pp collisions at $\sqrt{s}$ = 13 TeV (left panel of Fig. 2.4). It was shown that in the final comparison with the ATLAS experimental data one should take into account corrections for absorptive effects and also the contributions when one or both protons dissociate into hadronic continuum.

It was also shown that for the Odderon search in the central exclusive production (CEP) of single mesons is a valuable addition, and in fact an alternative, to the study of elastic pp scattering or CEP of two mesons. For the reaction pp pp $^+$ $^-$ (right panel of Fig. 2.4) we compared the purely diffractive contribution (Odderon-Pomeron fusion), calculated in the framework of the tensor-pomeron and vector-odderon model, to the photoproduction contribution (-P fusion) and to the $^+$ $^-$ continuum term. The deviations from the -P fusion contribution at large $p_{T,\ ^+\ ^-}$, can be treated as a signal of Odderon exchange. A combined analysis of both the K+K- and the $^+$ $^-$ channels should be the ultimate goal in searches for the Odderon exchange. We are looking forward to first experimental results on single and double (1020) CEP at the LHC.

Ultrarelativistic Heavy Ions are accompanied by a large flux of Weizsäcker–Williams photons. This offers the opportunity to study a variety of photo-induced nuclear processes as well as photon-photon processes. So far most investigations have been focused on ultraperipheral collisions. Interpreting Weizsäcker-Williams photons as partons of the nuclei, the coherent photon cloud contributes to peripheral and semi-central collisions, where the impact parameter of the collisions satisfies $b<2R_A$ (with R_A being the nuclear radius). It was realized

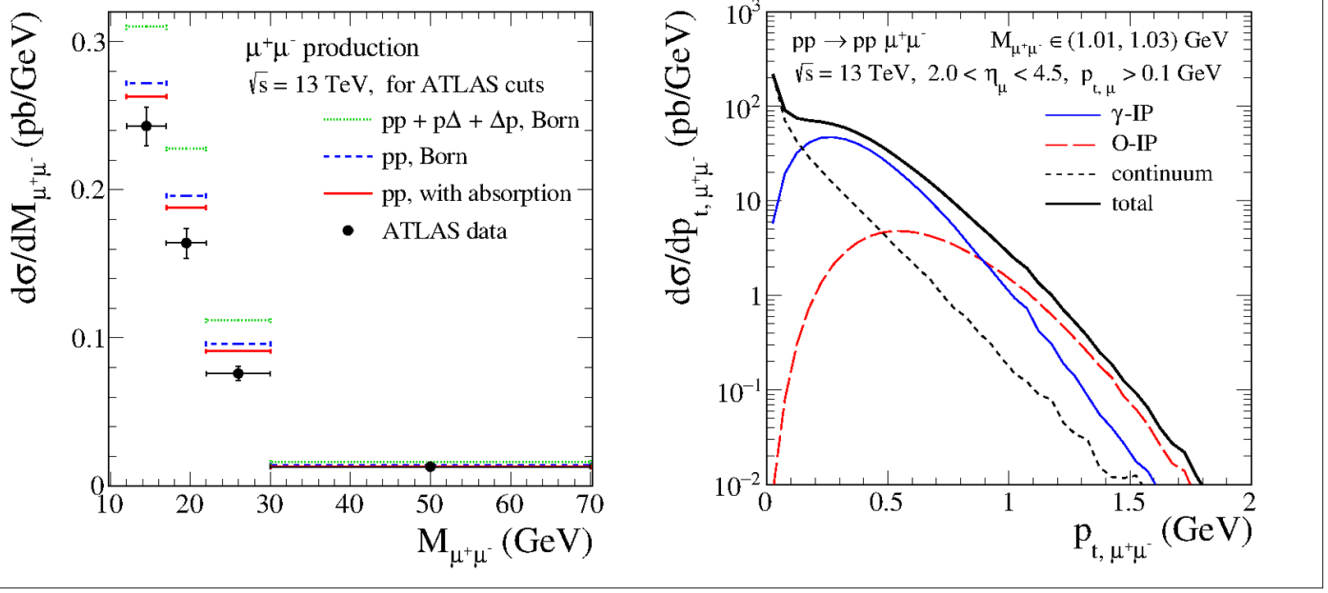

Fig. 2.4. **Left**: The differential cross section d /dM $_{+}$ $_{-}$ for the exclusive $^{+}$ $^{-}$ production at s = 13 TeV. Our "exact 2 4 kinematics" predictions including the pp pp $^{+}$ $^{-}$ and the pp p $^{+}$ $^{-}$ (p $^{+}$ $^{-}$) processes are compared with the ATLAS fiducial cross sections. [P. Lebiedowicz and A. Szczurek, Exclusive and semiexclusive production of + − pairs with isobars and other resonances in the final state and the size of absorption effects, Phys. Rev. D 98, 053007 (2018), https://doi.org/10.1103/PhysRevD.98.053007] **Right:** The distributions in transverse momentum of the $^{+}$ $^{-}$ pair for the pp pp $^{+}$ $^{-}$ reaction at s = 13 TeV in the (1020) resonance region and with the cuts relevant for the LHCb experiment. Here the −P and oderon−P fusion contributions and the $^{+}$ $^{-}$ continuum term are shown. [P. Lebiedowicz, O. Nachtmann, and A. Szczurek, Searching for the odderon in pp ppK+K− and pp pp $^{+}$ $^{-}$ reactions in the (1020) resonance region at the LHC, Phys. Rev. D 101, 094012 (2020), https://doi.org/10.1103/PhysRevD.101.094012].

recently that coherent photon-photon processes survive also in semi-central collisions.

Two years ago, the STAR collaboration at RHIC [Phys. Rev. Lett., 121(13):132301, 2018) observed a large enhancement at very low transverse momenta of the dielectron pair, P_T 0.15 GeV. In collaboration with Texas A&M University (USA), a group at IFJ performed a thorough **theoretical study of the centrality dependence of dilepton production at very low pair transverse momenta** [Phys. Lett. B 790, 339-344 (2019)]. For the first time, the interplay of dilepton production initial photon annihilation processes, l^+l^-, was studied. These processes were triggered by the coherent electromagnetic fields of the

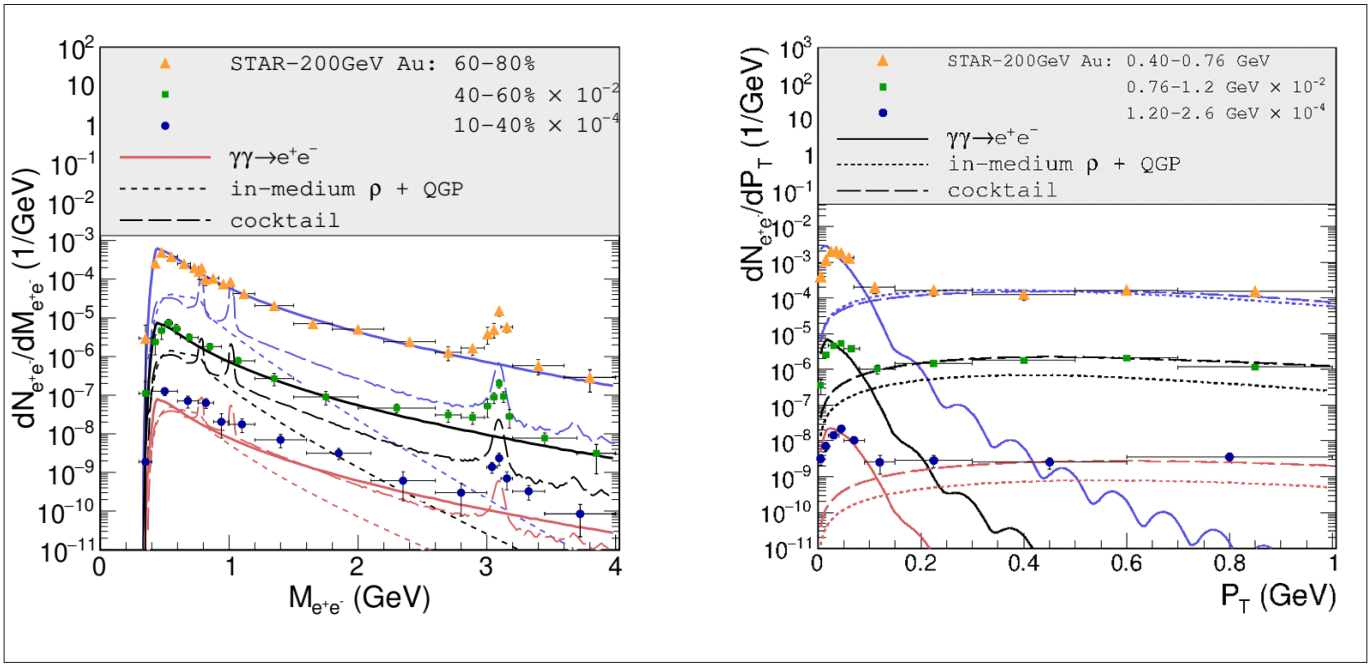

Fig. 2.5. Theoretical predictions vs. STAR experimental data at RHIC energy (s=200 GeV). Dielectron invariant mass spectra (**left panel**) for three ranges of centrality: 60 – 80% (upper curve), 40 – 60% (middle curve) and 10 – 40% (lower curve) and pair transverse momentum (**right panel**). Thermal radiation (dotted lines) and hadronic cocktail (dashed lines) contributions are compared with the e^+e^- process (solid lines) [Phys. Lett. B 790, 339-344 (2019)].

incoming nuclei with other mechanisms, such as thermal radiation from a quark-gluon plasma (QGP). For the thermal radiation (dotted lines), which includes the emission from the QGP and intermediate hadronic phases, an approach using in-medium vector spectral functions was employed. The approach describes the inclusive excess radiation observed over a wide range of collision energies. For the coherent photon fusion processes (solid lines), whose spectrum is much softer than for thermal radiation, the initial fluxes from the Fourier transform of charge distributions of the colliding nuclei in the equivalent-photon approximation were applied. It was verified for the first time that the combination of photon fusion, thermal radiation and final-state hadron decays (dashed lines) gives a fair description of the low-P_T dilepton mass spectra as recently measured by the STAR collaboration for different centrality classes, including experimental acceptance cuts (see Fig. 2.5 for the invariant mass and the pair transverse momentum distribution). The coherent contribution dominates in peripheral collisions (centrality = (60-80)%), while thermal radiation plays an important role only in small centralities.

plasma produced in ultrarelativistic heavy-Ion collisions. These experiments rely on comparisons of yields of charmonia in nucleus-nucleus collisions to those measured in proton-proton collisions. An understanding of the latter is therefore a pressing issue. At IFJ PAN, in collaboration with a group from Lund University, an approach to charmonium production via gluon-gluon fusion was worked out. In this approach, the production mechanism is described without the commonly used restriction to nonrelativistic internal motion of the produced cc pair.

The bound state structure of the charmonium is accounted for by the light-front wave function and includes relativistic corrections. The new approach was successfully applied to the production of çc- mesons in proton-proton collisions. While the data taken by LHCb in proton-proton collisions were a puzzle for other approaches, Fig. 2.6 shows that they are well described by the new approach using standard unintegrated gluon distributions from the literature at $\sqrt{s}$ = 8 TeV. At the higher energy of $\sqrt{s}$ = 13 TeV, the preliminary data seem to suggest additional mechanisms at large p_T.

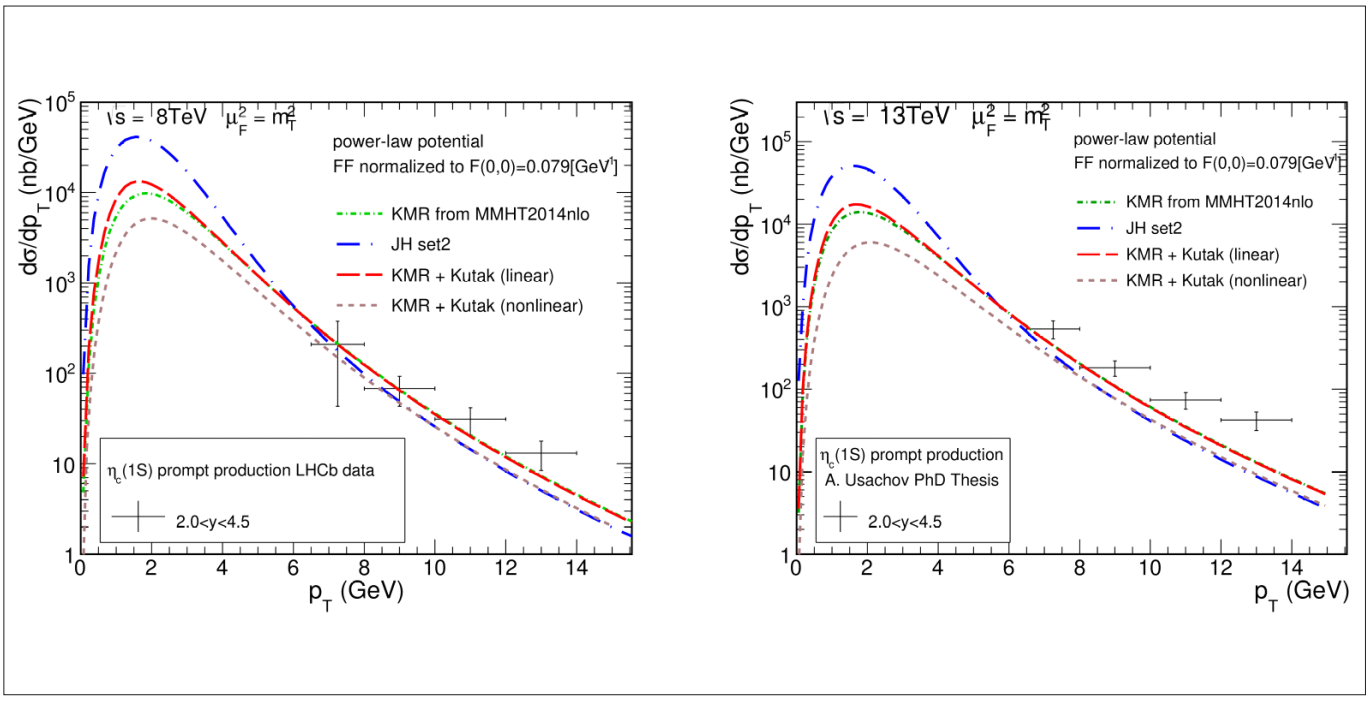

Fig. 2.6. Transverse momentum distribution for promt $_c$(1S) production compared with the LHCb data for $\sqrt{s}$ = 8 TeV (left panel) and with the preliminary experimental LHCb data for $\sqrt{s}$ = 13 TeV (right panel) [JHEP 02 (2020) 037].

Cross sections for the production of the ground state of the charmonium system, the $_c$-meson, were calculated in an approach including gluon transverse momenta [JHEP 02 (2020) 037]. In recent years charmonium physics has attracted a lot of attention owing to the special role played by heavy quarks as probes of the quark-gluon

The lifetime of the second 2^+ state in neutron-rich ^{20}O, $\tau(2_2) = 150^{\,80}_{\,30}$ fs, and an estimate for the lifetime of the second 2^+ state in ^{16}C were obtained for the first time [Phys. Rev. C101, 021303(R) (2020), EurekAlert!]. This achievement provided valuable experimental input to ongoing tests of the predictive power of *ab initio* nuclear

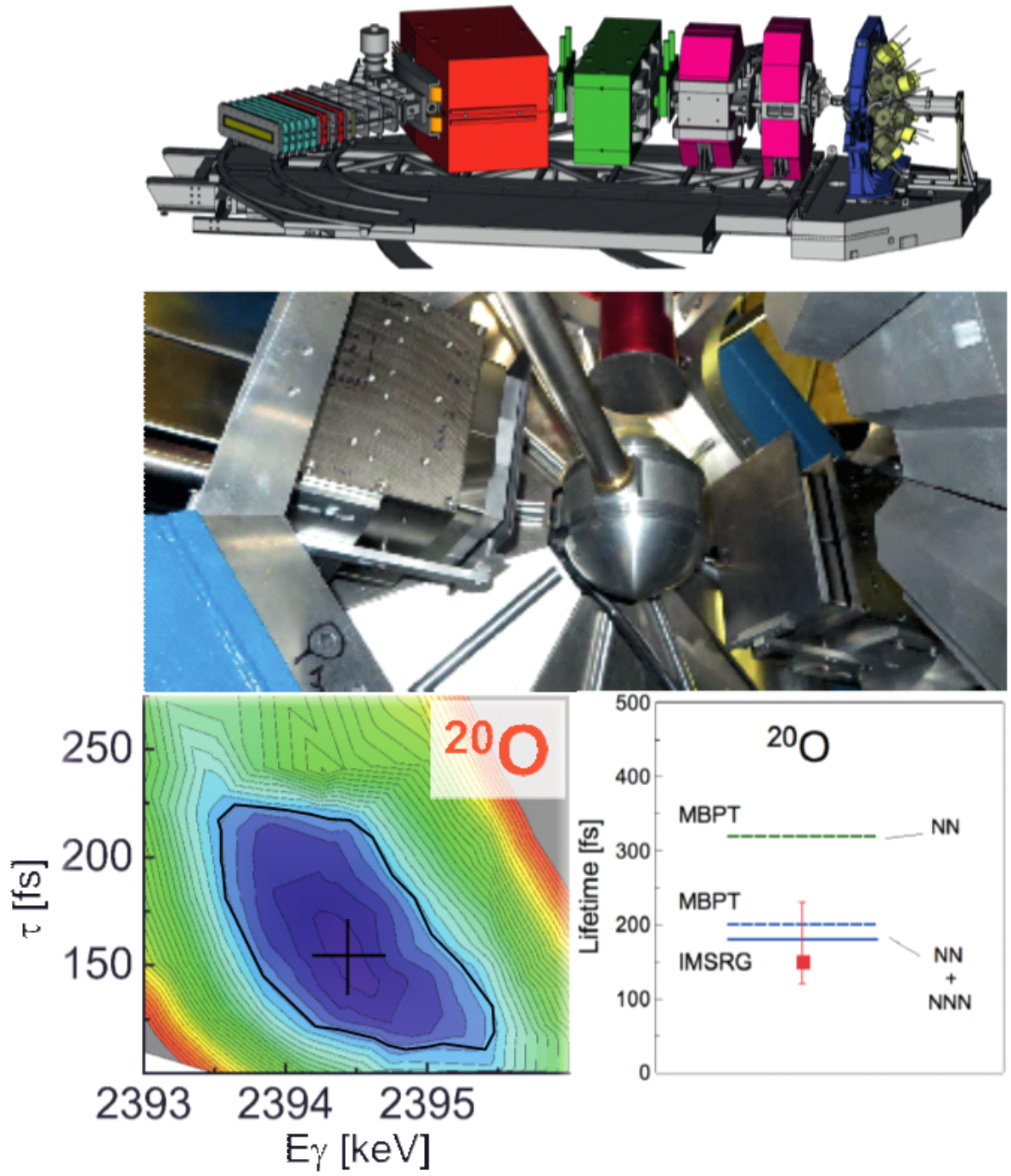

Fig. 2.7. **Up:** the experimental setup − a combination of AGATA and PARIS detectors (photo) installed at the entrance to the VAMOS mass separator (visualisation) at GANIL [EurekAlert!]. **Bottom left:** contour plot showing the quality of the gamma−line shape best fit as a function of the transition energy (E) and the lifetime ( ) of the 2_2 state in ^{20}O. The extracted values of E , and the area of uncertainty are indicated with a cross and a bold line respectively. **Bottom right:** comparison of the measured lifetime with results of *ab initio* shell model calculations; inclusion of 3N interactions is needed to reproduce the experimental value of . [Phys. Rev. C101, 021303(R) (2020)].

structure models. The experiment dedicated to measuring the lifetimes was carried out at the GANIL research center in Caen, France. The state-of-the-art gamma radiation detectors AGATA and PARIS combined with the VAMOS magnetic spectrometer were used in the measurements (Fig. 2.7).

The reaction of the ^{18}O beam with the ^{181}Ta target generated excited atomic nuclei of elements such as B, C, N, O and F as a result of deep-inelastic scattering or nucleon transfer processes. In the investigated moving nuclei, the excited quantum states decayed by the emission of high-energy photons, whose energy was shifted when compared to the energy of transitions in the rest frame. By

analyzing this Doppler-shifted gamma-transition line shapes via a novel Monte Carlo technique, nuclear state lifetimes in the tens to hundreds of femtoseconds were possible to be determined.

The experimental lifetimes agree with predictions of *ab initio* calculations using two- and three-nucleon interactions for ^{20}O and ^{16}C, which confirms the need to include the three-nucleon interactions in the description of electromagnetic transitions in the atomic nucleus. The present measurement shows the power of observables provided by electromagnetic transitions, determined with high-precision gamma spectroscopy, for assessing the quality of first-principles nuclear structure calculations.

Nuclear isomers play a key role in understanding nuclear structure physics. Of special interest are shape isomers: they may arise when the nuclear potential energy surface (PES), in the deformation space, has minima associated with different shapes and when these minima are separated by a high barrier. The transition from such minima toward the ground state minimum can be significantly hindered. So far, shape isomers, discovered in the 1960s, have been known to occur only in the heavy actinide nuclei, although in the 1980s mean-field models predicted their existence also in lighter systems, pointing to ^{66}Ni and ^{68}Ni as the lightest candidates. This concept encouraged studies of **shape isomers and shape coexistence in the nickel isotopes ^{64,66}Ni** [Phys. Rev. Lett., 125 (2020) 102502]. Recently, fully microscopic state-of-the-art shell-model calculations based on Monte Carlo computational schemes and the use of very powerful supercomputing confirmed the presence of a deep, local minimum at sizeable prolate deformation in the PES of ^{66}Ni, but not in ^{68}Ni. They also pointed to the existence of a similar minimum (Fig. 2.8) in the PES of ^{64}Ni, which until now has been considered purely spherical. Two experimental campaigns took place in order to search for shape isomers in the ^{64}Ni and ^{66}Ni nuclei.

The first one, having as the objective ^{66}Ni, was performed at the Tandem Laboratory of IFIN-HH and employed the two-neutron transfer reaction induced by an ^{18}O beam on a ^{64}Ni target, at the sub-Coulomb barrier energy of 39 MeV. All three lowest-excited 0^+ states in ^{66}Ni were populated and their gamma-decay was observed using gamma-coincidence technique. The 0^+ states lifetimes were assessed with the plunger method. A retardation of gamma-decay from the fourth excited 0^+ state, supposingly deformed, to spherical configuration was observed, B(E2)=0.2 W.u., resembling a shape-isomer-like behavior.

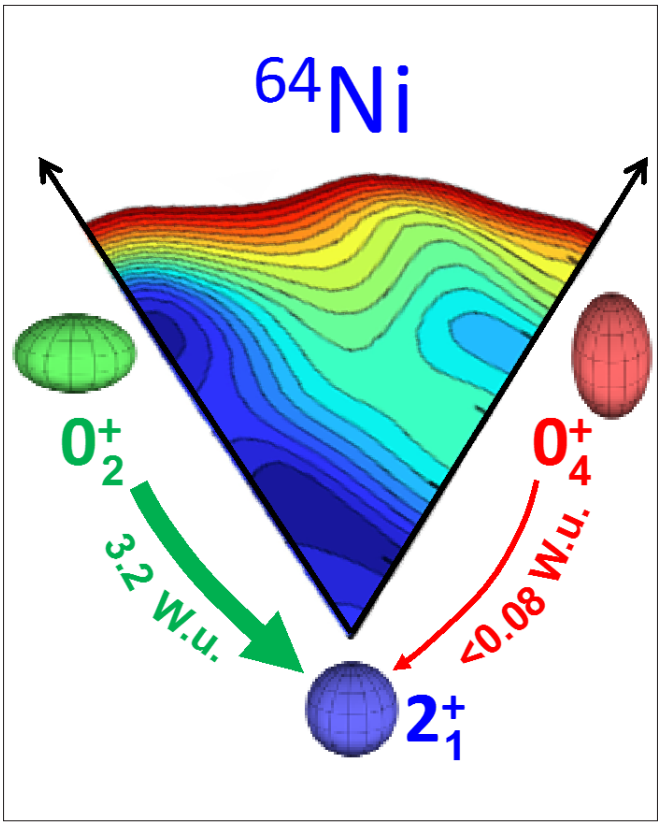

Fig. 2.8. The potential energy surface for the lowest 0^+ states of ^{64}Ni, as a function of prolate and oblate quadrupole moments (EurekAlert!).

The second campaign aimed at investigating the ^{64}Ni nucleus involved four experiments – they were performed at four different laboratories in Europe and the USA: Institut Laue-Langevin (Grenoble, France), IFIN-HH Tandem Laboratory (Romania), Argonne National Laboratory (Chicago, USA) and the Triangle Universities Nuclear Laboratory (TUNL, North Carolina, USA). Several 0^+ and 2^+ excited states were identified below 4.5 MeV in ^{64}Ni and their properties were established. This includes the deformed 0^+ state at 3463 keV, the gamma decay of which is hindered by more than one order of magnitude: B(E2) < 0.08 W.u.

These two campaigns resulted in an experimental identification of the shape-isomer like structures in ^{64}Ni and ^{66}Ni, achieved through high resolution gamma-ray spectroscopy and showing that shape isomerism is possible not only in very heavy nuclei: it remarkably appears in significantly lighter systems, as correctly predicted by theory, which points to the monopole tensor part of nucleus-nucleus interaction as the one governing this phenomenon.

Shape coexistence and the onset of quantum shape-phase transition in the A = 100 mass region were also the subject of investigations devoted to the structure of the ^{96}Y nucleus [Phys. Rev. C, 102 (2020) 054324]. In the isotopes with the proton number around Z = 40, a

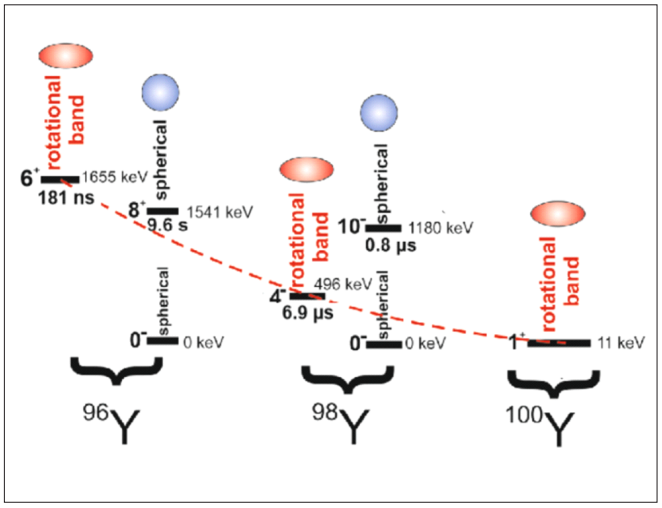

Fig. 2.9. Evolution of deformation across Y isotopic chain.

sudden change of nuclear structure occurs when the number of neutrons reaches N = 60. While the nuclei with N < 60 exhibit a spherical shape, the isotopes with N 60 are significantly deformed. This phenomenon is considered the most dramatic shape change in the nuclear chart. A question was raised whether the deformed structures appear just at N = 60 or if they reside also in the lighter isotopes. Indeed, deformed rotational bands built on excited isomeric states are placed in ^{95}Rb, ^{96}Sr, ^{98}Y, $^{98-99}$Zr, i.e., at N = 58 and 59; however, nothing was known about the location of such collective excitations at N < 58. In the course of the presented work, it was possible to extend significantly the level scheme of $^{96}Y_{57}$ via the gamma-coincidence spectroscopy technique. The data were collected at the Institut Laue-Langevin (ILL) in Grenoble during an experimental campaign where thermal neutrons from the nuclear reactor induced a fission reaction of ^{233}U and ^{235}U active targets. The emitted gamma rays were recorded by a new highly efficient germanium (HPGe) detector array named FIPPS (FIssion Product Prompt gamma-ray Spectrometer). The data analysis enabled the identification of a new (6^+), 181(9) ns isomeric state at 1655 keV excitation energy and a rotational band built on. This result points to the presence of deformed structures competing with spherical ones already at N = 57. With the increasing number of neutrons, these deformed structures gradually decrease in energy (Fig. 2.9), to become dominant at N 60. The presence of the rotational band in the $^{96}Y_{57}$ isotope can be explained by Hartree - Fock - Bogoliubov calculations if an oblate deformation is assumed.

Study of the structure of heavier nuclei resulted in the deduction the **most complex isomeric decay in ^{147}Gd** [Phys. Rev. C, 101 (2020) 064320]. In an extensive search for yrast traps performed in the early 1980s the high-spin isomer was identified in ^{147}Gd. In subsequent detailed studies the 0.5 s half-life and 8588 keV excitation energy were determined, the $49/2^+$ spin- parity was assigned and the isomer structure was understood. In spite of the complexity of the isomeric decay established in this study, only 40% of the decay intensity could be identified in its upper part. This indicated an unusual fragmentation of the decay and led to a striking conclusion that it must involve at least 50 decay branches which could not be observed because of their low intensity.

To resolve this puzzling phenomenon, the $49/2^+$ isomer decay in ^{147}Gd was now reinvestigated using much better tools of the modern gamma spectroscopy. The experiment was performed at the Legnaro NL using a ^{76}Ge beam on the ^{76}Ge target and collecting the reaction products in the ^{208}Pb catcher placed in the center of the GASP, an array of 40 detectors. The detection sensitivity down to the level below 10^{-3}/decay allowed one to resolve the bulk part of the complex isomeric decay. It confirmed the earlier anticipated complexity involving 400 transitions identified and clearly placed as populating 90 levels, all of them with

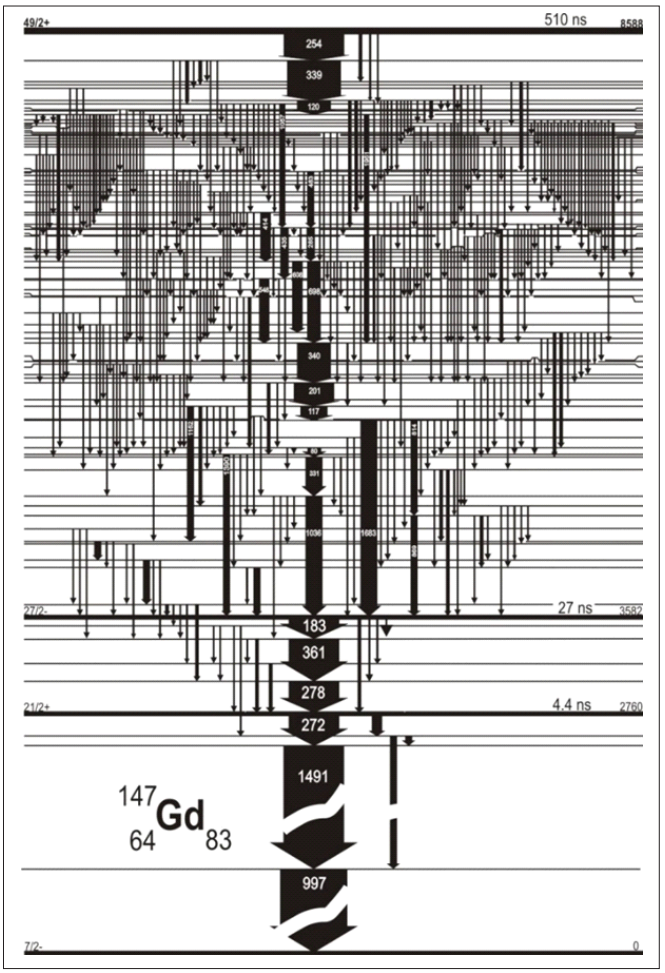

Fig. 2.10. The level scheme of ^{147}Gd – an example of the complex decay pattern of the $49/2^+$ isomeric state. Details of the level scheme available at [Phys. Rev. C, 101 (2020) 064320].

firmly assigned spin-parity. The overall view of this most complex isomeric decay observed in all of the chart of nuclides is displayed in Fig. 2.10. In the lower energy part, the observed state structures are rather well understood, but the structure of the most complex set of levels in the upper part is not at all transparent.

Nevertheless, it is clear that the decay fragmentation is initiated by fast low-energy M1 transitions which populate the group of levels closely spaced in a narrow excitation energy range between 7.8 and 8.0 MeV. This explains the observed complexity, which can be further illustrated by a few numbers characterizing some decay cascades selected from the extremely large number of decay paths between the $49/2^+$ isomer and the $7/2^-$ ground state. The shortest and longest gamma decay involves 10 and 22 transitions respectively, each of them happening with probability close to the 10^{-6}/decay. The decay probability selecting other paths ranges from 10^{-2}/decay for the most intense path down to the 10^{-17}/decay calculated for several cascades with the weakest intensity. Some other statistical features of the studied decay invite more detailed investigations.

Using proton beams provided by CCB at IFJ PAN **resulted in first results on the structure of high-lying single-particle states: M4 stretched resonances in ^{13}C** [Acta Phys. Pol. B Proc. Suppl., 13 (2020) 389]. The stretched excitations are dominated by a single particle-hole component for which the excited particle (proton or neutron) and the residual hole couple to the maximal possible spin value available on their respective shells. Because of the expected low density of other one-particle-one-hole configurations of high angular momenta in the energy region where the stretched states appear, their configurations should be relatively simple. This feature makes them attractive as their theoretical analysis could provide clear information about the role of continuum couplings in stretched excitations. The properties of stretched excitations are poorly known, even though they are of key importance to the physics of unbound systems. In light nuclei, as ^{13}C, they appear as high-lying resonances resulting from the $p_{3/2}$ $d_{5/2}$ M4 magnetic transitions. The direct measurement of stretched states properties, such as decay patterns,

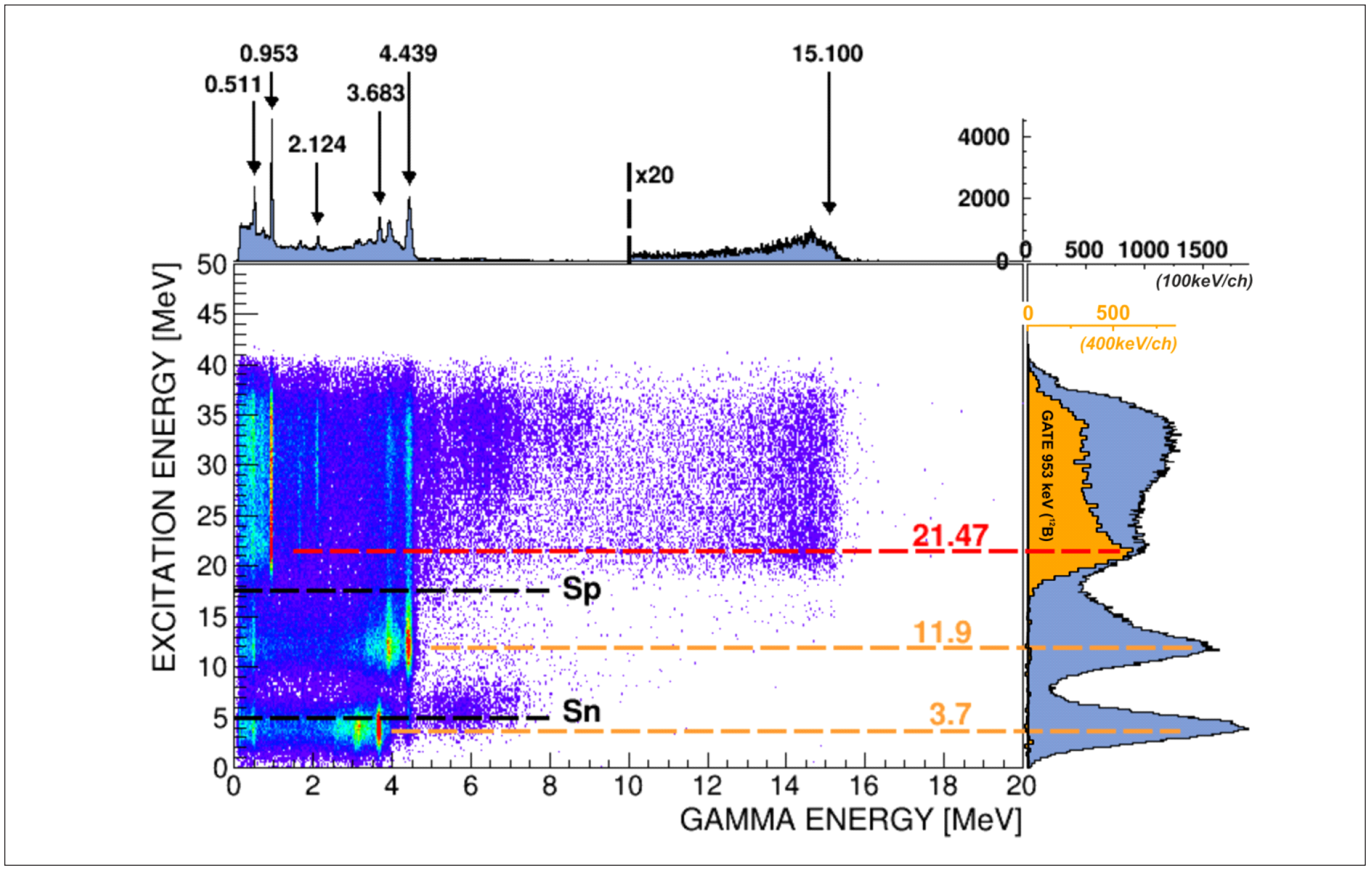

Fig. 2.11. Two−dimensional coincidence matrix showing the energy of the rays detected in the scintillator detectors vs. the excitation energy calculated from the energy of scattered protons (E_{beam}=135 MeV). Particle emission thresholds for neutron and proton in ^{13}C are given, as well as the location of the 21.47−MeV stretched resonance and of excited states in ^{13}C, which are followed by decays. Projections on the x axis (gamma energy) and y axis (excitation energy) are shown as blue spectra on the top and on the right, respectively. The excitation energy spectrum displayed after gating on the 953−keV transition from ^{12}B daughter nucleus (proton decay channel) is presented on the right (marked in orange). Labels in the top spectrum point to the decay from excited states in ^{12,13}C and ^{12}B.

should provide data which can be used as a very demanding test of state-of-the-art theory approaches.

The experiment performed at CCB aimed at the investigation of a stretched single-particle M4 state in ^{13}C, located at 21.47 MeV. The data was obtained by measuring inelastically scattered protons (which excite the resonance) in coincidence with charged particles from the resonance decay, and gamma rays from daughter nuclei. The detection setup consisted of: i) the KRATTA telescope array for detection of scattered protons, ii) two clusters of the PARIS scintillator array and an array of $LaBr_3$ detectors for gamma-ray measurement, and iii) a thick position-sensitive Si detector for light charged particles detection. In particular, the emitted gamma rays give a precise knowledge of the feeding to specific states in daughter nuclei, even in the case of a neutron decay from the resonance state. Thus, first experimental information (Fig. 2.11) on the proton and neutron decay channels of the 21.47-MeV resonance in ^{13}C, to ^{12}B and ^{12}C daughter nuclei, respectively, could be obtained. The experimental results on the decay of the 21.47-MeV stretched state in ^{13}C will be compared with the theoretical calculations based on the Gamow Shell Model approach.

Excitations of ^{208}Pb nuclei, such as pygmy states and giant resonances, were studied at CCB using a proton beam delivered by a medical cyclotron [Acta Phys. Pol. B, 51 (2020) 677]. Giant resonances are many nucleon excitations called "collective" and described as neutrons against protons vibrations. Among them the very important and most known is the giant dipole resonance (GDR). Very interesting is the giant quadrupole resonance (GQR) whose gamma decay has been observed only once so far. Pygmy states, also called pygmy dipole resonances (PDR), are less collective and may be described by a few nucleon excitations. The nature of this excitation is still under investigations. In the performed experiments, excited states were induced in the nuclei as a result of inelastic scattering of protons. The PDR, GDR and GQR were studied by measuring gamma rays emitted in their decay.

For the needs of nuclear physics research at CCB an experimental setup was constructed. It consisted of detectors for gamma ray and scattered protons measurement. At the first stage gamma rays were registered by 8 BaF_2 detectors of the HECTOR array, and protons were detected by the KRATTA triple (Si+CsI+CsI) telescopes, both surrounding a scattering chamber. The improved setup was based on a new big scattering chamber, large enough to mount the KRATTA inside it. In this case 4 large volume $LaBr_3$ scintillators and 2 PARIS clusters, each made of 9 $LaBr_3$+NaI or $CeBr_3$+NaI phoswiches, placed outside the chamber, were used for gamma ray measurement.

The experimental method was based on a simultaneous measurement of gamma rays and scattered protons giving information on excitation energy. An increase in the number of counts in the GQR energy regions of coincidence gamma spectrum was observed (Fig. 2.12, right panel). Another outcome was the observation (Fig. 2.12, left panel) of pygmy states at the energies in agreement with previous results achieved using an alpha particle scattering reaction.

After a three-year analysis of the data taken between 2015 and 2016 at the ultra-cold neutron source in Paul Scherrer Institute, Villigen, with the participation of physicists from our Institute, the **final value of the**

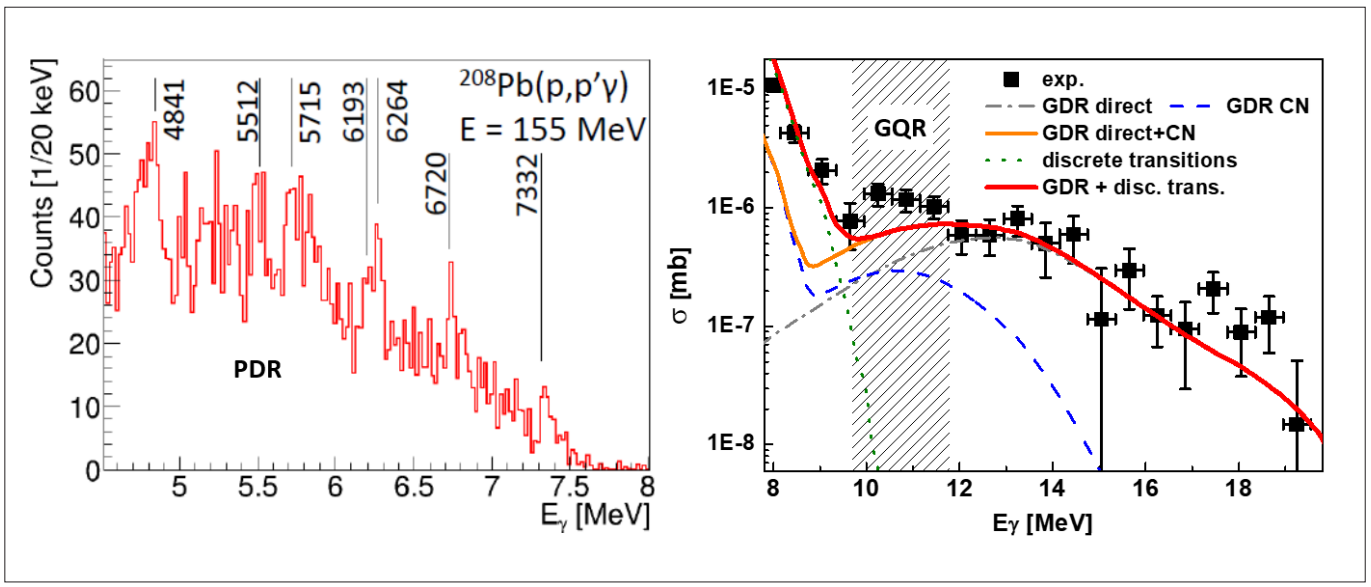

Fig 2.12. The gamma ray spectra showing **Left:** discreet [Acta Phys. Pol. B, 51 (2020) 677] and **Right:** continuous transitions feeding the ground state in ^{208}Pb.

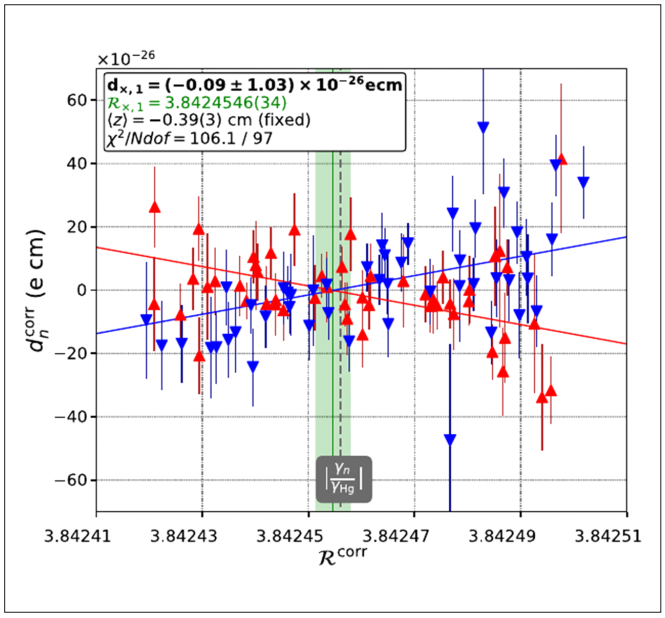

Fig. 2.13. The final results of the crossing-point analysis applied to account for the dominant systematic effect due to the relativistic motional field and the magnetic field gradient induced by the presence of gravitational shift of the center of mass of the UCNs in the chamber. The crossing point of blue and red lines, corresponding to the opposite directions of main magnetic field B0, indicates the neutron EDM (d_n) value. [Phys.Rev.Lett.124, 081803 (2020)].

neutron electric dipole moment (EDM) was obtained and published [Phys.Rev.Lett.124, 081803 (2020)]. The value is consistent with zero and may be interpreted as an upper limit of the neutron EDM 1.8 10^{-26} e cm, the most stringent one obtained in a single measurement of this observable. The experimental principle is based on Ramsey's method of separated oscillating magnetic fields with polarized ultra-cold neutrons from a solid deuterium source. The applied strategy involved a separate analysis of double blinded data performed by two independent groups. The experience gained as a result of this analysis is currently implemented in the construction of the next version of the measurement with completely new apparatus, significantly reduced systematic uncertainties and prospects for much higher statistics. Fig. 2.13 presents the results of a crossing-point analysis applied to account for the dominant systematic effect due to the relativistic motional field and the magnetic field gradient (see [Phys.Rev.Lett.124, 081803 (2020)] for the exact definition of indicated variables).

Physicists from our Division participated in **studies of dielectron radiation from baryon resonances in vacuum and dense nuclear matter with the High Acceptance Di-Electron Spectrometer** (HADES), installed at SIS18 in GSI, Darmstadt. It provided excellent detection for hadrons and rare dielectron production with powerful particle ($p/K/\ /e$) identification. It was designed to measure dielectron (e^+e^-) radiation from dense and hot baryonic matter. The microscopic description of the e^+e^- emissivity requires understanding of baryon-virtual photon couplings which can be studied in NN and ^-N reactions.

The elementary collisions, especially those with pion beams, offer a great opportunity to study the electromagnetic structure of baryonic resonances via baryon resonance Dalitz decays (time-like region) and their coupling to the light vector mesons and , which play an essential role in baryon N^* transitions. The studies of the vector meson–baryon interaction are motivated by the so-called vector-meson dominance model, predicting the low-mass vector mesons (, ,) as mediating fields in the hadron-photon interactions.

To understand resonance production mechanisms, a large dataset of -p scattering was obtained at four pion beam momenta 0.656, 0.69, 0.748 and 0.8 GeV/c [PRC 102, 024001, (2020)]. A precise normalization of these measurements was provided by the well known -p elastic scattering differential cross section. Two pion final states, ^-p $n^+\ ^-$ and ^-p $p\ ^0\ ^-$, were selected and included in a dedicated multichannel Partial Wave Analysis (PWA). In this way different contributions to the total amplitude, such as , N, N, were extracted together with their couplings to the main contributing baryon resonances, e.g. $N(1520)$, $N(1535)$, $N(1440)$ (Fig. 2.14). The $N(1520)$ resonance was found to dominate the N final state with the branching ratio BR = 12.2% ±1.9%. This value was used as

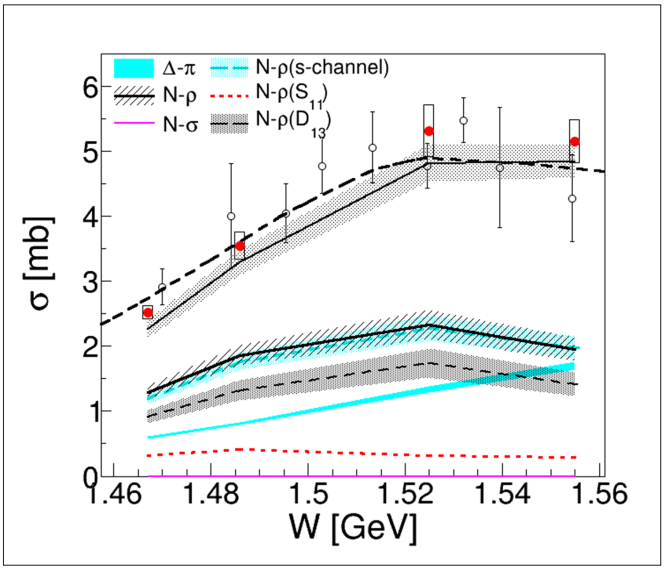

Fig. 2.14. Total production cross sections for the two-pion production in the ^-p $p\ ^0\ ^-$ reaction. The results from this work (red points) and from former experiments (black circles) are shown as a function of the total energy (W = s) in the c.m. frame. The black curves are the results from the Bonn–Gatchina PWA solution (solid) and from previous analyses (dashed). The other curves display the contribution to final states isobars listed in the legend. The bands reflect the systematic error of the PWA method. (adapted from [PRC 102, 024001, (2020)].

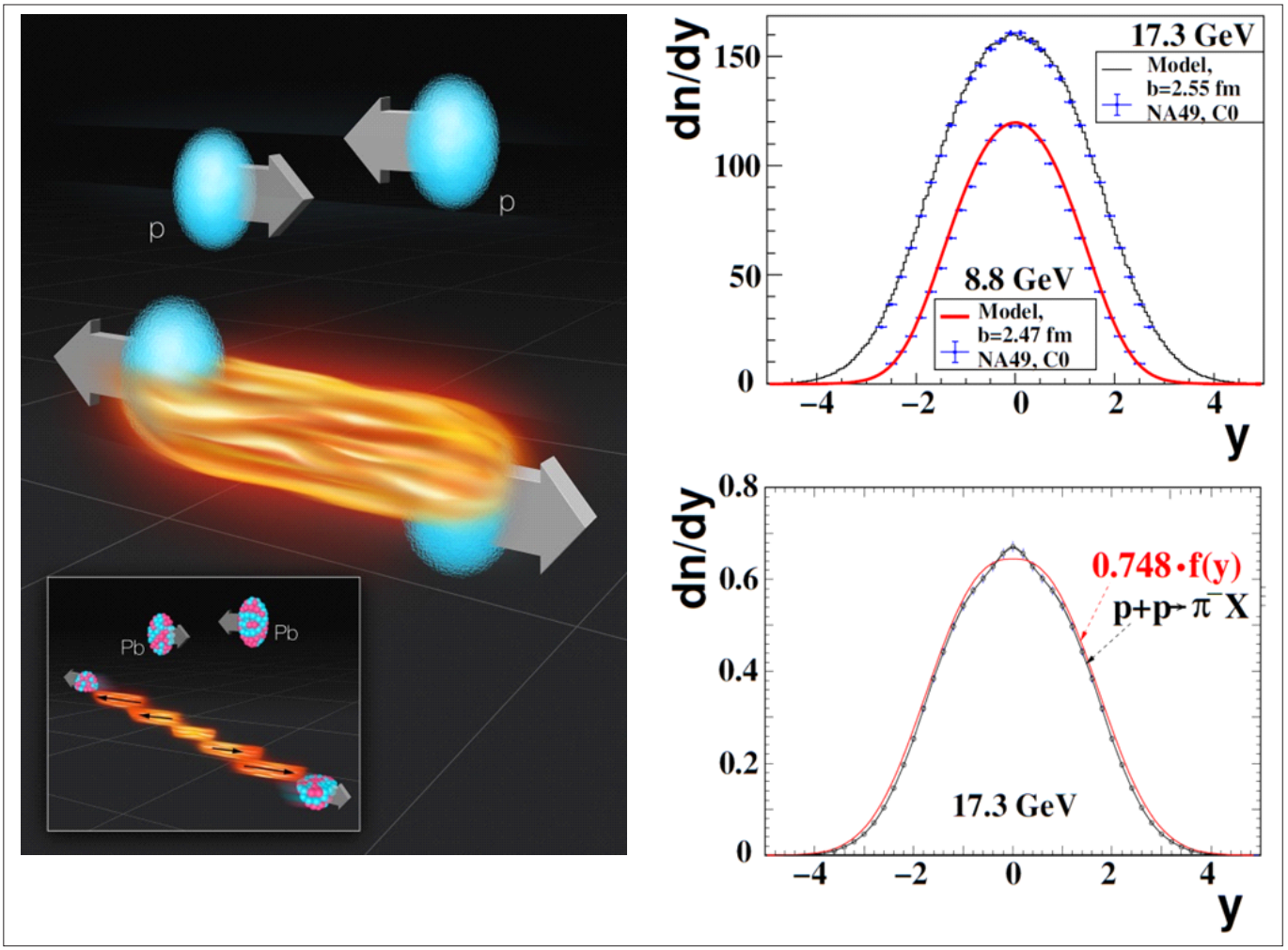

Fig. 2.15. Visualization of the model proposed by IFJ PAN physicists (left, picture by Dual Color) and its comparison to experimental data on p+p and Pb+Pb collisions, from Acta Phys. Polon. B 51 (2020) 1525 (right). See also [EurekAlert! 2017 and 2019].

an input for the description of the di-electron channels studied in this experiment.

Collisions of protons and nuclei at the energies in the range 9-17 GeV in the nucleon-nucleon center of mass system have been studied extensively – **a few main findings** are summarized below. In 2017, physicists from IFJ PAN presented a new model of the phenomena occurring during collisions of lead nuclei at high energies (Phys. Rev. C 95, 2017, 024908). This model assumed that the matter arising in the collisions, the quark-gluon plasma, moves away from the impact point in the form of numerous *streaks* stretching along the original direction of motion of the nuclei (Fig. 2.15, bottom left). The model described very well the entire impact parameter dependence of rapidity (relativistic velocity) distributions of mesons produced in lead-lead (Pb+Pb) collisions in the considered energy range (Fig. 2.15, top right). Then the researchers applied the same model to much simpler proton-proton collisions (Fig. 2.15, top left). After evaluating in detail the difference in the energy balance caused by the different amount of production of strange particles in p+p and Pb+Pb collisions, and by baryon stopping phenomena (discussed further below), all these differences appeared only to change the overall normalization by a simple factor of 0.748. The pion rapidity distribution from a single "*fire streak*"[1] was then compared to experimental data from the NA49 experiment (constructed and carried out at the CERN SPS accelerator with the participation of IFJ PAN). The compliance was strikingly good (Fig. 2.15, bottom right). The matter arising from proton-proton (p+p) collisions, cooler and qualitatively different than the quark-gluon plasma, seems therefore to behave like a *single fire streak* [Phys. Rev. C 99, 2019, 024908]. Since the quark-gluon plasma is formed at higher energies and in collisions of objects of greater complexity, it is legitimate to say

1) The term "fire streak" is used here in order to point out the partial similarity of this approach to several earlier works (e.g. Nucl. Phys. A296, 177 (1978), Phys. Rev. C18, 844 (1978)).

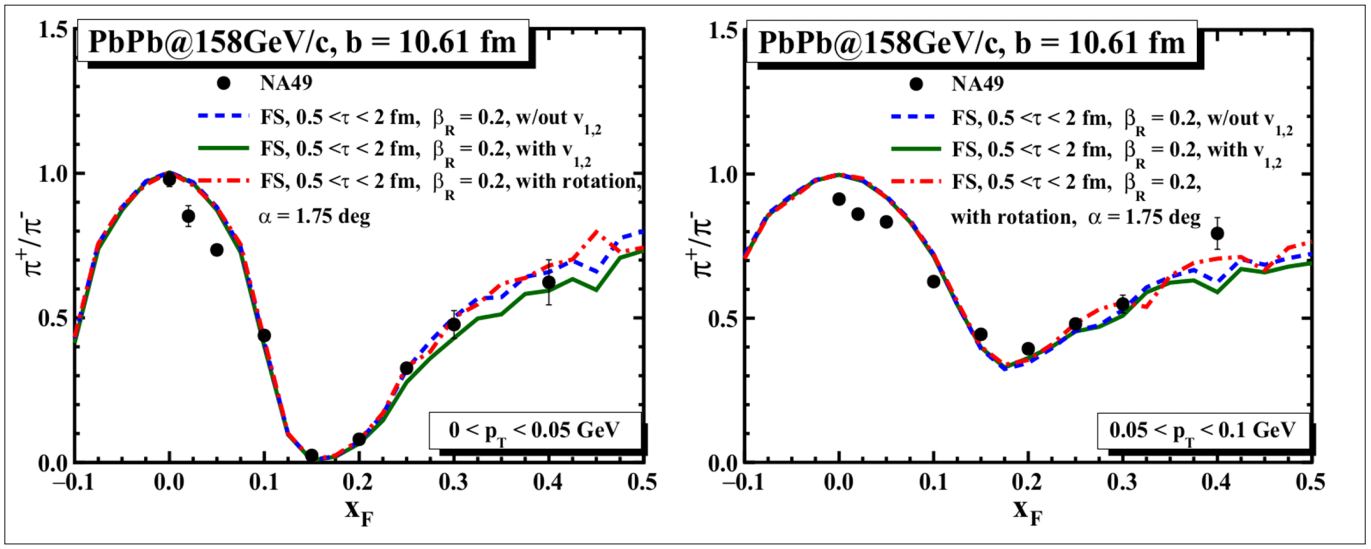

Fig. 2.16. First quantitative description of the electromagnetic distortion of $^{+}/^{-}$ ratios in Pb+Pb collisions at 158 GeV/nucleon beam energy ($x_F=2p_L/\sqrt{s_{NN}}$ is the scaled longitudinal momentum of the meson). [From Phys.Rev. C 102, 2020, 014901].

that it inherits some of the features of the matter that forms fire streaks in proton-proton collisions.

The success of the above model, apparently providing a good overall description for the longitudinal evolution of the system created in the collision, served as a basis for the **first ever quantitative description of the electromagnetic distortion of fast $^{+}$ and $^{-}$ meson spectra in peripheral collisions of lead nuclei** [Phys.Rev. C 102, 2020, 014901]. The electric charge of the nuclear remnants not participating in the collision (spectator systems) modifies the trajectories of electrically charged mesons and therefore distorts the charge ratios $^{+}/^{-}$ in the final state of the reaction. This distortion appeared to be a complex process, and the corresponding theoretical calculation included a number of different phenomena. These were (1) the influence of collision geometry, (2) the longitudinal evolution of the system, (3) transverse momentum (p_T) spectra of mesons, (4) the "lifetime" or pion creation time from the longitudinal elements of excited matter, (5) isospin effects, (6) directed and elliptic flow, (7) the transverse expansion of the system, (8) vorticity effects, (9) the fragmentation of spectator systems, and (10) relativistic effects on the electromagnetic field. The result is presented in Fig. 2.16. Interestingly, the quantitatively described experimental data indicate that the proper lifetime of forward moving streaks of excited matter (see above) is only of 0.5-2 fm/c, i.e. significantly shorter than for the central slower streaks which contribute to the bulk of particle production (see cited above Ref. for a detailed discussion).

The experimental database on the above electromagnetic distortions of charged mesons has been multiplied over the last three years. New experimental data on argon-scandium (Ar+Sc) collisions were collected by the NA61/SHINE detector at CERN and analyzed as a function of beam energy and collision impact parameter (centrality). Consequently, **first ever experimental results on electromagnetic effects in small systems at the CERN SPS** were obtained at 150A GeV/c beam momentum, followed by the corresponding first ever experimental results on these effects in peripheral small systems at 40A GeV/c. A set of examples is presented in Fig. 2.17, where the red arrow gives the x_F value for the meson at low-p_T moving at spectator (beam) velocity. The basic kinematical characteristics of the large electromagnetic distortion of $^{+}/^{-}$ ratios present in Pb+Pb collisions reappear, even if somewhat reduced, in the far smaller Ar+Sc systems. At least down to intermediate centrality collisions, these effects remain strong enough to break isospin symmetry, which unambiguously confirms their electromagnetic origin.

The importance of **baryon stopping** as a dynamical phenomenon significantly contributing to the differences between proton-proton and nuclear collisions addressed above had become evident in the course of the presented works. Here **a new phenomenological study** was performed in 2020 in the framework of the Dual Parton Model [Acta Phys. Polon. B51, 2020, 1207]. It was based on high quality data sets from the NA49 experiment on proton-proton and proton-carbon collisions [Eur. Phys. J. C65, 2010, 9, Eur. Phys. J. C73, 2013, 2364]. Unlike the earlier existing data, these combined the measurement of both protons and neutrons in the nearly complete projectile hemisphere in the collision c.m.s. with full coverage starting at $p_T=0$ (*sharp*).

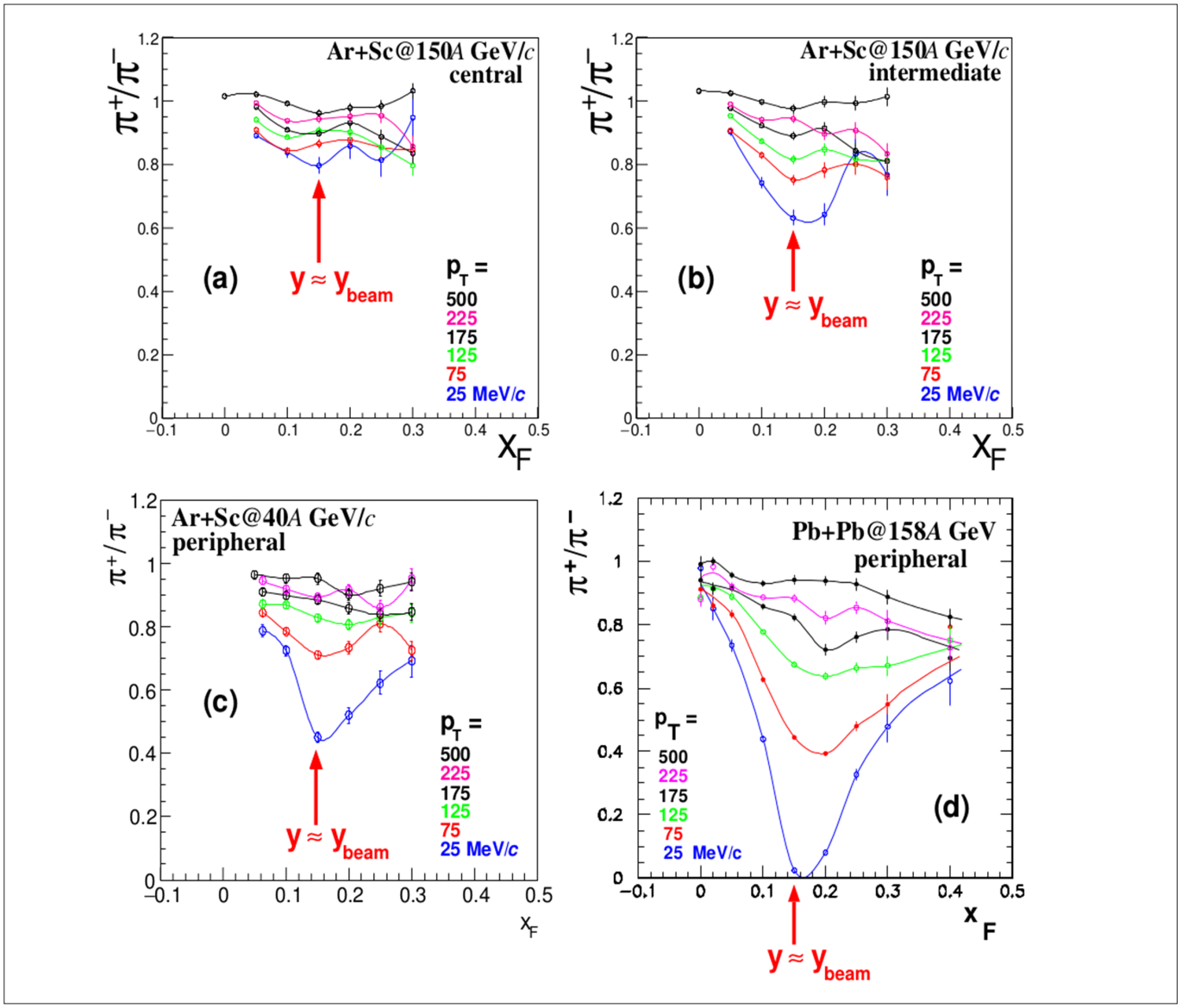

Fig. 2.17. Selected experimental results on electromagnetic effects in Ar+Sc and Pb+Pb collisions, from CERN-SPSC-2020-023, Acta Phys. Polon. B 50 (2019), 1127, and PoS(EPS-HEP 2009) 031.

This allowed IFJ PAN researchers to perform their analysis on full non-strange baryon spectra rather than using protons as an (insecure) proxy for the latter, and to isolate the latter distribution in "multiple" proton-carbon collisions in which the proton collides with more than one nucleon, as shown in Fig. 2.18. The analysis proved that baryon stopping mechanisms preserving the diquark in the proton (solid curve in the figure) cannot be held as the only responsible for the measured baryon stopping effect. An upper limit of about 60% was established for the latter contribution, leading to the conclusion that in multiple proton-nucleon collisions the diquark must be frequently disintegrated, at a level of 40% at least for the case of proton-carbon reactions.

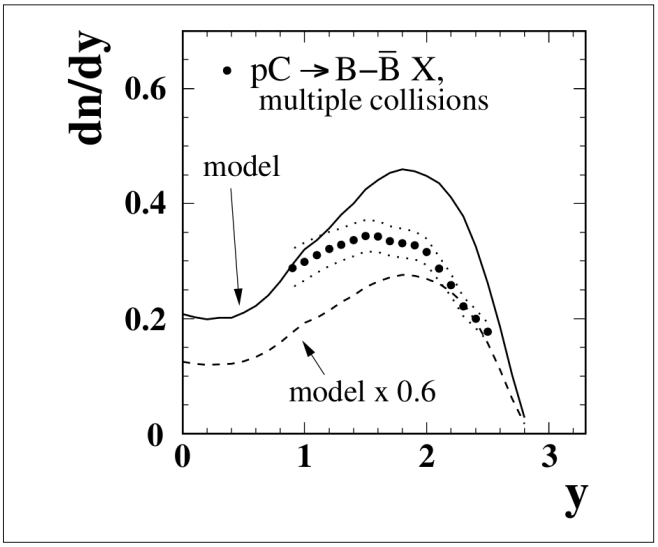

Fig. 2.18. Comparison of non−strange baryon rapidity distribution to the model analysis described in the text. [From Acta Phys. Polon. B51, 2020, 1207].

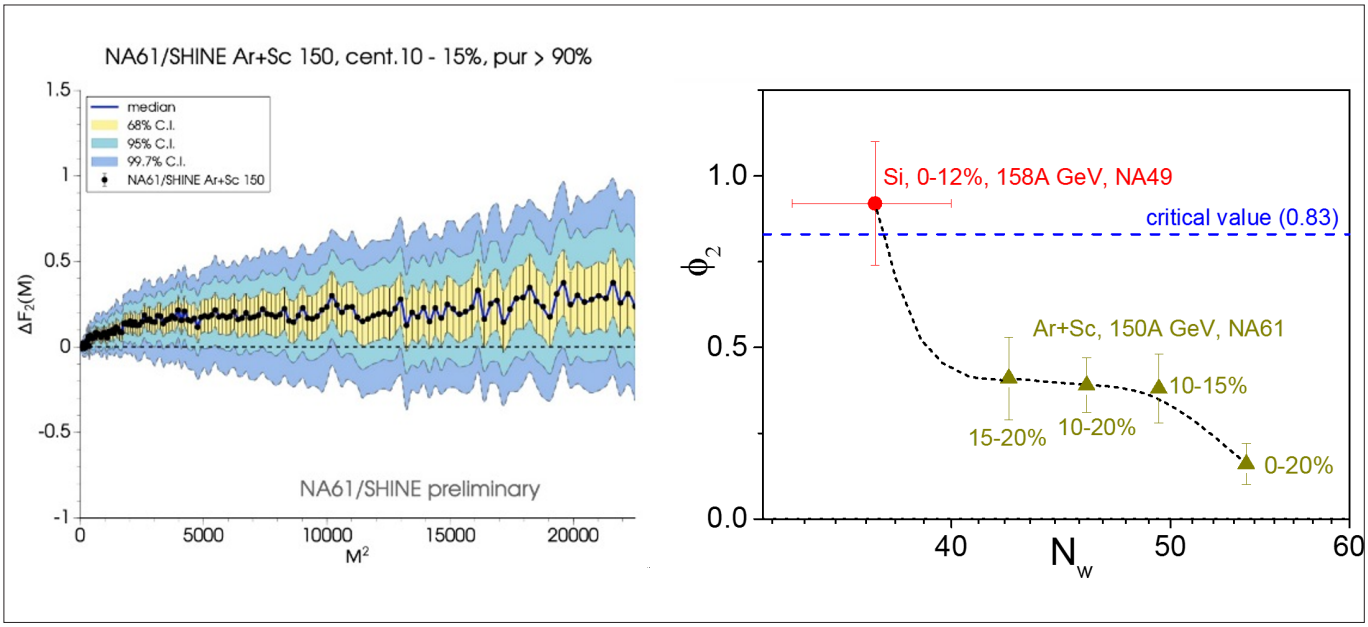

Fig 2.19. Factorial moments F_2 in Ar+Sc collisions [Nucl. Phys. A 1005, 2021, 121753] and extracted values of $_2$ for Ar+Sc and Si+Si reactions. [Reprinted from Nuclear Physics A 1003, N.G. Antoniou et al., "Decoding the QCD critical behaviour in A + A collisions", 122018, Copyright 2020, with permission from Elsevier. https://www.sciencedirect.com/journal/nuclear-physics-a].

Complementary to the above studies, new results on **proton intermittency** in Ar+Sc collisions became available from the NA61/SHINE experiment [Nucl. Phys. A 1005, 2021, 121753]. Intermittent behavior of emitted proton moments, that is power-law scaling behavior as a function of the number M^2 of subdivisions in a given area of transverse phase space (p_x, p_y), has been postulated as a signature for the created system to be located in the *Critical Point* (CP) of the phase diagram of strongly interacting matter – the point in which the phase transition between quark-gluon plasma and hadronic gas changes from first-order to "cross-over". Following this postulate, the power-law exponent $_2$ should approach the "critical value" of 5/6=0.83 for the system approaching the CP. The new measurements of 2nd order factorial moments $F_2(M)$ of proton multiplicity (see the cited Ref. for a precise definition) are shown in Fig. 2.19 (*left*). They display only a small, inconclusive deviation from zero. On the other hand, further analysis of these data was performed in the framework of A Model-Independent Analysis Scheme (AMIAS) in order to extract unbiased values for $_2$ [Nucl. Phys. A 1003, 2020, 122018]. The result of this analysis is presented in Fig. 2.19 (*right*), where the obtained values of $_2$ are plotted as a function of the number N_w of nucleons participating in the collision. For Ar+Sc collisions these remain below the critical value, but seem to display a growth with decreasing N_w, matching the critical value for collisions of silicon nuclei (Si+Si) obtained by the NA49 experiment [Eur. Phys. J. C 75, 2015, 587]. The exact interpretation of this result in the context of a possible approach of the system to criticality is still a matter for future studies.

The properties of hot and dense deconfined QCD matter, the Quark-Gluon Plasma (QGP), which is formed in high-energy heavy-ion collisions, can be characterized by the **measurement of high transverse momentum (p_T) particles** produced by hadronization of hard scattered partons in the early stage of the collision. It is expected that these partons lose energy by interactions with the QGP, which leads to the jet quenching. The ALICE Collaboration measured pT spectra of primary charged particles from pp, p-Pb and Pb-Pb collisions at a center-of-mass energy s_{NN} = 5.02 TeV in the kinematic range of 0.15 < pT < 50 GeV/c and | |<0.8, with an unprecedented precision [JHEP11 (2018) 013]. Spectra from Pb-Pb collisions are presented in nine centrality intervals and are compared to a reference spectrum from pp in terms of the nuclear modification factor (R_{PbPb}), defined as the ratio of the yield in Pb-Pb to the corresponding yield in pp collisions scaled by the number of binary nucleon-nucleon collisions. In 0-5% central collisions (Fig. 2.20), the p_T spectra are suppressed by more than a factor of 8 around 6-7 GeV/c with a significant reduction in suppression towards higher momenta up to 30 GeV/c. The suppression decreases with decreasing centrality and in the 70-80% central collisions reaches 30% at intermediate momenta and approaches unity for the highest p_T bin. The nuclear modification factor R_{pPb}, constructed from the pp and p-Pb spectra measured at the same collision energy, is consistent with

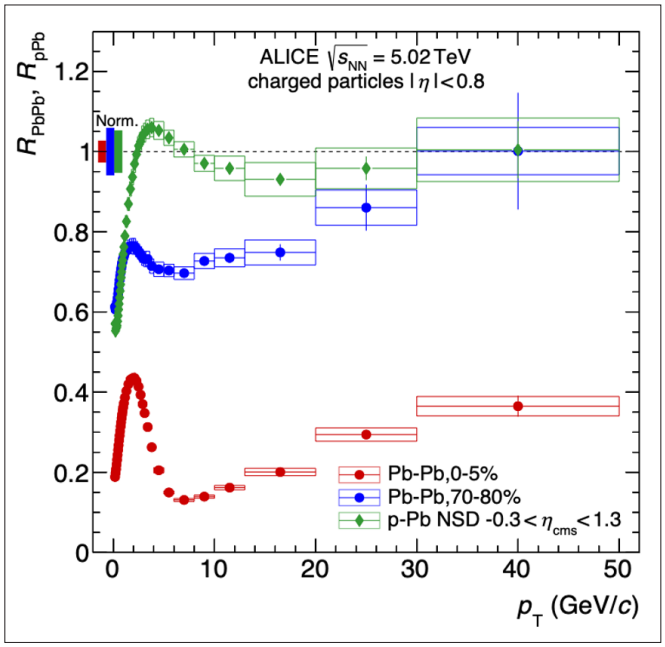

Fig. 2.20. Nuclear modification factors for charged particles in central (0–5%) and peripheral (70–80%) Pb–Pb and in p–Pb. [JHEP11 (2018) 013].

unity above 8 GeV/c. It indicates that the strong suppression observed in central Pb-Pb collisions is not due to initial state effects but rather due to final state partonic energy loss in the hot and dense QGP created in heavy-ion collisions. These results should provide further constraints on the parton energy loss calculations to determine the transport properties of the hot and dense QCD matter.

Analysis of event-by-event multiplicity correlations and fluctuations provides insight into the initial stages of ultra-relativistic heavy-ion collisions. Theoretical and experimental studies have shown that the analysis of correlations and fluctuations significantly benefits from using observables independent of system volume (geometrical) fluctuations. Recently, two families of such observables *called strongly intensive quantities* were introduced into heavy-ion physics. To one of those families belongs observable, defined as a combination of variances and correlation term of the extensive quantities (e.g., mean number of particles) distributions. Strongly intensive quantities are constructed in such a way that, under the assumption that particles are produced independently from a set of sources, they can provide direct information about these sources' properties. Fig. 2.21 shows first-ever results on the

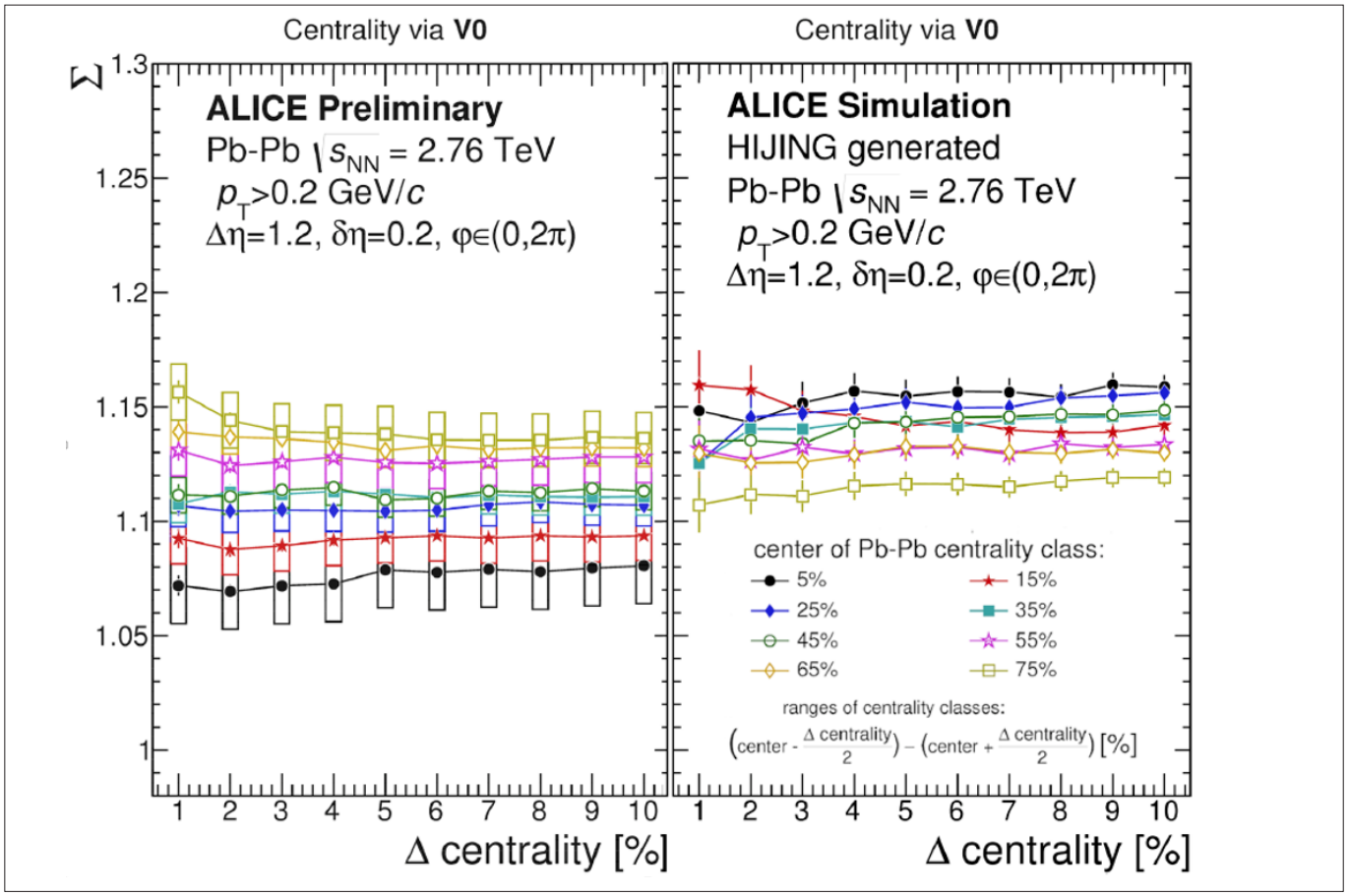

Fig. 2.21. Strongly intensive quantity as a function of the centrality bin width. The width of centrality class changes from 1% to 10% (large volume fluctuations). Results were obtained for charged particles multiplicity for the fixed value of pseudorapidity gap = 1.2 between forward and backward intervals. [MDPI-Proc. 219, EPS-HEP2019]

forward-backward multiplicity obtained for Pb–Pb collisions at s_{NN} = 2.76 TeV as a function of volume fluctuations (centrality bin width). The results revealed that the observable is indeed independent of variations in the initial state geometry. It is true for both experimental data and simulations with the HIJING model. The presented results also indicate that HIJING is not able to reproduce the observed dependence on the centrality of Pb–Pb collisions. Considering that provides direct information about the single source characteristics, the particle production mechanism implemented in the model differs from the scenario taking place in real physical events. This finding shows the scientific potential of strongly intensive quantities, which can be used to verify particle production models already at the level of initial sources.

Inclusive hadron measurements are essential to constrain theoretical models of particle production in both perturbative and non-perturbative regimes. Measurements of proton-nucleus collisions have unique sensitivity to the initial-state nuclear wave function and can elucidate the effects of cold nuclear matter in a wide range of observables of the QGP. **The neutral pion and meson invariant differential yields were precisely measured in non-single diffractive p-Pb collisions at s_{NN} = 5.02 TeV with the ALICE experiment** [Eur. Phys. J. C78 (2018) 624] in a broad transverse momentum range of 0.3 < p_T < 20 GeV/c and 0.7 < p_T < 20 GeV/c, respectively. A comparison of the measured high precision ^{0} and meson spectra with theoretical models in Fig. 2.22 clearly shows that different underlying pictures can describe the data qualitatively. However, systematic uncertainties of the theoretical models are not provided, or are sizable. Hydrodynamic models (EPOS3, VISHNU) agree with the data at low p_T, while jet production appears to be needed for a good description at p_T > 4 GeV/c. While the high p_T part of the spectra can be described by next-to-leading order (NLO) perturbative QCD calculations using different nuclear parton distribution functions, the precise data presented here will help to reduce model uncertainties significantly, for instance providing additional constraints on identified-particle fragmentation functions. Improved theoretical uncertainties are needed in order to discriminate among the models.

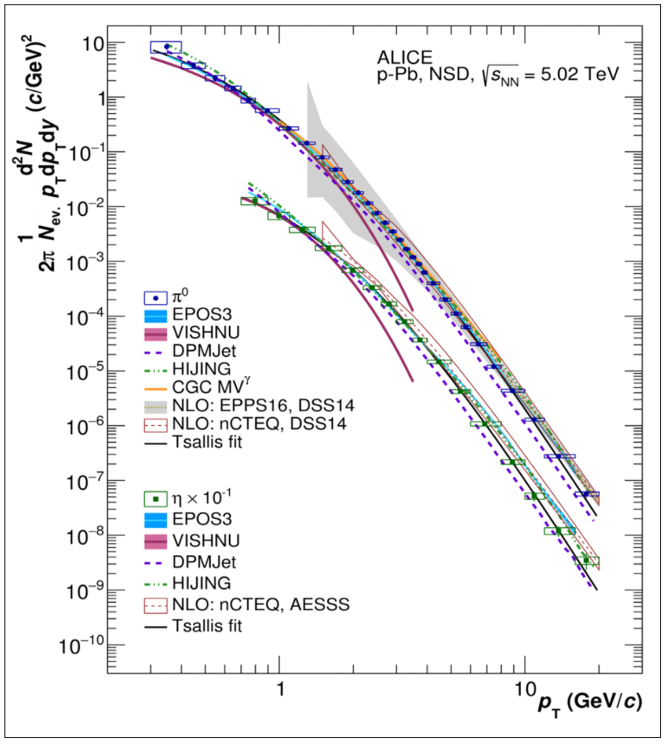

Fig. 2.22. Comparison of several theoretical calculations to the ^{0} and spectra in NSD p–Pb collisions at s_{NN} = 5.02 TeV. [Eur. Phys. J. C78 (2018) 624].

Recently, the ALICE Collaboration presented **the first measurement of the dependence on |t|, the square of the momentum transferred between the incoming and outgoing target nucleus, of coherent J/ photoproduction** [arXiv]. The data were measured with the ALICE detector in ultra-peripheral Pb–Pb collisions at a centre-of-mass energy per nucleon pair s_{NN} = 5.02 TeV with the J/ produced in the central rapidity region |y| < 0.8, which corresponds to the small Bjorken-x

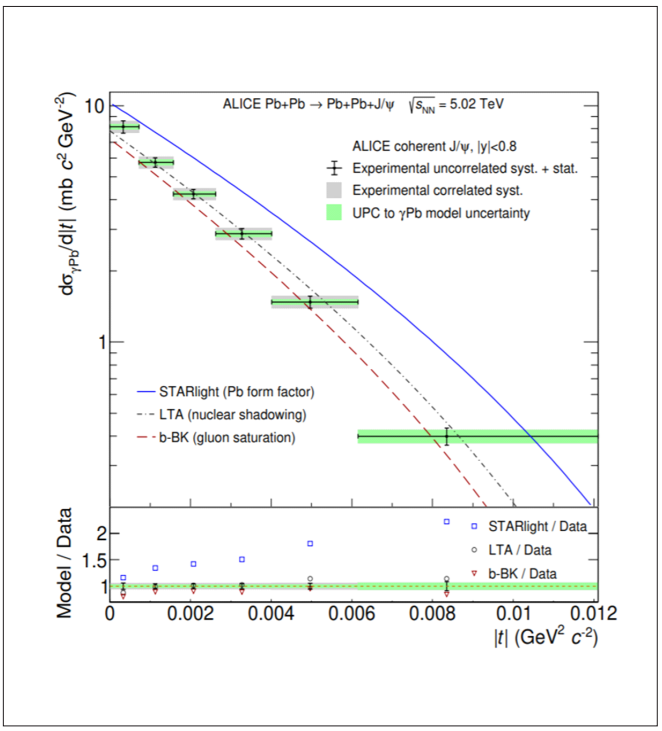

Fig. 2.23. Dependence on |t| of the photonuclear cross section for the coherent photoproduction of J/ off Pb compared with model predictions (**top panel**). Model to data ratio for each prediction in each measured point (**bottom panel**). [arXiv]

range (0.3–1.4)×10^{-3}. The measured |t|-dependence (see Fig. 2.23) is not described by computations based only on the Pb nuclear form factor, while the photonuclear cross section is reproduced better by models including shadowing according to the leading-twist approximation, or gluon-saturation effects from the impact-parameter dependent Balitsky-Kovchegov equation. These results highlight the importance of observables sensitive to the transverse gluonic structure of particles for extending the understanding of the high-energy limit of QCD.

❖

3. Division of Condensed Matter Physics

Overview

The physics of solids has shaped modern civilization. Suffice it to mention electronics, computer science, communication, energy and information storage, medicine, pharmacy, art, culture, entertainment… The wealth of phenomena encountered, on the one hand, and of applications on the other, earns it a unique position by combining pure curiosity-driven research with meeting practical needs. The growing interest in novel materials brings the researchers far beyond classically meant crystal state to more and more exotic and useful systems such as glasses, partly ordered materials, i.e. orientationally disordered and/or liquid crystals, known under the common name of soft matter. Low-dimensional objects, e.g. surfaces, interfaces, thin layers and nanoparticles are structurally fascinating but also useful in many areas of life. All the said systems belong to what is called the **condensed phase of matter**.

The works conducted at the **Division of Condensed Matter Physics** of the H. Niewodniczański Institute of Nuclear Physics Polish Academy of Sciences cover quite a number of the most topical research subjects reflected in the following formal structure of **departments**.

- Department of Structure Research of Condensed Matter (NZ31)
- Department for Functional Nanomaterials (NZ32)
- Department of Materials Research by Computers (NZ33)
- Department of Magnetic Materials and Nanostructures (NZ34)
- Department of Soft Matter Research (NZ35)
- Department of Molecular Engineering and Nanoelectronics (NZ36)
- Department of Molecular Magnetism (NZ37)

The structure has been evolving over time as new issues and methods have been appearing, e.g. the departments NZ32, NZ36 and NZ37 were established in 2019 only. The departments cooperate with each other and often share their equipment.

National and international collaborations are of vital importance because they provide inspiring contacts with producers of the most advanced samples as well as access to large scale instruments. To mention is the consortium of Polish scientific and research institutions "Neutrons for Polish Science" (Neutrony dla Polskiej Nauki, NDPN)[1]. The Joint Research Group "X-ray Irradiated Materials: Theory and Computation" of Deutsches Elektronen Synchrotron (DESY, Hamburg, Germany) and IFJ PAN is oriented towards studies relevant for materials science, diffractive imaging, plasma, and warm dense matter physics investigated with XFEL and synchrotron light sources (https://xm.cfel.de/). Numerous joint projects with Swiss Universities and Federal Research Institutes, dedicated mainly to energy-storage materials, are in progress. A long-lasting cooperation with the Universities of Tsukuba and Osaka (Japan) on calorimetric and complementary methods is now being extended to an agreement pertaining to cross appointment between IFJ PAN and Osaka University. Molecular magnetism is a subject of a cooperation with the Slovak Academy of Sciences whereas glass-formers and pharmaceutical materials are investigated in collaboration with the Italian National Center for Research. A COST Action CM1402 "From molecules to crystals" and a bilateral agreement with the Coimbra University (Portugal) turned out to be rather productive. The research concerning magnetism in systems with reduced dimensions are carried out in a close and long-term cooperation with Augsburg University and, recently in the frame of COST Action CA19140 "Focused Ion Technology for Nanomaterials (FIT4NANO)". Last but not least, our Division continues cooperation with the Joint Institute of Nuclear Research (JINR, Dubna, Russia) in the field of neutron

1) https://www.ill.eu/neutrons-for-society/stakeholder-relations/scientific-member-countries/poland.

scattering and positron annihilation spectroscopy. The number of Polish and foreign centers cooperating with our Division in a more and more fruitful way is systematically growing.

Biennial **international conferences** Multiscale Phenomena in Molecular Matter (MULTIS, 2017 and 2019) and Zakopane Schools of Physics Breaking Frontiers: Submicron Structures in Physics and Biology (2017, 2019) gather researchers from all over the world. In 2017 the 36th International Symposium on Dynamical Properties of Solids (DyProSo) was organized by the Division. Conferences and workshops on *ab initio* methods as applied to the dynamics of crystalline solids are organized yearly.

Below we present **selected achievements** of the Division in the years 2017 -2020. The first group of reports are on the soft matter studies. The recent works concern the effects of molecular structure onto the crystallization vs. vitrification of liquid crystalline materials both in bulk and in confined geometries. Particular attention has been paid to the kinetics of cold crystallization of a family of compounds exhibiting the chiral smectic C phase. The molecular disorder and motions are studied with diffraction, calorimetric and spectroscopic methods including neutron scattering (INS, SANS) in various materials such as medical-relevant substances, whose glassy state is essential for their bioavailability as drugs. A general formula unifying relaxation processes in a wide range of frequencies for rather different kinds of disordered dielectric media has been devised.

The impact of defects on the magnetic order has been observed experimentally and modelled numerically in a nanostructured multi-layered system. First order reversal curve has revealed the mechanism of the reversal of magnetization in a system of antiferromagnet sandwiched by ferromagnets. The roughness of interface has been found to affect the giant magnetoresistance with the use of conversion electron Mössbauer spectroscopy.

A number of molecular magnets, mainly CN-bridged, have been studied both experimentally and theoretically to elucidate the mechanisms of the magnetocaloric effect, percolation in a solid solution, and the effect of light onto the magnetic order.

In the area of nanoparticles a new, surprisingly efficient fabrication method of nano-corundum has been devised and applied. An interesting behavior of an array of single-molecule magnets on a curved surface of silica has been found. The use of the first in Poland holotomographic microscope Nanolive 3D CX-A has made possible long-term observations of living cancerous and healthy cells. New noble metal particles have been synthesized for cancer therapy and catalytic applications.

From among the results obtained with large scale instruments we mention the X-ray laser generated femtosecond pulses as a tool for studying the propagation of radiation damage in biologically relevant molecules and neutron scattering as a probe to determine distance between hydrogen atoms in metals. Positron annihilation spectroscopy, which is extremely sensitive to open volume defects in the crystal structure, has been used to study recrystallization in metals, especially in niobium, and gradient microstructure induced in magnesium by Surface Mechanical Attrition Treatment.

Density-Functional based *ab initio* methods of studies of the lattice dynamics provided an insight into the mechanism of the Verwey phase transition in Magnetite and in self-organized silicide nanostructures. We close our survey with combined theoretical and experimental studies of the topological Majorana states in low-dimensional systems.

We invite every interested reader to visit the web pages of our Division https://www.ifj.edu.pl/en/divisions/no3/.

Selected Research Highlights of the Division of Condensed Matter Physics

Glass-forming properties vs. molecular structure were in-depth studied in novel chiral liquid crystalline compounds exhibiting the antiferroelectric smectic C * phase (SmC *, Fig.3.1). Such compounds are nowadays intensively looked for because of their potential use in a new generation of liquid crystals displays (LCDs).

The most desired compounds are those for which the SmC * phase extends over a wide temperature range and which do not crystallize at room temperature. The crystallization consists of two stages: 1) nucleation and 2) growth of formed nuclei. If the temperature range of nucleation is below the temperature range of crystal growth and they overlap very weakly, the crystallization occurs only on slow cooling or is not possible on cooling at all, when the mentioned temperature ranges do not overlap. In such

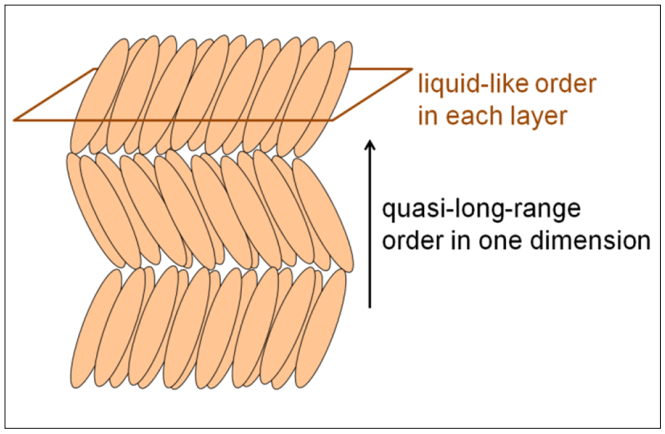

Fig. 3.1. The schematic structure of the antiferroelectric SmC * phase. Each ellipse represents a molecule. The tilting in neighbor layers is anticlinic. Additional helicoidal order is superimposed on the presented structure but the helix pitch exceeds significantly the layer thickness.

compounds, the glass transition (vitrification) is observed and crystallization may occur more easily during heating of the previously vitrified material (the so-called cold crystallization).

In the vitrified SmC * phase the movements of molecules within smectic layers are frozen and the molecules cannot be switched by an external electric field (the effect used in LCDs); therefore for practical purposes the most interesting compounds are those with a low glass transition temperature. The aim of our research was to find which details of the molecular structure prevent the crystallization and facilitate the glass transition from the SmC * phase at possibly low temperature. The materials chosen for this study were several $3FmX_1PhX_2n$[1)] chiral compounds (m = 5-7; X_1, X_2 = H, H or H, F; n = 6, 7; (Fig. 3.2a), known to exhibit the antiferroelectric SmC * phase in a wide temperature range. For $3FmX_1PhX_26$ homologues the strong influence of parity of the C_mH_{2m} chain and fluorination of the molecular core on glassforming properties was observed. Both even homologues 3F6HPhH6, 3F6FPhH6 as well as the odd 3F5FPhH6, undergo the melt crystallization, and their SmC * phase does not vitrify. 3F5HPhH6 and 3F7FPhH6 crystallize only upon slow cooling, otherwise they undergo the glass transition, followed by the cold crystallization during subsequent heating. Finally, 3F7HPhH6 homologue undergoes the vitrification even for the slowest applied cooling rate, 2 K/min. The conclusion is that the tendency to the glass transition increases with the increasing length of the C_mH_{2m} chain in odd homologues and that substitution of the fluorine atom at X_1 position facilitates the crystallization upon cooling.

A pretty **non-trivial kinetics of cold crystallization in the SmC * -forming $3FmX_1PhX_2n$ family** was established both in isothermal and non-isothermal mode [J. Mol. Liq. 319 (2020) 114153]. Both isothermal and non-isothermal crystallizations are mostly diffusion-controlled processes, as shown by in-depth analysis of 3F7HPhH7 (Fig. 3.2a). Besides calorimetric methods, infrared spectroscopy proved especially powerful in this work. The analysis of experimental FT-IR spectra, based on the perturbation-correlation moving window two-dimensional

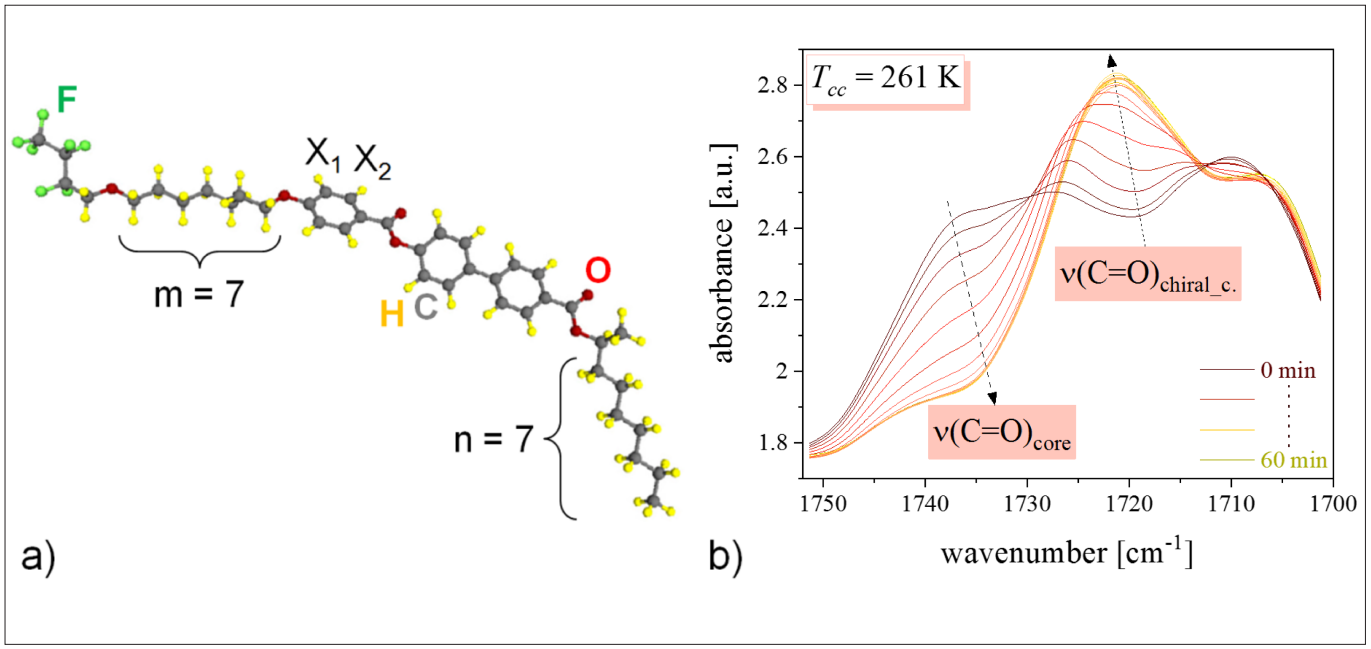

Fig. 3.2. Molecule of 3F7HPhH7 compound optimized with DFT method [adapted from Crystals 10 (2020) 655 under open access Creative Common CC BY license] (a) and evolution of FT−IR bands originating from C=O stretching during cold crystallization in 261 K (b).

1) (S)-4'-(1-methyl"m+1"alkoxycarbonyl) biphenyl-4-yl 4-["n"-(2,2,3,3,4,4,4-heptafluorobutoxy) "n"alkoxy]-benzoate

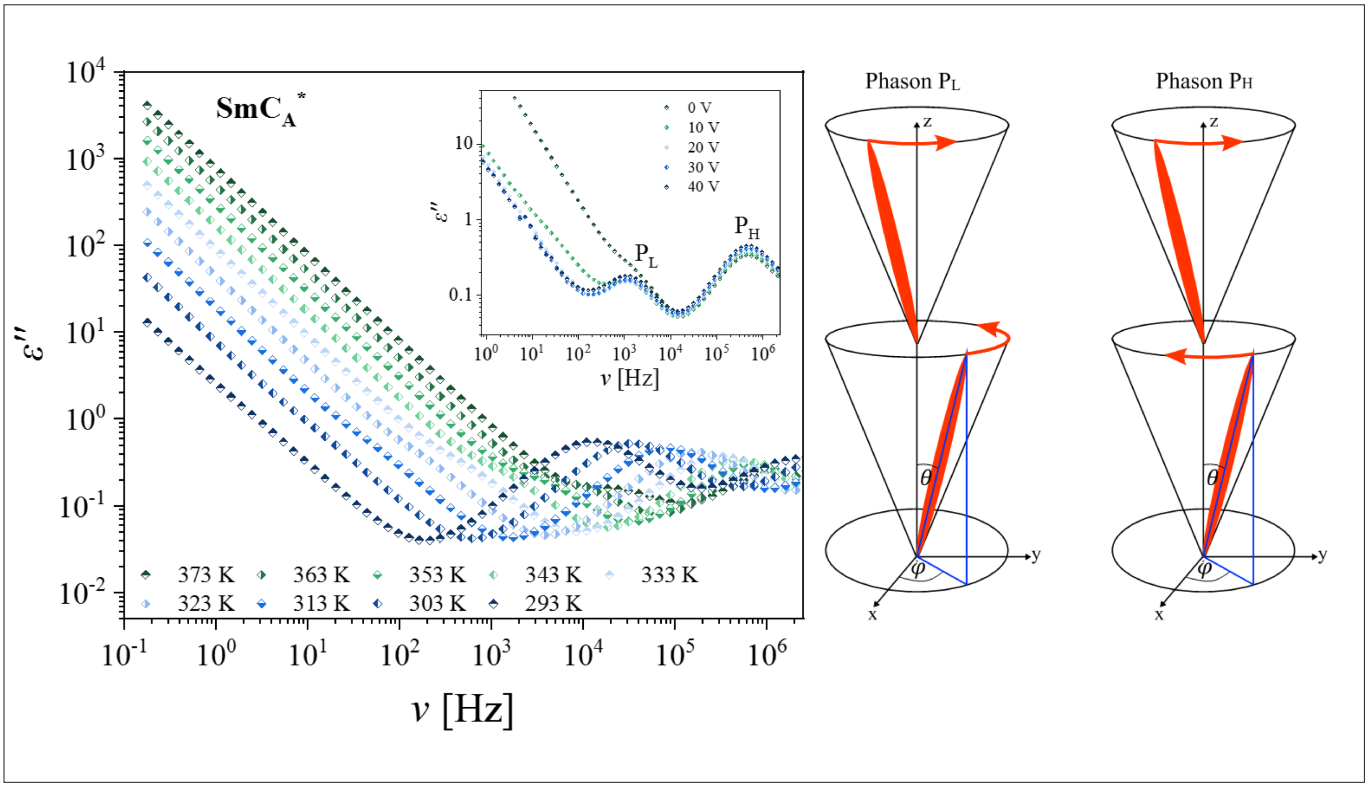

Fig. 3.3. The dielectric loss vs. frequency spectra observed in the SmC_A^* phase [adapted from Phys. Chem. Chem. Phys. 23 (2021) 8673 with permission from the PCCP Owner Societies]The inset shows spectra measured with an applied bias field in the SmC_A^* phase at 333 K. P_L and P_H are the low frequency in-phase and the high frequency anti-phase phasons, respectively.

analysis and two-dimensional correlation analysis, as well as DFT calculations [Crystals 10 (2020) 655] lead to the conclusion that the intra-molecular vibrations that are most sensitive to the glass transition and cold crystallization of 7HH7 turned out to be C-H, C-O-C and C=O stretching (Fig. 3.2b) as well as C-H rocking vibrations.

Pressure-induced crystallization of antiferroelectric liquid crystal was examined by Broadband Dielectric Spectroscopy (BDS), a method that – if additionally enhanced by the application of variable external pressure – proves especially powerful when it comes to revealing interesting aspects of crystallization of liquid crystals. This issue has been recently reviewed in Crystallization as Studied by Broadband Dielectric Spectroscopy, Springer, 2020, in particular in Chapter 5, pp 119–148.

The pressure–induced crystallization is well known among inorganic compounds, in mineralogy and geophysics. Not many works, however, refer to the high pressure crystallization at varying temperature of organic glass-formers. In our research we focused on the impact of hydrostatic pressure on the crystallization of glass-forming antiferroelectric smectic liquid crystal 3F7HPhH7[1]. This fluorinated chiral liquid crystal gained attention of liquid-crystals researches as a promising compound for use in new-generation liquid-crystal displays. During slow cooling the sample crystallizes, while fast cooling results in its vitrification [J. Mol. Liq. 319 (2020) 114153]. In order to elucidate the molecular dynamics processes in the antiferroelectric (SmC^*) phase, we analyzed the BDS spectra taken at ambient pressure, without and with a bias field, which is an additional electric field causing unwinding of the helix in the chiral smectic phases, Fig. 3.3. [Phys. Chem. Chem. Phys. 23 (2021) 8673]. The spectra reveal the presence of two relaxation processes related to the fluctuations in the azimuthal angle on the cone lateral surface at the SmC^* phase (and hence called phasons P_L and P_H).

We also registered the dielectric spectra at constant temperature (isotherms, Fig. 3.4a) or pressure (isobars, Fig. 3.4b) in the temperature range of the antiferroelectric phase of 3F7HPhH7 and during its crystallization. The movements of molecules generating individual relaxation processes become slower after sample compression (the loss spectra are shifted toward lower frequencies with increasing pressure or decreasing temperature and the cooling of the sample causes the rise of the dielectric loss value). The crystallization from the antiferroelectric phase took place at a higher pressure with increasing temperature or at

1) (S)-4'-(1-methyloctyloxycarbonyl) biphenyl-4-yl 4-[7-(2,2,3,3,4,4,4-heptafluorobutoxy) heptyl-1-oxy]-benzoate

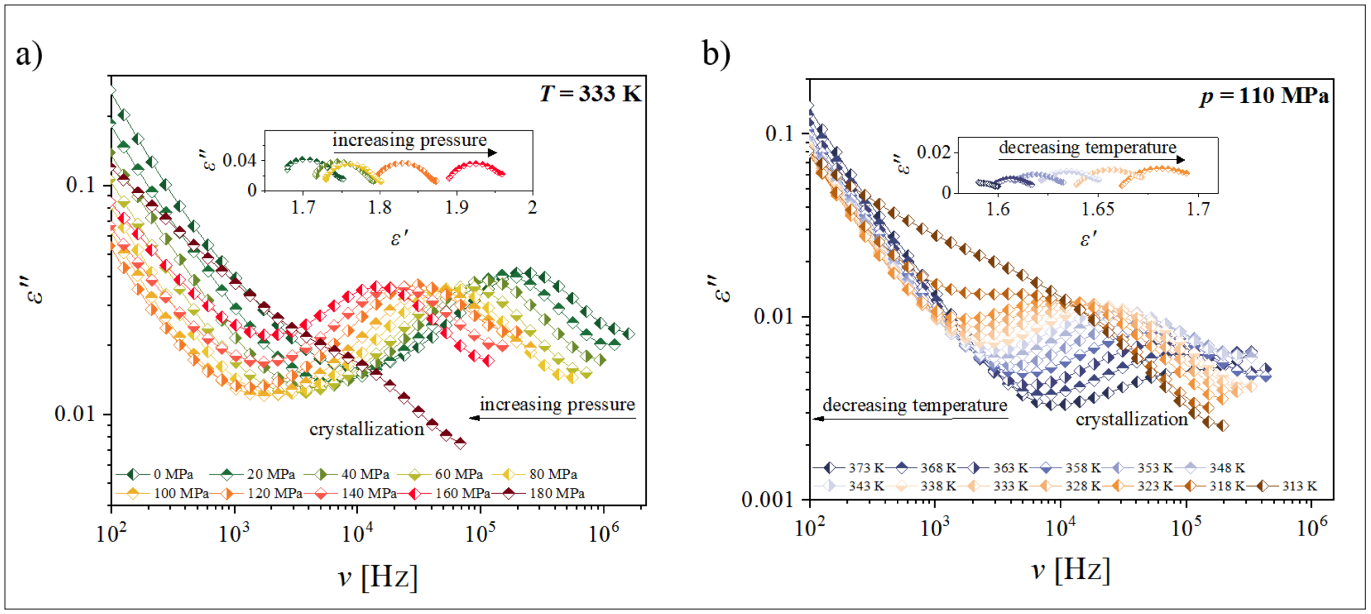

Fig. 3.4. The dielectric loss vs. frequency spectra measured at: a) one isotherm (333 K) under various pressure conditions; b) one isobar (110 MPa) under various temperatures. The insets present Cole–Cole plots for relaxation process.

a higher temperature with increasing pressure. Owing to the presence of the chiral center in the molecule (chiral compounds may form less ordered solid phases than achiral), and the perfluorinated terminal alkyl chain (fluorination of molecules causes an increase of dipole groups), we observed a weak relaxation process in the crystal phase. It means that this phase is the conformationally disordered (CONDIS) crystal type phase.

Amorphization optimizes drug performance and bioavailability. Very often, a dose of active pharmaceutical ingredients (APIs) administered to a patient can be decreased without compromising therapeutic effects, or the stability of APIs can be improved if in-depth knowledge is available on physical and physicochemical properties thereof. In particular, APIs, like many other organic compounds, often exhibit at least two polymorphic forms, which differ in physicochemical properties and sometimes also in therapeutic effects. Crystallization of polymorphs is governed by a combination of thermodynamic and kinetic factors.

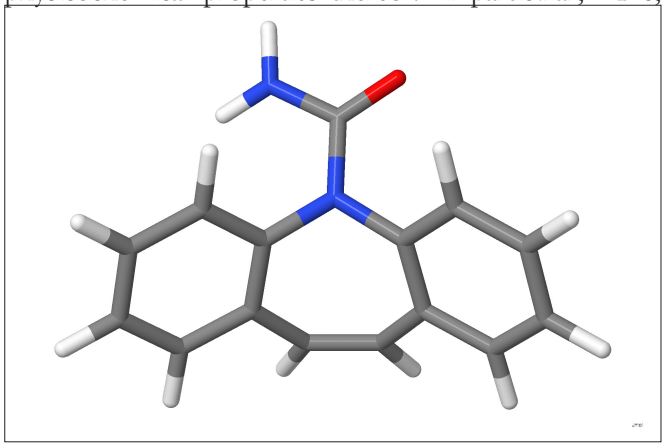

Fig. 3.5. Molecular structure of Carbamazepine.

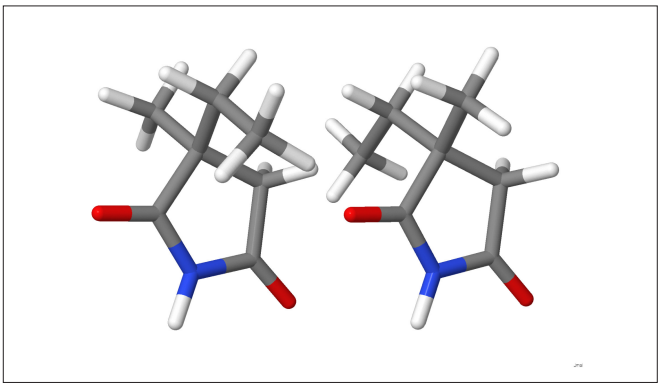

Fig. 3.6. S (left) and R (right) enantiomers of Ethosuximide (ETX). Various conformations of the side chain possible.

Two antiepileptic pharmaceuticals are 'on the carpet' with the ultimate aim of increasing their solubility in water and improving their bioavailability: carbamazepine CBZ[1], (Fig. 3.5) and ethosuximide ETX[2], the latter commercially available as a racemic mixture of two enantiomers (Fig. 3.6). Polymorphism and molecular dynamics of the mentioned substances have been studied in detail using several experimental methods.

Systematic studies using several methods (i.e.: DSC, X-ray diffraction, thermal analysis and FT-IR spectroscopy followed by moving window analysis MW, Fig. 3.7) provide

1) 5H-dibenzo[b,f]azepine-5-carboxamide
2) (RS)-3-ethyl-3-methyl-pyrrolidine-2,5-dione

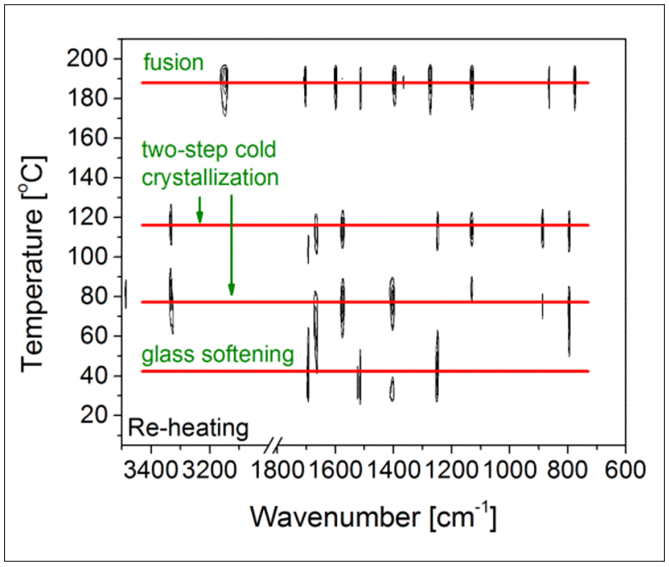

Fig. 3.7. Moving window analysis of spectra collected during re−heating of the CBZ sample [adapted by merging figures from Supplementary Material of J.Appl. Spectrosc., 74 (2020) 473-484].

a new insight into CBZ stability [J Pharm Sci 108(8) (2019) 2654, Appl. Spectrosc. 74(4) (2020) 473]. Our study demonstrates that the decomposition of CBZ starts around 195°C. Surprisingly, the issue of thermal instability of CBZ has not been commonly known and signalized in literature. To increase the thermal stability of CBZ the following procedures were proposed: (i) fast heating, (ii) hydrate forming and (iii) re-crystallizing CBZ from different organic solvents. Although all approaches enhance the thermal stability of CBZ, none of the concepts completely prevents CBZ decomposition.

The thermal analysis and DSC studies show that ETX exhibits a tendency to overcooling of isotropic liquid phase [J. Therm. Anal. Cal. 133(2) (2018) 961]. Only one crystal phase was detected during cooling and heating the sample, characterized as a conformationally disordered crystal (CONDIS). The CONDIS crystal of ETX vitrifies. Solid state polymorphism investigations were complemented by the studies of its dynamics [J. Pharm. Sci. 108(8) (2019) 102]. **ETX appears to be the first low-molecular-weight compound where a dynamical transition was assigned to the ODIC-CONDIS transformation with the help of dielectric relaxation studies.**

Liquid crystals under spatial confinement of nanometer size **become paranematic close to pore walls, and inside small pores they remain glassy** despite exhibiting more free volume, as shown recently by neutron scattering methods: Small Angle Scattering (SANS) and Inelastic Scattering (INS). Other complementary methods (cf. e.g. Liq. Cryst. 41(8) (2014) 1073) had already delivered some results evidencing that soft matter composed of rod-like mesogenic molecules exhibit properties different from those observed in bulk. The power of neutron scattering methods used in this work (neutrons interact with atomic nuclei) consists in that the experimental information is a sum of responses from individual atoms (with possible coherence effects in SANS) in contrast to e.g. broad-

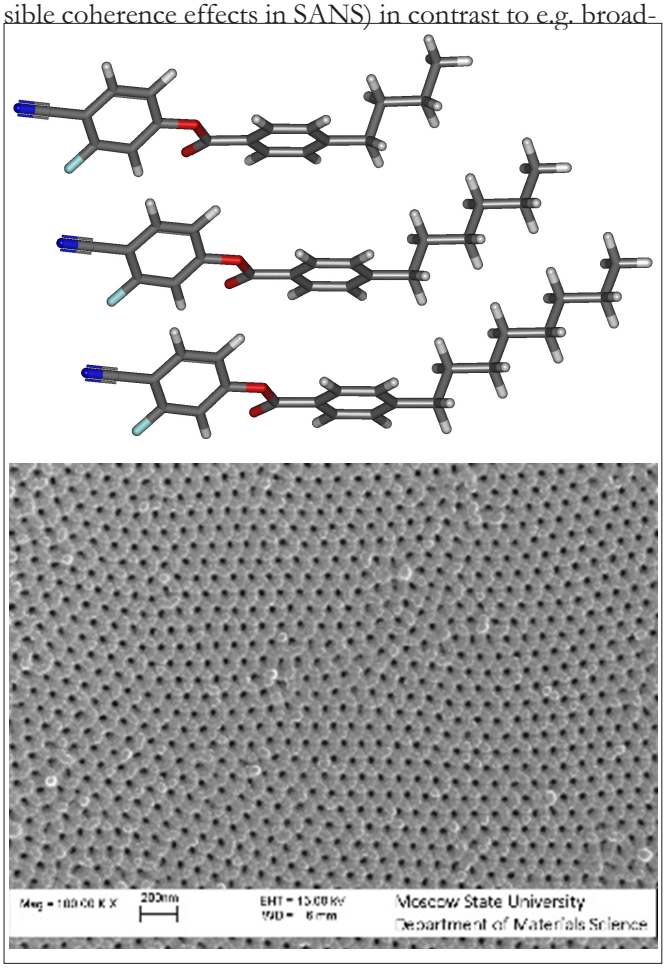

Fig. 3.8 Molecular structure of 4CFPB, 6CFPB, and 8CFPB. TEM photo of a nanopore membrane providing spatial confinement. [lower panel https://en.wikipedia.org/wiki/Anodic_aluminium_oxide].

band dielectric spectroscopy (BDS) which measures the properties of the whole sample. The liquid crystals studied were: 4-cyano-3-fluorophenyl 4-butylbenzoate (4CFPB), fluorophenyl 4-hexylbenzoate (6CFPB), and fluorophenyl 4-octylbenzoate (8CFPB), see Fig. 3.8, enclosed inside AAO nanoporous membranes of pore widths 20nm and 200nm.

SANS measurements provided evidence for the existence of a molecular layer adjacent to the pore walls, the more pronounced the narrower the nano-channels were. The thickness of such a layer could be estimated from SANS results, as shown in Fig. 3.9, using a core-shell cylinder scattering model.

INS spectra of 8CFPB revealed skeletal vibrations characteristic for steric hindrance being significantly decreased

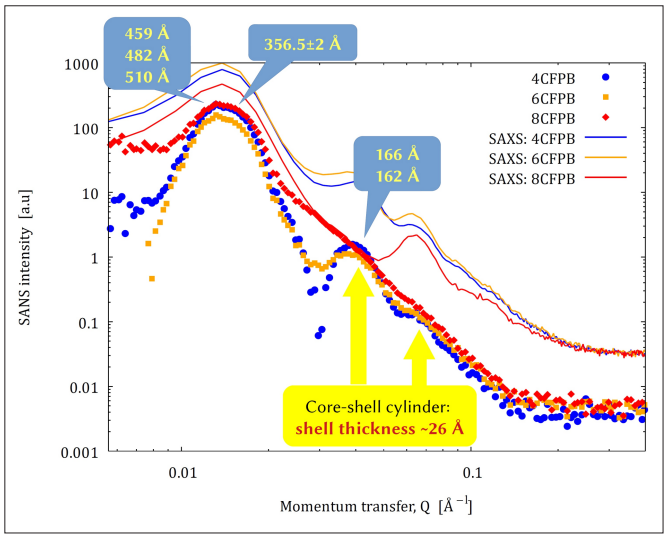

Fig. 3.9. SANS and SAXS results of 'n'CFPB under 20nm confinement.

under confinement. The latter prevents close-packing of the molecules easily attained in bulk. We arrived at this conclusion following model DFT calculations as shown in Fig. 3.10. This figure presents the density of vibrational states, G( ), derived from the experimental INS spectra. In contrast to 4CFPB and 6CFPB, the variation of density of 8CFPB in nanopores is almost undetectable via SANS (undefined inner core/shell boundaries). It is, however, recognizable in INS (through a difference in DOS of low-frequency skeletal vibrations). Inside 200nm cavities, there are conditions enabling the sample to crystallize, while

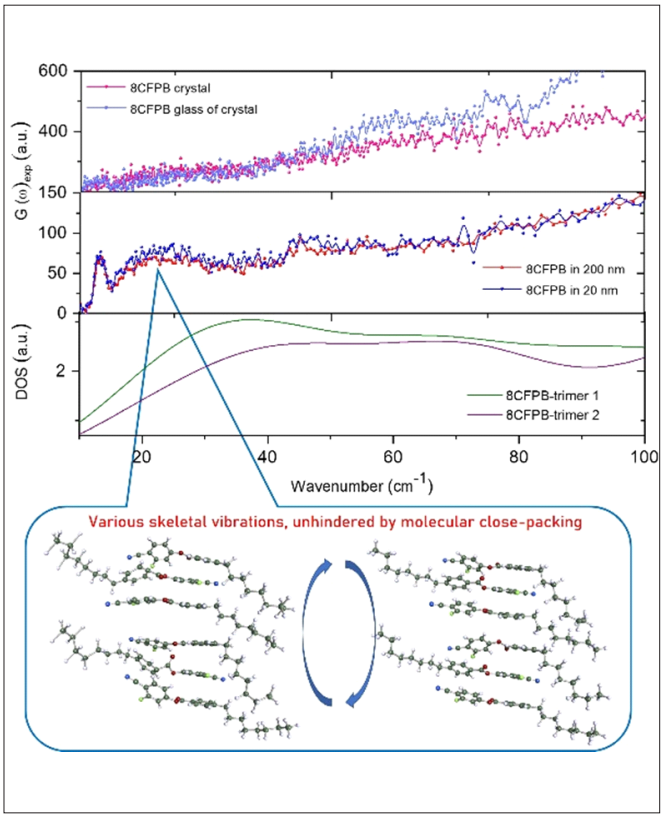

Fig. 3.10. INS spectra of 8CFPB inside 20nm pores. Interpretation aided by model calculations.

in small space it remains glassy. Both neutron scattering experiments were performed at the Frank laboratory of Neutron Physics, JINR, Dubna.

Inelastic Neutron Scattering unveils, otherwise partially concealed, **proton dynamics in glass-forming phenyl alcohols:**

(2-phenylbutan-1-ol, 2-(trifluoromethyl)phenethyl and 4-(trifluoromethyl)phenethyl alcohols, abbreviated BEP, 2TFMP and 4TFMP, respectively). They were studied complementarily by optical (FTIR) and neutron (INS) spectroscopic techniques. In particular, an analysis of the vibrational motions reveals intermolecular coupling brought about by hydrogen bonds in a wide temperature range. For the investigated compounds through the inelastic neutron scattering method, low-energy collective excitations in the title compounds can be studied, in states lacking molecular order. Such excitations manifest themselves in an excess density of states, often referred to as the boson peak. For 'proton glasses', its size indicates that the considered alcohols are in *'strong glassy'* states. Owing to the lack of selection rules and the specific sensitivity of INS to the vibrations of the light H atoms, INS reveals the characteristics of the sample that are hard to notice or '*covered*' by other effects in other methods. Neutron investigations of vibrations of both the skeleton (phenyl ring and alkyl chain) and the methyl group of the molecule, through the movements of protons, allow the separation of C-H, C-F and C-F•••H movements. Torsional motions of CH_3-CH_2- and -CH_2- groups are visible in the density of states G( ) spectra within the lattice vibrational region, see the upper figure,

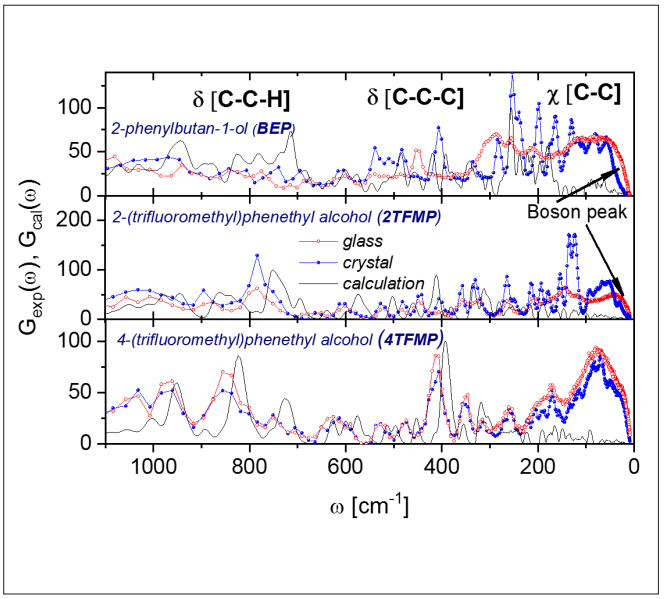

Fig. 3.11. Density of states spectra of solid phases, i.e., crystalline and glass of isotropic liquid at 5 K for BEP, 2TFMP and 4TFMP. Black lines correspond to results of theoretical calculation for tetramer clusters.

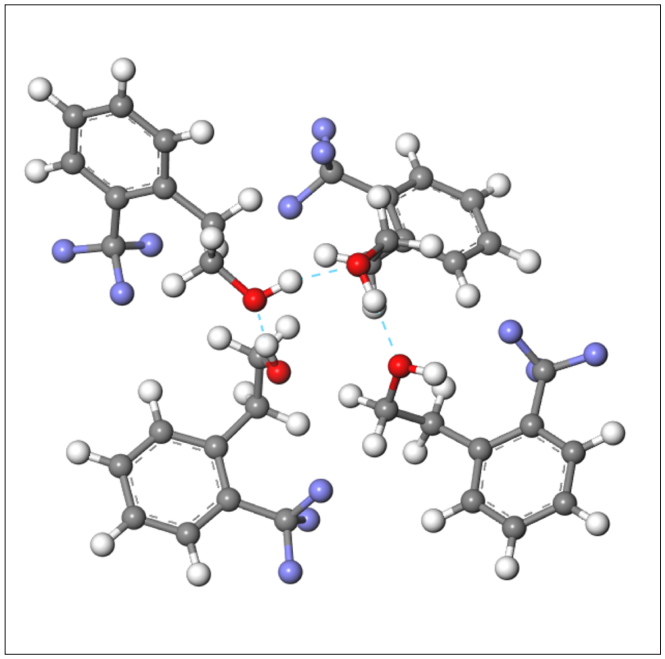

Fig. 3.12. Hydrogen bond structure of phenyl ring alcohols (2TFMP)

[Phase Transit. 91 (2018) 170-185]. The values of the hydrogen bonding strengths for fluorinated materials are very close to each other. Different positions of the CF_3 group create different energetic and, above all, steric conditions for adopting by the molecule possible conformations, and the latter significantly influence the vibrational dynamics. Such a statement inspired quantum chemical calculations using the DFT method, at a high level of theory, carried out both for isolated molecules and aggregates of a few molecules, maintained by non-covalent interactions. An example of the tetramer cluster for 2TFMP is shown in the bottom figure. Besides, these compounds show a tendency to cold crystallization, as a result of an achieved kinetic instability of the metastable supercooled thermodynamic state.

A special formula for dielectric relaxation related to molecular dynamics **in liquid-like phases** (isotropic liquid (IL), cholesteric, nematic, smectic A), solid-like phases (smectic B, conformationally disorder crystal phase (CONDIS), orientationally disordered plastic crystal phase (ODIC)) and supercooled disordered phases (sIL, sODIC) by a common master-curve was proposed by us, see Fig. 3.13. The proposed scaling of the dielectric response has been successfully applied to main relaxation processes. However, the existence of an excess wing (unresolved -relaxation), the resolved -relaxation, or both is often found in glass-forming materials. As it was shown, with the use of the scaling procedure, **the behavior of the resolved -relaxation and the excess wing strictly depend on the parameters of the main relaxation process**. Moreover, the behavior of supercooled disordered phases in any substances tends to the common power relation in glass transition temperature with the exponent depending on the long-range (1-*M*) and short-range (1-*N*) correlation coefficients. This indicates that the dynamics and the frequency behavior of permittivity have the same origin for all phases which can be described in terms of long-range and short-range correlation parameters. [Phase Transit. 91 (2018) 231].

The magnonic crystals were fabricated by depositing Co/Pd multilayers on polystyrene masks. It allowed us to obtain both arrays of separated magnetic

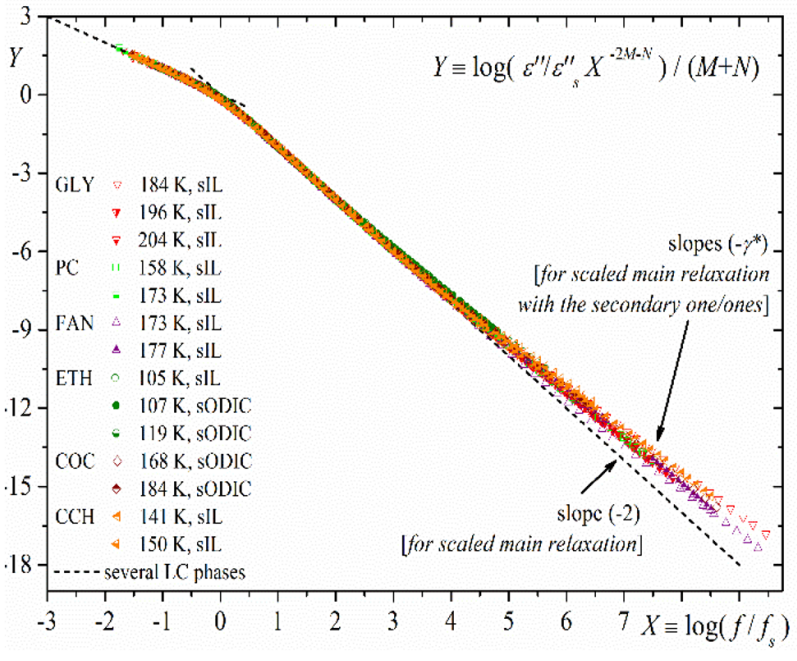

Fig. 3.13. Scaled data of imaginary part of dielectric permittivity for
GLY – glycerol,
PC – propylene carbonate,
FAN – 3-fluoroaniline,
ETH – ethanol,
COC – cyclooctanol,
CCH – cyanocyclohexane,
and several liquid-like and solid-like phases for liquid crystals (LC). GLY, PC, ETH show the existence of the excess wing phenomena;
FAN, COC – resolved -relaxation; and CCH – the excess wing and additional resolved -relaxation.

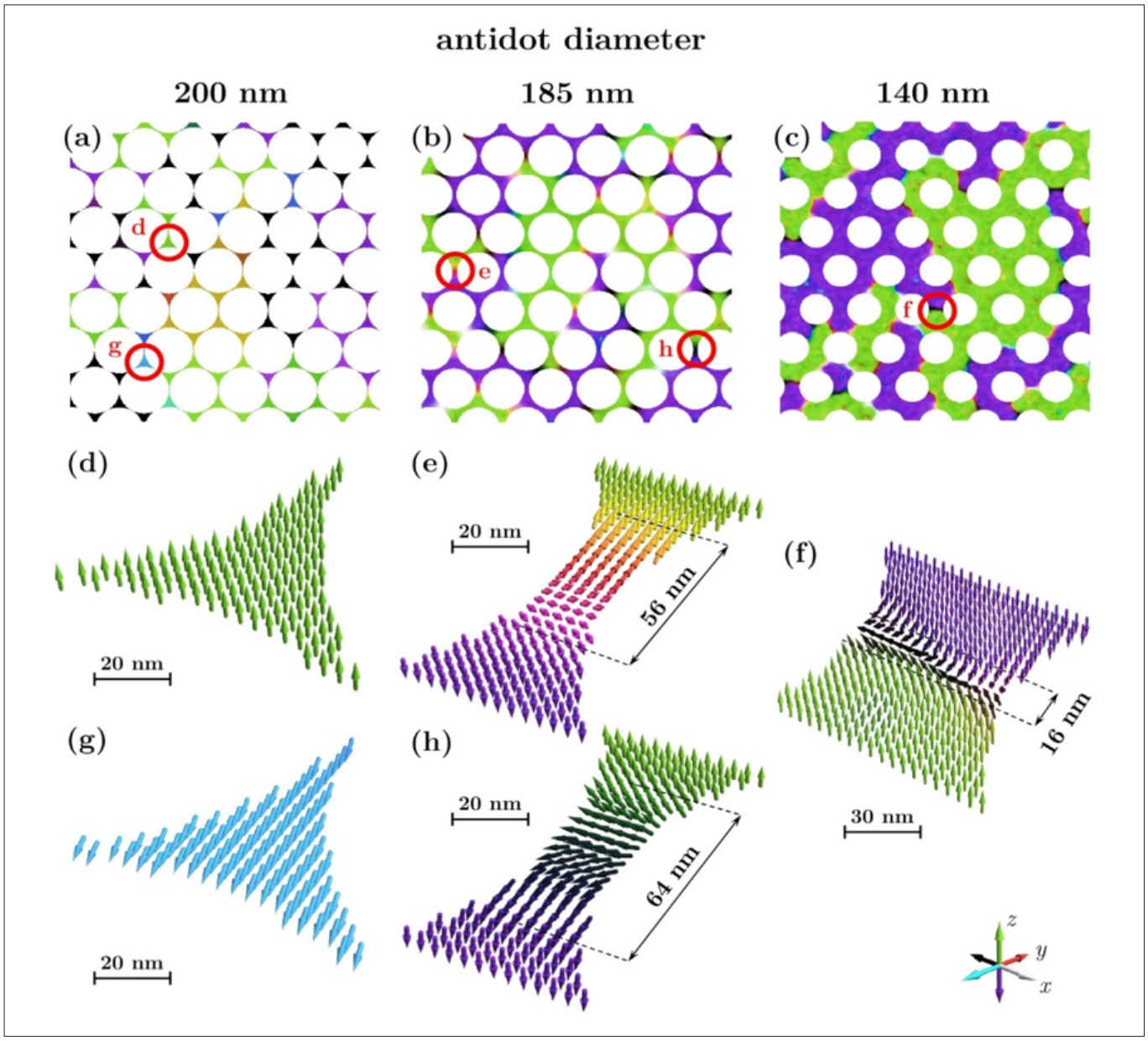

Fig. 3.14. Simulated domain structure after ac demagnetization for the arrays of antidots with diameters (a) 200 nm, (b) 185 nm and (c) 140 nm. Pictures (d – i) show details of the structure for the regions marked with red circles. [Reprinted from Sci Rep 9, 13276 (2019) under CC−BY license 4.0].

islands as well as arrays of antidots with adjustable sizes and perpendicular magnetic anisotropy which exhibited unusual magnetic properties. To explain these properties, we constructed **a micromagnetic model which accounts for intrinsic and extrinsic defects associated with the polycrystalline nature of the material and with corrugated edges of nanostructures.** We found that magnetic properties, magnetic reversal and the evolution of the domain pattern were strongly determined by density of defects, heterogeneity of nanostructures, and edge corrugations. In particular, an increase in the Néel domain walls, as compared to Bloch walls, was observed with an increase of the antidot diameters, suggesting that a neck between two antidots can behave like a nanowire with a width determined by the array period and antidot size. Furthermore, the presence of edge corrugations can lead to the formation of a network of magnetic bubbles, which are unstable in non-patterned flat films. A new, experimentally verified model was demonstrated, which for the first time makes it possible to simulate local changes in the magnetic properties of magnonic crystals, with great accuracy. Some peculiarities of the magnetic ordering in the system are represented in Fig. 3.14 [Sci Rep 9, 13276 (2019)].

We investigated a magnetization reversal mechanism in a $[Co/Pd_x]_7/CoO/[Co/Pd_y]_7$ thin-film composite, where an antiferromagnet is sandwiched

between a hard and soft ferromagnet with different coercivities. The antiferromagnet/ferromagnet interfaces give rise to the exchange bias effect. The application of soft and hard ferromagnetic films causes exchange-spring-like behavior, while the choice of the Co/Pd multilayers provides large out-of-plane magnetic anisotropy. We observed that the magnitude and the sign of the exchange bias anisotropy field are related to the arrangement of the magnetic moments in the antiferromagnetic layer. This ordering is induced by the spin orientation present in the neighboring ferromagnetic films, which is, in turn, dependent on the orientation and strength of the external magnetic field. **The First-Order-Reversal-Curve (FORC) studies showed that the magnetization reversal in the composite is driven by the nucleation of magnetic domains with opposite orientation followed by the domain-wall motion,** see Fig. 3.15 [ACS Appl. Mater. Interfaces 2020, 12, 35, 3992639934].

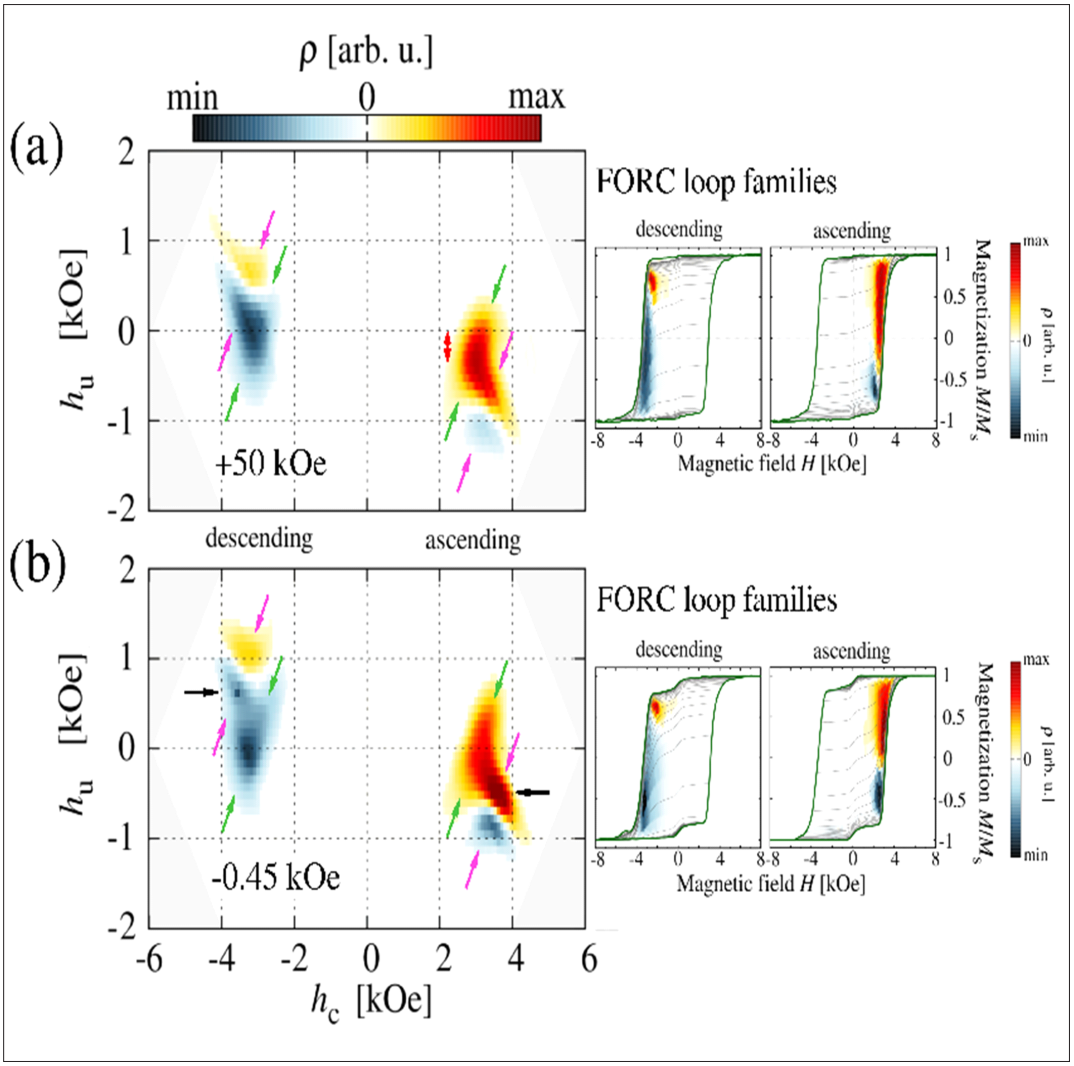

Fig. 3.15. FORC measurements for the $[Co/Pd_{0.6\ nm}]_7/CoO/[Co/Pd_{1.2\ nm}]_7$ composite obtained at 10 K for different H_{cool} cooling fields: (a) +50 kOe, and (b) −0.45 kOe. On the left side are shown $M(H,H_R)$ FORC loop families for ascending and descending magnetization branches, plotted in canvas of the hysteresis loops. The characteristic features are marked with color arrows. [Reprinted from ACS Appl. Mater. Interfaces 2020, 12, 35, 3992639934 under CC-BY license 4.0].

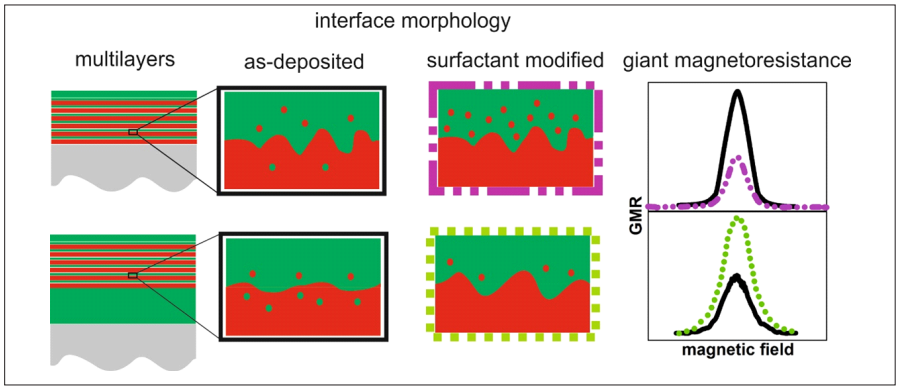

Fig 3.16. The influence of the interface roughness on the magnetoresistance effect presented graphically. [Reprinted from J. Alloys Compd. 824 (2020) 153877 under Elsevier Author Rights].

The Giant Magnetoresistance (GMR) effect in the Fe/Cr multilayered systems is sensitive to the interface structure, in particular **to the interface roughness**. But, despite huge progress in understanding of the GMR phenomena, the influence of the atomic scale interface structure on magnetic and magnetotransport properties is still an open question. In our investigations, in which we used the conversion electron Mössbauer

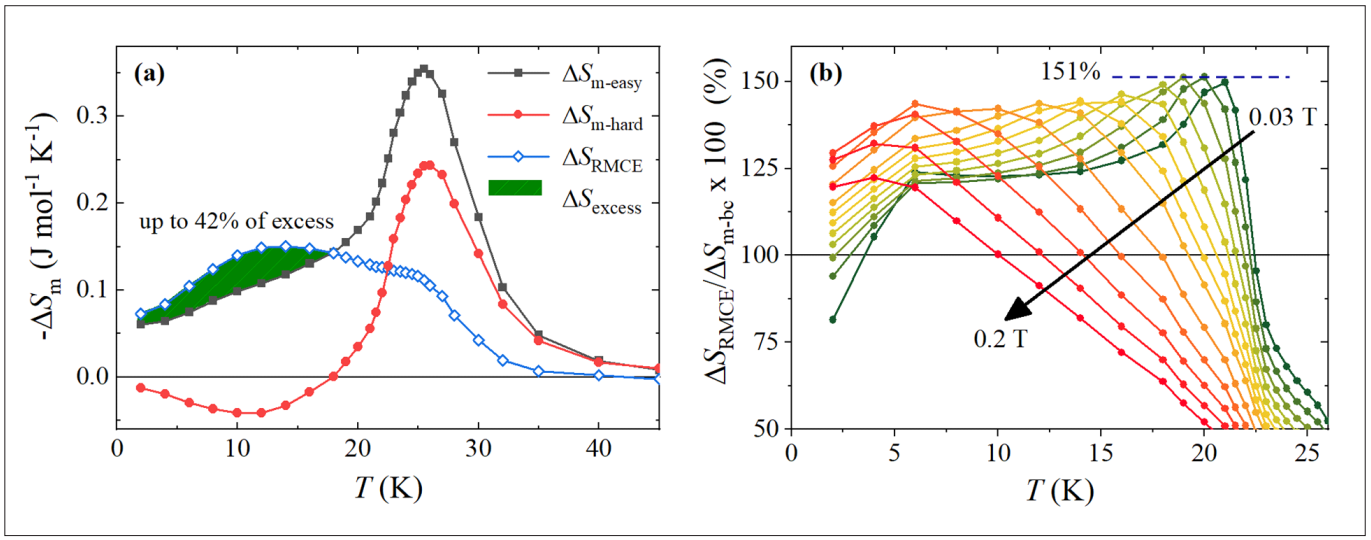

Fig. 3.17 (a) Comparison of the magnetic entropy change by applying magnetic field $_0$ $H = 0.12$ T for easy plane (black squares), hard axis (red circles) and due to RMCE in the field of 0.12 T (blue diamonds). The filled green area shows the excess part over the conventional MCE. (b) Enhancement of RMCE over conventional MCE showed as ratio of S_{RMCE} and S_{m-bc} as a function of temperature. In both plots solid lines are guides for the eyes.

spectroscopy, we were able to distinguish two kinds of interface roughness that affect the GMR in the opposite directions, thus leading to either an enhancement or to a reduction of the effect, see Fig. 3.16. The increase in the interface roughness that was mainly caused by atom interdiffusion resulted in a decrease in the magnetoresistance effect, while in the Fe/Cr multilayers that were deposited on a Cr buffer layer an increase in the interface roughness, which was mainly caused by interface corrugations, resulted in an enhancement of the magnetoresistance. [J. Alloys Compd. 824 (2020) 153877].

The magnetocaloric effect (MCE) is a magneto-thermodynamic process in which change of magnetic field is used to alter the temperature of a magnetic material. Recently, a new type of MCE has been developed, the rotating magnetocaloric effect (RMCE), in which the magnetic entropy change (– S_m) is achieved by rotating an anisotropic magnetic material in a constant field. The main advantages of the RMCE over MCE are: simple construction, high efficiency as a result of operation at higher frequencies than with conventional MCE, and lower energy consumption due to operation with permanent magnets. We studied the bulk magnetic properties and **the magnetocaloric effect of two 2D cyanido-bridged molecular ferrimagnets**

$\{[Mn^{II}(R\text{-}mpm)_2]_2[Nb^{IV}(CN)_8]\}\cdot 4H2O$
(mpm = -methyl-2-pyridinemethanol)

and

$\{(tetren)H_{)0.8}Cu^{II}{}_4[W^{V}(CN)_8]_4\cdot 7.2H_2O\}_n$
(tetren = tetraethylenepentamine)

with weak and significant magnetic anisotropy, respectively. Both compounds reveal an easy-plane type of anisotropy with a domination of intralayer superexchange interaction. A detailed study of MCE has showed a difference between - S_m in easy plane and hard axis. This inequality was used as a starting point to study the RMCE. It has been proved that the inverse part of MCE can enhance the RMCE reaching higher values of entropy change than in the conventional case.

In the case of $\{[Mn^{II}(R\text{-}mpm)_2]_2[Nb^{IV}(CN)_8]\}C4H_2O$ (with weak anisotropy) the excess of RMCE has increased up to 51 % more than the conventional non rotating easy plane MCE in low field limit (below 0.2 T).

On the other hand, the

$\{(tetren)H_5)_{0.8}Cu^{II}{}_4[W^{V}(CN)_8]_4\cdot 7.2H_2O\}_n$ compound

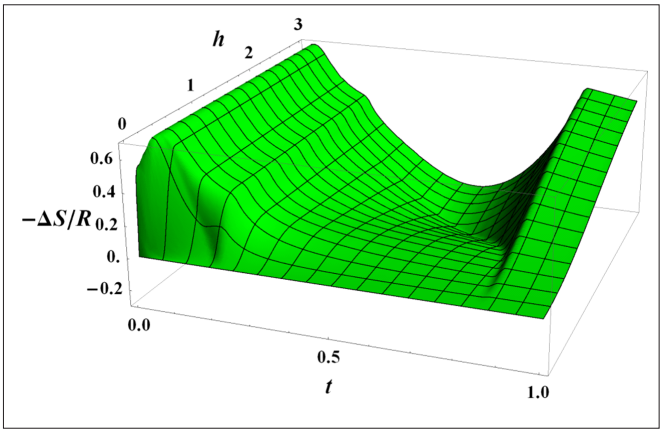

Fig. 3.18. Isothermal entropy change corresponding to the field change $h_i = 0$ $h_f = h$, with the field perpendicular to the bilayer as obtained within the CVMPA approach. [Reprinted with permission from Inorg. Chem. 2017, 56, 19, 11971-11980 © 2017 American Chemical Society].

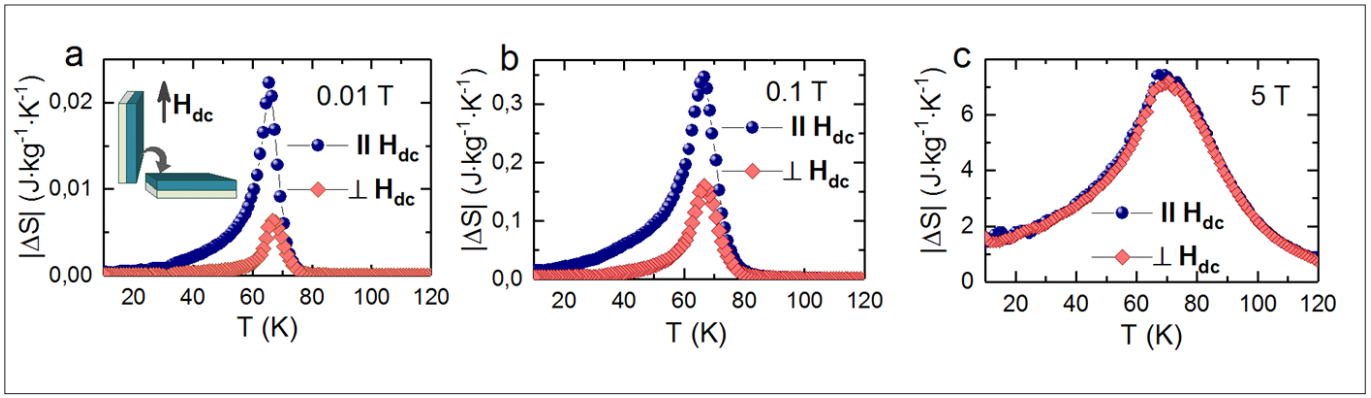

Fig. 3.19. The comparison of the temperature dependence of the magnetic entropy change in the $Ni_{3.1}[Cr(CN)_6]_2 \cdot nH_2O$ thin film obtained for $_0$ H from 0 to 0.01 (a), 0.1 (b), and 5 T (c) for in−plane (marked as blue circles) and out−of−plane (marked as grey diamonds) film orientation.

shows a similar enhancement (up to 47%), though in fields one order of magnitude higher than in the first compound. [Inorg. Chem. 2017, 56, 5, 27772783]. (Fig. 3.17).

Magnetocaloric effect has been explored theoretically in the two dimensional (2D) coordination polymer: $\{(tetren)\text{-}H_5)_{0.8}Cu^{II}_4[W^V(CN)_8]_4 \cdot 7.2H_2O\}_n$ (tetren = tetraethylene-pentamine). To get insight into the precise cause of the appearance of the inverse MCE for the studied compound, a simplified model assuming the anisotropic exchange coupling of the XY type (no coupling of the z components of the spins is present) was proposed. The coupling was further assumed to be ferromagnetic and confined to the nearest neighbors. The spins reside on the bilayer, i.e., two interacting monoatomic planes, each one of simple quadratic structure, which fixes unambiguously the coordination number of that lattice at $z = 5$. The system is immersed in the external magnetic field oriented perpendicular to the bilayer. To conform to the particular compound under study, all spins were assumed to be of magnitude 1/2. Using the molecular field approach and the cluster variational method in the pair approximation (CVMPA) it was confirmed that the exchange coupling anisotropy favoring the in-plane alignment of the spins gives rise to the inverse MCE for intermediate values of temperature, see Fig. 3.18. [Inorg. Chem. 56 (2017) 11971-11980].

The application of molecular material in a magnetic cooling device requires homogenous deposition of the substance on a determined surface. Therefore, the fabrication of well-defined molecule-based thin films and testing their magneto-thermal properties are one of the most important tasks of modern science. Recently, we have demonstrated **the first example of a study of the magnetocaloric effect in molecular magnets prepared in the form of a thin film**. The film of $Ni_{3.1}[Cr(CN)_6]_2CnH_2O$ Prussian blue analogue (PBA) was obtained using "layer by layer" deposition. The average film's thickness was 300 nm.

$Ni_{3.1}[Cr(CN)_6]_2CnH_2O$ is a ferromagnet with T_c= 66 K. To check the influence of the demagnetizing field, the magneto-thermal properties of the film were studied for the sample aligned parallel and perpendicular to the direction of an applied magnetic field, see Fig. 3.19. The values of the magnetic entropy change obtained for both film orientations are similar, reaching 7.43 $J \cdot kg^{-1}K^{-1}$ and 7.07 $J \cdot Ckg^{-1}K^{-1}$ at $_0H$=5T for parallel and perpendicular orientation respectively. The differences in the MCE results for parallel and perpendicular film orientation are essential only for fields lower than 1T. The relatively large value of the magnetic entropy change observed in our film allows us to consider the molecule-based nanoscale materials as efficient refrigerants for microdevices. [Eur. J. Inorg. Chem., 2017: 4817-4822].

Magnetic relaxations are widely studied in molecular magnets especially in individual molecules with paramagnetic cores: single-molecule magnets. Understanding and improving the magnetic dynamic properties are crucial in meeting the requirements of

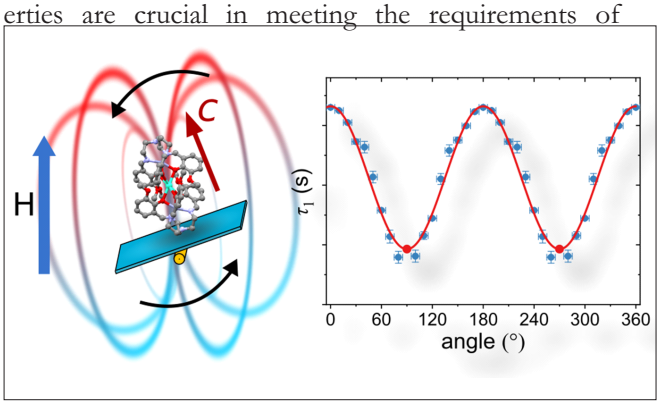

Fig. 3.20. Relaxation time $_1$ as a function of the angle at 2.0 K in applied field 1000 Oe. The 0 +k (k=0,1,2) corresponds to easy axis (H||c orientation) and the 90 +k (k=0,1,2) is the hard plane (H||ab geometry). The red solid line shows the best fit to the quantum tunneling of the magnetization equation.

molecule-based quantum computing or data storage applications. The slow relaxations of magnetization are inseparably related to magnetic anisotropy. However, a great majority of the relaxation measurements for molecular magnets were done for polycrystalline samples or a single direction of the crystal. **The angle dependence of spin-phonon relaxation has been studied with a new homemade probe** and the magnetic properties of single crystals of $[Tb^{3+}(ZnL)_2]CF_3SO_3$ (H_3L denotes a tripodal hexadentate Schiff-base ligand) were measured at low temperatures (down to 2 K). The dc magnetic measurements and crystal field calculations confirmed a strong uniaxial anisotropy. The obtained relaxation times strongly depend on the angle between the easy axis and the direction of an applied magnetic field, as it is visible in Fig. 3.20. This clear anisotropy of the magnetic relaxation was analyzed using the quantum tunneling of the magnetization, which was recognized as the dominant process. [J. Phys. Chem. C 2020, 124, 14, 79307937].

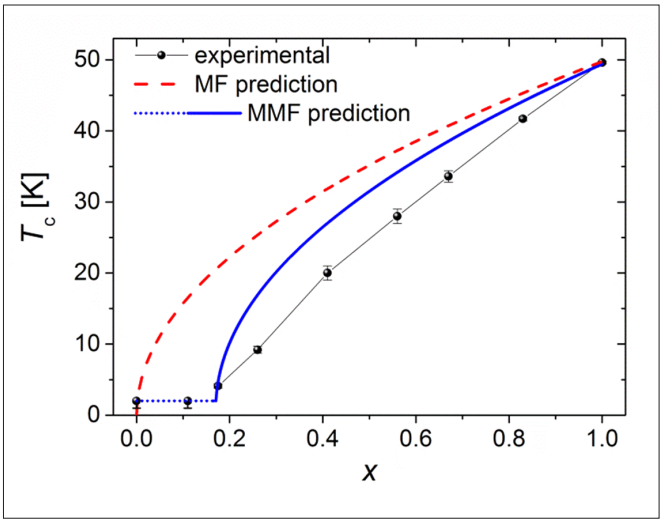

Fig. 3.21. Concentration dependence of the critical temperature. The dashed red line shows the molecular field (MF) prediction, while the solid/dotted blue line represents the modified molecular field (MMF) prediction. [Reprinted from Dalton Trans., 2018, 47, 11438-1144 with permission from The Royal Society of Chemistry].

A series of diluted molecular magnets $\{[Mn_{II}(H_2O)_2]_2[M^{IV}(CN)_8]\cdot 4H_2O\}_n$ (M = Nb/Mo) exhibiting a ferromagnetic phase have been investigated theoretically to demonstrate **the first example of site percolation in magnetic coordination polymers.** It is the first case of a magnetic percolation study with selective site substitution, where magnetic ions of only one type are replaced by their diamagnetic analogues, leaving the other magnetic sublattice untouched. A specially dedicated model within the molecular field approximation was devised to reproduce the Nb^{IV} concentration dependence of the magnetic ordering temperature T_c and to determine the percolation threshold. Fig. 3.21. [Dalton Trans., 2018, 47, 11438-1144]

Over the past few decades, molecular magnetic thin films have gained significant interest mainly owing to their potential in molecular spintronic devices. **The first example of an octacyanometallate-based molecular film was recently synthesized and characterized.** The crystalline $[Fe^{II}(H_2O)_2]_2[Nb^{IV}(CN)_8]C4H_2O$ film was prepared using the ion-exchange method. In this technique, the transition metal ions coordinate with policyanometallate anions, leading to the formation of microcrystals on the surface of the ion-sieving membrane.

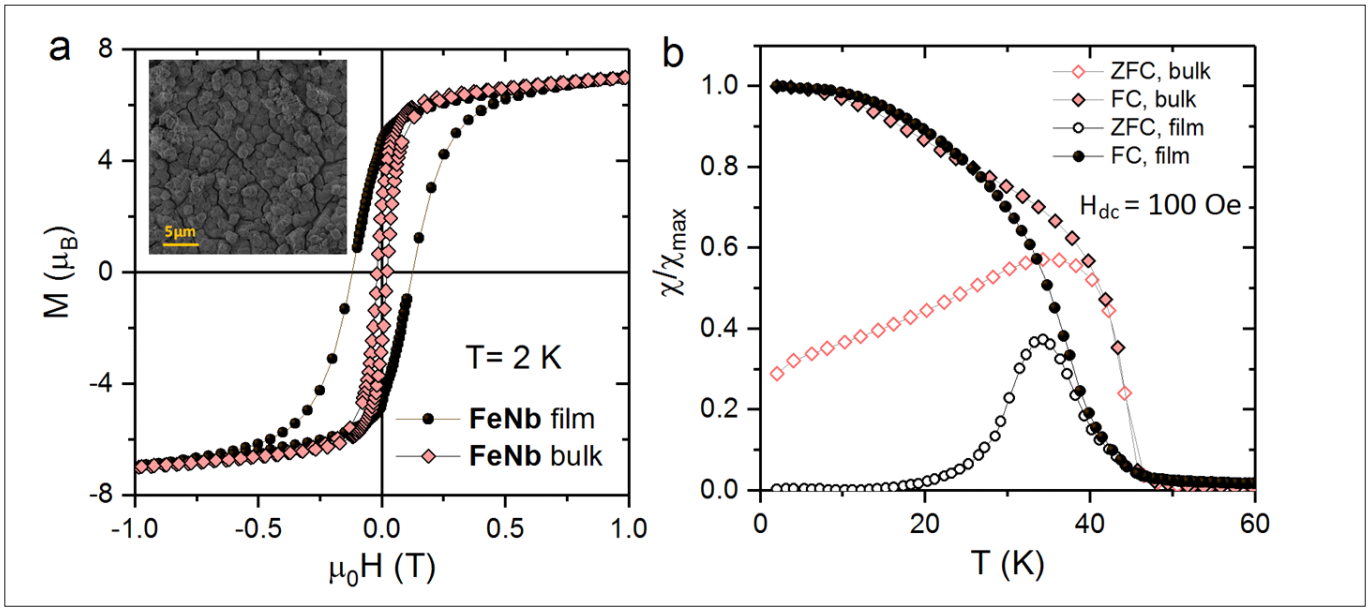

Fig. 3.22. The comparison of the magnetic properties measured for $[Fe(H_2O)_2]_2[Nb(CN)_8]\cdot 4H_2O$ obtained in a form of film and bulk: (a) hysteresis loops, (b) thermal variation of the DC susceptibility measured under zero−field cooled (ZFC) and field cooled (FC) conditions in the applied field of 100 Oe.

The process of the film's growth was monitored using UV-Vis spectroscopy as well as Scanning Electron Microscopy. During the ion-exchange reaction, the substrate was covered with octahedron-type crystals. With the increase of the reaction time, the size of the crystals increased, and then agglomerations appeared, which was accompanied by the change of the film's color from colorless to light violet.

The film's structural and spectroscopic properties are compatible with its bulk counterpart. Significant differences between the film and the powder sample were observed in the magnetic properties, see Fig. 3.22. Magnetic measurements reveal the critical temperature lowering (from 43 K to 40 K) and an increase in the coercive field (from 0.2 kOe to 1.2 kOe) upon material downsizing. The attained results open up a new perspective for the preparation of thin film molecular assemblies. [Materials 2020, 13(13), 30].

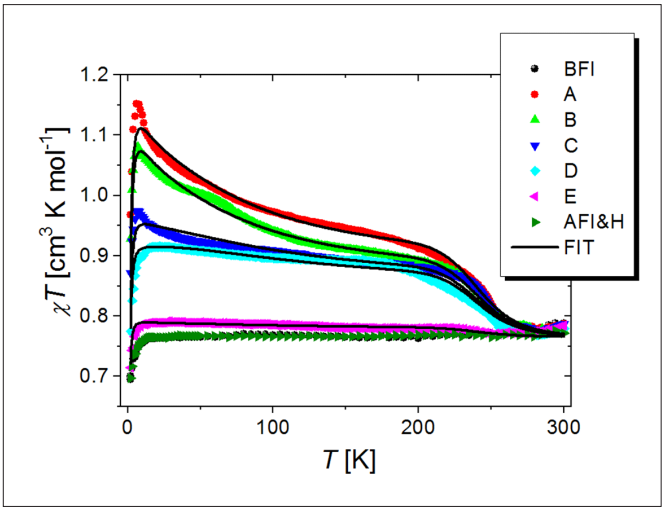

Fig. 3.23. T versus T plot of the sample before irradiation (BFI), upon irradiation in subsequent runs A– E with irradiation stage at 10 K (A), 50 K (B), 100 K (C), 150 K (D), 200 K (E), and after irradiation runs on heating up to 300 K (AFI&H) for the studied compound. [Adapted with permission from Inorg. Chem. 2018, 57, 14, 8137-8145. © 2018 American Chemical Society].

A new bimetallic cyanido-bridged trinuclear complex $[Cu^{II}(enpnen)]_2[Mo^{IV}(CN)_8]\cdot 6.75H_2O$ (enpnen = N,N -bis(2-aminoethyl)-1,3-propanediamine) that **shows a reversible photomagnetic effect** has been reported. The photoinduced increase of magnetization (Fig. 3.23) was explained through two possible processes simultaneously: the light-induced metal-to-metal charge transfer (MMCT) in the Cu^{II}–NC–Mo^{IV} pair and the light-induced excited spin-state trapping (LIESST) effect at the Mo^{IV} center. A numerical model assuming the simultaneous existence of three possible states after irradiation:

the MMCT Cu^{I}–NC–Mo^{V}–CN–Cu^{II} state,

the LIESST Cu^{II}–NC–Mo^{IV}(HS)–CN–Cu^{II} state (HS = high spin),

and the ground-state Cu^{II}–NC–Mo^{IV}(LS)–CN–Cu^{II} (LS = low spin),

enabled the determination of the exchange coupling constants and the relaxation times of the light-induced metastable states. Fractions of the respective states after irradiations at different temperatures were also calculated. The proposed model can provide an interpretative framework for testing and refinement of the mechanism of photomagnetic effect in other coordination networks with cyanido-bridged linkages. [Inorg. Chem. 2018, 57, 14, 81378145].

Mutual relation between the effective spectroscopic factors of the doublet ground state implied by the magnetization at saturation **and the low-temperature susceptibility** has been established. The major outcome of the EPR experiment for the doublet ground state is the threesome of the principal values of the spectroscopic tensor $\hat{g} = [g_{xx}, g_{yy}, g_{zz}]$. At the same time, the amplitudes of the isothermal magnetization or susceptibility detected in the magnetometric experiments depend crucially, albeit not always explicitly, on the components of the spectroscopic tensor. Useful tools for the comparison and consistency check of the outcome of both experiments were developed. Numerical values of the effective spectroscopic factor implied by the magnetization at saturation were provided for instant reference, see Fig. 3.24. The presented findings may be of valuable assistance in

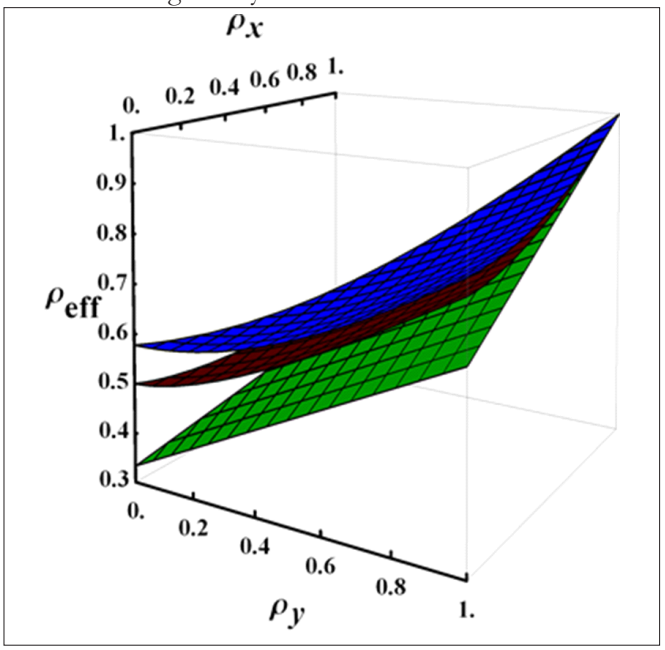

Fig. 3.24. The three measures of the effective spectroscopic factor ($_{eff}$ = g_{eff}/g_{xx} g_i/g_{zz} $(i = x, y)$): that implied by the powder sample measurement of zero−field susceptibility (blue), that implied by the magnetization powder measurement in the high field (red), and the arithmetic mean of the principal values of the spectroscopic tensor (green). [Reprinted from Physica B 581 (2020) 411960 © 2019 under Elsevier Author Rights].

rationalizing the physical implications of the powder sample EPR experiment. [Physica B 581 (2020) 411960_Hlk72521483].

The theoretical analysis of the octacyanide-bridged enantiomeric pair of 1-D chains $[Cu((R,R)\text{-chxn})_2]_2[Mo(CN)_8]\cdot H_2O$ (1R) and $[Cu((S,S)\text{-chxn})_2]_2[Mo(CN)_8]\cdot H_2O$ (1S) (chxn = (R,R)- and (S,S)-1,2-diaminocyclohexane for 1R and 1S, respectively), **exhibiting enantiopure structural helicity**, has been reported. The photomagnetic effects of 1R, 1S, and the racemic compound result from the blue light excitation (436 nm) of the photomagnetically active octacyanidomolybdate(IV) ions. As the efficiency of the irradiation process, i.e. the molar fraction of the $Mo(IV)_{HS}$ ions (HS = high spin), was unknown in advance, two independent thermodynamic models for the excited sample corresponding to two extremes of the excited state were considered. Model 1.0 corresponds to the situation where a relatively small fraction of the Mo(IV) becomes excited, while in model 1.1 a 100% efficiency of light irradiation was assumed. Using the models reflecting the structural details of the studied compounds their susceptibilities and magnetizations were reproduced, see Fig. 3.25. Model 1.1 turned out to be inconsistent with the revealed values of the $Mo(IV)_{HS}$ molar fractions. The calculations showed that in the excited state the $Mo(IV)_{HS}$ centers with $S = 1$ couple antiferromagnetically with the neighboring Cu^{II} centers with $S = 1/2$. Besides, the thermal relaxation energy barriers were estimated and $g_{Mo(HS)}$ was demonstrated to assume unusually high values. [Inorg. Chem. 2020, 59, 9, 5872-5882].

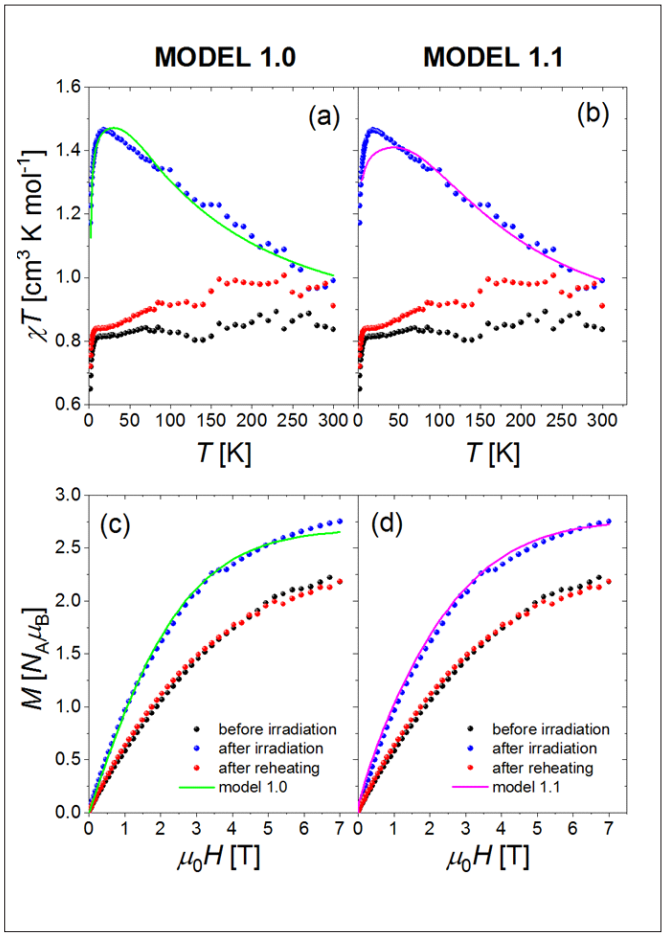

Fig. 3.25. Panels (a) and (b): T versus *T* plot for sample 1R before irradiation (black symbols), upon irradiation (blue symbols), upon reheating (red symbols), as obtained within model 1.0 (green solid line), and as obtained within model 1.1 (magenta solid line). Panels (c) and (d): Isothermal magnetization of sample 1R before irradiation (black symbols), upon irradiation (blue symbols), upon reheating (red symbols), as obtained within model 1.0 (green solid line), and as obtained within model 1.1 (magenta solid line). [Reprinted with permission from Inorg. Chem. 2020, 59, 9, 5872-5882 © 2020 American Chemical Society].

From the practical and societal perspective alumina is one of the most important oxides. Corundum, the most stable form of alumina, *alpha* – Al_2O_3 is a common mineral used as an abrasive owing to its hardness. Car catalytic converters are a popular application for alumina. Here, it serves as a porous undercoat for active transition metal particles (e.g. palladium), which are responsible for removing carbon monoxide and nitrogen oxides from exhaust fumes. The porosity of transition aluminas is related to thermodynamic stabilization of nanoparticles by very low surface energy. Under unfavorable thermodynamic conditions transition aluminas convert to corundum phase and abruptly lose porosity. A practical method of corundum nanoparticles formation was sought for decades. **The new method of nanocorundum production was developed** as part of a German-Polish cooperation of scientists from Mülheim an der Ruhr and Kraków. We noticed

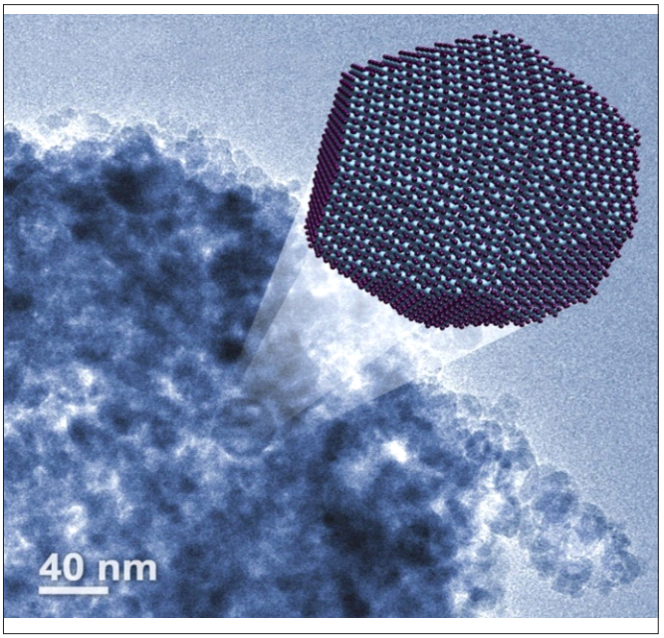

Fig. 3.26 Three−dimensional visualization of corundum nanoparticles. A real microscopic image in the background. [EurekAlert!].

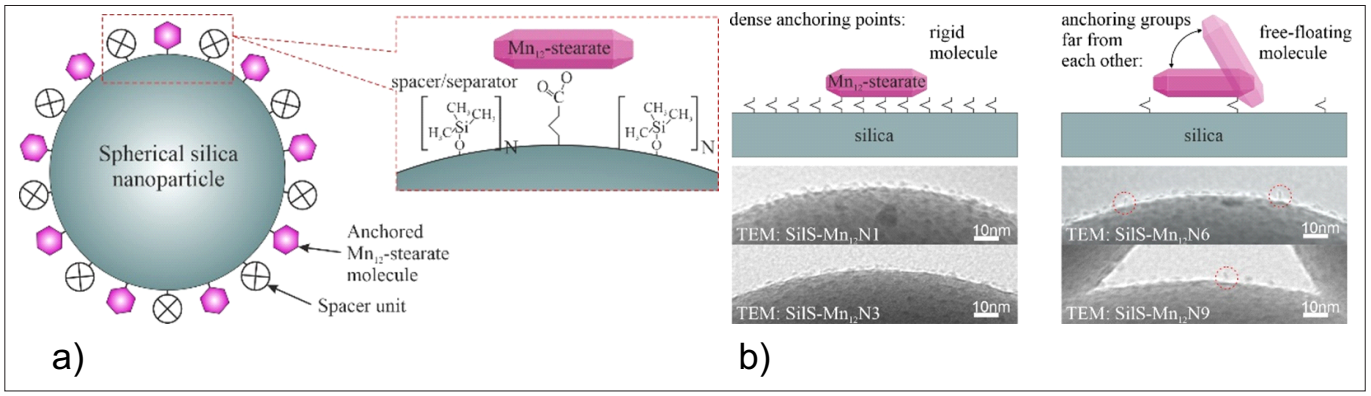

Fig. 3.27. A schematic illustration of the Mn12−silica nanocomposite (a) and visualization of the way of SMMs immobilization onto a silica surface (b), depending on the density of anchoring units (upper side), along with TEM images of samples (bottom part). [Reprinted from Materials 2020, 13(11), 2624 under CC−BY license 4.0].

that a simple and efficient production of nanometer-sized - alumina (Fig. 3.26) really boils down to removing the water molecules covering the bulk of aluminum hydroxide done with heat and/or high pressure to date. It was demonstrated, both practically and theoretically, that it was possible to obtain nanometer-sized corundum while maintaining its stability and significant porosity by using mechanical methods of water removal. This is done via delivering locally the amount of energy to the system exceeding the energy of bonding of water molecules by boehmite [Science 366, 485 (2019)].

A novel fabrication procedure has allowed us to obtain a material in which Mn_{12}-based **single-molecule magnets (SMMs) are regularly attached to a spherical silica's surface with a possibility of tuning their distribution** (Fig. 3.27). The synthesis procedure was based on the concept of the solid solvent [Int. J. Mol. Sci. 2020, 21(21), 8137]. The full functionalization [Nanomaterials 2019, 9(5), 764] and the possibility of tuning the distribution of SMMs [Nanomaterials 2019, 9(12), 1730] were achieved. Thorough investigations revealed that by modifying the number of anchoring units we could tune the magnetic molecules' number at the silica's surface and modify their mobility, as can be seen in Fig. 3.27b.

Moreover, the magnetic measurements showed that in spite of a different mobility of SMMs and different concentration of the spacer units, all the samples preserved their hysteretic magnetic behavior and slow relaxation, characteristic of Mn12 complex [Materials 2020, 13(11), 2624]. We have proven that a single-molecule magnet preserves its magnetic properties even when attached to the silica surface. To the best of our knowledge, it was done for the first time by our team.

The ageing effects of the Mn_{12}-silica nanocomposite were also investigated [Mater. Sci. Eng. B 261 (2020) 114670]. It was pointed out that the molecules attached on the surface preserve its magnetic characteristics (hysteresis in M(H) loops and slow magnetic relaxation). However, the observed magnetic properties evolve over time, revealing significant changes.

The shape size and chemical composition of nanoparticles (NPs) have a significant influence on their toxicity for living cells. We have undertaken a **study of the long-term influence of Au nanoparticles of different sizes and shapes on living organisms by holotomographic optical microscopy** (Fig 3.28). The first morphological changes in the glioblastoma cancer cells

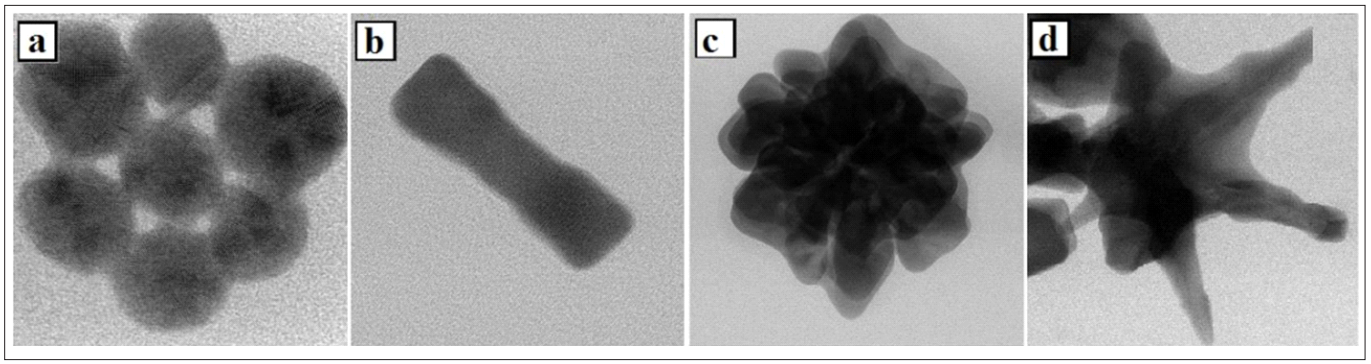

Fig 3.28. STEM HAADF overview images of the Au NPs: (a) spheres [Photodiagnosis Photodyn Ther 30 (2020) 101670]; (b) rod; (c) dahlia [adapted from J.Mater Sci 55, 25302543 (2020) with permission of Springer Nature]; (d) star [Reprinted from Int. J. Mol. Sci. 2019, 20(20), 5011 under CC−BY license 4.0].

cultured with spherical Au NPs occurred after 3h, Fig 3.29a, while star-shaped Au NPs caused changes already after 25 minutes, Fig 3.29b. Moreover, morphological changes in the cells caused by star-shaped Au NPs were progressing very fast.

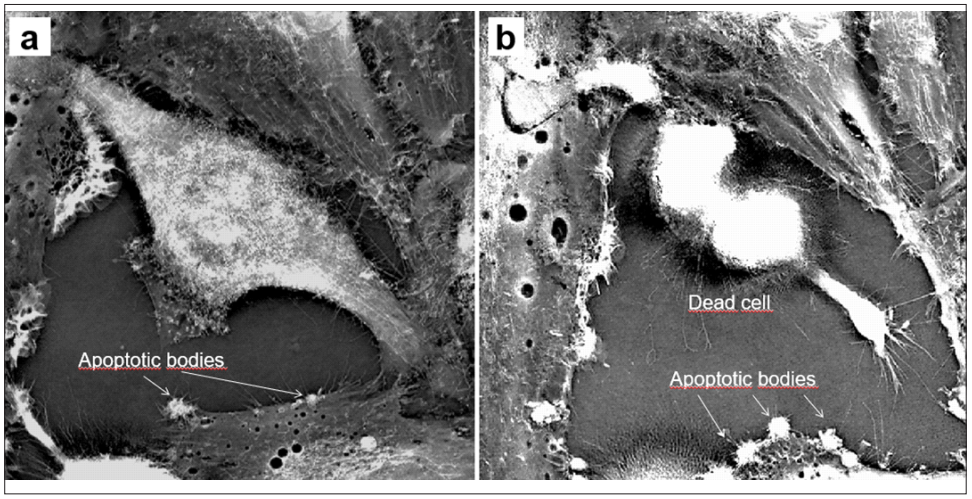

Fig. 3.29. Nanolive 3D CX−A photographs of morphological changes in glioblastoma cancer cells caused by Au NPs after: (a) 3h for spherical Au NPs; (b) 25 min. for star−shaped Au NPs.

Metallic nanoparticles composed of gold (Au NPs), platinum (Pt NPs) and palladium (Pd NPs), **are potential radiosensitizers in radiation-based anticancer therapies** (X-ray and proton radiotherapy). For this purpose, monometallic NPs as well as bi- and trimetallic nanocomplexes were synthesized. The addition of a non-cytotoxic concentration of NPs to colon cells culture (normal and cancer), followed by irradiation with a proton beam, results in a satisfactory therapeutic effect. Interestingly, the radiosensitizing properties of NPs depend not only on the type of metal, but also on the size of the NPs. Smaller NPs are more active because of the larger surface-to -volume ratio. In addition, the highly developed surface of bimetallic AuPt NPs (the so called AuPt nanocauliflowers) [Int. J. Mol. Sci. 2020, 21(24), 9610] results in the high radiosensitizing properties of such NPs. Also, the structure of the palladium shell in the case of bimetallic AuPd NPs plays an important role. The presence of a porous shell around a gold core (AuPd nanoraspberries) increases contact area of the NPs with the cell. Thus, such NPs show better radiosensizing properties compared to AuPd core-shell, with a continuous palladium shell. From the therapeutic point of view, it is important that this type of combined therapy causes more serious damage to cancer cells (SW480, SW620 and HCT116) than to normal colon cells (FHC). Exemplary results of the MTS assay for both types of bimetallic AuPd NPs and scanning transmission electron microscopy using high-angle annular dark field detector (STEM HAADF) images are presented in Fig. 3.30.

We developed a methodology to successfully synthesize in a repetitive way an innovative **catalyst made of platinum, rhenium and tin oxide**

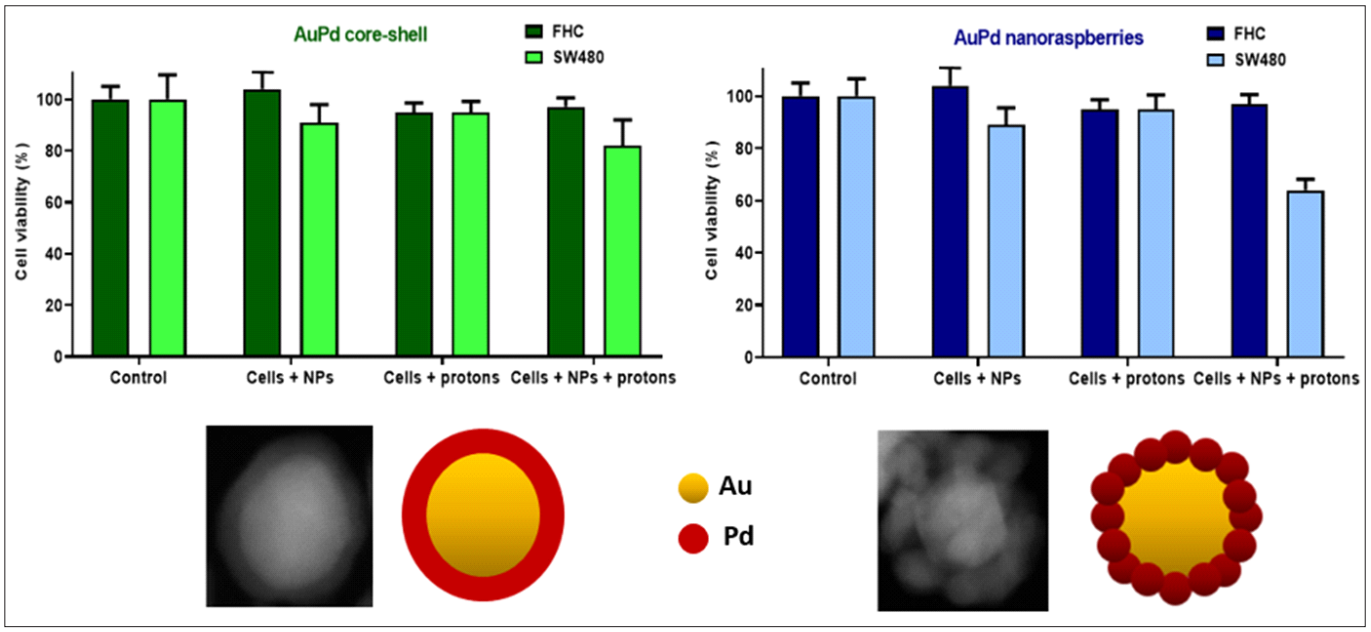

Fig. 3.30. Viability of SW480 colon cancer cells compared to FHC normal cells after the addition of AuPd core−shell/AuPd nanoraspberries and proton irradiation of a total dose of 15 Gy.

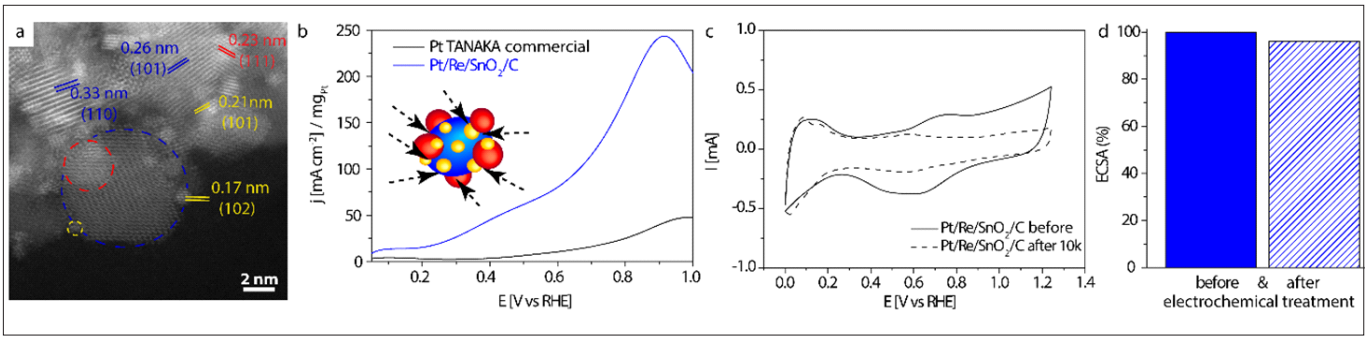

Fig. 3.31 a) High resolution HAADF−STEM image of the ternary Pt/Re/SnO_2/C catalyst with measured lattice distances corresponding to Pt (red), Re (yellow) and SnO_2 (blue); b) first EOR forward scan of the commercial Pt TANAKA and synthesized ternary Pt/Re/SnO_2/C catalyst with Schematic representation of 5 nm SnO_2 NPs (blue) surrounded by metallic Pt (red) and Re (yellow) nanoparticles (black dashed arrows indicate places of physical contact between individual NPs); c) cyclic voltammogram curves of the Pt/Re/SnO_2/C catalyst before and after 10 000 potential cycles with d) graphs showing the decrease in ECSA (%) [Figures reprinted from Nano Res. 13, 832842 (2020) under CC−BY license 4.0].

nanoparticles [J Nanopart Res (2018) 20: 144, Appl. Catal. A Gen. 570 (2019) 319] **for Direct Ethanol Fuel Cells** (DEFCs). Based on the electrostatic interactions, physical contact between the individual three types of NPs was ensured, which was confirmed by the high resolution HAADF-STEM image (Fig 3.31a). This is crucial in the ethanol oxidation reaction (EOR), because interfaces between the metal and oxide NPs are the active sites. Next, using the electrochemical methods, the electrocatalytic durability and activity towards EOR were investigated. The conducted experiments showed that the obtained ternary Pt/Re/SnO_2/C catalyst exhibited a catalytic activity towards EOR ten times higher than a commercial Pt catalyst (Fig 3.31b). Moreover, the onset potential of the synthesized ternary catalyst is shifted to more negative potentials, and after 10 000 potential cycles the electrochemical surface area of the catalyst decreased only slightly,

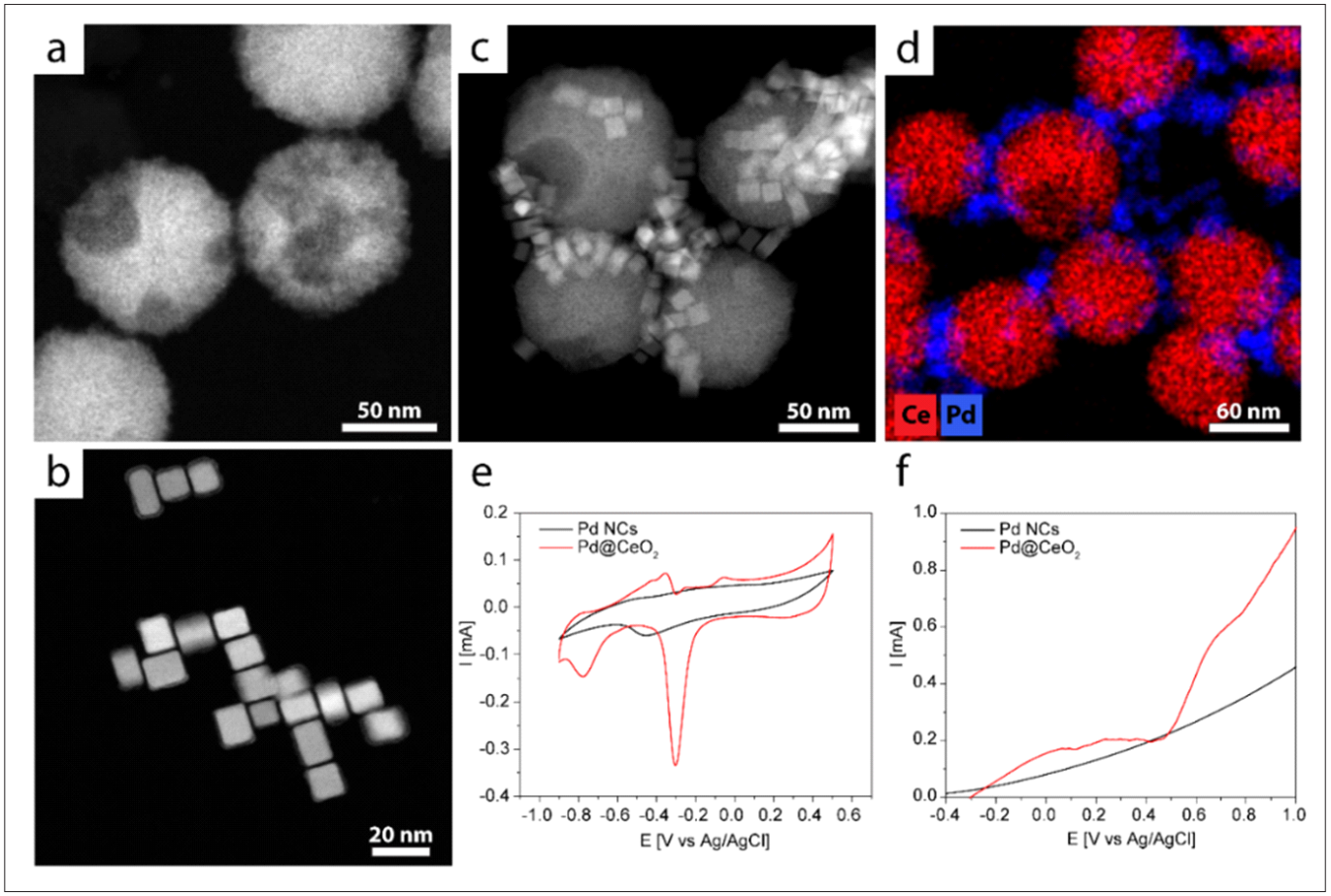

Fig. 3.32 (a) STEM HAADF image of the porous CeO_2 nanoparticles; (b) metallic palladium nanocubes; (c) CeO_2 NPs decorated by Pd NCs with (d) EDS map showing the distribution of Ce and Pd; (e) cyclic voltammetry of Pd NCs and Pd@CeO_2 nanocatalysts in 0.1 M NaOH and (f) first EOR forward scan of the Pd NCs and Pd@CeO_2 in 0.1 M NaOH with 0.5 M EtOH, sweep rate (20 mV/s).

demonstrating the high durability of the ternary Pt/Re/SnO_2/C catalysts (Fig 3.31 c,d).

Recently, **a platinum-free catalyst based on large, porous ~90 nm cerium oxide nanoparticles and palladium nanocubes (NCs) has been synthesized**, as confirmed by STEM HAADF images (Fig. 3.32a-c). Energy-dispersive X-ray spectroscopy (EDS) mappings showed the distribution of the Pd NCs on CeO_2 supports (Fig. 3.32d). The nanosystem was deposited on carbon Vulcan XC-72R and the electrochemical activity towards the ethanol oxidation reaction (EOR) was verified (Fig. 3.32 e,f). The obtained results indicate that the Pd@CeO_2/C catalysts show significantly higher activity for EOR than the catalyst composed only of Pd NCs.

Other nanoparticles for catalytic applications were studied by HAADF STEM and EDS in collaboration with Ulm University, resulting in several joint papers [Appl. Catal. B 282 (2021) 119483, Angew. Chem. Int. Ed. 2020, 59, 2276322770, Appl. Catal. B 270 (2020) 118846, ACS Catal. 2020, 10, 6, 35803594, J.Am. Chem. Soc. 2019, 141, 52015210].

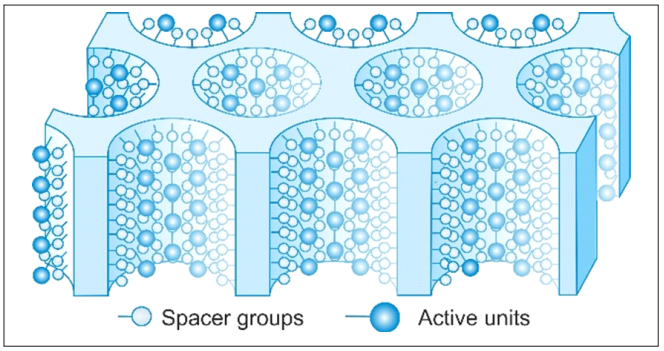

Fig. 3.33a. Schematic representation of a material with tuneable NLO properties: ordered porous silica thin layer. [Adapted from Andrii Fedorchuk, Magdalena Laskowska, The concept of 2D solid solvents: a new view on functionalized silica–based materials, doi:10.3390/IOCN2020-07945 under CC BY 4.0 license].

We also study **nonlinear optical (NLO) properties of novel nanocomposite materials** designed and synthesized for photonics applications. The proposed material consists of optically active polar units, regularly distributed inside a transparent matrix. Thin films of mesoporous silica with 2D hexagonally distributed pores having a diameter of ~2 nm, aligned perpendicular to the substrate, were used as the matrix (Fig. 3.33a). The matrix serves as a template which keeps the isolated functional units in an ordered arrangement and at specific distances. Propyl-copperphosphonate groups were used as active units. In order tos demonstrate the possibility of tuning the NLO response, samples with various concentrations of functional copper-containing groups were prepared. The nonlinear optics investigation, which included the second harmonic generation (SHG) and third harmonic generation (THG), confirmed that the geometry of the system strongly affects its NLO properties. The SHG and THG signals strongly depend on the degree of concentration of active units and can be tuned at the stage of sample synthesis in a very precise way (Fig. 3.33b). The investigation results confirm that the architecture of the compound can be effectively manipulated by changing the functionalization rate to enhance the values of the nonlinear optical susceptibilities. The proposed material can be used as an efficient tool for investigating structure-property relationships [Nanoscale 9, 2017, 12110].

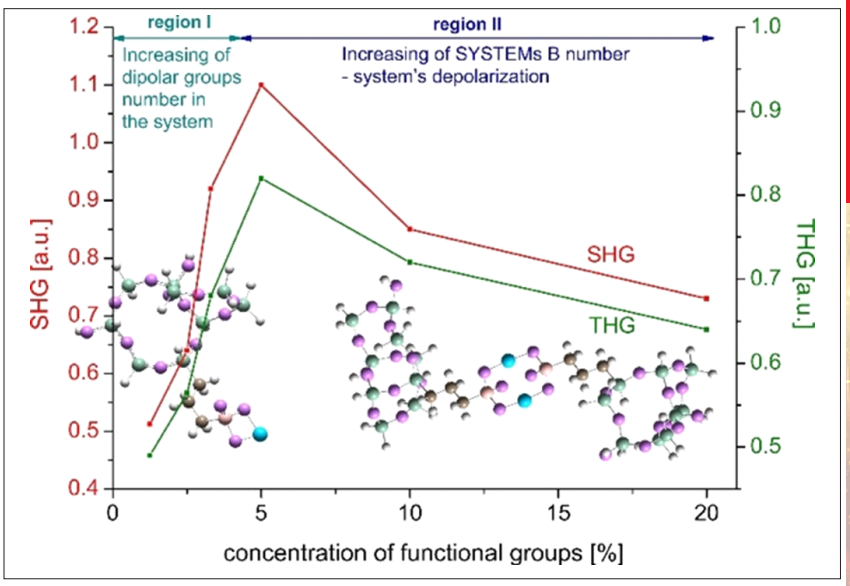

Fig. 3.33 b. The obtained dependence of the maximum fundamental intensity of SHG and THG signals versus the functional group content. [Adapted from Nanoscale, 2017, 9, 12110 by permission of The Royal Society of Chemistry (RSC)].

A study on the **nonlinear optical properties of nanocoposites based on silica matrix** was carried out for **a material consisting of nickel pyrophosphate nanocrystals** and SBA-15 silica [Microporous Mesoporous Mater. 306 (2020) 110435]. By applying a procedure of crystallization inside silica nanoreactors, we obtained nickel pyrophosphate nanocrystals with a diameter below 5 nm, which are clearly visible in TEM images (Fig. 3.34). Using thermogravimetry, transmission electron microscopy (TEM), Raman vibrational analysis, and N_2 sorption analysis, we analyzed the thermal behavior of the initial and

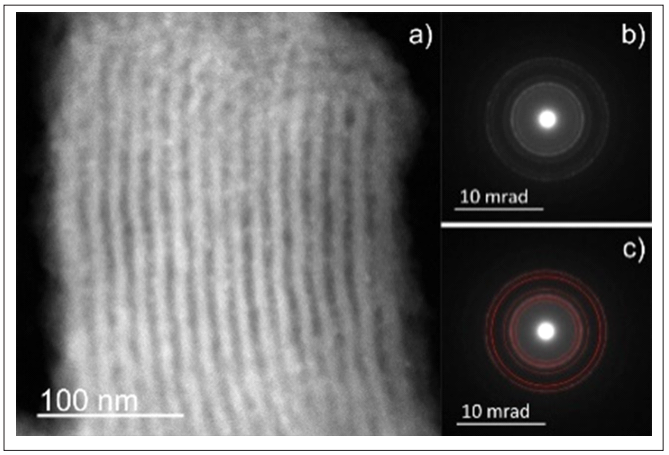

Fig. 3.34 (a) TEM image of the investigated material calcined in the air for 7 h at 350 C and (b) selected area electron diffraction (SAED) pattern showing the crystalline structure of the internal nanoobjects (c) SAED pattern with fitted theoretical diffraction rings for the nickel pyrophosphate structure.[Adapted from Microporous Mesoporous Mater. 306 (2020) 110435].

final material. The nonlinear optics investigation revealed that by the synthesis in silica nanoreactors, we can obtain a silica-based nanocomposite with enhanced and precisely tailored NLO properties. Crucial for second-harmonic generation is a strong spatial confinement during the creation of the nanocrystals that induce the acentricity of a charge.

X-ray lasers can reveal the spatial structures of biomolecules that are hard to obtain with other methods. The spatial structure of proteins tells us how these biomolecules work and how they might be targeted by drugs. **An international team of scientists has recently found the mechanism of spreading the X-ray triggered radiation damage in biomolecules to unprecedented detail.** The results are important for the design and interpretation of X-ray laser measurements. The scientists hit two types of crystallized biological molecules, the sweetener thaumatin and a complex of lysozyme (egg white) with the rare earth element, gadolinium, with pairs of X-ray laser pulses that had slightly different wavelengths and were up to 100 femtoseconds apart. A femtosecond is a millionth of a billionth of a second. The first pulse passed through the sample and was absorbed by an iron foil. The second one had a slightly different color that was not absorbed by the foil. It scattered off the sample and entered a detector, forming a diffraction pattern. The pattern could be analyzed to recover the structure of the sample and to detect any changes caused therein by the first pulse.

The scientists used two independent theoretical simulations: one from the DESY team comprised of Beata Ziaja (DESY & INP Krakow), Malik Abdullah, Zoltan Jurek and Robin Santra, and the other from the RMIT University in Melbourne and the University of Melbourne, to ensure that the conclusions were not biased. Their results show that in order to make reliable measurements, researchers need to model the specific parts of a sample rather than assuming that all parts of the molecule are equally damaged. The study enables a better understanding of how very short X-ray pulses produced by X-ray lasers modify the structure of biological molecules (see Fig. 3.35). [Nature Communications 11 (2020) 1814].

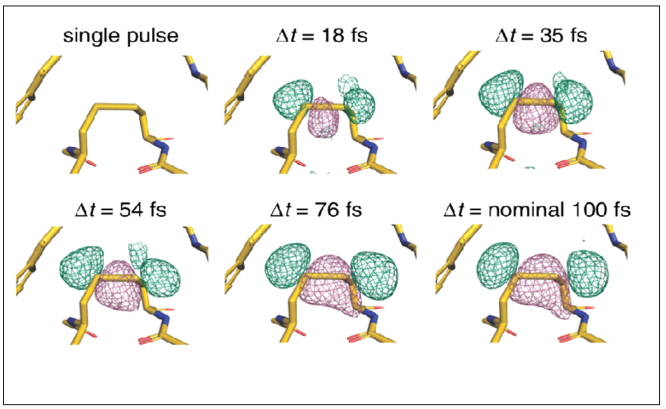

Fig.3.35. Difference density map of a thaumatin region with a bond between two sulphur atoms (dilsulfide bond). Negative (pink) and positive (green) structural differences, caused by stretching of the disulfide bond, increase with the delay between the two X−ray flashes. The other disulfide bonds in thaumatin show a similar effect. [Reprinted from Nat Commun 11, 1814 (2020) under CC−BY license 4.0].

Hydrogen in metals alters the electronic structure of such materials and hence modifies their physical and chemical properties. In conventional transition metal hydrides containing atomic hydrogen the minimum hydrogen -hydrogen distances are around 2.1 Å under ambient conditions (Switendick criterion). Although hints of H-H distances below 2.1 Å in AB_2 alloys have been

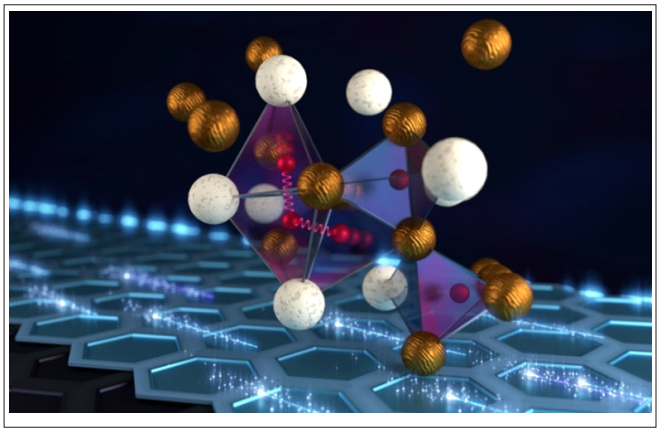

Fig. 3.36. Illustration of a zirconium vanadium hydride atomic structure at near ambient conditions as determined using neutron vibrational spectroscopy. The lattice is composed of vanadium atoms (in gold) and zirconium atoms (in white) enclosing hydrogen atoms (in red). Three hydrogen atoms are shown interacting at surprisingly small hydrogen−hydrogen atomic distances, as short as 1.6 angstroms. [Figure by Jill Hemman, Oak Ridge National Laboratory].

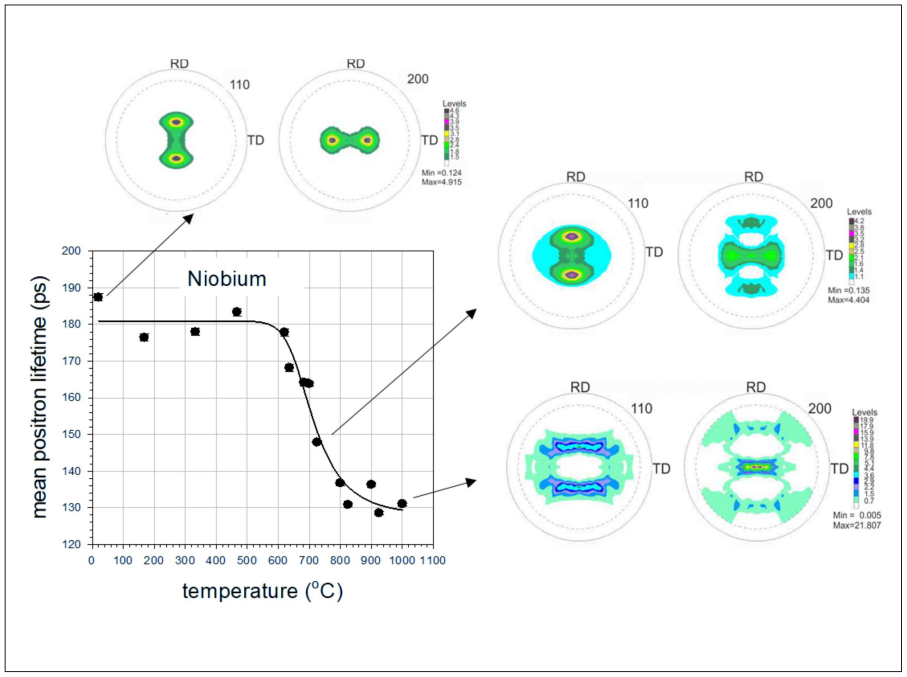

Fig. 3.37. The values of the mean positron lifetime as function of annealing temperature measured for the deformed Nb samples (left). Top and right: the {110} pole figures obtained for samples annealed at different temperatures, as indicated by the arrows. [Adapted from Phys. Status Solidi B 2018, 255, 1800051].

reported, evidence is inconclusive as hydrogen positions are difficult to locate by diffraction techniques. **We have used an inelastic neutron scattering as a local probe of the hydrogen interactions in metals.** These measurements combined together with electronic structure modeling of a well-studied and prototypical metal hydride ZrV_2H_x provide evidence for anomalous hydrogen–hydrogen distances as short as 1.6 Å (Fig. 3.36). The findings provide insights leading to the creation of materials with properties such as very high T_c superconductivity and other quantum behaviors [PNAS February 25, 2020 117 (8) 4021-4026].

Recrystallization is a fundamental process in metallurgy. It occurs by nucleation and growth of grains with new crystallographic orientations which fill the deformed regions. Figure 3.37 shows the mean positron lifetime as a function of the annealing temperature and pole figures, which are sensitive to the crystallographic texture contained for pure niobium deformed by cold rolling. The characteristic decrease in the positron lifetime in the temperature range 600-800°C is accompanied by significant changes in pole figures as a result of recrystallization. Positron data allows one to determine the activation energy of grain boundary migration for Nb equals to 2.26±0.4 eV.

Gradient microstructure induced in magnesium by Surface Mechanical Attrition Treatment (SMAT) was studied by combination of **Positron Annihilation Spectroscopy (PAS) and complementary methods**. The presence of the plastically deformed region rich in crystal lattice defects near the treated surface was indicated by the high values of the mean positron lifetime visible in Fig. 3.38. The defects present are vacancies associated with dislocations. The decrease of the mean positron lifetime with the depth from the surface indicates a reduction of the defect concentration. It corresponds with the visible decreasing density of deformation twins. Additionally, SMAT strongly influences the behavior of magnesium during electrochemical corrosion tests. Better corrosion resistance of the sample SMATed for 120 s was connected to a thicker oxide layer on its surface indicated by Variable Energy Positron (VEP) beam measurements.

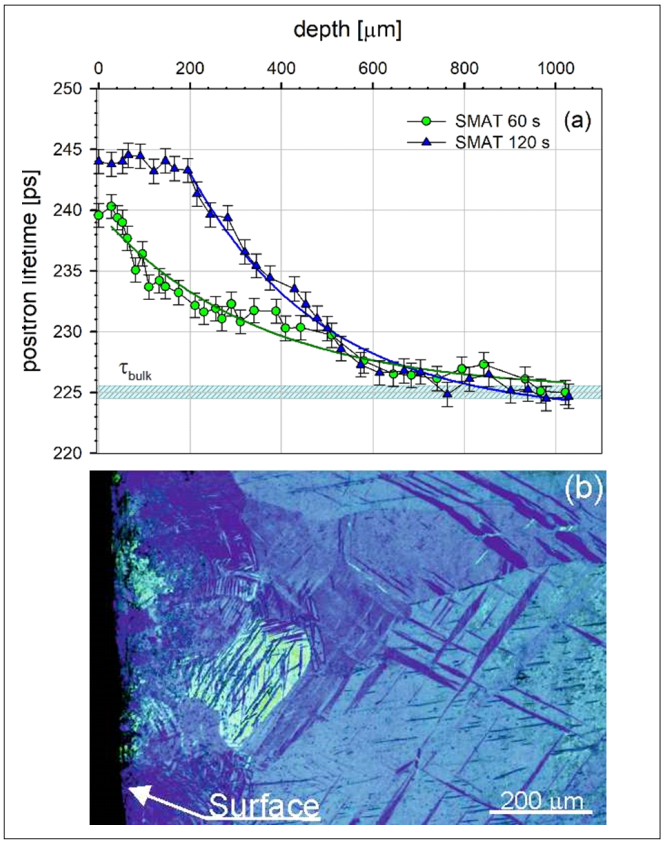

Fig.3.38. Depth profiles of the mean positron lifetime for the magnesium samples SMATed for 120 and 60 s (a) and optical microscopy image (polarized light) of the microstructure for the sample SMATed for 120 s. [Adapted from Materials 2020, 13(18), 4002 under CC-BY license 4.0].

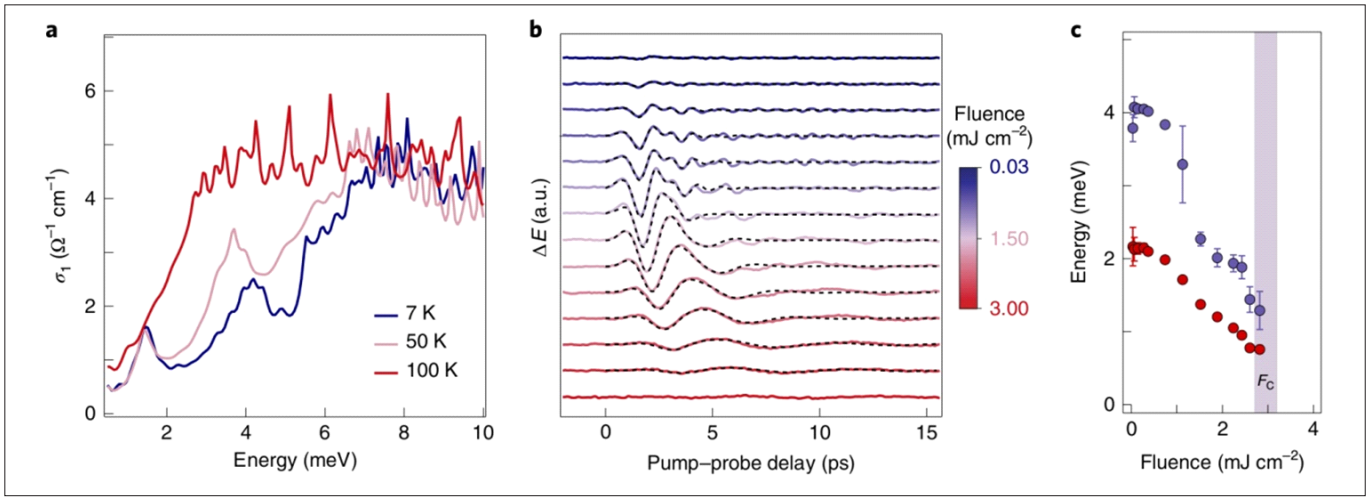

Fig. 3.39 (a) The real part of the equilibrium optical conductivity of magnetite. (b) The pump–induced change in the terahertz electric field transmitted through the sample at 7 K following photoexcitation with a near–infrared (1.55 eV) pump pulse at various absorbed fluences. (c) The energy of each oscillation extracted from the fits as a function of fluence. [Reproduced from Nature Physics 16, 541-545 (2020) with permission of Springer Nature].

New type of soft polaronic waves was discovered in magnetite. The Verwey transition in magnetite was the first metal-to-insulator transformation observed historically. During this extremely complex process, the electrical conductivity changes by as much as two orders of magnitude and a transformation of the crystal structure takes place. Below the Verwey transition, the charge-orbital order consisting of three-site polarons (trimerons) was found. Optical measurements performed at MIT revealed the existence of low-energy excitations of the trimeron order, which correspond to charge oscillations coupled to lattice vibrations (Fig. 3.39). The energy of two coherent modes decreases to zero when approaching the Verwey transition, indicating their critical behavior near this transformation. The theoretical model allowed us to describe the newly-discovered excitations as a coherent tunneling of polarons. The energy barrier for the tunneling process and other model parameters were calculated using the density functional theory (DFT). The involvement of these waves in the Verwey transition was confirmed within the Ginzburg-Landau model. Finally, the calculations also ruled out other possible explanations for the observed phenomenon, including conventional phonons and orbital excitations. The obtained results indicate that the trimeron order in magnetite has elementary excitations with a very low energy, absorbing radiation in the far-infrared region of the electromagnetic spectrum. These excitations are collective fluctuations of charge and lattice deformations that exhibit critical behavior and are thus involved in the Verwey transition [Nature Physics 16, 541545 (2020)].

Self-organized silicide nanostructures are considered **as building blocks of future nanoelectronics or spintronics**. In nanostructures, the lattice vibrational waves (phonons) deviate drastically from those in bulk crystals, which gives rise to anomalies in thermodynamic, elastic, electronic, and magnetic properties. Combined experimental (nuclear inelastic scattering) and theoretical (density functional theory) studies allowed us to determine the lattice dynamics of metastable, surface-stabilized -phase $FeSi_2$ nanoislands epitaxially grown on the Si(111) surface and endotaxial -$FeSi_2$ nanowires embedded into the Si(110) surface. The experimental phonon

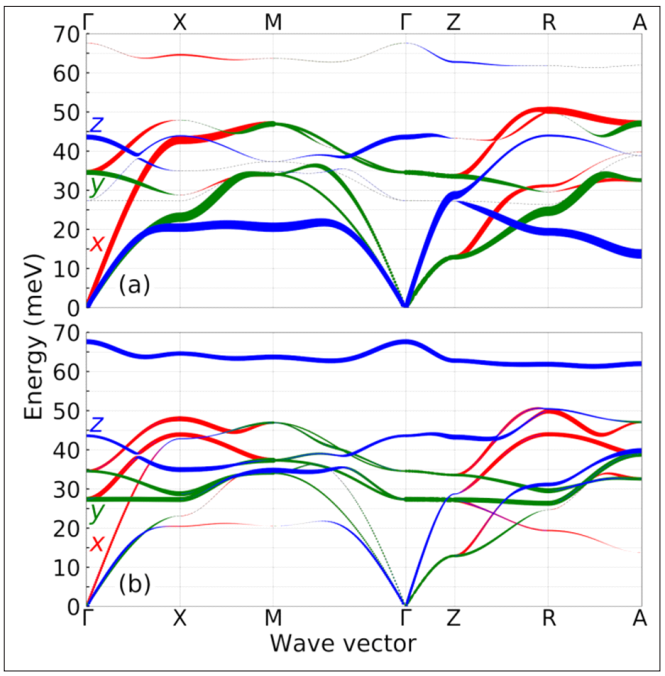

Fig. 3.40. Ab initio–calculated polarization–resolved phonon dispersion relations of the bulk –$FeSi_2$ projected on (a) Fe atom and (b) one of the Si atoms in the unit cell. [Reprinted from Phys. Rev. B 101, 165406 with permission of the American Physical Society].

density of states obtained with the wave vector of the x-ray beam being parallel to a certain crystallographic direction of the substrate is composed of a specific combination of x-, y- and z -polarized phonons of the tetragonal -$FeSi_2$ unit cell (Fig. 3.40). A pronounced vibrational anisotropy of experimental spectra, taken along distinct directions, originated from the specific orientation of the -$FeSi_2$ unit cell on the Si surface, is fully consistent with the results of the first-principles calculations [Phys. Rev. B 101 (2020) 165406, Phys. Rev. B 102 (2020) 195414].

Realization of the nontrivial topological phase in low dimensional structures is a consequence of the interplay between superconductivity, spin-orbit coupling, and magnetic field. The existence of this non-trivial topological phase is found to be at the origin of the emergence of the bound states - the most famous example is the Majorana state. The signatures of Majorana bound states at the ends of magnetic chains deposited on a superconducting substrate were reported experimentally, and recent studies suggest a possibility of realization of the topological superconducting domain in a magnetic nanostructure coupled with a bulk superconductor. In the case of magnetic monoatomic chains (see Fig. 3.41a), we employed the first

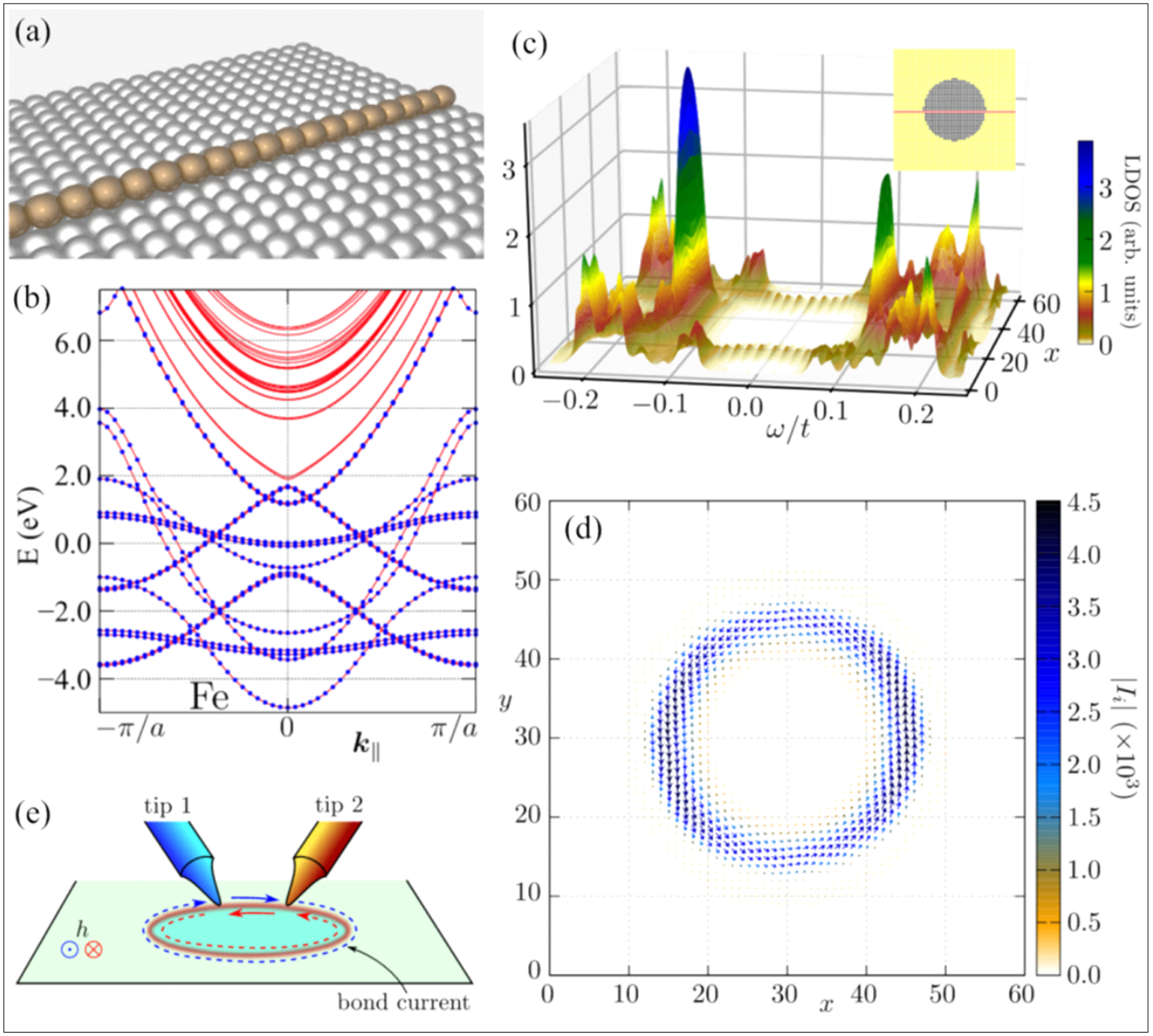

Fig. 3.41 (a) Schematic representation of the monoatomic chain (brown atoms) at the surface of superconductor (gray atoms). (b) Comparison of the iron band structures obtained from the DFT and tight−binding model calculations (solid red line and blue dots, respectively). (c) Local density of states along the nanoflake. (d) Vector map of the bond current showing the boundary between trivial and non−trivial topological phases. (e) Setup of a double−tip experiment probing the chirality of the edge states [Adapted by combining five figures reproduced from Phys. Rev. B 101, 205143 (2020) and Phys. Rev. B 102, 245405 (2020) with permission of the American Physical Society].

principles (DFT) calculations to directly investigate the topological properties of transition metal nanochains (i.e., Mn, Cr, Fe and Co) [Phys. Rev. B 101 205143 (2020)], see Fig. 3.41b. In contrast to the previous studies, we found the exact tight-binding models in the Wannier orbital basis for the isolated chains as well as for the surface-deposited wires. Based on these models, we calculated the topological invariants for all the systems. Firstly, for the isolated chains we demonstrated the existence of the topological phase only in the Mn and Co systems. Secondly, we showed that a coupling between the chain and substrate leads to strong modification of the band structure. Moreover, the analysis of the topological invariant indicates the possibility of the topological phase in all the studied nanochains deposited on the Pb surface. Therefore, our results demonstrate an important role of the coupling between deposited atoms and a substrate for topological properties of nanosystems, that should be implemented in future studies. In the second case, we studied the nontrivial topological phase in a nanoflake [Phys. Rev. B 102 245405 (2020)]. The boundary between trivial and topological phases is "marked" by a nearly-zero in-gap bound state (Fig. 3.41d). The analysis of the topological phase diagram of such a system shows that a similar phase separation can be induced by tuning the chemical potential of the nanoflake (Fig. 3.41c). We study such a possibility in detail, analyzing the spatial extent of the edge modes circulating around the nanoflake and discussing some practical implementations. Moreover, the chirality of Majorana edge states can be probed by non-local differential conductance using scanning tunneling spectroscopy with a double tip setup (Fig. 3.41e).

❖

4. Division of Theoretical Physics

In the years 2017-2020 the Division of Theoretical Physics consisted of four departments: of Structure-of-Matter Theory, of Particle Theory, of Complex Systems Theory and of Mathematical Physics. The research conducted at the Division can be therefore accordingly grouped in four areas:

Department of Structure of Matter Theory carries out research on the properties and experimental signatures of quark-gluon plasma created in heavy ion collisions at the LHC and RHIC colliders as well as in low energy experiments with a high density of baryon number, such as HADES, NA61/SHINE, BES@RHIC (present) and FAIR, NICA (future). The Department is also involved in studies on density distributions of quarks and gluons in nucleons and mesons, in particular their saturation, and in analysis of final states in scattering processes at colliders in KEK, CERN and Jefferson Lab. The analyses are carried out with a variety of methods: quantum field theory, effective quark models, and relativistic hydrodynamics.

Department of Particle Theory focuses on calculations: analytical, numerical and stochastic in order to explain and provide precise predictions for experiments carried out at existing and planned particle colliders, such as the LHC, meson factories, ILC, CLIC, FCC-ee, FCC-hh, CEPC, EIC. The calculations, which involve electromagnetic, weak and strong interactions, are conducted within the framework of quantum field theory and their precision is a crucial parameter which should be better than the experimental one.

Research in **Department of Mathematical Physics** covers various topics: probabilistic models and correlations in the theory of quanta; analysis of paradigms of interpretation and paradoxes in the theory of quanta; construction of generalized coherent states and generalization of the Bargmann scheme; analysis of quantization methods based on generalized coherent states; solving evolution equations, also with fractional derivatives, with the application of operatorial methods; application of anomalous transport models to the description of anomalous diffusion and relaxation processes, in particular in dielectrics.

Department of **Complex Systems Theory** focuses its activities on interdisciplinary research in the following areas: theory of complex systems, nonlinear dynamics, analysis of empirical data, and modelling of biological and socioeconomic systems. In particular, current research is devoted to the following fields: Econophysics, Quantitative linguistics, Neuroscience, Fractal analysis, Complex networks.

In the next paragraphs we present the results of our research, followed by the selected research highlights.

❖

Monte Carlo accounting for transverse momentum dependence of initial state partons. The Division of Theoretical Physics possesses valuable expertise in the calculation of high energy processes at hadron colliders, for which the fraction x of the energy of the colliding hadrons transmitted to the hard scattering process is relatively small. In this situation, the momentum components of the hadron's constituents transverse to the overall momentum of the hadron become non-negligible, and need to be consistently accounted for in the description. This activity is in accord with the recent growing interest in the so-called Transverse Momentum Dependent factorization and TMD parton densities. In particular the tomography of TMD parton densities will be a topic of research at a future collider facility called the Electron Ion Collider.

Essential aspects of the findings reported in the Division have been made publicly available in the form of the parton level Monte Carlo program KaTie. It can generate event files for processes with essentially arbitrary final-state

particles, and differs from other parton-level generators in that it can provide space-like initial-state momenta accompanied with consistent matrix elements. It has subsequently been used in various studies, ranging from the inclusive Drell-Yan process to multi-jet production, both stand-alone and interfaced with parton shower programs, and even including medium effects in ultra-relativistic nuclear collisions. In all cases the description of the data worked very well, thus demonstrating the crucial role of kinematic effects.

Physics at the future electron-positron colliders. Research on various aspects of physics at electron-positron colliders has intensified in the last few years. In particular, the Bhabha cross section at LEP was reanalyzed with the help of the Bhlumi Monte Carlo program. The precision of two key components – vacuum polarization and pair production – was improved. The analysis reduced the cross section and its uncertainty by 0.048% and from 0.061% to 0.037%, respectively. Bhabha cross section was used at LEP to measure the luminosity. As a consequence, the number of neutrino species has been changed in the presented work to 2.9963±0.0074 and the 20-year-old 2sigma tension with the Standard Model is gone. Researchers from IFJ PAN participated in numerous studies related to an electron-positron accelerator proposed as the next big project at CERN – the FCC-ee. In one of the studies the precise path of further reduction of the Bhabha cross section precision down to 0.01% was proposed. The study based on Bhlumi Monte Carlo program identified two key ingredients to be improved: vacuum polarization and improvements of the photon and fermion pair production matrix element beyond second order. Both tasks were judged feasible but they will require technical innovations. Some improvements needed in Bhlumi are already available in other programs (Bhwide) or are available analytically. Another study was devoted to the comprehensive analysis of theoretical precision of several key electroweak observables at the Z-peak and at the WW threshold. The giant increase of statistics from LEP to FCC-ee (10^5 times at Z-peak) calls for theory improvements of 5-200 times. The introductory study showed that it is feasible, but would require new calculations and tools beyond what is available today. The two really difficult observables turned out to be: total cross section at WW threshold and forward-backward asymmetry at Z-peak. Studies dedicated to these two cases were done at IFJ. In the first case the new seminal method of the exponentiation of multiple real and virtual photons from charged W bosons was outlined. All real and virtual infrared singularities in the standard analysis of the perturbative QED (like in classic Yennie-Frautschi-Suura work) are associated with photon emissions from the external legs in the scattering process. A solution was proposed to the long-standing problem of the systematic treatment of the soft and hard photon emission from the unstable charged particles, like W boson, and the interferences between the production and decay parts of the process, at any perturbative order. In the second analysis the important question was discussed whether the effect of interference between photon emission in the initial and final state of the Z boson production and decay process could be removed from the experimental data for the angular charge asymmetry A_{FB} at the precision 100 times higher within resumed perturbative QED calculations. The first quantitative study was done with the help of the KKMC program and a newly developed calculation based on soft photon resummation, matched with NLO and NNLO fixed-order calculations. It was concluded that a factor of 10 improvement with respect to the past state of art (LEP) is obtained and another factor of 10 is feasible. Exploiting the KKMC program, two other studies were also completed. The aim of the first one was to archive four versions of the electroweak libraries, alternative to the one published 20 years ago, which were instrumental for the precision Standard Model calculation from the end of the LEP era till now. They will be used as a reference in the applications/comparisons for the future electron-positron colliders, in particular for the FCC-ee related studies. The main result of the second study was that by means of exploiting the interference between s-channel Z exchange and t-channel W exchange in the e^+e^- X+ process the coupling constant of Z boson to electron neutrino can be measured at the FCC-ee high luminosity with the statistical error of ~1%, that is a factor ~20 better than the present error. The researchers from IFJ PAN contributed actively to the two-year process of preparation of the Conceptual Design Report of FCC-ee, finally published in 2020.

Monte Carlo and phenomenology of Tau lepton and precision electroweak physics. The work on new modelling of tau decays profited in particular from studies on final states with an additional light fermion pair. The new version of tau decay library has recently been installed as part of the Belle2 collaboration software. It was done in mixed Fortran and C++ languages. Electroweak libraries for precision predictions of experiments at LHC, FCC and of the past LEP were revisited, and phenomenological studies were completed to assure the cutting-edge precision for the developed software: KKMC Monte Carlo for FCC and Tauspinner re-weighting tool for

LHC. Studies on machine learning applications were continued, this time in the domain of fitting Higgs CP parity mixing angle.

General Purpose Monte Carlo event generators and LHC phenomenology. One of the greatest challenges for obtaining accurate theoretical predictions to make discoveries in modern HEP comes from the fact that there is a huge gap between the one-line formula of a fundamental theory, like the Lagrangian of Standard Model (SM), and the experimental reality that it implies. General Purpose Monte Carlo (GPMC) event generators have been constructed to bridge that gap. One can think of a GPMC as a "Virtual Collider" that produces simulated collisions similar to those that are produced in the actual LHC experiments, and therefore its results can be directly compared to the experimental data. It is for this reason why not only the Higgs boson discovery but almost all measurements and discoveries in modern HEP experiments have relied on these "virtual" machines[1]. It is clear that these tools are highly valued within the HEP community and will become more important in the future as we explore uncharted territories.

In the past four years significant improvements of Herwig generator were made, leading to the new public release of a program[2] described in details in the publication from 2020. Researchers from the Theory Division have worked on various aspects of the Herwig developments, starting with matching perturbative parton cascades with higher-order matrix elements, and ending with improvements of non-perturbative color structure of an event in hadron-hadron collisions. The latter aspect is one of the least-understood elements needed to describe hadron-hadron events, thus it is responsible for a large uncertainty of the predictions.

Finally, the generator was also used to propose new measurements and to study quark-gluon jet discrimination documented in the publications.

Jet quenching and transverse momentum branching rate. Quantum chromodynamics (QCD) is well-established as the theory of strong interactions. However, there are QCD phenomena that still require better understanding. One of such phenomena is jet quenching observed in the context of RHIC physics, i.e. stopping of a hadronic jet produced in an early stage of heavy ion collisions and propagating through quark-gluon plasma (QGP) which is formed in a later stage of the collisions. With the LHC being in operation, the jet quenching can be observed at much higher available energies in collisions of lead nuclei. Still one of the open problems is to understand the details of the jet–QGP interaction mechanism and the pattern of energy loss. Various approaches have been proposed which differ in assumptions about the properties of plasma and jet–plasma interactions. So far transverse momentum dependence in quenching of jets was largely neglected. The researchers from IFJ PAN, IF UJ and AGH-UST focused on this problem and investigated the generation of transverse momenta via cascades of subsequently emitted jets from an energetic jet traversing QGP. In particular they studied an equation which describes time evolution of longitudinal as well as transverse momenta distributions of gluons emitted from the energetic jet. While the equation was formulated around the year 2010, only its reformulation as a parton shower equation allowed for a solution. The solution was obtained by the newly constructed Monte Carlo program MINCAS. It had interesting physical properties as it turned out not to be Gaussian.

In the follow up study the researchers proposed a factorization formula combining kT-factorization and medium–jet interactions. Using this formula and its implementation in Monte Carlo generators, a study of combined effects of transverse moment a of initial-state partons with transverse moment a of partons in the final state generated because of medium–jet interactions was performed. This approach allowed the scientists at IFJ PAN to address di-jet observables accounting for exact kinematics of the initial state. Using this framework, the researchers provided a description of RAA data and studied azimuthal decorrelations of the produced di-jets. In particular, a novel phenomenon was found, namely that the resulting di-jet observables demonstrate behavior deviating from that of jet-pairs which undergo transverse-momentum broadening following the Gaussian distribution. In the future the framework is going to be generalized to account for quarks and vacuum-like showers that also contribute to the description of the complete final state.

1) The indispensability of GPMCs is demonstrated in the number of citations that they receive from the three main LHC experiments: ATLAS, CMS, and LHCb. As of 28 January 2019, according to the inSPIRE-HEP database, these collaborations published 2252 papers, of which 1888 publications (84%) directly cited one of the main GPMCs: Herwig, Pythia or Sherpa.
2) It is worth mentioning that the document describing the previous release of Herwig [Eur.Phys.J.C 76 (2016)] received sufficient citations to place it in the top 1% within the academic field of Physics, according to Web of Science (WoS). It is the most cited non-experimental publication of the last decade (since 2010) from the IFJ PAN according to Web HEP INSPIRE.

Higher order predictions in Quantum Chromodynamics. A robust framework for calculations of higher order corrections in Quantum Chromodynamics (QCD) for a range of quantities has been created. The approach was developed within the Soft Collinear Effective Theory (SCET), which allows for systematic study of a limit of QCD in which emissions of partons are soft or collinear. It turns out that, in this limit, the cross section factorizes into simpler objects called beam, soft and hard functions. Activities in the Theory Division focused on computing those quantities at higher orders in the perturbative expansion. To evaluate divergent integrals appearing in the calculation, a method based on sector decomposition and differential equations was developed. It required mappings of kinematic variables to be found which would then allow for disentangling the overlapping singularities. The framework was extensively validated. In particular, the results predicted by the renormalization group, which constitutes a direct demonstration of validity of the small-qT factorization at NNLO, were recovered. Therefore, the first complete result for the real and imaginary part of the small-qT soft function at NNLO, which was the last missing element needed to calculate the NNLO cross section for top quark pair production by means of the qT slicing method, was obtained. The researchers further developed the framework to use it for the calculation of the N3LO beam function. This object is even more challenging, hence the need to design a specific sector-decomposition algorithm in order to handle all the divergent integrals. The algorithm was completed, allowing preliminary results to be produced.

Double parton distributions and their evolution. The Large Hadron Collider opened a new kinematic domain for exploring the dynamics of the strong interactions, characterized by large parton densities. In this domain, multi-parton processes with more than one hard parton-parton interaction per one collision of incoming protons are becoming important. The simplest multi-parton process is the double parton scattering. In the QCD description of such a scattering, the double parton distributions (DPDs) play a basic role. They are generalizations of the standard single parton distributions, describing correlations between two partons in the proton. Their QCD evolution in the collinear limit was intensively studied in the years prior to 2017. The natural development of these studies was to go beyond the collinear limit by taking into account the transverse momentum dependence of the double parton distributions. Following the method of Kimber, Martin and Ryskin, the transverse momentum dependent unintegrated double parton distributions (UDPDs) were theoretically constructed from the DPDFs by the group. Then, their QCD evolution, i.e. the dependence on factorization scales, was analyzed using a numerical program which was constructed for this purpose. In particular, the issue of factorization of the UDPDFs into a product of two single unintegrated parton distributions was addressed. Surprisingly, the so-called splitting term in the evolution equations appeared to be crucial for such a factorization at small values of the parton momentum fractions.

The Drell-Yan process as a probe of QCD dynamics. The Drell-Yan (DY) lepton pair production is one of the most important processes to study the QCD dynamics of the colliding hadrons. One of the most interesting aspects of this dynamics is the so-called BFKL evolution which results from the high energy limit of QCD. The BFKL evolution was intensively studied at the ep collider HERA and is also important at the pp collider LHC for carefully selected processes. One of such processes is the DY pair production accompanied by a jet separated by a large rapidity interval, proposed by researchers from IFJ PAN and IF UJ. It was shown that the dependence of the cross section on the azimuthal angle between the transverse momentum of the DY pair and the jet is a good indicator of the BFKL dynamics as well as the angular dependence of the DY structure functions.

In the follow-up studies, the low mass lepton pair DY production was investigated, using the CCFM-K evolution equations with coherence encoded in angular ordering of parton emissions. It was shown that the resulting transverse momentum dependent parton distributions (TMDs) allow for a successful description of lepton pair spectra in transverse momentum up to the values equal to the lepton pair mass, which is not the case for the TMDs without coherence.

Partonic structure of the pion. In the on-going studies of partonic structure of hadrons undertaken by researchers from IFJ PAN and the University of Granada, the double parton distributions (DPDFs) of the pion in effective chiral quark models were investigated, resulting in a deeper understanding of the properties of DPDFs, such as the pertinent Gaunt-Stirling sum rules. The so-called good lattice cross sections of the pion, which are specific correlators yielding information on the partonic Ioffe-time distributions, were also examined. The results compare very favorably to recent lattice QCD data.

Low energy multichannel interactions. Studies of CP violation and of final state interactions in D0-meson decays into a kaon and two charged pions measured at BaBar were undertaken by researchers from IFJ PAN in collaboration with the LPNHE Laboratory in Paris. The heavy-meson decay amplitudes were constructed in the QCD factorization framework. Unitarity plays an important role in constraining the number of free parameters required in the description of experimental data obtained in D-meson factories.

Multichannel two-meson interactions below 2 GeV were studied. A full set of partial wave amplitudes was constructed and tested by comparison with experimental data and the crossing symmetry constraint. A scalar-isoscalar form factor was calculated and compared to experimental data and with theoretical constraints. The spectrum of light mesons decaying into various two meson channels was investigated using newly derived theoretical amplitudes. The contribution of multi-channel two-meson scattering to the final Y-meson family decays was calculated and compared with the available data and with various theoretical predictions.

The photoproduction of resonances and two-meson interactions below 2 GeV was investigated for the S, P and D waves. The results of the Born approximation and of analysis with the final state interactions were compared. For this purpose, previously obtained unitary multichannel amplitudes and the amplitudes with crossing symmetries were used. These predictions were compared with experimental data from CLAS12 and GlueX. Amplitudes for photoproduction on the nucleon processes were calculated for application in the Jefferson Laboratory and compared with the data.

Physics of heavy-ion collisions and quark-gluon plasma. The physics of relativistic heavy-ion collisions aims at answering one of the most fundamental problems in modern physics, namely understanding the structure and properties of nuclear matter in extreme conditions. Quantum chromodynamics (QCD) states that partons forming nucleons at high temperatures or densities undergo the so-called asymptotic freedom phenomenon, according to which they are liberated creating a new state of hot and dense strongly-interacting matter dubbed the quark-gluon plasma (QGP). The properties of this exotic state of matter are of great interest to the physics community as it is commonly believed that it existed in the early Universe and forms the cores of compact stellar objects. Similar physical conditions may be reproduced in laboratory conditions by colliding head-on bare heavy nuclei at relativistic speeds in the collider facilities, such as Relativistic Heavy- Ion Collider (RHIC) at BNL and the Large Hadron Collider (LHC) at CERN, as well as at somewhat lower energies at fixed-target experiments, such as HADES at GSI and NA61/SHINE at CERN. The studies performed by the researchers at the Department of Structure of Matter Theory in collaboration with theorists from other leading institutions (GSI, FIAS, INFN, NISER, Illinois Univ., CERN, Tech. Univ. Darmstadt) are primarily focused on constructing the theoretical and phenomenological models which may be used for the description of the systems produced in experiments as well as for the interpretation of the extracted data. One of the most successful theoretical descriptions of the collective behavior observed in these processes is provided by relativistic hydrodynamics. The current focus of the community is on further improvements of the models to correctly include bulk viscous effects and higher-order transport coefficients. The main goal is to constrain key properties of the QGP and to provide a reliable soft-background model of evolution required to compute QGP modification of hard probes, such as jets or heavy quark bound states.

Matter and space. Conceptual, philosophical, and phenomenological issues concerning the expected connection between the properties of matter and the nature of macroscopic space have been discussed at some length and from a couple of standpoints.

Assuming the Aristotelian view of space as an attribute of matter, it was argued that the research on the possible quantum origin of space should not be restricted to the experimentally inaccessible miniscule Planck length scale of 10^{-33} cm. It was furthermore pointed out that important relevant information on the issues of the nature and possible emergence of space is most likely hidden in the spectrum and at the distance and mass scales of elementary particles (leptons, quarks, and hadrons) [Foundations of Science 24 (2019) 287–305]. The supporting arguments included: a novel generalization of the concept of mass, phenomenological hints on the spatial structure of excited baryons, and the discussion of what are the possibly most natural values of the fundamental mass and distance scales. The arguments involved in particular a discussion of the phase-space-based explanation of the Harari-Shupe rishon model of fundamental fermions, the surprising regularities observed in the mass spectra of leptons and quarks [Open Phys. 16 (2018) 427-429], and the question of the relevance of different fundamental physical constants, such as: h - the quantum constant and a variety of space-related constants (i.e. c – the

speed of light, G – Newton's gravitational constant, – the cosmological constant, or a_M - the MOND limiting acceleration scale) [Mod. Phys. Lett. A 34 (2019) 37, 1950306].

Weak radiative hyperon decays. Triggered by a recent paper, the issue of weak radiative hyperon decays was discussed anew. The contribution from the intermediate (1405) state was analyzed in some detail. It was pointed out that the measurement of the n decay asymmetry could resolve the encountered ambiguities and definitely answer the question of whether Hara's theorem is violated or not [ActaPhys. Pol. B51(2020)2111].

Selected Research Highlights of the Division of Theoretical Physics

One question regarding the internal structure of hadrons is what happens with the density of its constituents, gluons in particular, for small values of the energy fraction x. The density is expected to stop rising for decreasing values of x, referred to as saturation. On the theoretical side, saturation is incorporated via non-linear evolution of the density, or more precise - the parton density function (PDF), with the energy scale. On the experimental side, it is for example expected to be observed in the forward production of jets. Such final-state configurations imply that one of the colliding hadrons was acting as a dilute probe, with only a few but highly energetic constituents, while the other was acting as a target densely populated with low-energy gluons. In particular those observables which are sensitive to the transverse momentum of the low-x gluons are expected to be indicators of saturation. One of those indicators is the angle between the two jets in the plane transverse to the momenta of the colliding hadrons. **Using the previously formulated ITMD factorization and accounting for resummation of soft gluons in terms of the Sudakov form factors, researchers from IFJ PAN successfully described in [Phys.Lett.B795(2019)511-515] spectra of angular decorrelations of forward-forward di-jets in p-p and p-Pb collisions. The description provided strong further evidence for the onset of nonlinear effects once the gluonic fields become large.** (Fig. 4.1). This result was also reported by the EurekAlert.

In analogy to the nucleon structure, which can be described by parton distribution functions (PDFs), the quark and gluon content of atomic nuclei can be described in terms of nuclear PDFs (nPDFs). We know that such nPDFs are modified compared to the PDFs of free protons. The form of such modifications is quite well measured in the case of quarks, where we distinguish four different regions: shadowing region, anti-shadowing region, EMC region, Fermi-motion region. Analogical behavior is expected to be present for gluon nPDFs; however, this is much less confirmed in particular for the shadowing and anti-shadowing regions. In a recent work [Phys. Rev. Lett. 121 (2018) 5, 052004] **it was shown with minimal statistical significance of 7-sigma that the nuclear gluon parton distribution is indeed shadowed.** (Fig. 4.2). The novel use of the LHC heavy-flavor (D, J/Psi, B->J/Psi, Upsilon(1S)) data from proton-lead collisions allowed us also to corroborate the existence of gluon

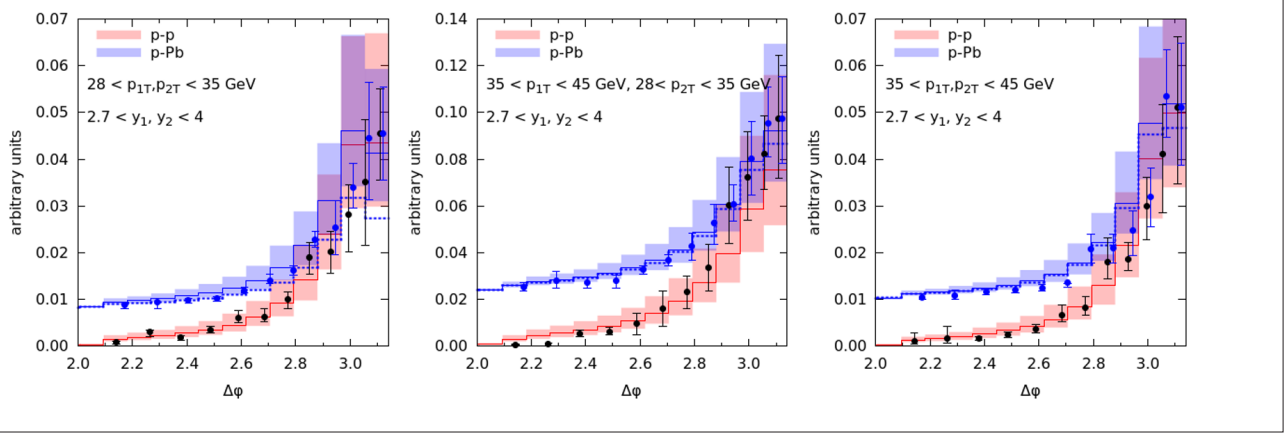

Fig. 4.1 Broadening of distributions in p−Pb collisions vs p−p collisions for different sets of cuts imposed on the jets' transverse momenta. The plots show normalized cross sections as functions of the azimuthal distance between the two leading jets, [from Phys. Lett. B 795 (2019) 511-515, under CC-BY 4.0].

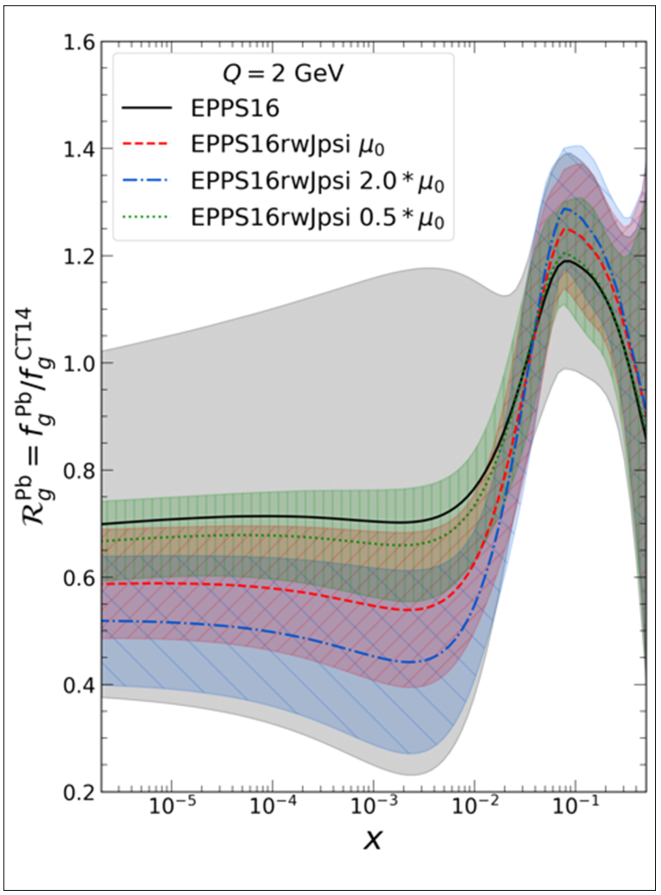

Fig 4.2. The figure shows nuclear modification factor for lead nucleus which is a ratio of lead nPDF to a PDF of a free−proton. The large grey band quantifies the initial uncertainty of such a modification as described by the EPPS16 nPDFs. The red, blue, and green bands show the corresponding nuclear modifications after including the (a) D−meson, (b) J/psi−meson heavy−flavor LHC data into the analysis. The colored bands quantify the additional uncertainty due to the factorization scale which in the case of heavy−flavor data is of big importance. It is clear that after including the new data the uncertainty of the gluon distribution is very much reduced and the obtained gluon nPDF is shadowed (at small x values nuclear modification is smaller than one) [Phys. Rev. Lett. 121, 052004 (Creative Commons Attribution 4.0 International license)].

anti-shadowing and showed that such data have great potential to dramatically improve our knowledge of the nuclear gluon distribution.

Unexpectedly, low viscosity of the quark-gluon plasma has been revealed**.** One of the issues faced by practitioners of traditional second-order viscous hydrodynamics is that the quark-gluon plasma (QGP) possesses a high degree of momentum-space anisotropy arising because of its initial rapid expansion in the beam-direction. In this case viscous hydrodynamics is being pushed to its limits, resulting in rapidly growing uncertainties of its predictions. As a way to address these problems, it was proposed to reorganize the hydrodynamic expansion in a way that the intrinsic anisotropies are treated non-perturbatively – this method was developed at IFJ PAN in a seminal work [Phys. Rev. C 83 (2011) 034907] and became known as anisotropic hydrodynamics. A recent joint work of Polish and American groups [Phys. Rev. Lett. 119, 042301 (2017)] based on anisotropic hydrodynamics framework, for the first time confronting realistic theoretical predictions (aHydroQP) with actual measurements, shows that **the anisotropic hydrodynamics is able to provide the most accurate description of the phenomena occurring in QGP**. In particular, it was possible to obtain an excellent description of the soft-hadronic observables (see Fig. 4.3) with a much smaller value of the bulk viscosity than in previous studies. These phenomenological results suggest that, if non-conformal aspects are carefully taken into account, one can obtain a very good description of many key heavy-ion observables with the values of the physical parameters characterizing QGP, which are quite different from the previously extracted ones.

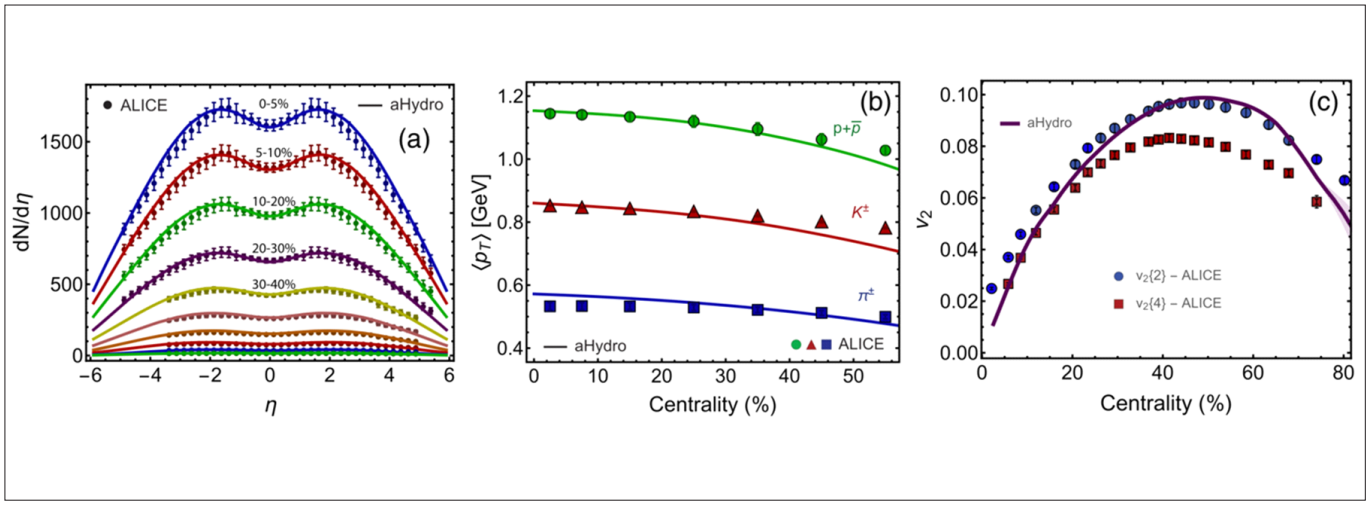

Fig. 4.3 Three panels showing (a) the charged−hadron multiplicity in different centrality classes as a function of pseudorapidity, (b) the average transverse momentum of pions, kaons, and protons as a function of centrality, and (c) the integrated v2 for charged hadrons as a function of centrality. All results are obtained with anisotropic hydrodynamics aHydroQP for 2.76 TeV Pb−Pb collisions. Data in panels are from the ALICE Collaboration [from Phys. Rev. Lett. 119, 042301 (2017), APS Reuse and Permissions Licence].

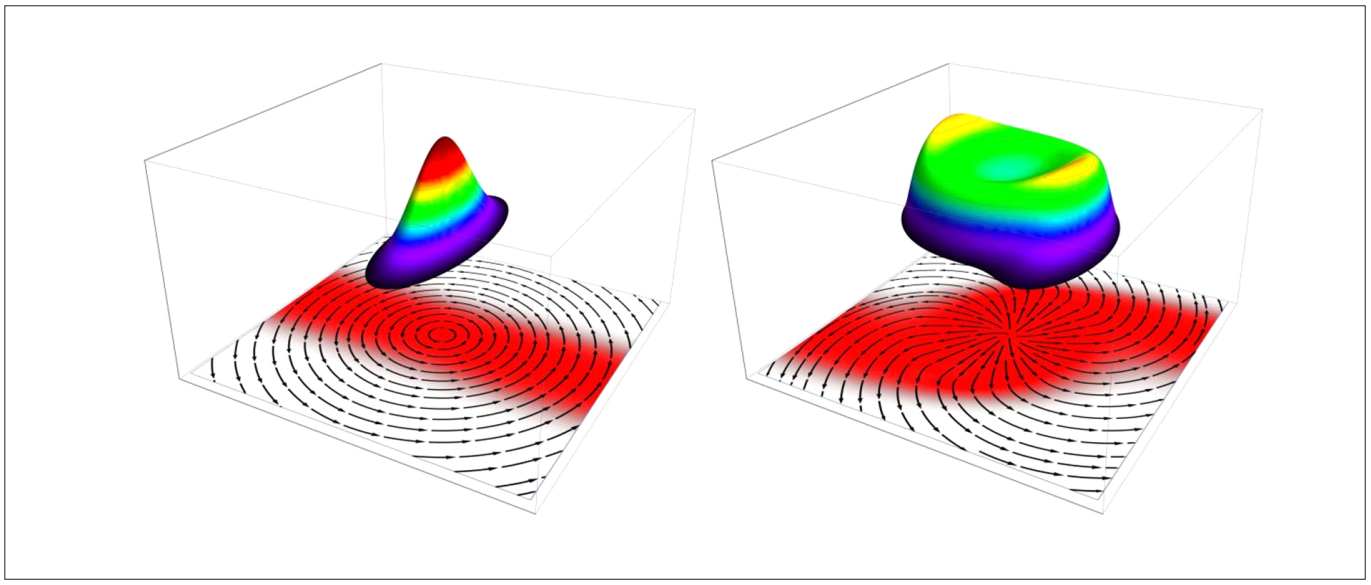

Fig. 4.4 Ultrarelativistic flow of quark−gluon plasma with spin. On the left, the initial state of the system, on the right −− the result of hydrodynamic evolution. The arrows on the bottom view show the plasma flow lines. The red area is the region of polarized particles that evolves according to the flow of matter. The top graphs show plasma temperature profiles.

It is known that fireballs created in non-central heavy-ion collisions possess large global angular momenta which may generate a spin polarization of the quark-gluon plasma (QGP) in a way resembling the magnetomechanical effects of Einstein-de Haas and Barnett. It has been suggested that the latter should be reflected in the finite global polarization of the hadrons emitted from the system, such as lambda hyperons and vector mesons, thus providing unique access to the purely quantum phenomena in relativistic systems. Much effort has recently been invested in studies of such systems, both from the experimental and theoretical points of view. While recent works have contributed significantly to our understanding of global equilibrium and stationary states, no hydrodynamical framework has been developed so far which would allow for space-time evolution of polarization effects. The first relativistic hydrodynamic model for the evolution of the polarized system of charged particles with spin 1/2 was first discussed in 2018 by the group in collaboration with researchers from IFJ PAN. However, only now, **it has been shown** [Prog.Part.Nucl.Phys. 108 (2019) 103709] **how the conservation laws can be used to construct formalism for the spin-polarized fluids in a fully consistent form** (see Fig. 4.4.). Moreover, it was found that the description of spin in the hydrodynamic models is tightly connected with other intriguing problems related to the so-called pseudogauge transformations and localization of energy in quantum systems. The newly proposed hydrodynamics with spin sheds more light on the relations between these concepts as well as provides a new practical tool to study the properties of the strongly-interacting matter under extreme conditions,

Initial deformation of a quark-gluon plasma droplet can be tuned with polarized deuterons. Understanding of the origin of collective correlations in collisions involving small nuclei is one of the most important and actively pursued topics in the field of ultra-relativistic nuclear collisions. It is widely believed that studies of such systems can provide the limits of applicability of relativistic hydrodynamics, as well as scrutinize more fundamental QCD-based approaches, such as the color glass condensate. In an article [Phy. Rev. Lett. 121(2018)20,202301] it was proposed to study collisions of polarized deuterons with heavy nuclei. Owing to the D-wave admixture in the wave function, the polarized deuteron is a spatially-deformed object (see Fig. 4.5). **A collision of the polarized deuteron with a „wall" of a heavy nucleus forms a correspondingly deformed initial fireball, which then via hydrodynamic expansion yields azimuthal asymmetry in the spectra of emitted hadrons.** The fixed target AFTER@LHC experiments, planned after the LHC Long Shutdown 3, in particular SMOG2@LHCb, will be able to study collisions of the 2.76 TeV Pb beam on polarized deuterium targets, giving an opportunity to observe our effect. The straightforward measurement of the angular distributions with respect to the polarization axis would provide an unequivocal way to probe the mechanism responsible for the observed collectivity in small systems.

Punctuation plays a key role in the linguistic networks. Natural language is commonly considered the principal trait of humanity. At the same time, it constitutes one of the most vivid examples of complex systems where

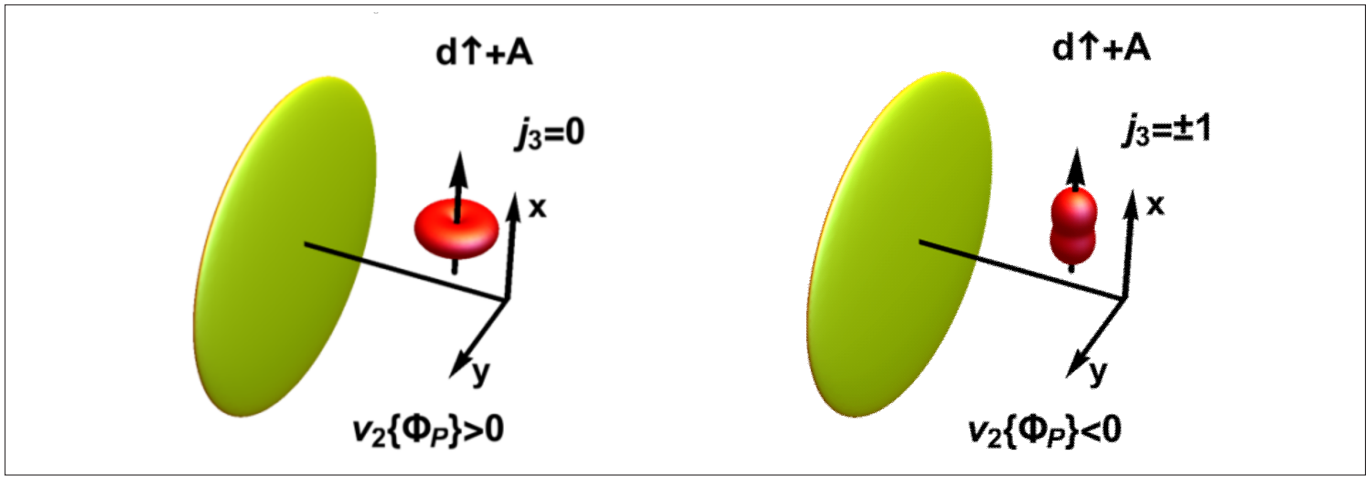

Fig. 4.5 Schematic view of the ultra−relativistic collision of a heavy nucleus on the deuteron target polarized along (j3 = ±1, left) and perpendicular (j3 = 0, right) to the fixed polarization axis $_P$. The deformation of the created fireball in the transverse plane reflects the intrinsic deformation of the polarized deuteron. The collective shape−flow transmutation mechanism results in the one body elliptic flow coefficient with respect to the polarization axis, $v_2\{\ _P\}$, with the signs as indicated in the figure [adapted from Phy. Rev. Lett. 121(2018)20,202301 under APS Reuse and Permissions License].

the term *more is different,* like no other, succinctly reflects its essence. Indeed, the relatively small number of elementary items, the phonemes and letters, allows one to express virtually an infinite amount of information. Mapping the linguistic expressions into writing requires the use of punctuation; otherwise some expressions might be ambiguous and deceptive. Punctuation also allows one to denote separate logical units into which any compound message can be divided. From this perspective, the punctuation marks are something more than merely technical signs serving to allow a reader to comprehend the consecutive pieces of texts more easily. **It appears** [Information Sciences 375 (2017) 98–113] **that, from a statistical viewpoint, the punctuation marks reveal properties that are qualitatively similar to the properties of the most frequent words like articles, conjunctions, pronouns, and prepositions**. This refers to both the Zipfian analysis and the network analysis. By adding the punctuation marks to the Zipf plots, it is shown (Fig. 4.6) that these plots that are normally described by the Zipf–Mandelbrot distribution largely restore the power-law Zipfian behavior for the most frequent items. These results indicate that the punctuation marks can fruitfully be considered in the linguistic studies as their inclusion effectively extends dimensionality of an analysis and, therefore, it opens more space for a possible manifestation of some previously unobserved effects.

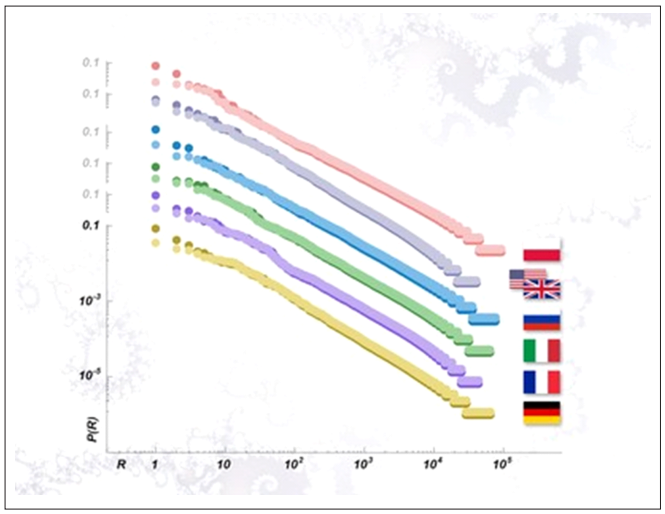

Fig.4.6 Probability of occurrence of words (vertical axis) versus their rank (horizontal axis) for corpora representing different European languages. The original puzzling downward departure from the straight line for ranks close to unity, observed for the ordinary words (brighter colors), disappears (corresponding darker colors) when the punctuation marks are also taken into account.

Essential features of many real-world systems can be expressed by networks. A written text can be represented by a network whose nodes correspond to the words and links among them are determined by their co-occurrence, as an example shown in Fig. 4.7 and 4.8 indicates. Though simple in construction and intuitive, they carry within their structure exploitable information on the underlying language sample. **Constructing such networks from English and Polish literary texts and studying their properties** [Information Sciences 482 (2019) 301-320], **and then determining the resulting relations through dendrograms have led to the possibility of identifying groupings of the texts and thus distinguishing individual writing styles. The fact that the presented approach works well for both Polish and English texts suggests that it can probably be treated as applicable to a vast group of languages – as Polish and English are examples of the languages**

Fig.4.7 The author of an unsigned text can be identified by analyzing the network relationship between just a few most frequent words of the text, provided the punctuation marks are also included. (Elsevier license terms and conditions).

substantially different from each other, in terms of the origin, morphology, and grammar features.

Entanglement is hiding in particle indistinguishability. Intuition suggests that a necessary condition for the emergence of entanglement is the requirement that at some point in their evolution the particles touch one another or, at least, indirect contact should take place through another particle or physical field to convey the interaction. How else can they establish this mysterious bond, which is quantum entanglement? Paradoxically, however, it turns out that this is possible. **Quantum mechanics allows entanglement to occur without the need for any, even indirect, contact.** The research shows that activation of particle entanglement from their fundamental indistinguishability is possible and can be directly observed.

To justify such a surprising conclusion, a scheme should be presented in which the particles will show non-local

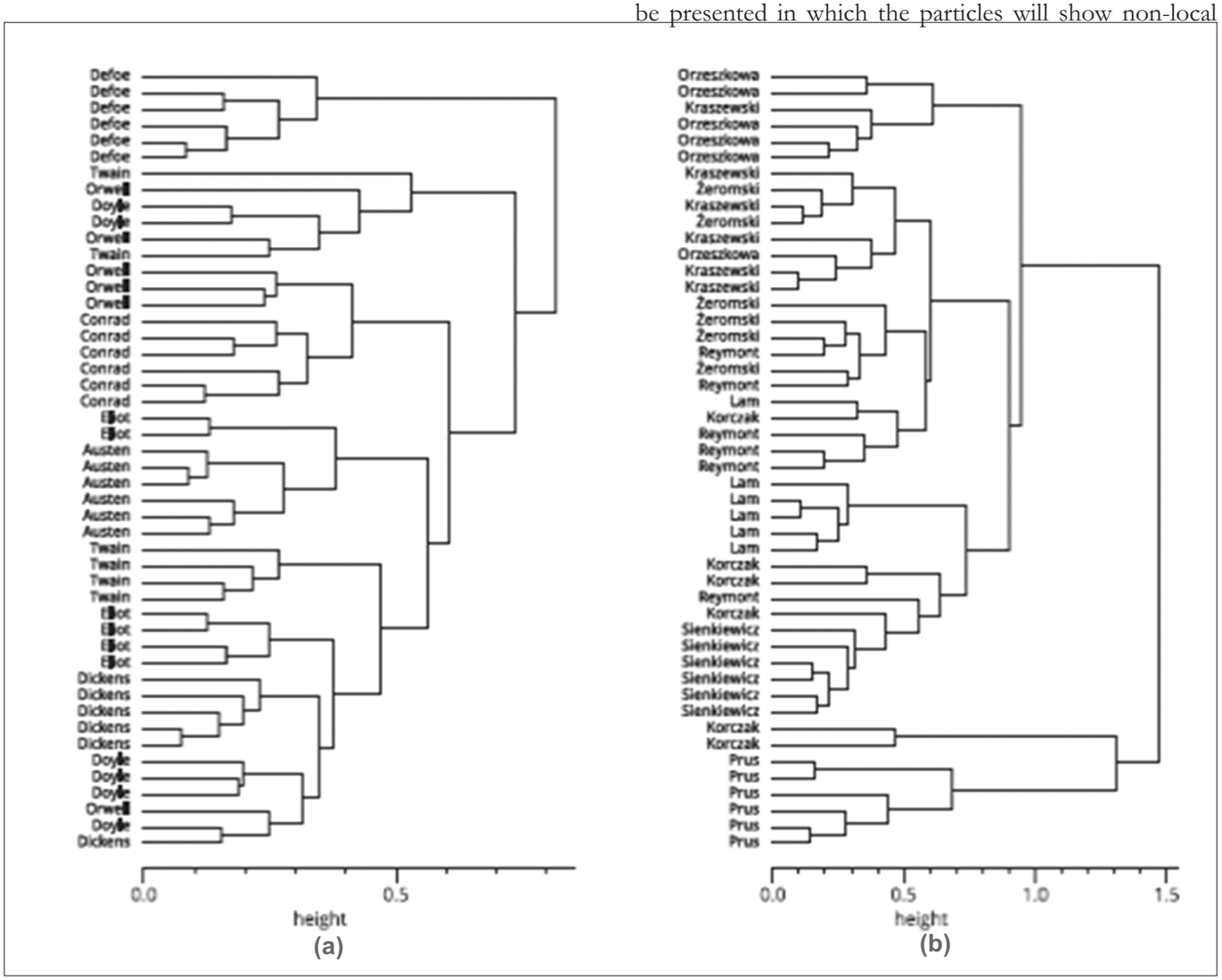

Fig. 4.8 The dendrograms of the hierarchical clustering of (a) English and (b) Polish different books in the space of the weighted clustering coefficients of networks' nodes corresponding to 12 most frequent words and punctuations marks. Each text is labelled by the surname of its author. (from [Information Sciences 482 (2019) 301-320] under Elsevier license terms and conditions).

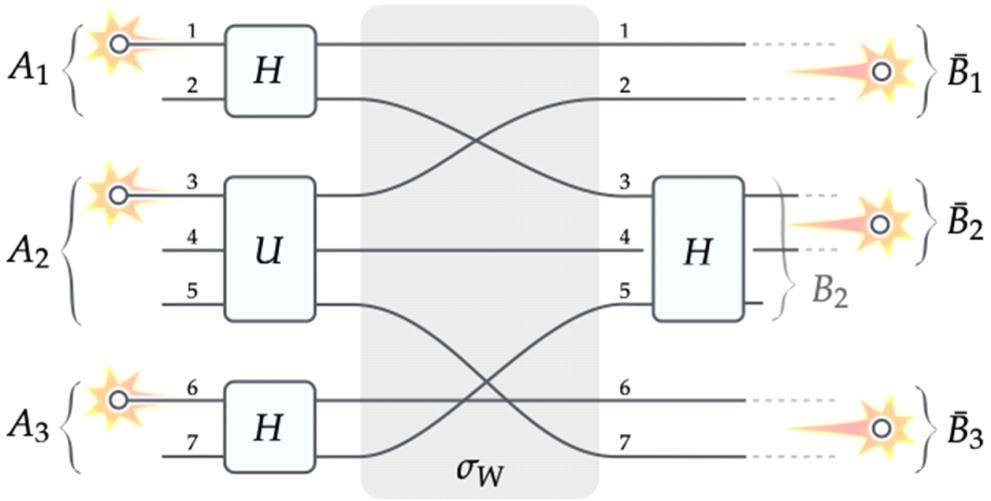

Fig 4.9 Three independent particles injected on the left follow the path in a simple optical circuit. Post−selection at the end guarantees that the particles never touched each other along the way. The scheme generates a nontrivial entangled state of three particles on the right, the so−called W state [from Scientific Reports 9, 20131 (2019) (Under CC-BY licence 4.0)].

correlations at a distance (in a Bell-type experiment). The subtlety of this approach is to exclude the possibility of an interaction understood as some form of contact along the way. Such a scheme should also be very economical, so it must exclude the presence of force carriers which could mediate this interaction (physical field or intermediate particles). In an article Scientific Reports 9, 20131 (2019) it is shown how this can be done. The authors' approach consists of a clever permutation of paths traversed by the particles which start from independent sources and undergo post-selection at the end of the procedure (see Fig.4.9) . This new paradigm allows generating any entangled states of two and three particles avoiding any contact. The proposed approach can be easily extended to more particles.

Within this framework indistinguishability of particles presents itself as a useful resource of entanglement accessible for practical applications. On the foundational side, it is interesting to see how an innocuous symmetrisation postulate for identical particles takes flesh and in its pure form leads to the consequences observed in laboratories.

❖

5. Division of Interdisciplinary Research

The research performed at the **Division of Interdisciplinary Research** is focused on three main areas: life and health science, culture heritage, and material science. The Division consists of four Departments which carry out their research using mainly vibrational spectroscopy, magnetic resonance imaging, ion, X-ray, and synchrotron radiation microprobes, sophisticated X-ray spectroscopies at Free Electron Laser facilities, and atomic force microscopy (AFM). In addition, the classic cytogenetic and molecular cytogenetic techniques are applied to studies in the health science area. The Departments are equipped with modern world-class apparatus which include:

NanoIR2 system which in this configuration is the only one in Poland and the second one in the world. It combines Fourier Transform – InfraRed spectrometer providing chemical sensibility with AFM precision. The system configuration with two lasers (OPO and QCL) enables performing analysis in the broad spectral range for various types of samples even of the size and thickness of a nanometer.

The integrated RAMAN-AFM system for performing Raman microspectroscopy and Raman nanospectroscopy. It has equipment for in vivo cell measurements.

Vacuum FTIR spectrometer equipped with vacuum IR microscope, bolometer, MCT and FPA detectors that allow us to perform both spectra acquisition and mapping in transmission, reflection as well as ATR modes.

FTIR fast imaging microscope equipped with MCT, MCT linear array and DLATGS detectors.

Atomic force microscope (AFM) combined with the fluorescence microscope capable of measuring live cells properties in aqueous media, suitable for all AFM-based experiments, including those on living cells.

UV-VIS spectrometer with plate reader - for the use of multiple absorption, fluorescence and luminescence markers.

RT-PCR system Real Time (Reverse Transcription) Polymerase Chain Reaction for the real-time RNA sequence expression measurements. Used in dosimetric, and spectroscopic studies.

System for automatic analysis of chromosome aberrations – AxioImager.Z2 microscope that serves to automatically detect chromosomal aberrations and identify chromosomes.

2.5 MV van de Graaff accelerator providing a proton microbeam for spatial imaging of biological and environmental materials.

Hamamatsu X-ray tube providing a 2 mm X-ray beam for computer microtomography imaging and investigation of microstructures in complex systems.

Two X-ray tubes in Von Hamos geometry making it possible to perform XAS and XES measurements simultaneously.

Bruker Biospec Magnetic Resonance Imaging scanner.

The research performed at the Division would not be so successful without broad international collaborations that include: Paul Scherrer Institute, Villigen, Switzerland; Uppsala University, Sweden; Wigner Research Institute, Budapest, Hungary; PTB Berlin Germany; University of Vienna, Austria; Extreme Light Infrastructure, Prague, Czech Republic; SACLA Facility, Japan; European XFEL and DESY, Hamburg, Germany; SwissFEL, Villigen, Switzerland; Linac Coherent Light Source, USA; Université Paris-Saclay, and Newcastle University, UK.

❖

The **Department of Experimental Physics of Complex Systems** deals with interdisciplinary studies in the fields of biology, medicine, culture heritage, and environment protection using mainly vibrational

microspectroscopy. The classic cytogenetic method is also applied to study biomedical subjects.

The research carried out with the use of new devices purchased within the frame of the project co-funded by the Małopolska Regional Operational Programme Measure 5.1 Krakow Metropolitan Area, as an important hub of the European Research Area for 2007-2013, No. MRPO.05.01.00-12-013/15, sheds new light on the possibility of imaging various types of complex systems with micro- and nano-scale spatial resolution.

Atomic Force Microscopy (AFM), in combination with an infrared spectrometer (NanoIR-2), plays a crucial role in our studies and further extends the experimental capabilities of the Department. It has to be emphasized that this is the only one such a spectrometer in Poland.

The wide spectrum of research activities is undoubtedly of great social importance in the field of health and environmental protection. The research is also carried out in the inter-domain collaboration with specialists from different Polish and international institutions.

One of the research paths in the field of biomedicine relates to the analysis and modeling of drugs/metal nanoparticle systems using advanced vibrational spectroscopic methods. This line of research aims to analyze and develop innovations in the cellular response to drug treatment and to study the cell sensitivity to anticancer agents. Another topic of research carried out by our Research Team involves the use of drug nanocarriers to increase the effectiveness of their delivery to the target sites. Simultaneously, we perform the analysis of ionizing radiation influence on living organisms by determining the biochemical alterations in cells subjected to irradiation. Special emphasis has to be placed on studying the effects of changes in lymphocytes as a result of ionizing irradiation.

Moving from the cellular level to higher-order structures, we explore changes in tissues and body fluids that have been damaged by disease processes. Therefore, it is extremely important to search for spectroscopic markers of pathological changes, which play a key role not only in the diagnosis of a disease but also provides a better understanding of the disease development basis.

Another branch of research is devoted to investigation of the modified biomaterials. In this case we focus on the study of various surface modification factors that affect the corrosion processes of materials.

The Department also conducts research in the field of broadly understood protection of cultural heritage through interdisciplinary cooperation on the border of physics, chemistry, and art history. The use of advanced methods of vibrational spectroscopy turns out to be extremely effective not only in determining the composition of the tested material, but also in the assessment of the progressive degradation process of the work. It helps conservation and renovation treatments to be planned better, and gives an opportunity to obtain valuable information about the origin and history of the tested object.

In 2019 a part of the Department of Experimental Physics of Complex Systems was converted into the **Department of Applied Spectroscopy**, which explores the properties of X-rays in applied and fundamental research. Particularly, the research focuses on studying processes occurring in biological systems at the cellular and molecular level using synchrotron facilities, free electron lasers, and classical X-ray sources. Furthermore, X-ray research is explored for real-time determination of electron dynamics and electronic structure of atoms and molecules in energy related materials. Fundamental studies are oriented towards investigating X-ray interactions with matter and studying multiple ionization processes with the use of X-ray laser pulses. A large part of X-ray research is devoted to the development of the laboratory setups that would allow XAS (X-ray Absorption Spectroscopy) and XES (X-ray Emission Spectroscopy) techniques to be applied simultaneously to electronic structure determination of the studied material. The setup is designed in Von Hamos geometry. It is worth mentioning that our laboratory setup offers XAS/XES measurements on liquid-jet samples as the only one in Poland.

Research in the Department of Applied Spectroscopy is further focused on exploration and application of X-ray Free Electron Lasers (XFEL) to study time-resolved phenomena in biological and chemical systems as well as to investigate fundamental mechanisms driving X-ray interaction with matter. The Department contributes to the global effort to develop the diagnostics methods dedicated to femtosecond X-ray pulse measurements and takes part in developing techniques for performing single- and shot-to-shot X-ray spectroscopic measurements. The Department of Applied Spectroscopy exploited the first available X-ray Free Electron Lasers world-wide: Linac Coherent Light Source in US and SACLA facility in Japan. Since 2018, the Department staff have been exploring newly opened European XFEL laser facilities and have contributed to the success of the first experiment executed at the SwissFEL X-ray Laser at Paul Scherrer Institute in Switzerland. The Department also takes part in research and technique developments at the FXE station of the European XFEL in Hamburg, Germany, for example in

a joint effort to develop an X-ray diagnostic instrument dedicated to single-shot X-ray energy distribution measurements.

In general, our basic research is complemented with X-ray microscopy studies and methods using ion beams from a 2.5 MeV Van de Graaff accelerator for spatial imaging of biological and environmental materials, determining their elemental and chemical compositions. In addition, we perform experiments with the use of computed microtomography, including phase contrast tomography allowing 3D imaging of low contrast objects.

The research conducted at the **Department of the Biophysical Microstructures** mainly focuses on mechanical, micro-, and macro-rheological, and adhesive properties of single molecules, individual living cells and tissues, including cancer cell lines, neoplastic, and tumor tissues. The basic methods used are atomic force microscopy (AFM) to assess properties at the nanoscale and a rheometer working at the macroscale. A wide range of other fluorescent microscopy methods, such as live-cell imaging system, cell viability assessments (ELISA reader) and Western blots, is also applied to complement the studies. Within the scientific interest of the Department are such issues as biophysical and biochemical cues in cancer progression, drug effectiveness measured through biomechanical parameters, alterations of mechanical and rheological properties in non-cancer related diseases (muscular dystrophy, multiple sclerosis) and lung diseases (asthma or COPD).

In the **Department of Magnetic Resonance Imaging**, interdisciplinary biomedical and material problems are investigated as well as new MRI techniques are developed. The main MRI research system is the Bruker Biospec MRI scanner, based on a 9.4 T horizontal magnet, equipped with gradient coils capable of generating magnetic field gradients up to 1.5 T/m, and with a number of dedicated ^{1}H, ^{31}P, ^{19}F, ^{13}C and ^{129}Xe RF probe heads, including the CryoProbe™. This system is also equipped with an advanced animal monitoring and control system and is used predominantly for interdisciplinary biomedical studies *in vitro* or *in vivo* based on animal models of civilization diseases. Another area of research is focused on the properties of novel theranostic drug nanocarriers, MRI contrast agents, and pharmaceutical dosage forms. Apart from biomedical and material studies, the Department staff also concentrate their efforts on the design and development of dedicated actively shielded gradient coils and RF coils.

Selected Research Highlights of the Division of Interdisciplinary Research

One of the directions towards the enhancement of cancer therapy is to develop a more precise supply of the therapeutic agents to the target cells. The main goal of this research was to **improve cancer therapy through the use of well-defined drug/carrier conjugates as an effective drug delivery system**.[1)]

This approach entails two important benefits. First, the more effective accumulation of the therapeutic agent inside the tumor cells, the greater antitumor efficiency. Second, the more controlled distribution of the drug, the lower its concentration necessary to achieve the cytotoxic effect. This should prevent the patient from bothersome side effects. The crucial factor determining the design of the stable drug/carrier conjugates is the precise characterization of how the drug adsorbs on the potential carrier surface. Even the smallest perturbation in the structure of the drug molecule can affect its biological activity. The conducted research is focused on the drugs used in non-small cell lung cancer therapy and on the application of metal nanoparticles as their effective vehicles. Owing to the surface plasmon resonance effect of metal nanoparticles, the performed surface-enhanced vibrational spectroscopy investigations enable comprehensive analysis of how the drug anchors to these potential carriers and how this connection is affected by such factors as pH conditions, temperature, time of incubation, drug concentration, presence of the nanoparticles stabilizers on the metal surface.

In our efforts to characterize the molecular structure of the erlotinib drug and its adsorption behavior changes on the silver and gold nanoparticles (stabilized using different

1) This research was supported by the National Science Centre, Poland (Grant no. 2016/21/D/ST4/02178). The measurements were performed using the equipment purchased in the frame of the project co-funded by the Małopolska Regional Operational Program Measure 5.1 Krakow Metropolitan Area as an important hub of the European Research Area for 2007-2013, project no. MRPO.05.01.00-12-013/15.

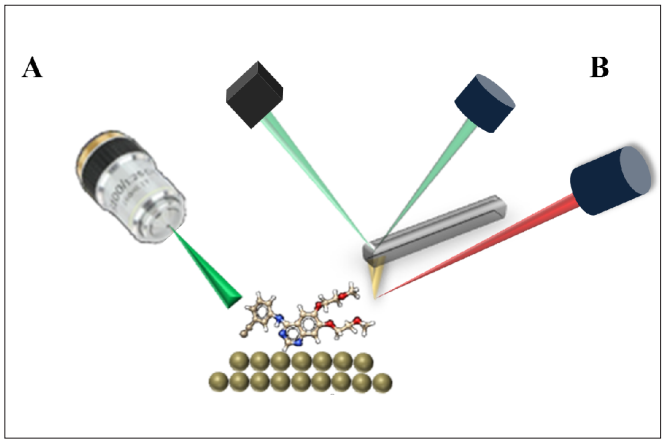

Fig. 5.1. Experimental scheme of SERS (A) and AFM−IR (B)

reagents) under the conditions mentioned above, we used the following advanced techniques/methods: Raman spectroscopy, Fourier transformed infrared spectroscopy, surface-enhanced infrared absorption (SEIRA) and surface-enhanced Raman (SERS) spectroscopies, and atomic force microscopy in combination with IR (AFM-IR) (see an experimental scheme in Fig. 5.1).

The performed analysis indicated that in the acidic environment the protonation of the –NH+ and –C=N+ groups of erlotinib takes place [J. Spectrosc. 2019 (2019) 9191328]. This had an influence on the adsorption of erlotinib on the investigated nanoparticles. Briefly, the strong interaction of erlotinib *via* the N-C bond with silver nanoparticles (AgNPs) was characterized in the acidic medium, while for neutral and alkaline environments this interaction occured mainly through the C C bond [J. Raman Spectrosc. 49 (2018) 1265; Spectrochim. Acta A 228 (2020) 117737]. Additionally, extending the drug/metal nanocarrier incubation time weakens the drug-nanocarrier linkage. This is especially noticeable at 37 C.

Additionally, the investigations (spectra collection and chemical maps acquisition) at the nanoscale conducted with the use of the AFM-IR technique provided possibilities to describe the adsorption process of erlotinib on the metal monolayers consisting of 15 nm silver and gold nanoparticles, respectively, with the resolution of a single metal nanoparticle (see Fig. 5.2). Moreover, this pioneering study proves that AFM-IR is a useful technique for the investigation of the drug/metal monolayer interaction and also provides an image of the drug distribution on the applied metal monolayers [Nano Res. 13 (2020) 1020]. This may be crucial for understanding the drug/nanocarrier connection stability.

Finally, the results obtained using the SERS and AFM-IR (with the polarized IR radiation) techniques for erlotinib immobilized on the metal nanoparticles stabilized using different reagents imply that the presence of a stabilizing layer on the metal surface has a strong influence on the drug/metal nanocarrier conjugates stability [Appl. Surf. Sci. 537 (2021) 147897].

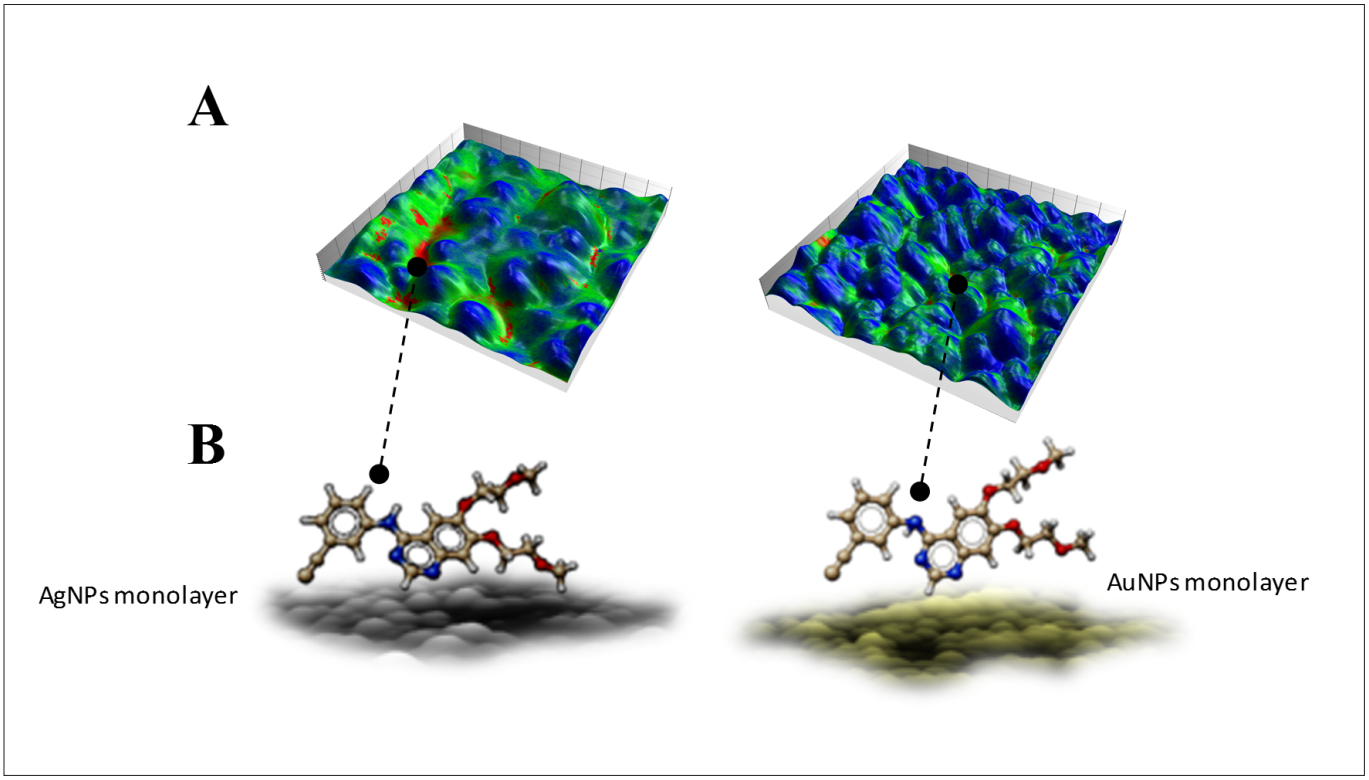

Fig. 5.2. The AFM−IR chemical signal distribution (A) of erlotinib on the silver (AgNPs) and gold nanoparticles (AuNPs) monolayers together with the suggested drug adsorption geometries on these metals (B) [adapted from Nano Res. 13 (2020) 1020].

In our next study we strived to develop an innovative approach to define the sensitivity of breast cells to drug/nanosensor conjugates using high-definition micro-and nanospectroscopy imaging at the single-cell level.[1] Thanks to the use of high-resolution imaging methods in Fourier-transform infrared spectroscopy (FTIR), Raman spectroscopy (RS), and a new technique combining the advantages of IR spectroscopy with atomic force microscopy (AFM), it was possible to obtain in-depth information at the single-cell level.

In the first stage of our investigations, particular emphasis was put on the study of the molecular structure using theoretical predictions based on density functional theory calculations (DFT) and experimental results (RS, FTIR). There is no doubt that the FTIR and RS methods are unique tools to determine the molecular structure of various compounds. Nevertheless, the adsorption of molecules on the roughened metal substrate may cause noticeable changes in its optical properties. The most commonly known techniques to investigate this interfacial behavior are surface-enhanced Raman (SERS), surface-enhanced infrared absorption (SEIRA) spectroscopy, and polarization-modulated SEIRA at the nanoscale (PM-SEIRA).

Then, the investigation focused on the drug behavior on the metal nanostructure and on testing the strength of interaction of the molecule with the metal sensor using specific surface-enhanced vibrational spectroscopic techniques (SERS, SEIRA, PM-SEIRA) [Appl. Surf. Sci. 499 (2020) 143975]. The subject of the analysis were compounds with antitumor activity and potential drugs not yet used in therapy adsorbed on the gold nanoparticles surface [Appl. Surf. Sci. 404 (2017) 168]. Fig. 5.3 shows a schematic representation of the performed study.

The usefulness of the FTIR method for assessing various alterations in tumorigenic and non-tumorigenic cells [Sensors and Actuators B: Chemical, 313 (2020) 128039] was determined in our next study. FTIR is a very sensitive and fast tool that gives information about the chemical component and morphology of cells and ensures the evaluation and tracking of the effects caused by drugs. Nonetheless, only the development of imaging methods has opened new possibilities in cancer diagnosis and therapy. The main concept of this work was to develop a more accurate way to define the sensitivity of cancer cells to drugs. It offered the possibility of a precise search for spectroscopic correlation and variations between the spectroscopic results obtained for control cells and cells treated only with Au nanoparticles (AuNPs) and cells treated with drug/AuNPs conjugates. a-Methyl-DL-tryptophan was used as a chemotherapeutic agent. Three human breast cell lines, i.e. MCF10A (non-tumorigenic), MCF7 (metastatic, pleural effusion, mildly malignant) and MDA-MB-231 (metastatic, pleural effusion, malignant) were treated with different concentrations of AuNPs and drug/AuNPs.

This type of research is currently of great importance as it may prove to be a key to a better understanding of biochemical changes resulting from cell exposure to drug-nanosensor conjugates. In a broader sense, this investigation provides not only the effective distinction between non-tumorigenic, mildly malignant, and malignant cells, but above all it offers a novel approach to define the sensitivity of cancer cells to drugs. It has been found that spectral

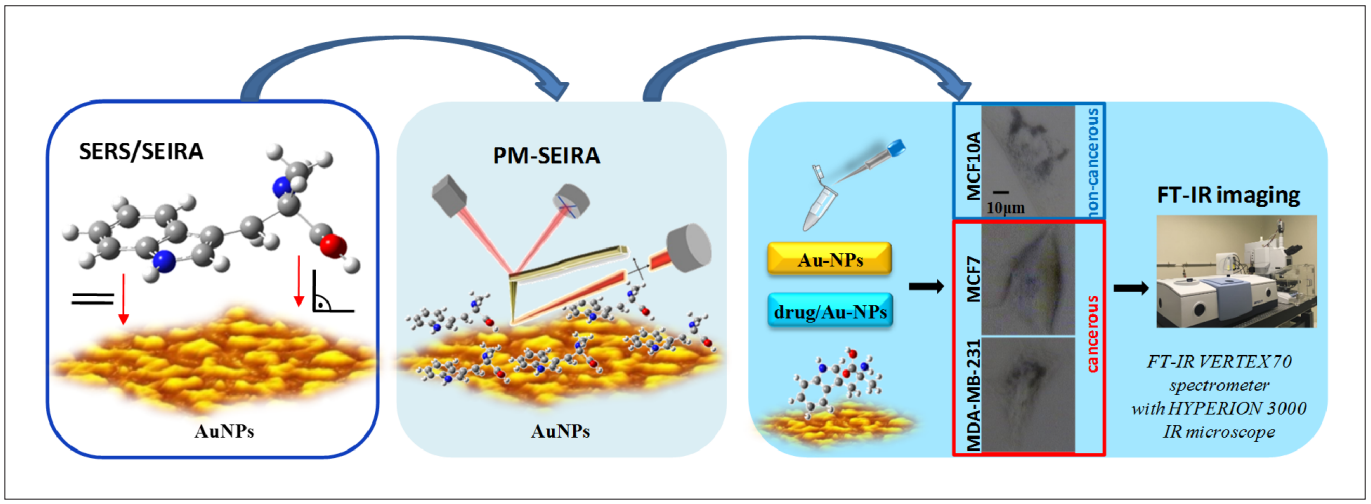

Fig. 5.3. The main research paths including SERS, SEIRA, PM−SEIRA and cellular studies

1) This research was supported by the National Science Centre, Poland (Grant no. 2017/01/X/ST4/00428). The measurements were performed using the equipment purchased in the frame of the project co-funded by the Małopolska Regional Operational Program Measure 5.1 Krakow Metropolitan Area as an important hub of the European Research Area for 2007-2013, project no. MRPO.05.01.00-12-013/15.

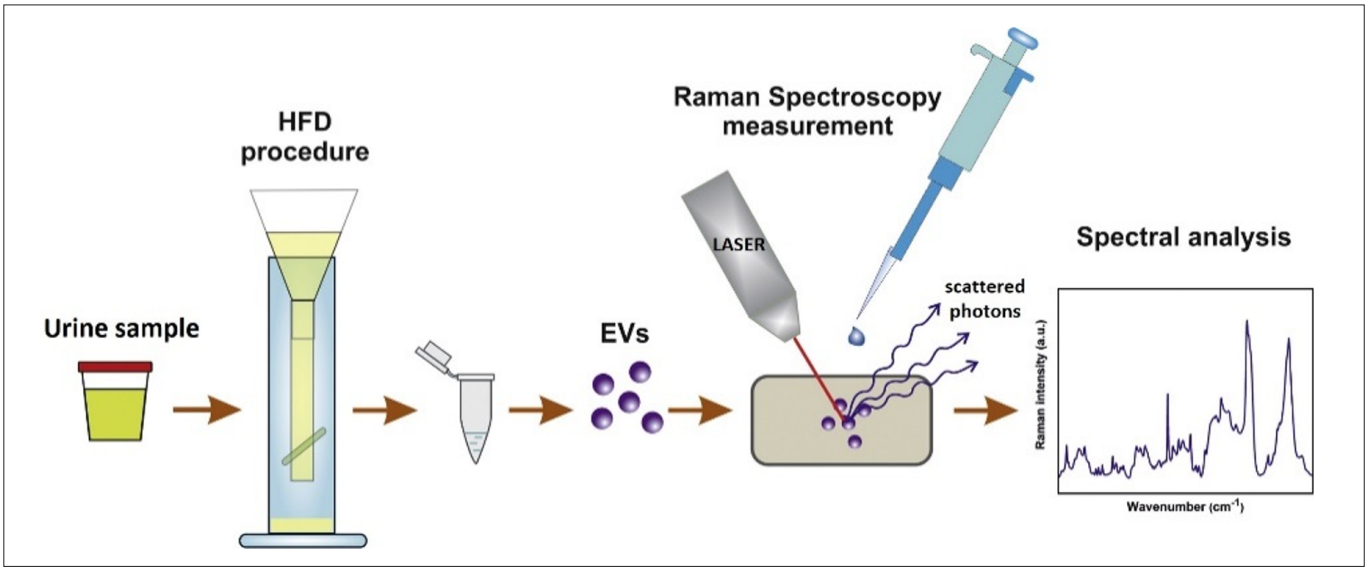

Fig. 5.4. Schematic layout of the performed experiments [adapted from Nanomedicine Nanotechnology, Biol. Med. 17 (2019) 137].

signals responsible for the data separation between control cells and cells exposed to drug/AuNPs containing medium are connected with changes in nucleic acids, lipids, and amide I and II oscillations.

Type 2 diabetes mellitus (T2DM) is a form of diabetes that is characterized by high blood sugar, insulin resistance, and a relative lack of insulin. T2DM diagnosis is based on the control of blood parameters (serum glucose and glycated hemoglobin), usually after the onset of symptoms in the form of frequent urination (polyuria), increased thirst (polydipsia), increased hunger (polyphagia), and weight loss. Thus, the detection of early-stage T2DM (with no classical symptoms) is very challenging. In the last decade there has been a growing interest in new methods for the early diagnosis of this type of disease. Recently, much attention has been focused on **the use of cell-derived extracellular vesicles (EVs) for the early detection of type 2 diabetes mellitus**. These nano-sized membranous vesicles play a crucial role in many biological processes, such as coagulation and fibrinolysis, intercellular communication, inflammation, and angiogenesis. Owing to their presence in almost all body fluids, EVs appear as potential biomarkers of diseases. Urine has shown to be a particularly rich reservoir of EVs released by glomerular epithelial cells that line the urinary tract. It has been suggested that the number and content of urinary EVs (UEVs) can reflect the stage of renal damage in diabetes. This makes urine of great interest for the diagnosis of this disease. Many optical and non-optical techniques have been used for several decades to characterize EVs, including high-resolution imaging with electron microscopy, nanoparticle tracking analysis (NTA), dynamic light scattering (DLS), tunable resistive pulse sensing (tRPS), flow cytometry, atomic force microscopy, and many others. However, none of these techniques have proven to be without limitations and the EV community has not adapted a "gold standard" protocol for analysis. Raman spectroscopy is a non-destructive, label-free method, based on inelastic scattering of monochromatic light which provides information about the chemical content of EVs. Furthermore, Raman spectroscopy is a promising tool for clinical applications because it enables specific detection of hemoglobin and albumin glycation which can be useful for diabetes monitoring. Taking into account the potential usefulness of UEVs as biomarkers of diseases, together with the Institute of Physics, Jagiellonian University, we explored the application of Raman spectroscopy in laboratory medicine to distinguish UEVs collected from diabetic patients and healthy controls (denoted by 'C') (Fig. 5.4). Additionally, we used the spectral signature to compare diabetic patients having glycemic control on different levels (controlled ('CD') and uncontrolled ('UD') diabetes).

Average Raman spectra of samples from the study groups show distinct differences in the fingerprint region (Fig. 5.5A). A clear separation between the groups was also confirmed by chemometric analysis. Moreover, the spectroscopic analysis was supported with Partial Least Squares Regression (PLSR) analysis to find biochemical differences between samples from all the studied groups. PLSR models revealed significant differences in the content of lipids, proteins, and nucleic acids. Based on the performed study, one may assume that Raman spectroscopy distinguishes between CD and UD diabetic patients as well as between diabetics and healthy subjects. Finally, it is of great interest to compare spectral data with clinical characteristics. Thus,

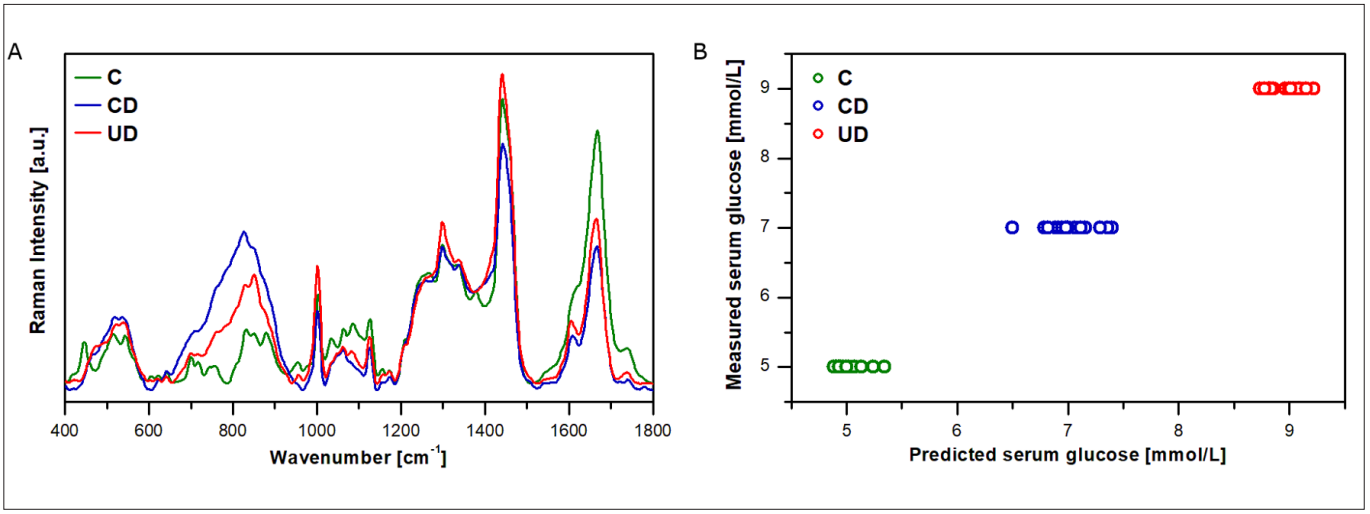

Fig. 5.5. Average Raman spectra of UEVs isolated from C, CD and UD groups (A) with TEM image of the representative UEVs (insert), predicted and measured serum glucose calculated from PLSR models (B) [adapted from Nanomedicine Nanotechnology, Biol. Med. 17 (2019) 137].

the PLSR method was applied to correlate Raman signatures with selected clinical parameters. As can be seen in Fig. 5.5B, the correlation between the measured Raman spectra and serum glucose concentration is good. It suggests that the PLSR method is a useful tool to characterize spectral changes in Raman spectra, which correlate with clinical parameters related to T2DM.

The investigation confirmed that Raman spectroscopy is a powerful tool for searching for abnormalities in UEVs derived from pathologically altered tissues, which can be very useful for the diagnosis of diabetic complications at an early stage. The results of this research were published in a prestigious journal *Nanomedicine: Nanotechnology, Biology and Medicine* [Nanomedicine Nanotechnology, Biol. Med. 17 (2019) 137]. Furthermore, an invention based on the obtained results was applied for patent protection in Poland.[1)] In the next step, the patent was expanded to international protection.[2)]

Nowadays, non-communicable (chronic) diseases are considered as responsible for the majority of global deaths. Moreover, cancer is predicted to be the leading cause of human death in the 21st century. One of the most important elements of cancer treatment is radiotherapy, which applies ionizing radiation (e.g. X-rays or protons) to damage vital biomolecules (mainly DNA) and induce cell death. Recently, much attention has been focused on the

application of vibrational spectroscopy methods for the detection and analysis of radiation-induced damage and response of cancer cells. [3)]

Spectroscopic methods are highly suitable for the detection and characterization of complex biological systems. In particular, Raman spectroscopy has shown promise as it provides detailed molecular information about the sample and can easily detect structural changes. However, the recent development of the AFM-IR technique, which combines nanoscale imaging with chemical contrast through infrared spectroscopy, has opened up new fields for the exploration of subcellular biochemistry. Furthermore, as optical techniques, both methods are label-free, non-invasive, and non-destructive, allowing the simultaneous detection of a variety of biomolecules (nucleic acids (DNA, RNA), proteins, lipids, etc.) in a single acquisition. Thus, vibrational spectroscopy methods appear to be promising for studying biochemical changes induced by ionizing radiation. Since spectroscopic measurements based on single acquisition per cell take an inherent risk of omitting important information when only a small and random subset of a cell area is probed, spectroscopic imaging shows the potential to provide more insight into chemical changes that occur in the whole cell body.

In the conducted research, Raman and AFM-IR imaging techniques were applied to monitor subcellular changes induced by ionizing radiation (X-ray) in PC-3 prostate cancer cells. Spectroscopic analysis was supported with Partial

1) Patent no. PAT.235682, title: "Sposób wykrywania i diagnozowania przebiegu cukrzycy"
2) International PCT application no. PCT/PL2018/050059, title: "A method of detecting and diagnosing the progression of diabetes"
3) This research was supported by the National Science Centre, Poland (Grant no. 2015/19/D/ST4/01943).
The measurements were performed using the equipment purchased in the frame of the project co-funded by the Małopolska Regional Operational Program Measure 5.1 Krakow Metropolitan Area as an important hub of the European Research Area for 2007-2013, project no. MRPO.05.01.00-12-013/15.

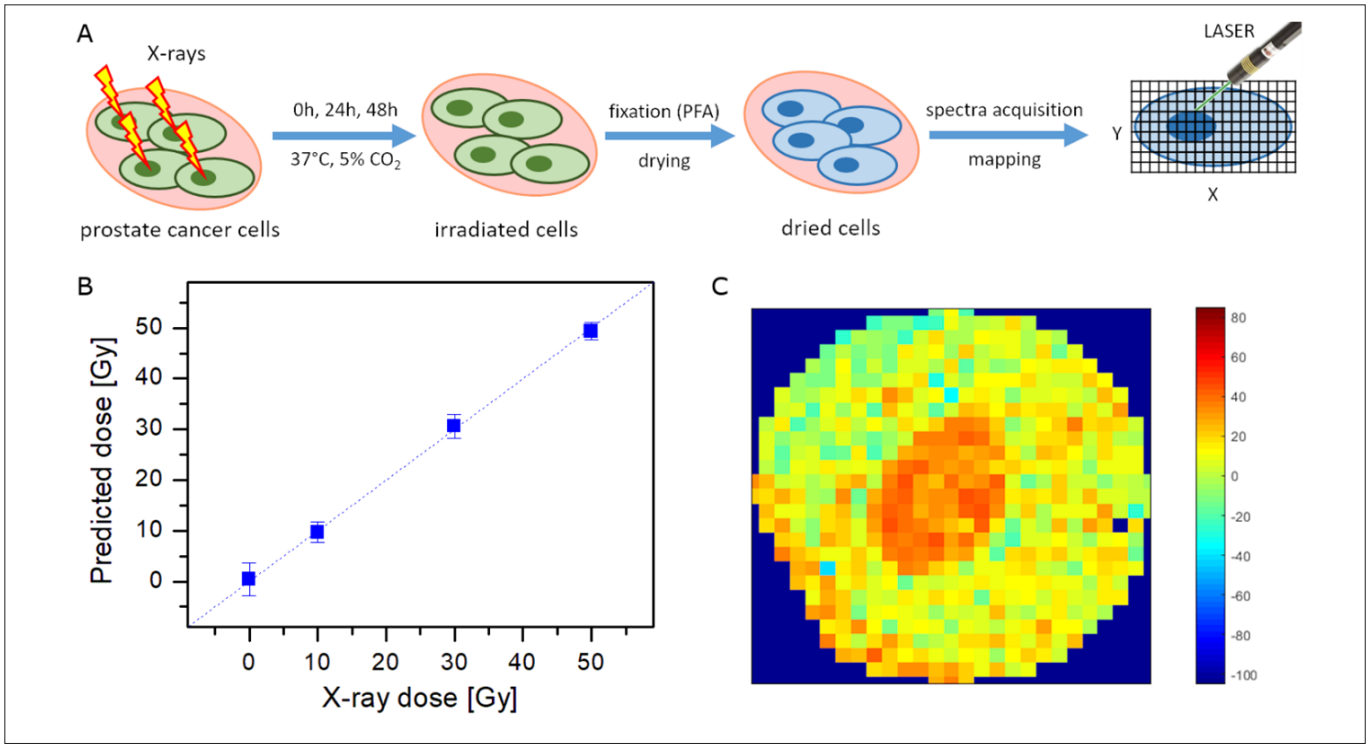

Fig. 5.6. Schematic layout of the performed experiments (A), PLSR model for cells fixed 48 h after irradiation (B), Raman map of the predicted X−ray dose for the 48 h timepoint and X−ray dose of 10 Gy (C) [adapted from Sci. Rep. 9 (2019) 8715].

Least Squares Regression (PLSR) analysis to elucidate the time-dependent evolution of chemical changes induced in cells by irradiation (Fig. 5.6A) [Sci. Rep. 9 (2019) 8715]. The obtained regression models show good correlations between the applied and predicted X-ray dose (clear biochemical changes with a dose identified by spectroscopic methods, Fig. 5.6B), even for early-stage cell response (cells fixed just after the irradiation). It confirms the high utility of spectroscopic methods in exploring biochemical changes induced by increasing the dose of radiation in cancer cells. Moreover, such changes seem to be similar for two main cell components, i.e. cytoplasm and the nuclear region. However, response strength depends strongly on time and X-ray dose. On the other hand, the application of the Raman mapping technique enables component-specific prediction of the delivered X-ray dose (Fig. 5.6C). This novel approach shows that the calculated radiation dose deposited in cytoplasm and nucleus is different within the cells and is dependent on the time of cell response (fixation time after irradiation) and X-ray dose. It suggests that the cytoplasm and nuclear region should be analyzed independently. Additionally, a clear advantage of Raman mapping over single-point measurements can be confirmed by comparison of PLSR models for average spectra of the whole cell and randomly selected single pixels.

Spectroscopic analysis of the investigated cells reveals significant heterogeneity of the lipid content. Prostate cancer cells show a unique lipid metabolism manifested by an increased requirement for lipid accumulation in cytosolic lipid droplets (LDs). Thus, these cell organelles were tested for their composition and the effect of X-ray irradiation [BBA - Mol. Cell Biol. Lipids. 1865 (2020) 158753]. The analysis of Raman spectra shows that LDs in PC-3 cells are composed of either triacylglycerols (TAGs) or cholesterol esters (CEs). Moreover, LDs exhibit significant heterogeneity of chemical composition. Further investigation shows that X-ray irradiation has a smaller impact on LDs composition and to a greater extent affects lipid concentration. Since LDs are usually less than 1 m in size, AFM-IR imaging was applied for detailed analysis of LDs distribution in untreated and irradiated cells [Nanotechnology. 30 (2019) 425502]. Apart from large LDs aggregates rich in CEs, small spots of high lipid signal can be found across the cell body. LDs as small as 150 nm in size can be successfully revealed in the cytoplasm using the AFM-IR technique (Fig. 5.7), which is definitely below the diffraction limit of standard FT-IR and Raman measurements. The analysis of AFM-IR spectra indicates the homogeneous composition of LDs in single cells and their heterogeneous composition within the cell population. As can be seen, both Raman and AFM-IR techniques show high usefulness in analyzing LDs accumulated in the cytoplasm of cancer cells in terms of spatial distribution, composition, and the effect of irradiation.

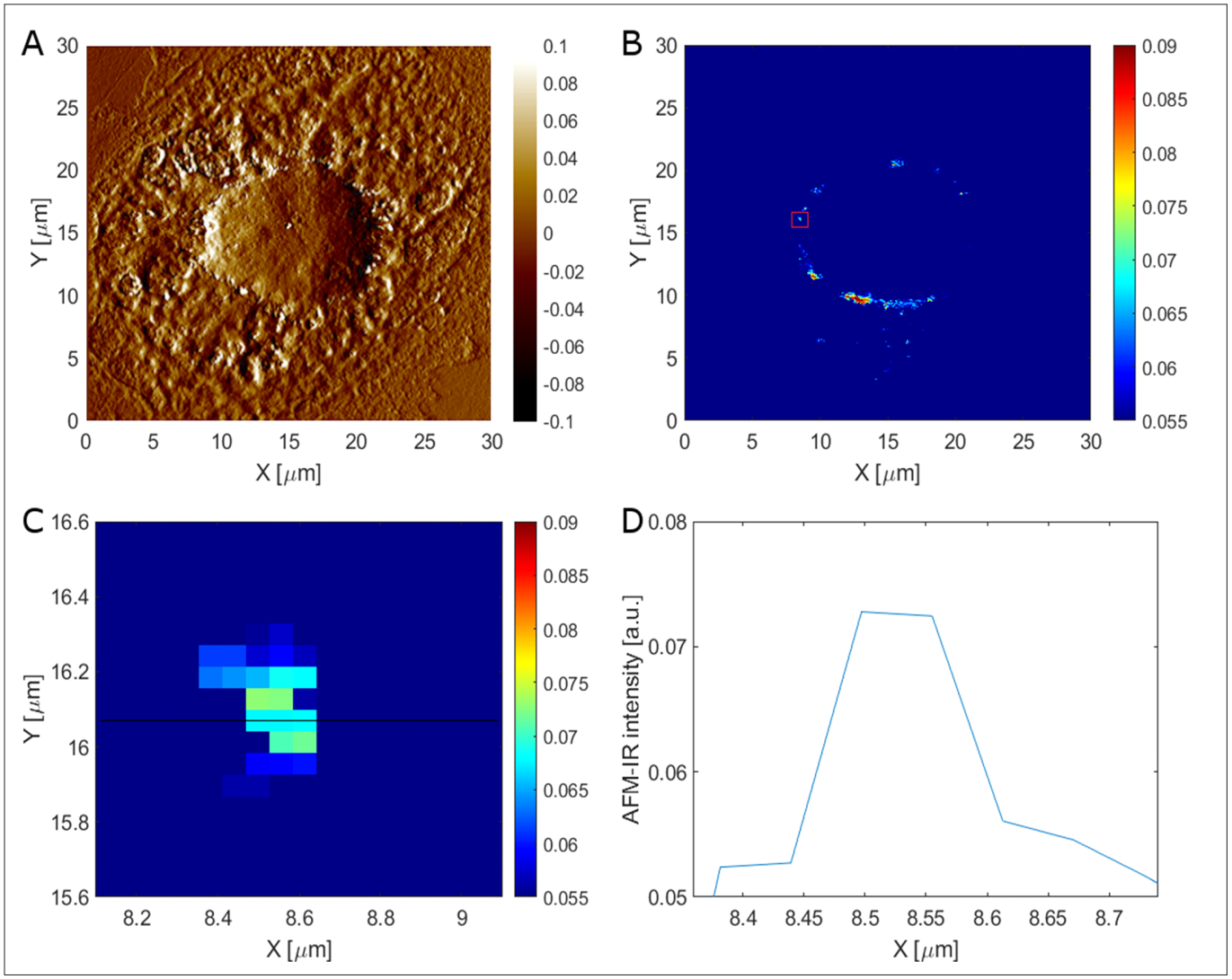

Fig. 5.7. AFM (deflection) image of a PC−3 cell (**A**). AFM−IR signal image (1730 cm^{-1} band) of the cell with marked area (red square) of the selected LDs (**B**). Magnified area of the LDs selected at (B) with a profile line (**C**). AFM−IR signal profile (indicated in (C) with a black line) (**D**).

Finally, the effect of irradiation should be considered at two stages, i.e. the physicochemical stage and the biological response. Both effects induce different biochemical changes in the cells and should be analyzed as two separate phenomena. The obtained regression models, performed separately for cytoplasmic and nuclear regions, show good correlations for both effects [J. Biophotonics. 13 (2020) e202000252]. However, the physicochemical damage models show weaker dose-dependence than the biological response models. This suggests that the effect of the physicochemical damage to cell components is more subtle than the early-stage biological response of the cells to irradiation. Furthermore, a comparison of Raman signatures related to regression models proves that both effects are associated with different biochemical changes and the early-stage biological response of the cells cannot be confused with the physicochemical damage caused by X-ray irradiation. The research shows that spectroscopic studies of radiation effects are sensitive enough to discriminate between the initial damage and the response of the cell. This fact/finding seems to be particularly important as identifying the mechanisms of radiation-induced cell responses, both in terms of damage and repair, has potential clinical implications for improving outcomes with radiation therapy.

The activity of metal complexes in biological systems is commonly studied with the use of X-rays. In addition to the compounds occurring naturally in the human body, metal ions are also required the role they play as pharmaceuticals as well as diagnostic agents. Due to the increasing number of cancer cases in the world, investigations into new anti-tumor drugs containing metal ions are particularly important. The lack of molecular mechanistic **understanding of the interaction between metal complexes and biomolecules** hampers their potential medical use. Until now, the formation of metal– biomolecule

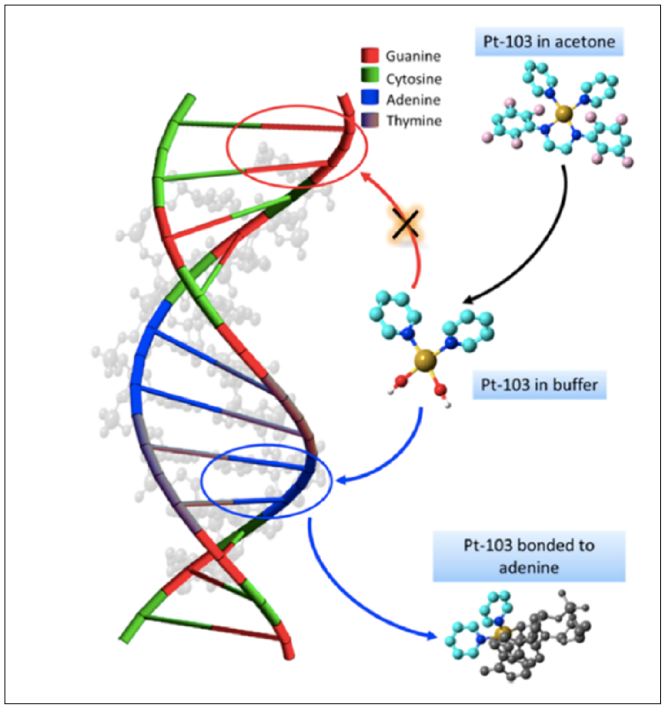

Fig. 5. 8. Representation of hydrolysis and DNA binding of Pt103 [Reproduced with permission from: J. Phys. Chem. Lett. 8 (2017) 805, Copyright 2021American Chemical Society].

adducts could be monitored only by indirect methods that evidence the existence of interactions. In this project we presented an original method to reveal the interactions of metal complexes with biocompounds based on resonant X-ray emission spectroscopy (RXES) and theoretical simulations [J. Phys. Chem. Lett. 8 (2017) 805]. The proposed methodology, called atomic telemetry, is label free and can be employed for in situ and in vivo measurements, enabling the direct study of the interaction between the complex and biomolecules within times that are shorter than those in current practices. One important advantage of atomic telemetry with respect to other complementary methods currently in use is that low drug dosages commonly used in the treatment of cancer can be detected and analysed.

The report unveils a hydrolysis process and DNA binding of [Pt{N(p-HC_6F_4)CH_2}$_2$py$_2$], known as Pt103 (Fig. 5.8.), which showed potential cytotoxic activity against cancer cells. The results of RXES experimental data analysis and molecular dynamics simulations confirmed that Pt103 preferentially coordinates to adjacent adenine sites, instead of guanine sites as in cisplatin, because of its hydrogen bond ability. That may explain large biological activity of Pt103 and can be useful in further designing of new anticancer drugs.

The proposed approach was also successfully implemented to the studies of hydrolysis mechanism of Pt103 oxidation product, namely Pt103$(OH)_2$ [J. Inorg. Biochem. 187 (2018) 56]. As a result, it was revealed that hydrolysis preceded any reduction of the metal center, which may play an important role in explaining its antitumor activity.

Transition metal compounds constitute one of the most interesting classes of materials with unique properties, such as superconductivity, magnetoresistance, ferroelectricity, thermoelectricity, and optical and catalytic activity. This makes them attractive in areas such as optics, electronics, catalysis, sensors, and energy conversion and storage. The functional properties of these materials are very sensitive to the electronic band structure of the central transition metal, in particular the composition of occupied and unoccupied electronic states in the vicinity of Fermi energies. Thus, the knowledge about the electronic structure of transition metal elements, especially orbital contribution and the relative energy position of the highest occupied (valence band) and the lowest unoccupied states (conduction band), is crucial for the design of innovative and efficient materials.

In this project, the combination of resonant and non-resonant X-ray emission spectroscopies and theoretical modelling was used to provide a quantitative analysis of 5d metal-oxide total electronic structures (occupied and unoccupied states) [J. Synchrotron Rad. 27 (2020) 689]. Metal and metal-oxide material cases studies (W and WO_3, respectively) were evaluated to show the ability of the approach to assess simultaneously the composition of the electronic states around-Fermi, band gap energies, and the strength of crystal field splitting. The experimental RXES plane for tungsten (VI) oxide material is presented in Fig. 5.9. The dominant feature in the WO_3 RXES plane is strong $2p_{3/2}$ 5d signal, with two intense resonances whose

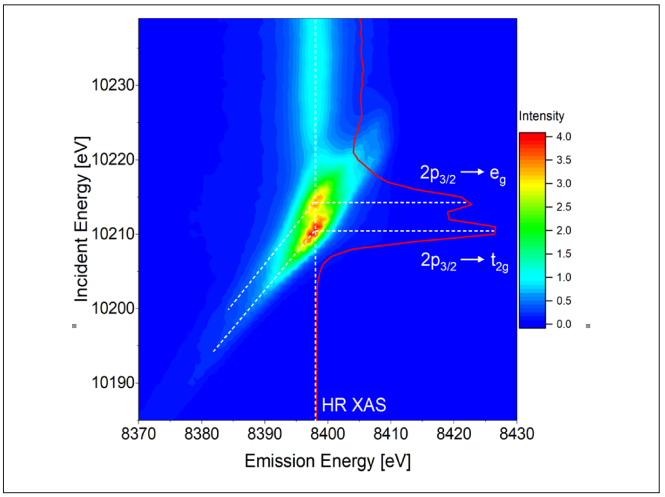

Fig. 5.9. RXES plane measured around the W L_3 absorption edge for WO_3 material. The extracted HR-XAS spectrum is plotted as the red line on the plane. [Reproduced from J. Synchrotron Rad. 27 (2020) 689 by permission].

appearance is due to splitting of the W 5d states into the W t_{2g} and e_g orbitals by the crystal field of the surrounding oxygen atoms. The composition of occupied and unoccupied electronic states of a material in the vicinity of Fermi energies is vital because it underpins its physical, chemical and mechanical properties. The results obtained in the project study are important for the rational design of metal-oxide materials and may be adapted to study other transition metal compounds with different composition, morphology and structures.

For many years X-ray studies on complex systems have been accompanied by a concern about the damage inflicted onto the studied material by an incident X-ray beam, especially when using the bright 3rd and 4th generation radiation sources such as X-ray free-electron lasers (XFELs). The radiation damage is the unwanted consequence of the high ionization of the studied material by an intense probe beam: electronic structure change, bond breaking, Coulomb explosion, structural change. Progress in overcoming the X-ray damage influence on the experimental data has been made possible on the part of the excitation beam itself with the advent of the 4th generation X-ray sources. The new X-ray source shortens the X-ray pulse duration to femtoseconds while maintaining a high number of photons. This improvement opened the way to develop the so-called *probe-before-destroy* approach allowing molecular systems to be probed before the radiation damage causes observable changes in them. The radiation damage is typically considered in terms of the Coulomb explosion leading to a structural change, while it has been shown that the much faster electronic structure change may also have a significant influence on the X-ray diffraction (XRD) results.

We irradiated 0.1 M solvent of potassium hexacyanoferrate(II) trihydrate ($K_4[Fe(CN)_6 \cdot 3H_2O]$) in distilled water with XFEL pulses of different photon fluxes and observed a monotonic change in the Fe K emission spectrum with increasing photon flux [Structural Dynamics 6 (2019) 024901]. This finding cannot be related to the metal-site direct absorption, which may be considered only as a higher order contribution. A detailed analysis revealed an additional strong contribution to the probed atoms' electronic structure modification much faster than direct photoabsorption. This contribution originated from the ionization of the probed Fe atoms' environment and led to the creation of short-lived high valence states which is an unexpected phenomenon because the probe-before-destruction methodology, a strategy pioneered for structure-related measurements free of beam damage, does not predict it. Therefore such a study should be continued since this work

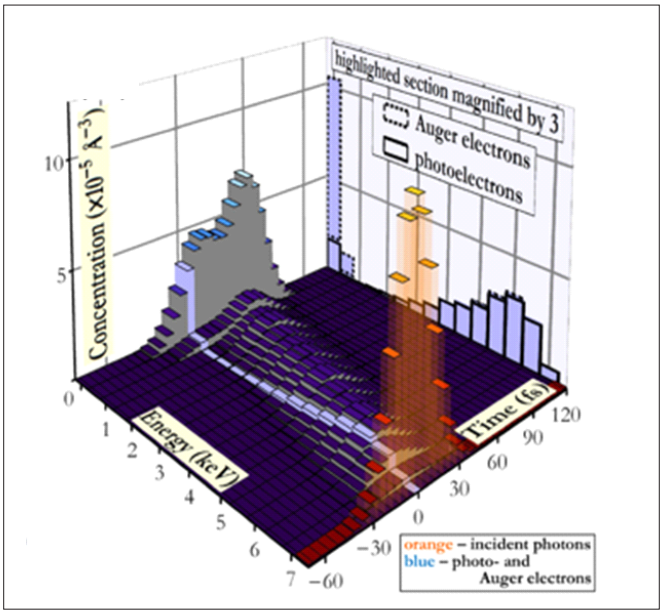

Fig. 5.10. Simulated energy and time distributions of incident photons as well as energetic photo− and Auger electrons under ultrashort intense X−ray pulse irradiation [Figure reproduced from: Structural Dynamics 6 (2019) 024901 published under CC BY 4.0 license].

calls for consideration of the electronic structure change in experiments with XFEL sources focused on samples embedded in e.g., solutions or in matrices, which in fact concerns most of the experimental studies.

Particle Induced X-ray Spectroscopy in Cultural Heritage has come into common use by historians. The largest numismatic collection of silver denarii dating back to the earliest development of the Polish medieval state was studied using proton microprobe induced X-ray emission spectroscopy (PIXE).

The whole collection, housed in the National Museum in Krakow, encompasses over 70 objects, attributed to Mieszko (Misico) and Boleslaus the Brave. The basic aim of the study was to determine the denarii elemental composition in order to cross-compare the results with previous micro-X-ray fluorescence data and to perform a better quantification of the denarii elemental composition,

Fig. 5.11. Silver denar of the Boleslaus the Brave [Reprinted from J.Radioanal Nucl Chem, 314 (2017) 2309 under CC BY 4.0 license].

especially with regard to trace elements [J. Radioanal Nucl Chem, 314 (2017) 2309, Surf. and Int. Anal., 50 (2018) 78]. The major elements detected were Ag, Cu, and Pb, but minor elements, such as Fe, Au, Bi, Hg, and Zn, were also present, indicating the provenance of the alloy compounds. Among the others significantly elevated level of Mercury content determined in 11 denarii suggests the Central Asian origin of the alloy material, obtained probably by way of re–melting Islamic coins. The more strict elemental composition of the denarii attributed to Mieszko is most probably a result of a more developed technology, which supports the hypothesis that they were minted later – not during the rule of Mieszko I, but of Mieszko II Lambert, the son of Boleslaus.

Rheology of muscles has become a mechanical fingerprint of muscular dystrophy. Duchenne muscular dystrophy (DMD) is still an incurable disease; therefore, there is much ongoing research on potential treatment strategies, such as gene or stem cell-based therapeutic approaches applied to DMD animal models (*mdx* mice). We evaluated biochemical and biomechanical changes in *mdx* skeletal muscles subjected to an autologous cell transplantation approach, whereby the transplanted mesoangioblast cells (MABs) were treated to express full-length dystrophin (Fig. 5.12). As expected, a biochemical analysis of the dystrophin level showed a substantial decrease of the dystrophin amount in *mdx*/SCID muscles with respect to wild-type (B6/SCID) muscles associated with the decrease of Young's and shear modulus, indicating the muscle weakening. The biomechanical characteristics of MABs transplanted muscles depend on the scale, i.e. nano- or macro-indentation. The nanomechanical properties of *mdx*/SCID 1T muscles showed no amelioration of the muscles mechanical properties. In *mdx*/SCID 3T samples, a bimodal modulus distribution was observed, showing muscle fibers function restoration [Mol. Ther. 26 (2018) 1093]. Macro-rheological studies showed that autologous cell therapy results in muscle function restoration as storage modulus values of transplanted samples are close to the shear modulus of wild-type muscles, regardless of the number of transplantations. Shear rheology measurements also

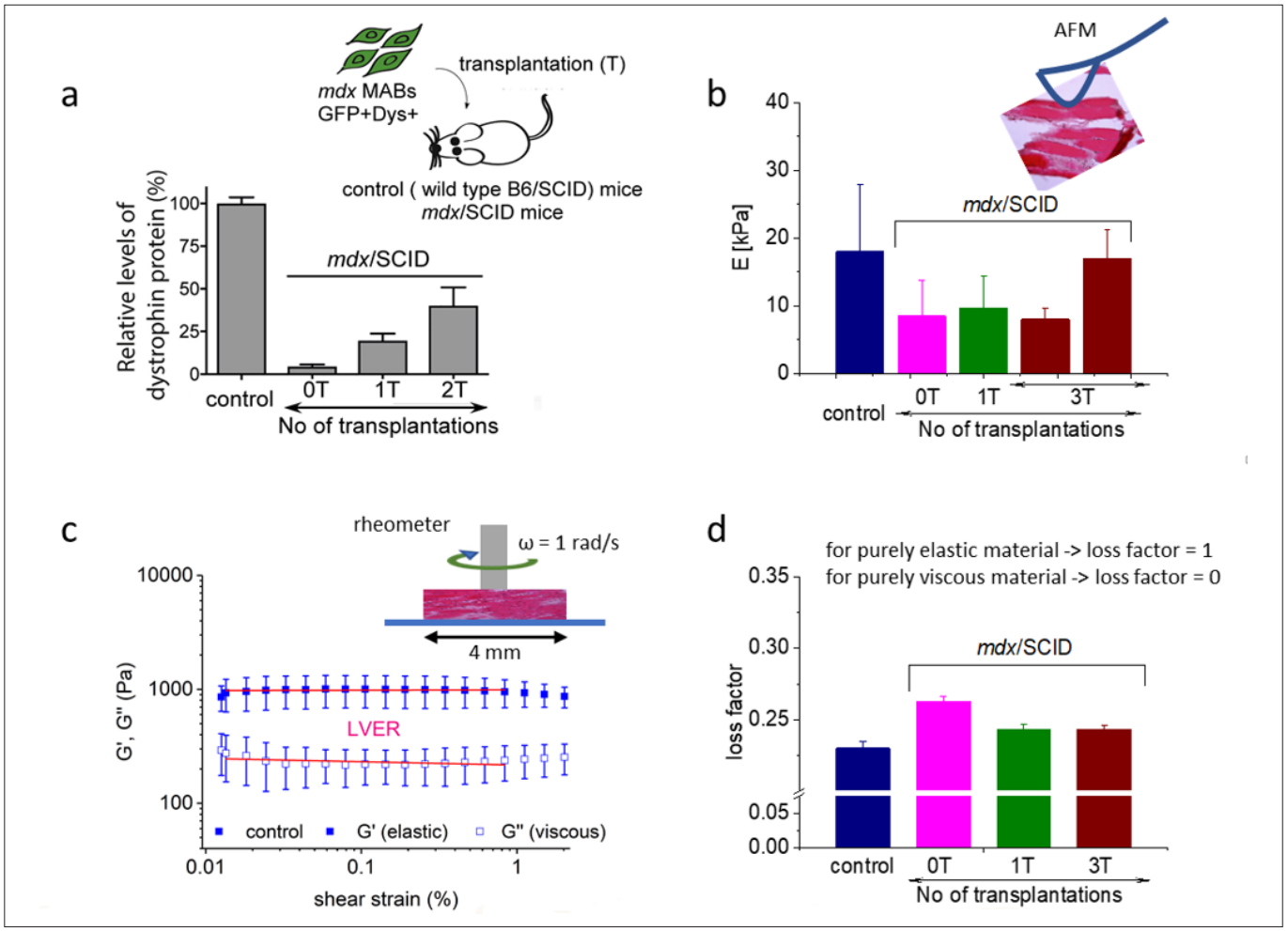

Fig. 5.12. (**a**) Dystrophin expression in wild−type (B6/SCID), dystrophic (mdx/SCID) and mesoangioblasts (MABs, GFP+Dys+) transplanted mdx/SCID muscles, and (**b**) elasticity (E) of muscle fibers obtained with AFM. (**c&d**) Macrorheological properties of normal, diseased, and MABs transplanted tibialis anterior muscles. [Mol. Ther. 26 (2018) 1093].

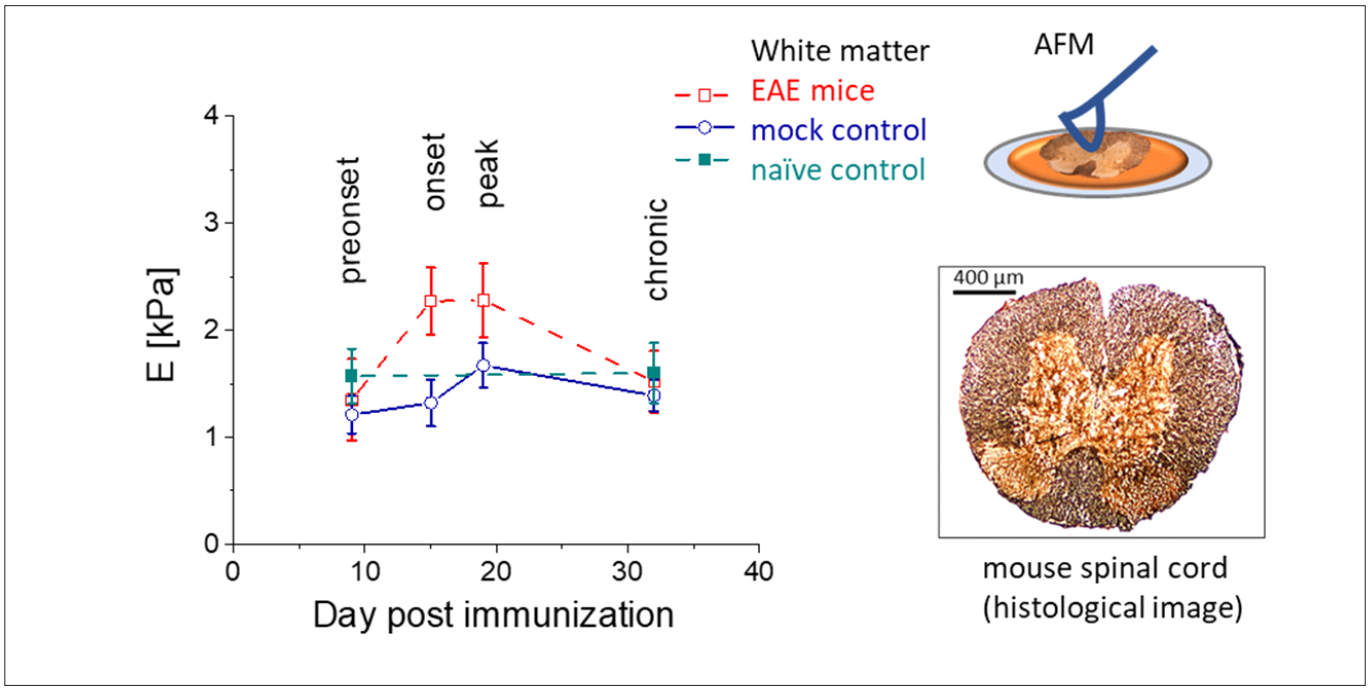

Fig. 5.13. In the mice model of multiple sclerosis, spinal cord tissues stiffen in the disease course. The increased rigidity appears before histopathological alterations and clinical symptoms. From [Arch Biochem. Biophys. 680 (2020) 108221] under license No. 5032110528243.

revealed that viscous properties, described by loss modulus or loss factor, cannot be neglected. The obtained results confirm that biomechanical measurements are a useful tool supporting the disease diagnosis and detection.

Rigidity increase in the spinal cord tissue during the MD onset phase occurs before significant alterations in histopathological and clinical symptoms. The increase in white matter rigidity can be regarded as an early signature of experimental autoimmune encephalomyelitis (EAE) being a mouse model of multiple sclerosis (MS), a chronic inflammatory disease of the central nervous system. We postulate that biological and biomechanical properties play an important role in spinal cord function impairments. Atomic force microscopy (AFM) was applied to investigate spinal cords' mechanical properties collected from EAE mice in preonset, onset, peak, and chronic disease phases (Fig. 5.13). Biomechanical changes were compared with histopathological alterations observed in the successive phases. Tissue rigidity increased in the onset phase before histopathological and clinical symptoms altered significantly — these findings point to elastography as methods for early MS detection and the use of drugs releasing tissue tension [Arch. Biochem. Biophys. 680 (2020) 108221].

Syndecans are receptors that, together with integrins, control **cell interactions with extracellular matrix components** such as vitronectin (VN). Despite structural similarities between all syndecan families, their specific attachment to extracellular matrix proteins is defined by heparan and chondroitin chains. Force spectroscopy data, recorded by an atomic force microscope (AFM, Fig. 14a), were analyzed using two theoretical approaches describing force-induced unbinding, authored by Bell-Evans Dudko-Hummer-Szabo. The results reveal various unbinding kinetics for each type of single syndecan complex [J. Phys. Chem. Let. 9 (2018) 1509]. One of the syndecan family members, syndecan-4, unbinds by crossing over only one energy barrier. Syndecan-4 located at the cell membrane interacts with vitronectin; therefore, its unbinding properties were compared to the interaction of V 1 integrin to VN, too (Fig. 5.14b). As each ECM protein, vitronectin possesses two binding sites specific to integrins and syndecans. The obtained data enabled us to reconstruct the unbinding pathways and propose the model showing that the unbinding of V 1 from VN proceeds before the unbinding of SDC-4, suggesting the regulatory role of syndecan-4 in cell adhesion (Fig. 5.14c).

Diagnostic techniques such as **Magnetic Resonance Imaging (MRI) and Spectroscopy (MRS) are sensitive to the tissue structure as well as biochemical composition.** Localized MRS was used for the non-invasive evaluation of brain metabolism in the model of anorexia nervosa (AN). Anorectic patients present aberrant eating behaviors leading to the reduction of energy intake, caused by an intense fear of gaining weight

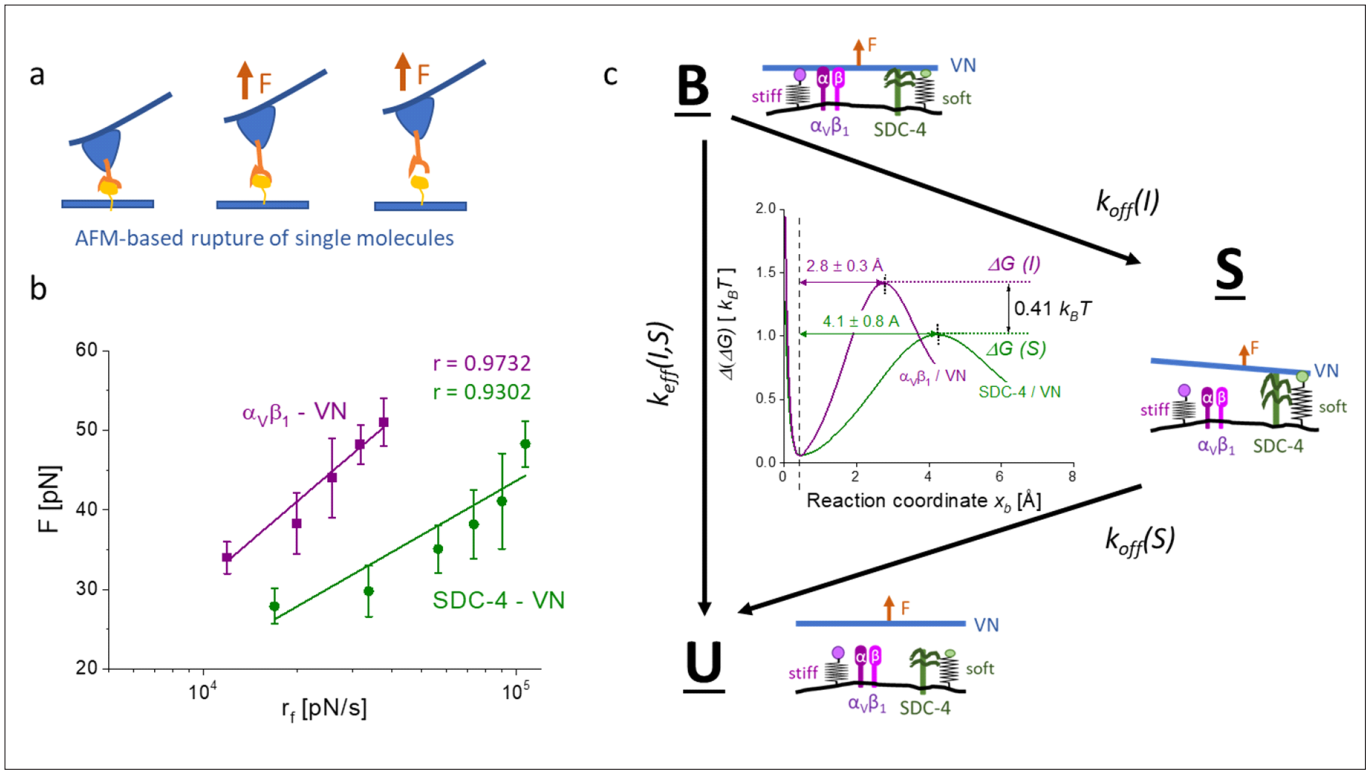

Fig. 5.14. Unbinding of individual complexes by AFM (**a**) delivers the so−called dynamic force spectra (**b**) that can be applied to reconstruct the energy landscape during the unbinding (**c**). Obtained parameters served to model the unbinding pathway in the co−operative interactions between syndecans and integrins. [J. Phys. Chem. Let. 9 (2018) 1509 and from Micron 137 (2020) 102888] under license No. 5032110280467.

and distortion of the body image. For this study, a rat model of activity-based anorexia (ABA) was used. The hypothalamus and the brain stem were chosen as regions of interest for the *in vivo* spectroscopic studies since those structures play an important role in the regulation of metabolism in humans. Single voxel ^{1}H MRS, using the point-resolved spectroscopy (PRESS) sequence, was used to assess the neurochemical composition of those regions (Fig. 5. 15). Especially the levels of glutamate (Glu) and -aminobutyric acid (GABA) were assessed. The spectra were analyzed with the LCModel software to obtain quantitative

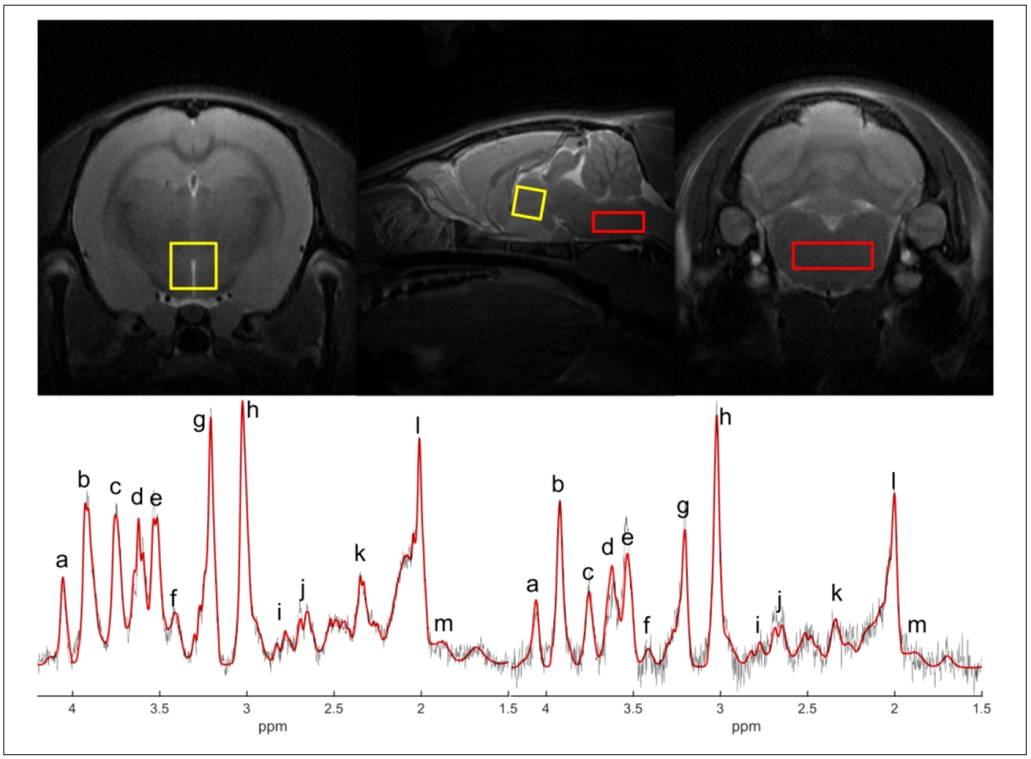

Fig. 5. 15. Schematic view of the position of MRS voxels in the hypothalamus (yellow) and in the brain stem (red) overlaid over the three orthogonal cross−sections through T_2 weighted image of the rat brain. Below examples of proton spectra from the hypothalamus (left drawing, the yellow region) and the brain stem (right drawing, the red region). The black line is the measured data and the red line is the LCModel fit. The following peaks can be assigned to the metabolites as follows: a − Ins; b − Cr, PCr; c − Glu, Gln, GSH; d − Ins, PCh; e − Ins; f − Tau; g −GPC, PCh; h − Cr, PCr; i − Asp; j − NAA; k − Glu; l − NAA; m − GABA. From [NMR Biomed.,33(2020)e4306002/nbm.4306] by permission.

information on the content of 17 metabolites. Moreover, the effect of subcutaneously administered kisspeptin-10 on the measured brain metabolites level was quantified.

The obtained results showed that kisspeptin reinforced food consumption in this model of anorexia is changing a pattern of weight loss. A statistically significant change in the concentration of creatine (Cr), phosphocreatine, GABA, glutathione and inositol compared to the control group was detected. Subcutaneous administration of kisspeptin reversed the decrease in GABA and Cr levels in the hypothalamus as well as restored Glu level in the brain stem.

This experiment confirms that excessive exercise and food restriction alter the balance of main neurotransmitters while peripherally administered kisspeptin appears to partially restore Glu and GABA signalling, as well as alleviate the fluctuations in other brain metabolites [NMR Biomed.,33(2020)e4306002/nbm.4306].

The theranostic potential of various nanocomposites was investigated using Magnetic Resonance Relaxometry and Imaging. The term 'theranostic' relates to an object that combines two modalities: therapy and diagnostic imaging. The utilization of such materials instead of two separate substances for each application introduces a possibility of overcoming differences in biodistribution and selectivity of administered therapeutic and imaging agents. Magnetic resonance imaging can be used to obtain a spatial distribution of nanoparticles owing

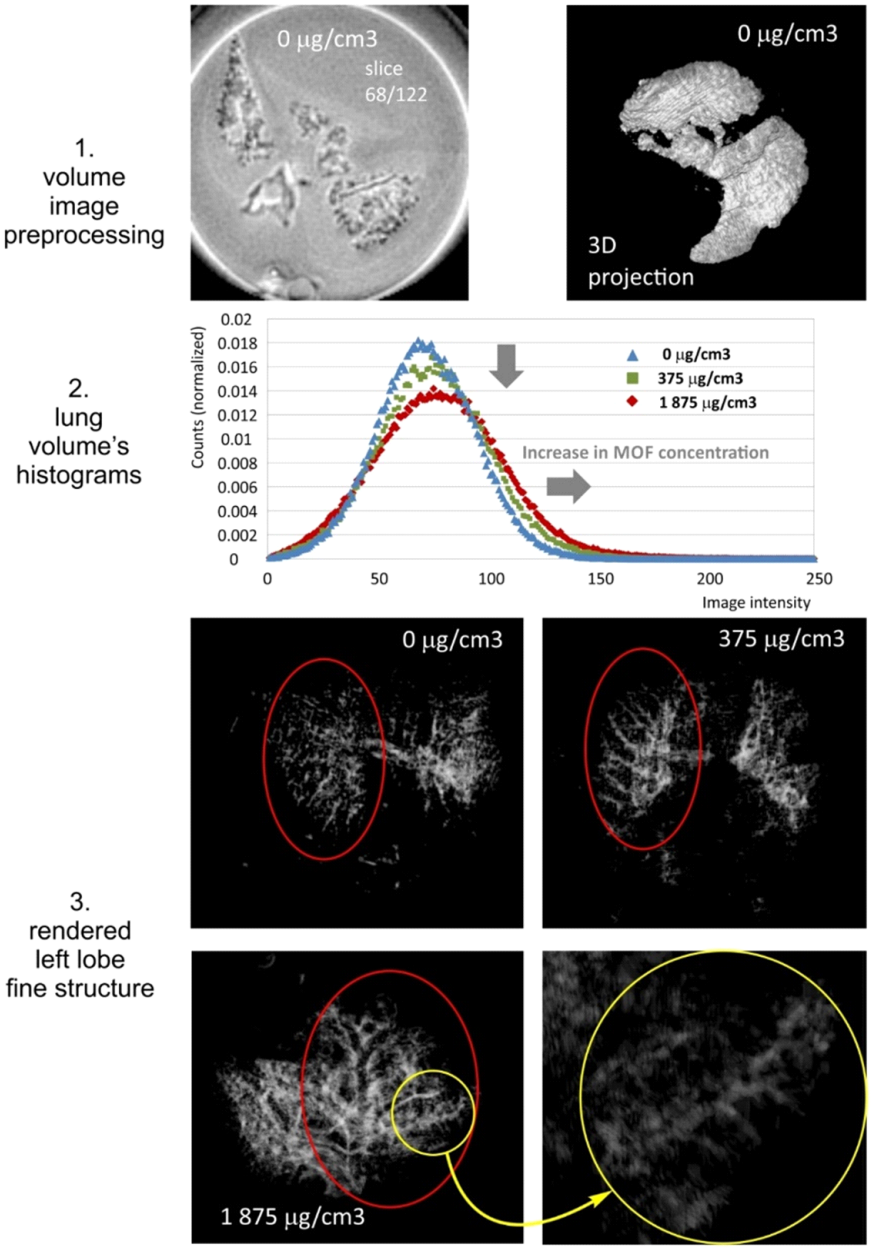

Fig. 5.16. Qualitative and quantitative analysis of MRI volume images of lungs.

1: Single slice from the MRI image volume (left) and 3D projection of segmented lung image volume (right);

2: histograms of volume lung images obtained for three different MOF concentrations (the grey arrows show the influence of MOF concentration on the image intensity histogram; i.e., decrease in maximum histogram value and expansion in the image intensity range towards higher intensities);

3: views of rendered left lobe fine structure (the yellow circle shows details of deeper lung areas contrasted with MOF).
From Pharmaceutics2019,11(12) 687], under CC BY4.0 license.

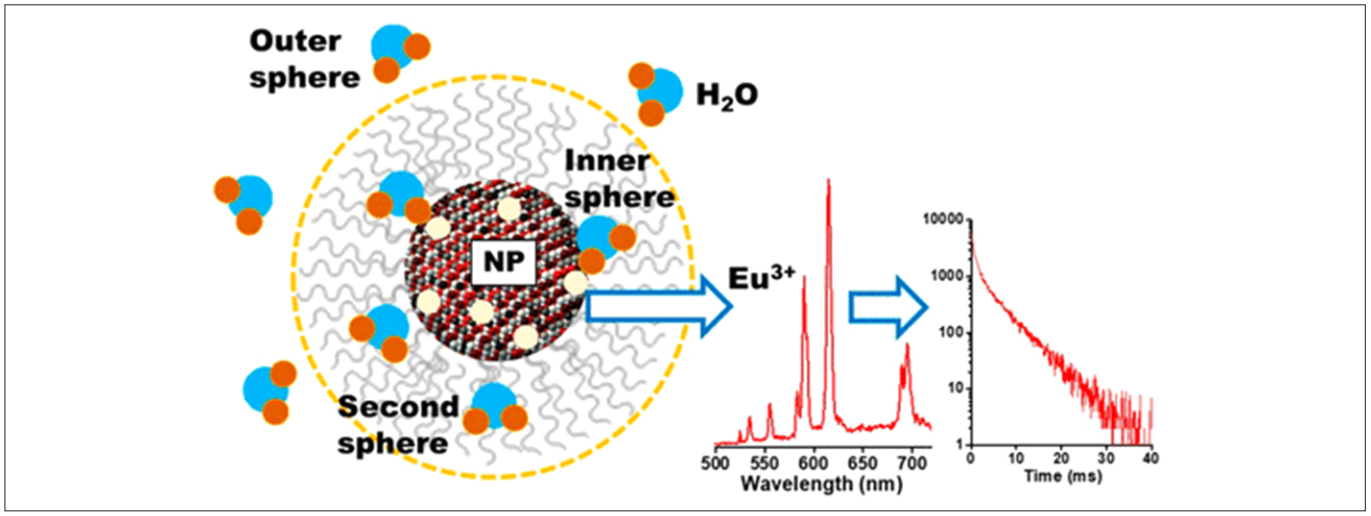

Fig.5.17. Scheme of the experimental verification of the contrasting mechanism of waterdispersed, Eu3+ based NPs. From [J. Phys. Chem. C2018, 122, 21, 11557 by permission.

to contrast changes in ^{1}H image caused by an interaction between water and paramagnetic ions, superparamagnetic iron oxides or by utilising an additional signal of x-nucleus (e.g ^{19}F). **The theranostic approach to local tuberculosis treatment enables drug delivery and imaging of the lungs for a better control and personalization of antibiotic therapy.** Metal-organic framework (MOF) Fe-MIL-101-NH2 nanoparticles were loaded with isoniazid. Magnetic resonance imaging (MRI) contrast capabilities were tested on porous lung tissue phantom and ex vivo rat lungs. The final product showed good aerodynamic properties, modified drug release, easier uptake by macrophages in relation to raw isoniazid-MOF, and MRI contrast capabilities. Starting from raw MOF, a fully functional inhalable theranostic system with a potential application in personalized tuberculosis pulmonary therapy was developedain [Pharm Res. 35, (2018)144, Pharm. 2019, 11(12)].

Other investigated materials were nanocapsules for anti-cancerous drugs delivery, containing substances commonly used as MRI contrast agents: magnetite (Fe_3O_4) or gadolinium (Gd) nanoparticles [Col. Surf. B 183 (219) 110396, RSC Adv. 2020, 43607]. An anti-cancerous drug (Paclitaxel, PTX) was encapsulated in multifunctional hybrid nanocarriers formed via the layer-by-layer technique with biodegradable polyelectrolytes labelled with gadolinium or with iron oxide nanoparticles (SPIONs). In both cases, we confirmed that the obtained NCs could be successfully used as MRI-detectable drug delivery systems. We demonstrated that nanocarriers with Gd display positive contrasting properties while nanocapsules with Fe_3O_4 can serve as negative MRI contrast agents. We carried out similar experiments for Fe_3O_4@SiOang2057 2@Au nanoparticles for MRI-guided chemo/NIR photothermal therapy of cancer cells [RSC Adv. 2020,10,26508]. In order to evaluate their theranostic potential, we investigated the MRI contrasting properties of the active element of the nanoparticle (i.e. Fe_3O_4@SiO_2). Very high R2 relaxivity rate value results in strong MR contrast.

Paramagnetic lanthanide-based NPs are currently designed MRI contrast agents to obtain optimal relaxivities at high magnetic fields of 7, 9.4, and 11.7 T where human imaging has been possible yielding high contrast to noise ratio compared to the clinical field of 3 T. However, the underlying longitudinal (T_1) and transverse (T_2) relaxation mechanisms of the NP-based contrast agents based on the spatial motion and proximity of water protons with respect to the paramagnetic ions on the surface of NPs are still not well understood, specifically in terms of contributions from inner, second, and outer spheres of coordination of water molecules to the NPs. We showed that the Gd3+-based NPs, e.g., NaGdF4, are promising T1 contrast agents owing to the paramagnetic Gd3+ possessing a symmetric 8S7/2-state and slow electronic relaxation relevant to its eficiency to produce a positive (T1) contrast. Water-dispersed NaGdF4:Eu3+ and NaY–NaGdF4:Eu3+ core–shell NPs were studied at 9.4 T. Excited state lifetime decays of Eu3+ dopants, which are highly sensitive to proximate water molecules, were analyzed, demonstrating a dominance of inner and second sphere contribution over outer sphere to the T1 and T2 relaxations in smaller NaGdF4:Eu3+ NPs while exclusively outer sphere in NaYF4–NaGdF4:Eu3+ core–shell NPs [Chem. C 2018, 122, 21, 11557]. (Fig 5.17).

Nanocarriers containing fluorine were another group of investigated materials. In our study we investigated nanocarriers formed via the layer-by-layer technique with biodegradable polyelectrolytes and with Nafion®: polymer with high ^{19}F content [Langmuir 2020, 36, 32, 9543,

Nanomaterials 2020, 10(11), 2127]. The close to zero natural concentration of ^{19}F nuclei in the human body makes fluorine atoms a perfect MRI marker without any natural background signal. This creates the opportunity of localizing and identifying only exogenous fluorinated compounds with 100% specificity of the signal. The application of heteronuclear magnetic resonance imaging results in obtaining a spatial distribution of X-nucleus imposed on a conventional 1H image. Such a contrast is so called hot-spot contrast. To overcome limitations due to such short T2, the 3D UTE pulse sequence was applied to ^{19}F MR imaging. Images of Nafion®- containing samples with SNR 5 with acquisition time below 30 min for ^{19}F concentration as low as 1.53×10^{-2} mmol $^{19}F/g$ of sample were obtained. This is comparable with the results obtained for the molecules which exhibit more preferable MR characteristics.

Multimodal probes are an asset to simplified and improved medical imaging. In particular, the combination of fluorescence imaging and magnetic resonance imaging (MRI) offers sought-after capabilities. We showed that pyrrolidin-2-one-capped manganese oxide nanoparticles (**MnO^{pyr}** NPs) combine MRI with fluorescence microscopy to function as efficient bifunctional bio-nanoprobes [ASC Appl. Mater. Interfaces 2019, 11,14 13069]. The **MnO^{pyr}** NPs are soluble in water without any further postsynthetic modifications. The r_1 relaxivity and r_2/r_1 ratio indicated that these NPs are potential T_1 MRI contrast agents at clinical (3 T) and ultrahigh (9.4 T) magnetic fields. Serendipitously, the as-prepared NPs were photoluminescent. The unexpected luminescence can be ascribed to the modification of the pyrrolidin-2-one during the thermal treatment. **MnO^{pyr}** NPs were successfully used to enable fluorescence microscopy of HeLa cells, demonstrating bifunctional imaging capabilities. A low cytotoxic response in two distinct cell types (HeLa, HepG2) supports the suitability of **MnO^{pyr}** NPs for biological imaging applications.

❖

6. Division of Applications of Physics

Energy production, human health and climate changes are major and closely interrelated challenges for the future of mankind. The rapid increase in world's population over the 20th century, together with its increasing energy consumption will soon exhaust the potentially limited natural resources of oil and gas, and of environmentally unacceptable coal. This stimulates and extends the search for environmentally friendly and renewable energy sources. Nuclear and thermonuclear sources of energy, such as that produced by the current nuclear fission reactors and the future nuclear fusion reactors, are environmentally clean and able to operate under any climatic conditions. Environmentally clean and renewable energy production should then relieve the symptoms of climate warming, observed, e.g., by glacier retreatment in the polar or high mountain regions of the world. Abundance of energy supply, while improving the quality of life and further extending the average life expectancy, will result not only in major societal changes but will also lead to a more frequent occurrence of cancer diseases - which must be offset by the development of means to fight and cure cancer more efficiently than today.

The activities of our Division of Applications of Physics are focused on three main research areas: future sources of energy, monitoring of the environment, and further advancing the fight against cancer. We are involved in the ITER (International Thermonuclear Experimental Reactor) project – a major world-wide effort to develop the future thermonuclear energy source. By operating and developing extremely sensitive instruments we are able to monitor and provide expert analysis of radiation in the environment, including the Arctic and mountain glaciers. Since February 2011, cancer patients are routinely treated with latest state-of-art proton radiotherapy at our Institute. Along with clinical work involving patient treatment, we conduct a broad programme of research in dosimetry and medical physics to improve the clinical outcome of such radiotherapy. We also continue our long tradition of developing innovative radiation detectors, mainly exploiting thermally or optically stimulated luminescence (TL, OSL), which are broadly applied in clinical dosimetry, environmental dosimetry and individual monitoring.

The **Department of Radiation Transport Physics** is actively engaged in a world-wide programme to develop future sources of energy - thermonuclear reactors, based on tokamak or stellarator principles. Working as partners of the European consortia - EUROfusion and Fusion for Energy, this Department develops high-resolution neutron diagnostics to study and control the plasma at the ITER tokamak. We are also heavily involved in the DONES project to prepare the design of the International Fusion Materials Irradiation Facility, DEMO-Oriented Neutron Source (IFMIF-DONES). The mission of IFMIF-DONES will be to test and validate the properties of materials irradiated by a fusion-type spectrum of fast neutrons at relevant doses and temperatures. Our activity in this project concentrates on modelling the neutron radiation doses, on the design of the Start-up Monitoring Module and on the design of facilities for complementary physics experiments. At our home laboratory we operate a 14 MeV neutron generator and our Plasma Focus Z-pinch device, mainly for purposes of basic research. This includes studies of plasma compression dynamics, of plasma pinch evolution, and of symmetry and stability of hot and dense high current-conducting electron-ion plasma with various plasma admixtures. Within another area of this activity, an expert Monte-Carlo modelling group develops extensive calculations of radiation transport in complex systems, applied in the design of neutron and gamma diagnostics, and in the evaluation and interpretation of results of experiments in various disciplines, including medical physics, plasma physics and nuclear borehole geophysics.

The **Department of Radiation Research and Proton Radiotherapy** is involved mainly in research on dosimetry for proton therapy, but also in dosimetry for GRID - spatially fractionated therapy and FLASH - high dose-rate

therapy. Analysis and measurements of out-of-field doses of scattered radiation in cancer radiotherapy have been performed in collaboration with the European Radiation Dosimetry Group EURADOS. The FRED Monte Carlo transport code was adapted to fast graphics card computing and applied in verifying treatment plans of proton therapy patients at the Cyclotron Centre Bronowice. A major facility used by this Department is the AIC-144 60 MeV proton cyclotron with two beam lines: a horizontal line to the eye therapy hall and a high intensity proton line to the AIC-144 experimental hall. These irradiation facilities enable proton irradiation to be performed very accurately over a wide range of doses (proton fluences) and dose rates. The adjustable range of the proton beam current is 2- 60 nA, its energy range is 10-60 MeV, with proton flux values ranging between 5 10^5 p cm^{-2} s^{-1} and 10^9 p cm^{-2} s^{-1}. The total absorbed doses delivered to fields of about 10 cm in diameter may range between 5 mGy and 120 kGy. This very precisely controlled and reproducible set of beam parameters allows proton beams to be applied in testing and quality control of clinical radiation detectors designed for radiotherapy purposes, in irradiating biological samples, including radiobiological experiments with animals, and in designing and performing tests of radiation hardness of electronics and materials applied in the space industry or around research accelerators (such as equipment for the LHCb experiment at CERN, or for the FAIR facility at GSI, Darmstadt). Irradiation of biological cells and small animals is also possible and has been performed. Adequate beam-time at this stand-alone 60 MeV proton facility is readily available to external users, unlike in other such facilities which typically share their beams on "parasitic" principles, competing with principal research or patient irradiation.

The **Department of Radiation Physics and Dosimetry** is involved mainly in solid state dosimetry research. This Department heavily engages in developing new methods of dose measurement and new types of luminescence detectors of ionizing radiation for applications in medical physics and radiation protection. The leading expertise and world recognition of this Department is in thermoluminescence (TL) dosimetry, stemming from its extensive over 30-year experience in the development, manufacture and application of TL detectors for radiation protection, environmental monitoring and clinical dosimetry. TL detectors produced in the Department's laboratory have been applied in the dosimetry of cosmic radiation on board of the International Space Station. In this Department, unique two-dimensional (2D) TL dosimetry systems have been developed and constructed for clinical applications in medical physics. Over the recent years increasing attention has been paid to optically stimulated luminescence (OSL) and radiophoto-luminescence (RPL) – based radiation detection and dosimetry. The Department currently engages in studies and development of novel luminescent materials, such as crystals grown *in situ* by micro-pulling-down and Czochralski methods at temperatures exceeding 2000°C. The Department of Radiation Physics and Dosimetry is well-equipped with a variety of research instruments which include research equipment for luminescence measurements, a Risø DA-20 TL/OSL reader, a fluorescence microscope, and several optical spectrometers.

Civilization hazards and issues related to environmental changes are the main topics studied at the **Department of Nuclear Physical Chemistry**. Here, radiochemical methods are applied to analyse radioactivity in the environment and to separate radionuclides produced by irradiating suitable elements by cyclotron beams. Within studies of environmental radioactivity, detection and measurements of activity of plutonium, americium, uranium, thorium, polonium, ^{90}Sr, ^{63}Ni, ^{7}Be, ^{99}Tc and ^{137}Cs in various environmental samples are performed. The Department's equipment consists mainly of low background, high resolution (germanium) gamma-ray spectrometers, semiconductor alpha-ray spectrometers and a liquid scintillator spectrometer. From 1990 onwards, the Laboratory is part of the national network to monitor radioactive contamination, organized by the Polish National Atomic Energy Agency (PAA) and the Central Laboratory for Radiation Protection (CLOR). In a dedicated control station, ambient air is continuously pumped through special filters and the radioactive aerosol content deposited on such filters analysed every week to assess the presence and activity of gamma-emitting elements in these aerosols. The system is extremely sensitive, with a detection limit below 1 Bq/m^3. Apart from alpha-spectrometry, beta and gamma-spectrometry routinely applied in analysing aerosols, mass spectrometry has also been introduced as a measurement technique, in collaboration with the Institute of Geological Sciences of the Polish Academy of Sciences. Over the recent years, investigations of radioactive contamination in the environment over polar areas of both the Arctic and the Antarctic became a very important part of environmental studies conducted in this Department. Radionuclides to be applied in nuclear medicine or tracers to be used in environmental radioactivity studies are also produced in this Department by irradiating suitable target materials with proton beams accelerated in the AIC-144 cyclotron.

The **Department of Mass Spectrometry** has recently been established in order to further extend our capabilities in performing environmental studies of natural and man-made radioactivity and of the contribution of potentially harmful chemical elements in the environment. Application of mass spectrometry is particularly useful in several of our projects concerning radioactivity in the environment over polar regions of Spitsbergen and the Antarctic. The presence of airborne artificial radionuclides (^{137}Cs, ^{238,239,240}Pu, ^{241}Am) and ^{240}Pu/^{239}Pu mass ratios is now being systematically studied over glacial areas throughout the world. The Department of Mass Spectrometry is also currently investigating potential applications of mass spectrometry in various branches of medicine. For nuclear medicine applications, new methods of measuring the internal radioactive contamination of medical personnel are being developed. Investigations of the metabolism of citrates and gluconates by isotope labelling techniques may also be applied in oncology. Installation of a new ICPMS mass spectrometer is planned in 2021.

Selected Research Highlights of the Division of Applications of Physics

In the quest for fusion energy, scientists have spent decades in finding ways of increasing the temperature of the plasma fuel. Very hot plasma is required to generate significant fusion power. The standard technique to heat plasma is to apply radio-frequency waves. In most reactors, plasma is made up of only two ion species. **Within a new approach**, developed by an international team where IFJ PAN researchers contributed [Nat. Phys. 13 (2017) 10] **fuel is made up of three ion species: e.g., hydrogen, deuterium, and trace amounts of helium-3**. Focusing the radio-frequency wave energy on ^{3}He ions heats these ions to much higher energies, due to ^{3}He ions being a much smaller fraction of the total density. **This allows the plasma to reach temperatures much higher than those previously observed**. This approach was tested at the Joint European Torus (JET) - Europe's largest fusion device and at the Alcator C-Mod reactor at MIT. Efficient acceleration of ^{3}He ions to high energies in dedicated plasma mixtures was demonstrated. Additionally, effective plasma heating was observed, as a result of the slowing-down of the fast ^{3}He ions. The developed approach is not only limited to laboratory plasmas, but may also explain observations of energetic ions in space-plasma environment, e.g., in ^{3}He-rich solar flares. (Fig. 6.1)

In the era of big data and machine learning we benefit from such digital tools to retrieve information on heavy impurity radiation and transport in thermonuclear plasma confined in tokamaks. This knowledge of impurity transport is critical for the performance of the tokamak device. Recent experiments and analysis have been conducted as part of the EUROfusion Medium-Size Tokamak work package on several machines: ASDEX Upgrade tokamak [Nucl. Fusion 59 (2019) 112014], the TCV tokamak [Nucl. Fusion 59 (2019) 112023] and on the Tore Supra & WEST tokamaks using various plasma heating schemes. A series of plasma discharges were performed at the ASDEX Upgrade to study the transport of tungsten (W) impurities, following controlled injections of their small amount by laser blow-off of a solid-state sample. This allowed investigation to be performed of the relative impact of radio-frequency (RF) heating at the ion cyclotron frequency and neutral beam injection on the in-out W asymmetries visible in the soft X-ray (SXR) distribution. A transient up-down SXR asymmetry potentially affecting central impurity accumulation was also reported at TCV during RF heating at electron cyclotron frequency, following controlled gas injections of neon and krypton. The SXR emissivity distribution is

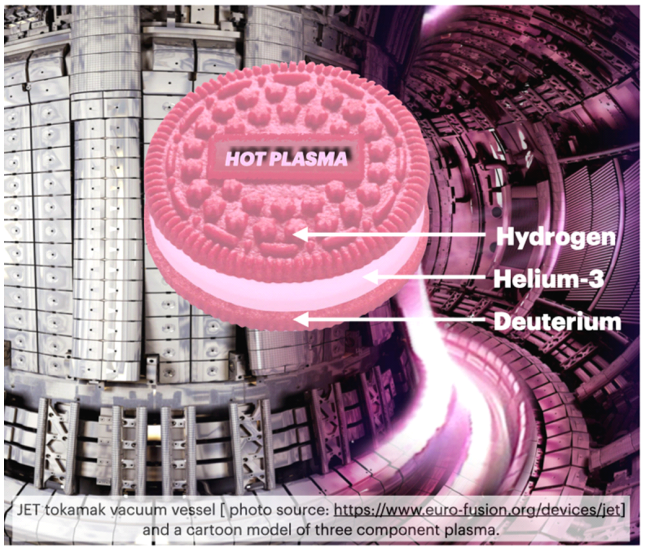

Fig. 6.1 The JET tokamak vacuum vessel [adapted from https://euro-fusion.org/devices/jet] and a cartoon model of a three−component plasma. In most reactors, the plasma is made up of two ion species. Here, a small amount of the third type of ions (Helium−3) is added to the plasma to capture the energy of radio−frequency waves.

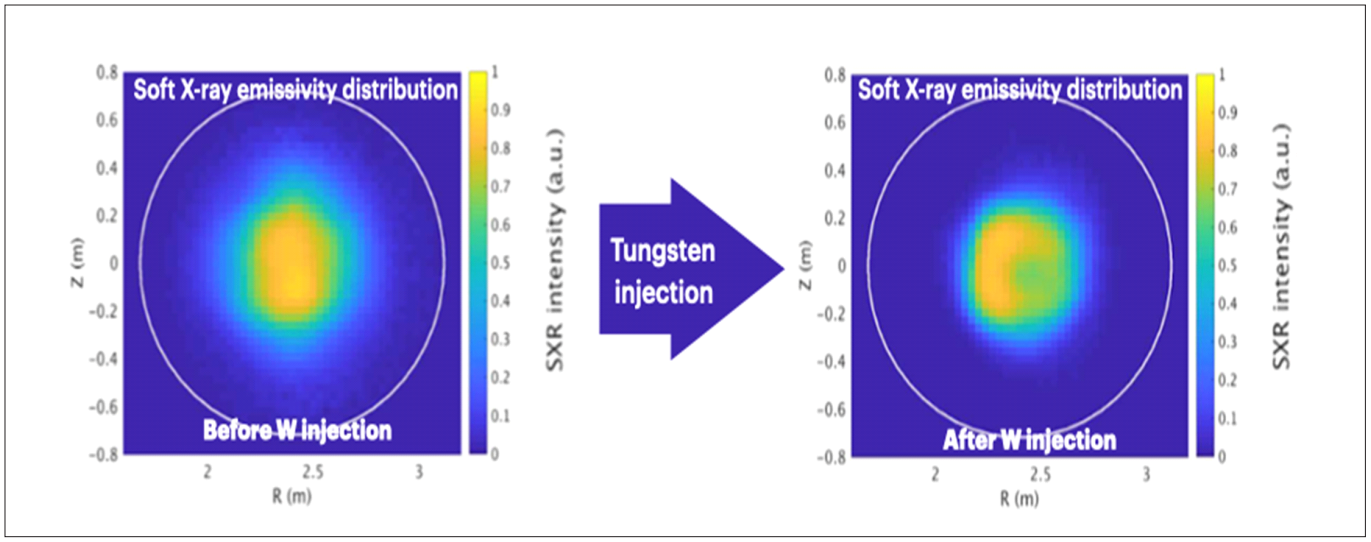

Fig 6.2. Tomographic reconstruction of soft X−ray emitted from plasma. For the reconstruction, a method based on neural networks was applied to the data from Tore Supra plasma discharge. Left: Distribution of soft X−ray plasma emissivity before injection of small amounts of tungsten using laser−blow off of a solid−state sample. Left: The same type of plot but after the injection of tungsten.

recovered by plasma 2D tomography, either using Tikhonov regularization or, more recently, using neural networks [Laser Part. Beams 37 (2019) 171]. An example of SXR tomographic reconstruction performed before and after W injection on Tore Supra is shown in Fig. 6.2. **The obtained data make it possible to recover the impurity distribution and to estimate diffusive and convective transport coefficients of impurities using the gradient-flux technique** [J. Fusion Energy 39 (2020) 240].

We reported novel research focused on plasma generated in our Z-pinch device called Plasma Focus. In a recent study the parameters of plasma pinch (i.e., a small plasma column) compression were studied and modelled using the 5-phase Lee model code to validate a simple description of Plasma Focus discharge. A new set of parameters and indicators was proposed to assess the occurrence of radiative compression and its strength in pure gases and gas mixtures. We found no, or relatively weak, radiative compression during all discharges in D_2 and D_2+Ar mixtures, under a constant total pressure of about 2.9 mbar [IEEE Trans. Plasma Sci. 47 (2019) 4301]. Relatively strong radiative compression was achieved only for some discharges in pure Ar. In the next step, discharges in D_2+Ne mixtures and pure Ne are currently being performed and analysed, using new diagnostic systems which include an ultra-fast 4-frame pinhole camera for vacuum ultra violet (VUV) and soft X-ray (SXR) imaging of the plasma column. An example of a 4-frame image captured using this camera is shown in Fig. 6.3. The measured and computed total neutron yield from D-D fusion was equal to 2.53 10^8 n/discharge and 2.96 10^8 n/discharge, respectively. **This demonstrates that a good approximation of plasma discharge parameters can be achieved using the Lee model code.**

The plasma-facing components of future thermonuclear reactors, such as DEMO, will be constantly exposed to a high flux of neutron radiation. To ensure their safe operation it is necessary to develop and validate its construction materials. None of the presently available neutron sources can adequately reproduce the

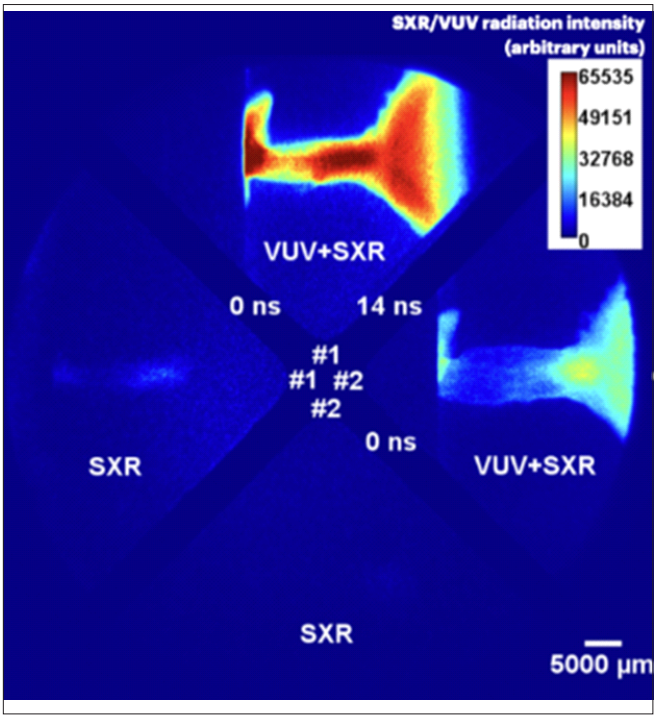

Fig. 6.3. Imaging of a plasma pinch in the Plasma Focus device using a four−frame camera with two SXR filters and two SXR+VUV filters. Due to the time delay of only 14 ns between consecutive frames, the plasma pinch compression dynamics and evolution may be studied. The colour scale in the image indicates the intensity of the registered radiation, in arbitrary units.

Fig. 6.4. Layout of the new IFMIF−DONES facility for neutron irradiation, to be constructed as part of the European programme for achieving electricity from fusion. The laboratory is essential for testing and validation of plasma−facing components able to withstand harsh radiation and temperature condition in the thermonuclear reactors, such as DEMO.

neutron fluxes predicted for DEMO. **This mission is foreseen for the IFMIF-DONES** (International Fusion Materials Irradiation Facility, DEMO-Oriented Neutron Source) laboratory which is planned as a neutron irradiation facility for testing and validation of materials to be used in the future fusion reactors [Nucl. Fusion 58 (2018) 105002]. A high intensity neutron flux with a spectrum similar to that observed in the D+T fusion reaction will be produced in stripping reactions of a 40 MeV D beam impinging on a liquid Li target. The general layout of the facility is shown in Fig. 6.4.

However, before the experiments at IFMIF-DONES can be performed, a detailed study of the produced neutron flux must be carried out. For this purpose, a Start-Up Monitoring Module (STUMM) for IFMIF-DONES is being designed at the Institute of Nuclear Physics PAN. The STUMM module will be used during the commissioning phase and before each series of irradiations, in order to validate radiation transport modelling and to ensure that material samples are exposed to the required dose and to the required neutron spectra in well-controlled conditions [Acta Phys. Pol. B 48 (2017) 687]. The general view of the module is shown in Fig. 6.5. The central part located ahead of the neutron beam is a

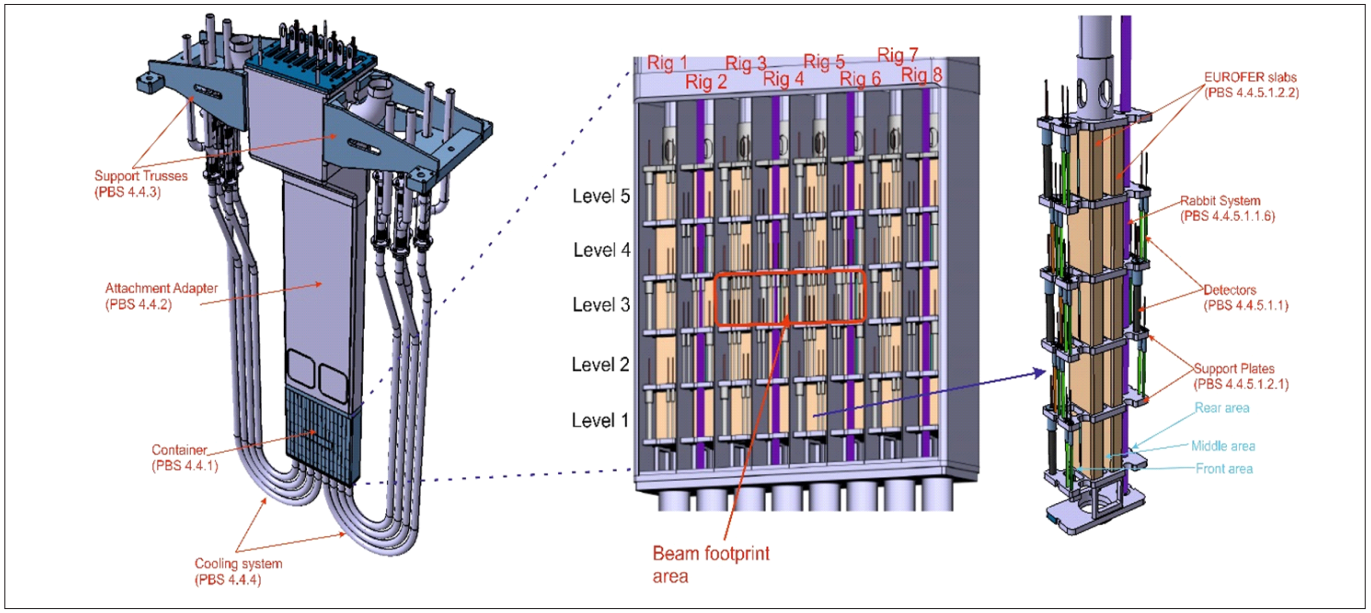

Fig. 6.5. Start−Up Monitoring Module for the IFMIF−DONES designed at IFJ PAN. Left: general view, centre: container, right: active part of the rig. The module will be filled with an array or radiation sensors and neutron and gamma detectors to evaluate the conditions under which samples will be irradiated and to validate the modelling of radiation transport.

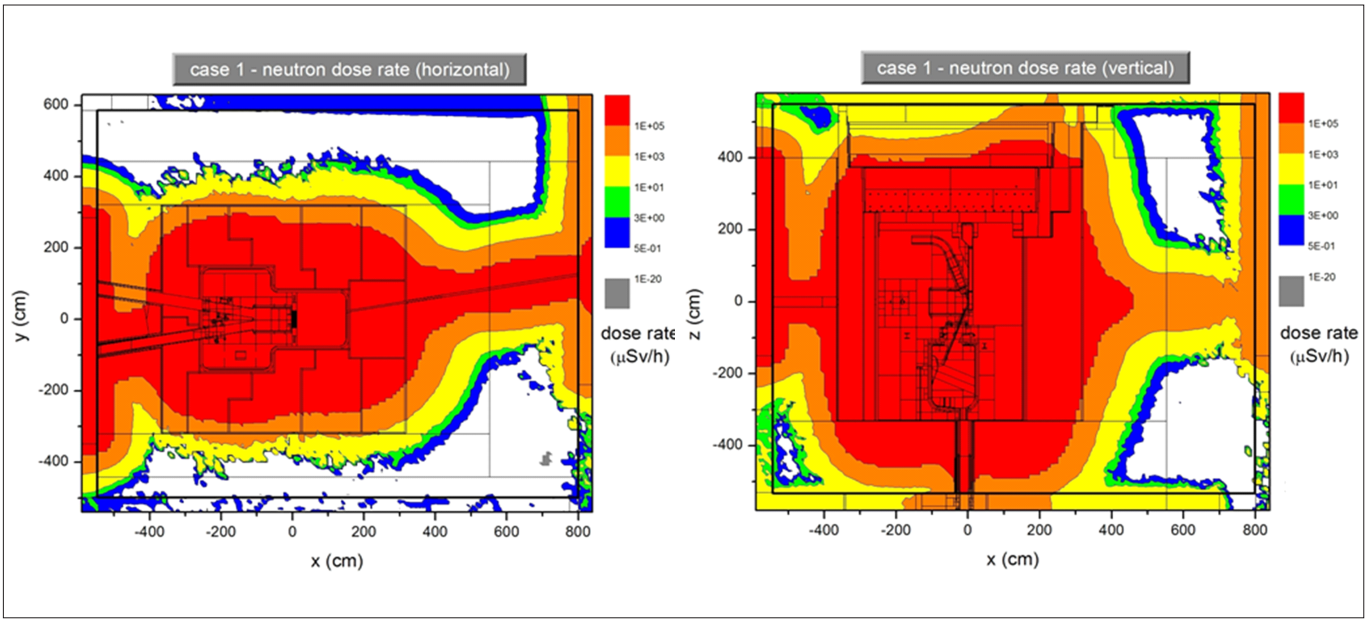

Fig. 6.6. Horizontal (left) and vertical (right) maps of neutron-induced dose rates calculated in the IFMIF-DONES Test Cell during operation of the facility. According to these maps, the neutron dose rate in the TC during its operation exceeds 10^5 Sv/hour (red colour). With such calculations the adequacy of the concrete biological shielding in ensuring safe working conditions in the adjacent rooms may be confirmed and verified [adapted from the "Radiation field during operation in the TC and surrounding rooms for the maintainable TC concept", Eurofusion Report EFDA_D_2M6SB6]

container which is the active area of the STUMM setup. An array of carefully selected radiation detectors is installed in eight rigs, of five levels each. During its operation the module will absorb considerable energy of radiation and will be cooled by liquid helium in order to remain in a stable thermal condition. The sensors selected for the STUMM must be compatible with the operating conditions of the module – they must be radiation-resistant and of relatively low radiation sensitivity to avoid detector saturation, yet must provide reliable dosimetry over a wide range of conditions (especially over the development phase of the facility). **The neutron flux at the module position during full power operation of IFMIF-DONES will be extremely high - expected to reach 5×10^{18} n m^{-2} s^{-1}.** Module prototyping and validation of components and sensors for the STUMM unit will continue over the next few years.

Large scale particle transport calculations using the MCNP (Monte Carlo N-particle) code coupled to the McDeLicious package were performed to simulate D-Li reaction in the neutron target of the IFMIF-DONES facility. The aim of this work was to provide input for the design and optimization of selected IFMIF-DONES systems [Fusion Eng. Des. 146 (2019) 1276]. Three-dimensional spatial distributions of dose rates and fluxes were computed for the irradiation Test Cell (TC), surrounding shielding walls, and in adjacent rooms, to verify the shielding efficiency and confirm the radiation classification of these areas. Computation of dose maps inside and outside the TC walls required that variance reduction techniques, such as the ADVANTG 3.0.3 (AutomateD VAriaNce reducTion Generator) code, be used. **According to these calculations, the neutron dose rate in the Test Cell during its operation will significantly exceed 10^5 Sv/hour (Fig. 6..6). Adequacy of the concrete biological shielding was verified to ensure safe working conditions in neighbouring rooms. These analyses are essential for planning operations and maintenance activities within various areas of the IFMIF-DONES facility [J. Fusion Energy. 37 (2018) 168].**

Measurements of neutron streaming through penetrations in the biological shield are being carried out at the JET tokamak using thermoluminescence detectors (TLD) in order to validate the neutronics codes and nuclear data applied to ITER analyses in a real fusion environment. This work is carried out within the framework of the EUROfusion Consortium. The response of TLDs to the neutron component of the radiation field is related to neutron fluence in a well-defined neutron energy spectrum. Calibration of TLDs in real fusion radiation conditions was essential to ensure correct evaluation of the neutron fluence at JET at various locations. Irradiation of TLD samples was performed in a bare configuration and inside moderators with 2.5 MeV (DD reaction) and 14 MeV (DT reaction) neutrons at the Frascati Neutron Generator (FNG). The new factors (Fig. 6.7) which resulted from these calibrations will be applied in past and future JET measurements and will reduce the observed discrepancy between calculations and measurements noted in

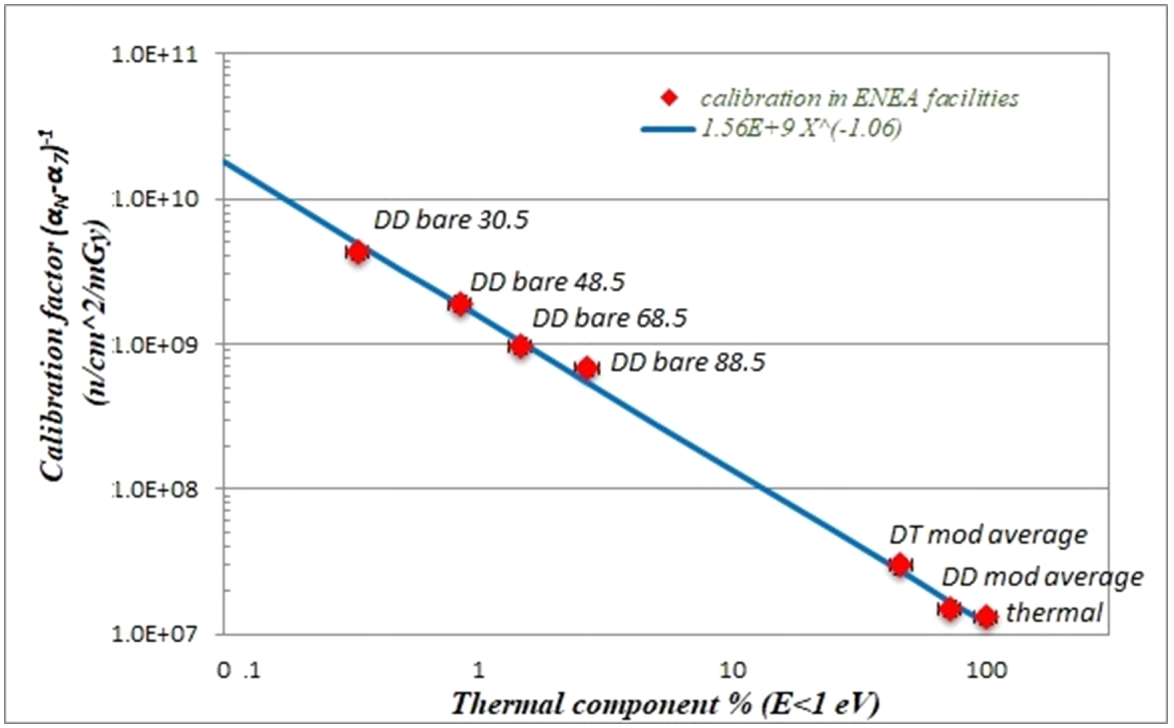

Fig. 6.7. Calibration factor ($_{N}$− $_{7}$)$^{-1}$ versus the percentage of the thermal neutron component in the calibration campaigns at the ENEA facilities. [adapted from Nucl. Instrum. Methods Phys. Res., Sect. A 904 (2018) 202]

a past neutron streaming experiment at JET. **The detection system based on TLDs developed and calibrated for JET experiments can be applied more generally in fusion neutron fields - for example at ITER, to monitor neutron fluence outside the biological shield.**

Selection of materials for ITER components was a most challenging task due to the unique operational conditions. Despite the experience from other tokamaks, and knowledge gained at fission neutron irradiation programs and also from theoretical calculations, the choice of materials was not simple, since for a number of materials the existing databases were neither complete nor sufficient. The scope of the Eurofusion WPJET3 ACT subproject was to perform benchmark irradiation experiments at the JET tokamak, to irradiate samples of actual ITER materials. Within the JET C38 D-D campaign a total of 27 ITER material samples (foils) were irradiated. The foils were then distributed between four European laboratories for subsequent analysis. The study carried out at IFJ PAN and based on low background gamma spectrometry identified ^{57}Co, ^{58}Co, ^{60}Co, ^{59}Fe, ^{51}Cr, ^{54}Mn for a sample of radial closure plates of toroidal field coils, ^{57}Co, ^{58}Co, ^{60}Co, ^{59}Fe, ^{51}Cr, ^{54}Mn, ^{65}Zn for a shield as well as ^{60}Co, ^{51}Cr, ^{65}Zn for CuCrZn pipes for divertor tungsten monoblocks. **The results are relevant for the prediction of future ITER shutdown dose rates and decommissioning strategies.**

One of the main research directions is development and investigation of new luminescent materials for applications in dosimetry of ionizing radiation. Several new dosimetry materials in the form of crystals grown by micro-pulling-down (m-PD) and Czochralski methods were systematically studied. Recently, lithium magnesium phosphate ($LiMgPO_4$, LMP) (Fig.6.8) has gained wide recognition because it offers substantial advantages against the well-known LiF-based dosimeters. Among these advantages are, in particular, linear dose-response [Radiat. Meas 85 (2016), 88] extending beyond 1 kGy (no saturation effects were observed within this dose range) as well as high radio-sensitivity, if doped with appropriate rare-earth (RE) elements. These features are directly related to the increased efficiency of this material to alpha particles [Radiat. Meas. 113 (2018), 14]. Moreover, radioluminescence was recently reported in this material [Radiat. Meas. 136 (2020), 106408], also suggesting its potential application as a scintillation detector. **Promising results recently obtained for differently doped LMP crystals** [Materials 12 (2019), 2861; Materials 13 (2020), 2032] **also suggest that, in the nearest future, LMP may well become the standard material in modern radiation dosimetry**.

Another group of materials that are currently considered for luminescent applications are perovskite structure materials. These are nowadays of particular

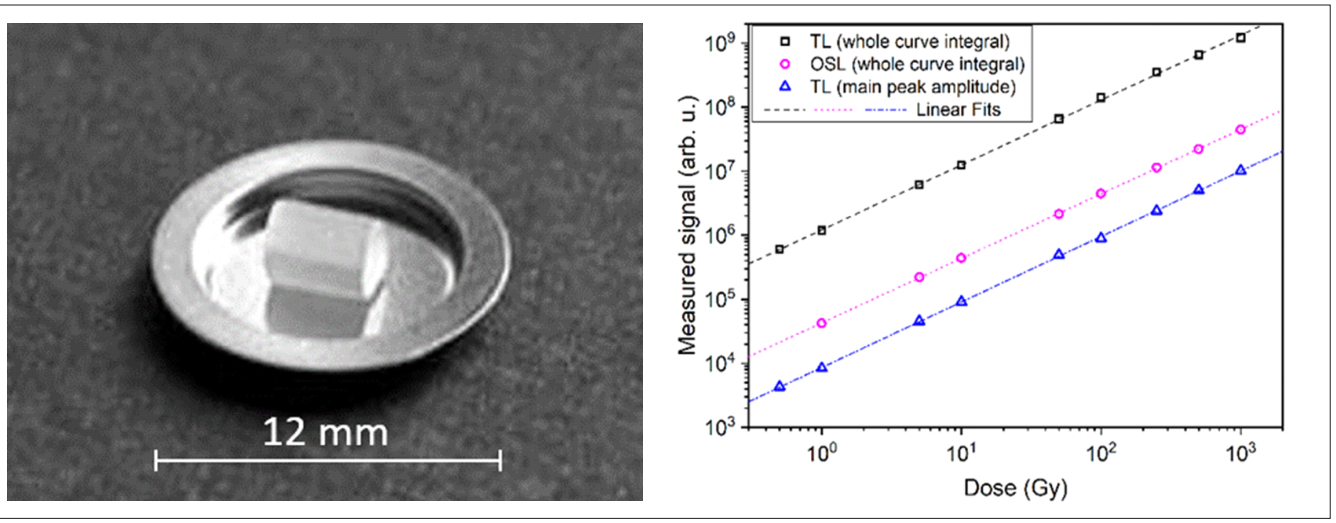

Fig. 6.8. Example of an LMP crystal grown from the melt by the micro-pulling-down method (left), and linear dose-response measured for the LiMgPO4 crystal over the dose range up to 1 kGy (right)) [adapted from Radiat.Meas. 85 92016), 88].

significance due to the wide range of their potential applications (e.g., in optoelectronics, solid-state lasers, radiation detectors, and solar cells). Differently-doped perovskite crystals were successively grown at the IFJ PAN crystal growth facility and their luminescent properties were investigated in detail. It was shown that the Ce^{3+} dopant incorporated in Y_2O_3-Lu_2O_3-Al_2O_3 triple oxide system may be utilized as an effective indicator of perovskite and garnet crystallographic phases, as the Ce^{3+} emission in these phases is spectrally well separated [Opt. Mater. 89 (2019) 408]. Partial substitution of Y with Lu and further, of Lu with Gd ($Lu_xY_{1-x}AlO_3$ and $Gd_xLun_{1-x}AlO_3$, respectively) as well as complete substitution of Y with Lu and Gd ($LuAlO_3$ and $GdAlO_3$) increased the Z number of the host material and made it possible to improve the energy transfer from RE-based host cations to Eu^{3+} and Tb^{3+} ions [Radiat. Meas. 126 (2019) 106140; Crystals 10 (20200 385)]. (Fig.6.9). **These observations suggest that the studied perovskites, besides being fast and efficient scintillators, may also become very promising energy-storage phosphors for dosimetry applications.**

A novel method of radiation detection has been developed, basing on the fluorescence of lithium fluoride crystals [J. Lumin. 213 (2019) 82, Opt Mater. 90 (2019) 1,

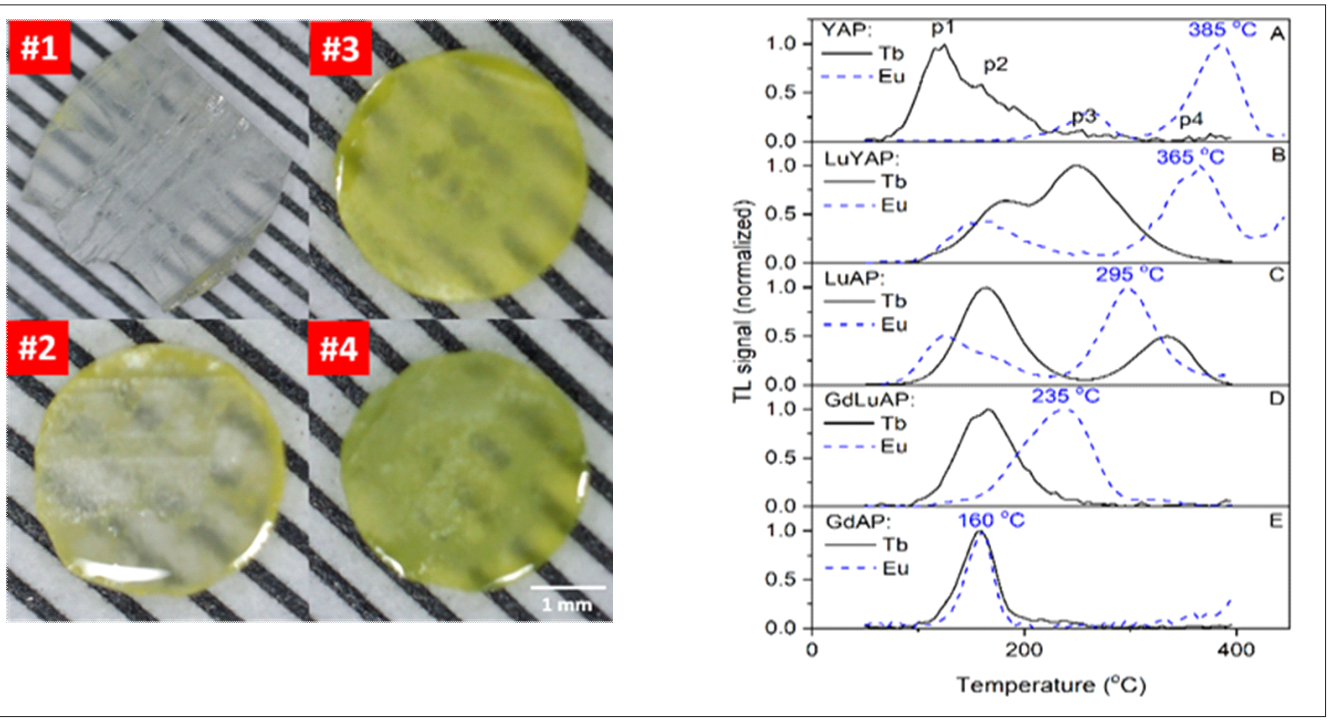

Fig. 6.9. Crystals of Ce-doped Y2O3-Lu2O3-Al2O3 triple oxide system grown from the melt by micro-pulling-down method (left). Defects engineering realized by RE-based host cation substitution and related changes of the measured glow-curves (right) [adapted from Opt. Mat. 89 (2019), 408] .

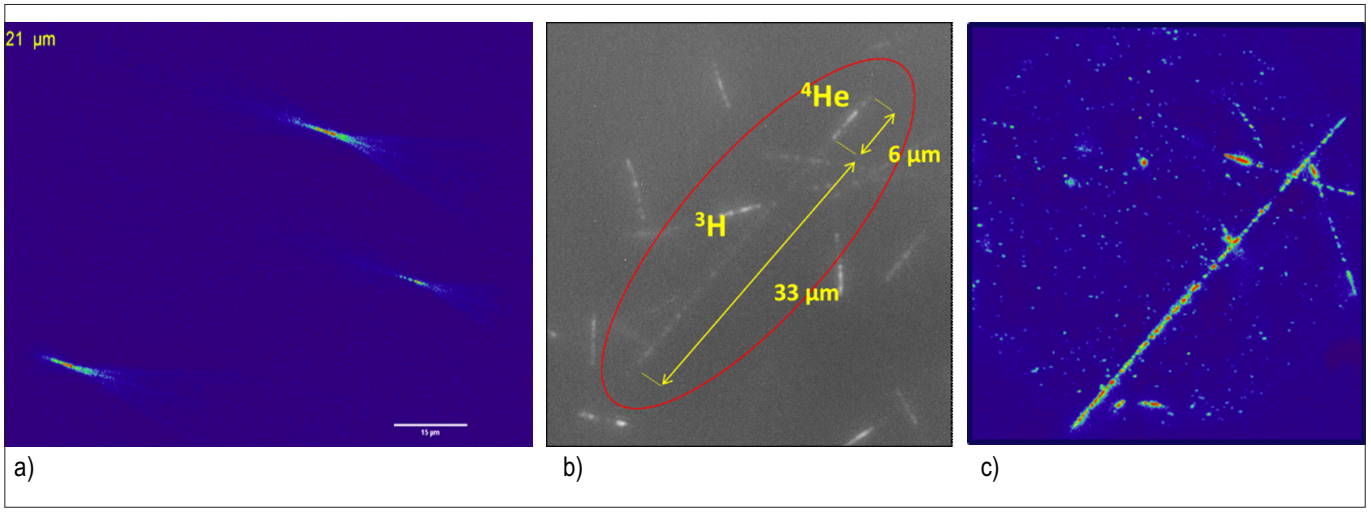

Fig. 6.10. Examples of fluorescent tracks in LiF crystals: a) iron ions with energy 145 MeV/amu, b) alpha−particle and tritium nuclei – products of ^{6}Li(n,) reaction, c) cosmic radiation at the Earth orbit.

Radiat. Meas. 116 (2018) 35]. Charged particles traversing the crystal produce anion vacancies, mainly F_2 centres, composed of two anion vacancies with two bounded electrons and F_3^+ of three vacancies with two electrons. If an irradiated LiF crystal is illuminated by blue light, photoluminescence emission is observed at about 670 nm, related to F_2 and at about 530 nm - related to F_3^+centres. Using a wide-field fluorescent microscope with a highly sensitive digital camera, we succeeded in imaging tracks produced by just single nuclear particles. It was possible to obtain images of high-energy ions, alpha-particles, as well as the products of ^{6}Li(n,) reaction (Figs. 6.10). These investigations were performed using LiF crystals grown in our laboratory with the Czochralski method. Analysis of fluorescent track images in 3D enabled us to develop a method of alpha particle spectrometry based on track-length measurements [Measurement 160 (2020) 107837]. **LiF fluorescent track detectors were used within the DOSIS-3D experiment at the International Space Station on the Earth orbit to register tracks of cosmic radiation particles** (Fig. 6.10c).

A new ultra-low-level gamma spectrometer with an active shield was constructed [J. Radioanal. Nucl. Chem. 322 (2019) 1311]. The achieved level of background reduction is equivalent to placing this spectrometer some 20-30 m (of water) below ground level. The modular construction of the spectrometer and the applied digital data acquisition format, including off-line data analysis, made it possible to further extend the range of this research device. This spectrometer is currently used in studies of radioactivity of air filters from the Antarctic (in collaboration with the Finnish Meteorological Institute) or in evaluating radionuclides present in meteorites. Owing to its digital data acquisition system, it became possible to significantly expand the research potential of this gamma-ray spectrometer. Indeed, as initiated in September 2019, the flux of cosmic-ray muons, registered by the active shield detectors, could be monitored concurrently with spectrometry measurements (Fig. 6.11). **Thus, within a single instrument - a low-background digital gamma gamma-ray spectrometer - two different branches of physics may be concurrently addressed: low-background gamma-ray spectrometry and astrophysics (e.g., the CREDO project).**

At the IFJ PAN, regular proton therapy of cancer patients began in February 2011. This activity is accompanied by a broad range of applied research

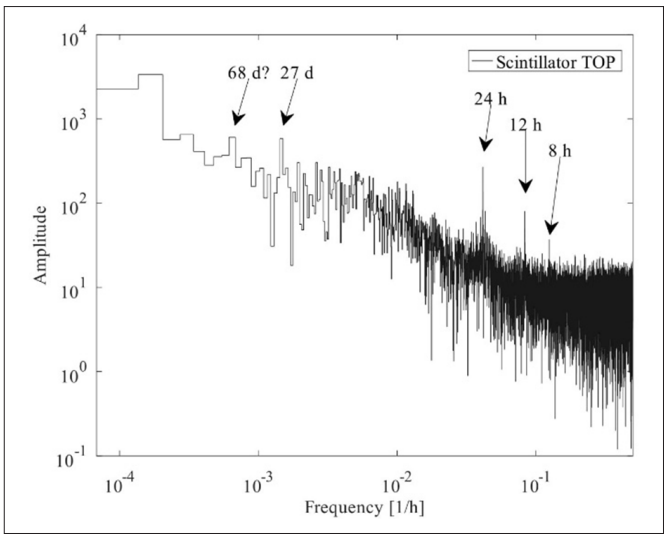

Fig. 6.11. Frequency distribution of the secondary muon flux (normalized at standard air pressure) registered in the largest scintillator of the active shield of the ultra−low−level gamma spectrometer. The Earth's rotation cycle (24h) and Sun's rotation (27 days) as well as harmonic day cycles of 12 h and 8 h may be distinguished. The nature of the 68−day cycle remains unclear.

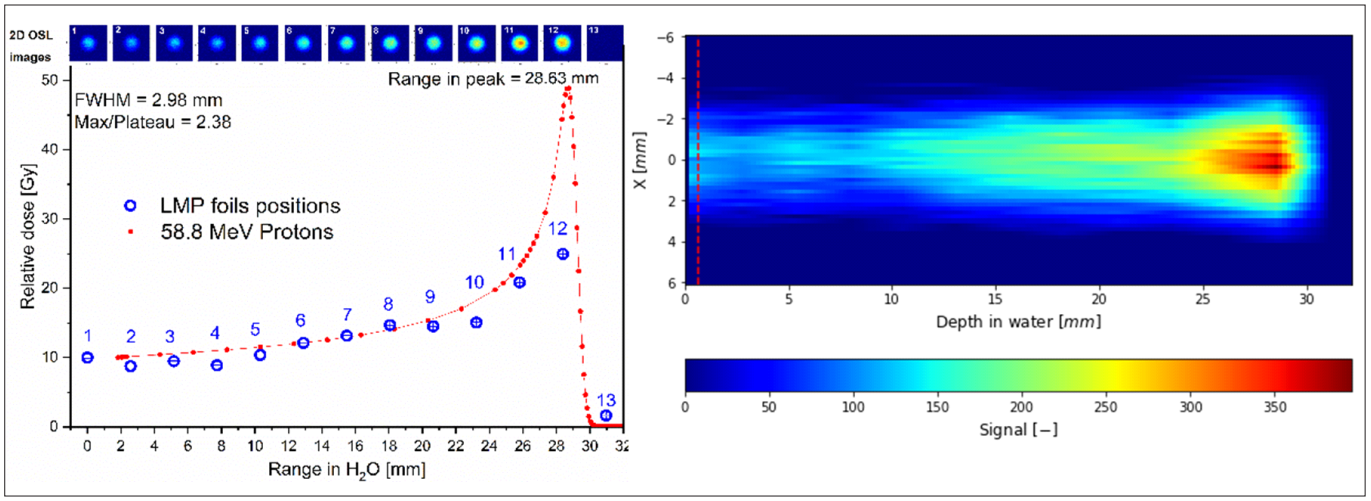

Fig. 6.12. Relative dose–response obtained from 2DOSL foils placed at different depths in the Bragg Peak (right), together with a reconstructed image of the actual 2D proton depth dose distribution, obtained from captured 2D OSL images. [Radiat. Meas. 133 (2020) 106255]

including clinical radiation dosimetry, medical physics and radiobiology. In modern radiation therapy two-dimensional (2D) dosimetry is required to validate complex treatment plans and in Quality Assurance procedures. A novel and promising approach in 2D dosimetry developed at the Department of Radiation Physics and Dosimetry is based on the optically-stimulated luminescence (OSL) phenomenon. By investigating prototype 2D OSL dosimeters in the form of flat and flexible sheets made of a polymer containing the embedded OSL material in the form of powder ($LiMgPO_4$, LMP), accompanied by an in-house-developed optical imaging setup consisting of an illuminating light source and a high-sensitive CCD camera, the possibility was verified of obtaining 2D dose distributions for clinical applications. The newly developed 2D dosimetry foils based on OSL readout are flexible and water-resistant, and applicable even in strong magnetic fields where electronic devices fail. **The newly developed 2D OSL system has been tested by verifying proton depth dose distributions in the treatment of eyeball melanoma at the Proton Eye Radiotherapy Facility at IFJ PAN**, using a dedicated patient collimator and a 60 MeV unmodulated proton beam (Fig. 6.12).

The range of a proton beam can be monitored by detection of secondary radiation produced by the interaction of protons in the therapeutic beam with patient tissues and emitted by the patient. Within the project *J-PET technology for proton beam therapy range monitoring* (LIDER/26/0157/ L-8/16/NCBR/2017) a novel plastic-scintillator setup, designed for diagnostic PET imaging (J-PET) and developed at the Jagiellonian University, was applied in a feasibility study of proton beam range monitoring at the CCB patient irradiation facility of IFJ PAN. The sensitivity of different geometry configurations of the J-PET detector was assessed by Monte Carlo simulations and tested in pilot experiments at CCB. The GATE/Geant4 Monte Carlo toolkit was used for calculating the + activity induced by proton beams in phantoms and in patients, and the expected J-PET detector response. CASTOR software was used to reconstruct in three-dimensions the + activity distributions. **The studies suggest that J-PET technology might be considered as a novel approach for beam range monitoring in proton therapy.** (Fig.6.13). [Acta Phys. Pol., B 51 (2020) 409]

A dose measurement method currently being under development is real-time dosimetry based on measurement of radioluminescence (RL) emitted by a detector in the form of a small luminophore crystal [Radiat. Meas. 136 (2020) 106408]. RL relies on an emission of light under irradiation which accompanies transitions between energy levels in a luminophore crystal. This light occurs spontaneously during exposure of the RL detector to ionizing radiation, and is dependent on the dose rate. A novel PORTOS (portable OSL/RL) optical system was constructed at IFJ PAN as a small, portable and remotely acting device consisting of a Hamamatsu H10682-210 photomultiplier located at one end of a 15 m quartz optical fibre, at the other end of which a detector, in the form of a slice of a crystal, is placed. A piece of a $LiMgPO_4$ luminophore crystal rod (of 3 mm diameter and 1 mm thickness) grown at IFJ PAN by the micro-pulling-down method is sensitive to ionizing radiation and can be applied as a radiation detector. The PORTOS system is controlled by software enabling the signal to be recorded with sampling times of 1 s up to a few seconds and over measurement duration times ranging between milliseconds and a

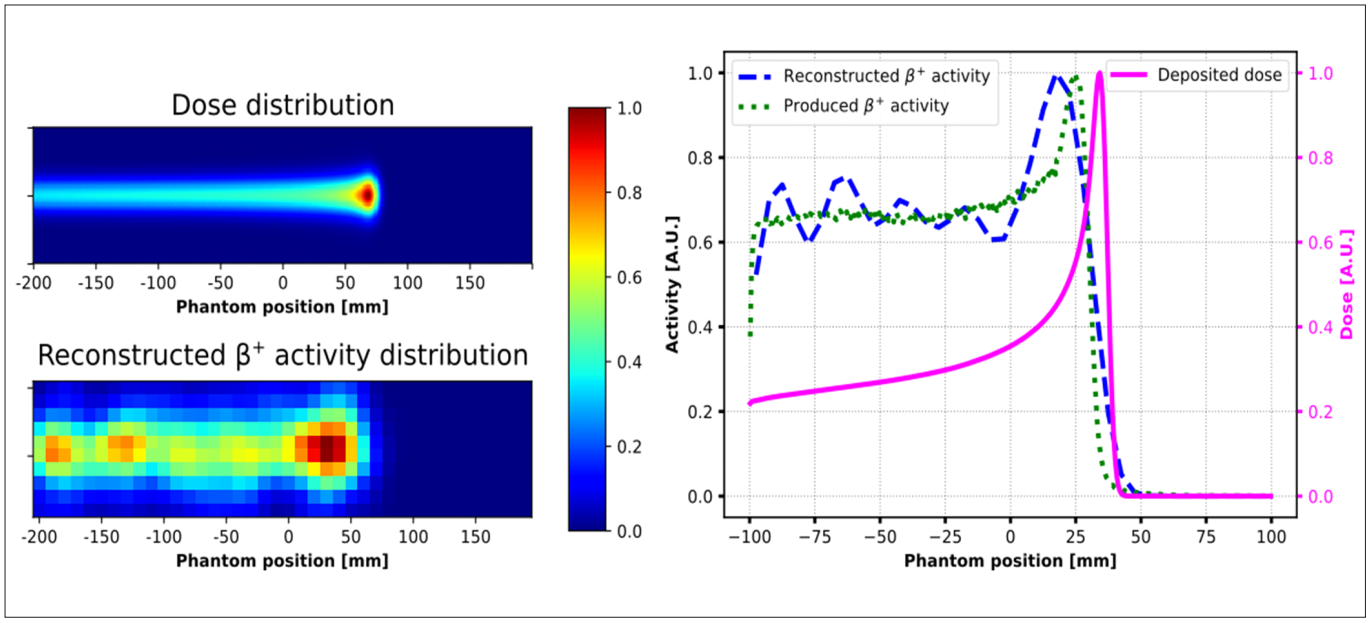

Fig. 6.13. Monte Carlo simulations of dose (top−left) and reconstructed + activity (bottom−left) produced in a homogenous phantom by a 150 MeV proton beam. Profiles of dose, + production and reconstructed + activity detected with J−PET (right) suggest a correlation between dose activity – which may then be used for monitoring the proton beam range during therapy [adapted from [Acta Phys. Pol., B 51 (2020) 9]

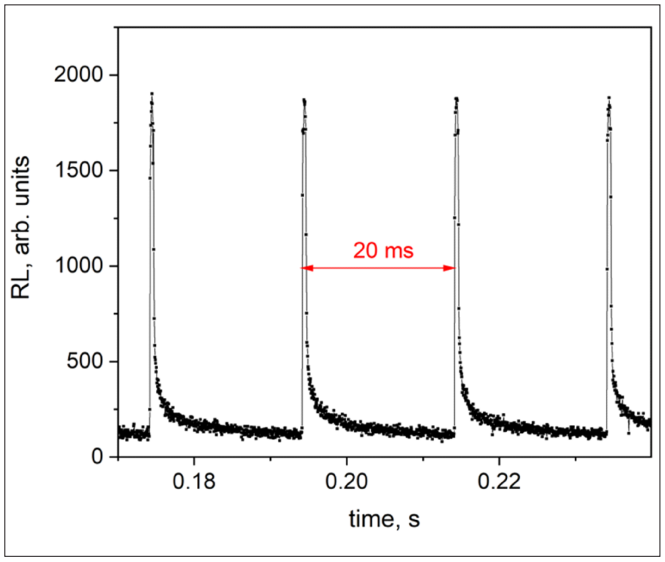

Fig. 6.14 Proton beam structure of the AIC−144 cyclotron, measured with the PORTOS device.[adapted from Radiat. Meas. 136 (2020) 106408]

few hours (Fig. 6.14) **The developed system with a millimetre-sized detector could be applied, e.g., as a point-like dosimeter in proton radiotherapy.**

Undesirable doses to healthy tissues distant from the target volume largely depend on the beam delivery technique. In proton therapy of children, special attention should be given to the treatment of shallowly-located tumours because lesions might be located closer than a few centimetres beneath the patient's skin. In facilities with PBS technology, the lowest energy of the proton beam typically ranges between 60 MeV and 100 MeV, which corresponds to a range of about 3.1-7.5 cm of water-equivalent thickness. In our work radiation doses in 5-year and 10-year anthropomorphic phantoms and in the treatment room were experimentally determined for two types of pre-absorbers – a range shifter (RS) and a personalized 3D-printed proton beam compensator (PC). The results of the measurements performed with European Radiation Dosimetry Group EURADOS and within the Horizon 2020 INSPIRE project confirmed that **the use of beam compensator as a pre-absorber does not significantly increase, and in many cases slightly decreases, out-of-field-doses** (Fig. 6.15). **Personalized 3D-printed proton compensators can be safely used to treat paediatric patients.**

In protocols of clinical proton therapy, it is assumed that the effect of nuclear fragmentation on the biological effectiveness of the proton beam may be neglected. It was suggested [Radiat. Prot. Dosim. 180 (2018) 296] that inclusion of secondary fragments leads to a significant increase in values of calculated average LET in proton beams which may also indicate a possible enhancement of their radiobiological effectiveness. Within an international initiative – MoVe-IT, an *in-silico* Monte-Carlo experiment to simulate the interaction of a monoenergetic beam with liquid water was performed using the Prometheus supercomputer [Physica Med. 80 (2020) 342]. It was shown that **the highest contribution to cell killing may appear over the entrance channel of the proton beam. Enhanced cell killing is caused by excess production of helium ions and of secondary protons, mostly in the central region**

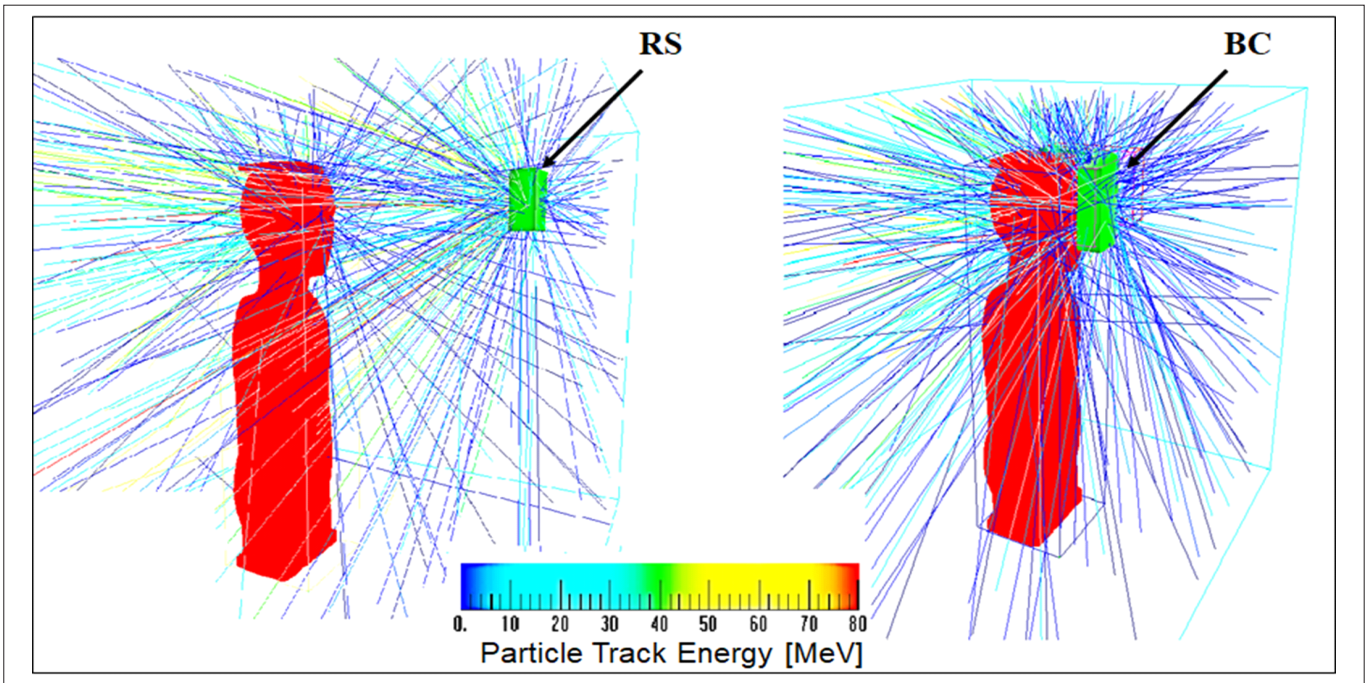

Fig. 6.15 Visualization of neutron paths produced by a therapeutic proton beam in two pre−absorbers (left – Range Shifter, right – Beam Compensator), for a nozzle angle of 0°.

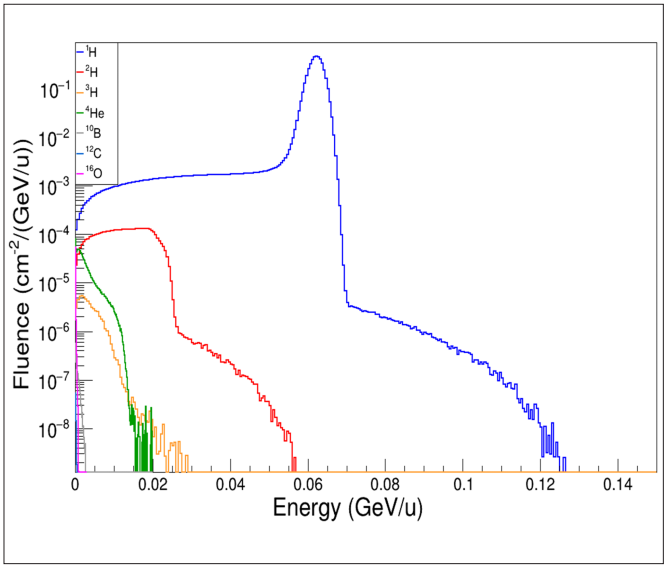

Fig 6.16 The energy−fluence spectrum of fragments generated by 150 MeV protons in liquid water, calculated at the depth of 12.5 cm. The highest contribution of secondary radiation arises from secondary protons and ^{4}He ions [adapted from Physica Med. 80 (2020) 342].

around one-half of the beam range (Fig. 6.16). The outcome of such studies may lead to improvements in treatment planning and to a better understanding of radiation action. Software tools developed during that project were made freely available in the public domain and have been frequently applied by our research partners.

Physical and biological range uncertainties, i.e., uncertainty of the distance that protons travel inside a patient body, limit the clinical potential of proton beam therapy. Fast Monte Carlo simulations to verify the patient treatment plan are essential in reducing physical and biological range uncertainties in the patient body and in achieving more accurate treatment with proton beams. Within the project *Quantification of biological range uncertainties towards an improved patient treatment in CCB Cracow proton beam therapy centre* (POIR.04.04.00-00-2475/16-00) performed within a broad international collaboration including the Sapienza University of Rome and INFN at Frascati, the FRED GPU-accelerated Monte Carlo (MC) simulation toolkit was adopted for calculations of physical (depth) and biological dose distributions in scanned proton beams (Fig.6.17). MC simulation results were found to be in excellent agreement with a large number of dose distributions measured in water and in heterogeneous phantoms. Systematic studies were performed to quantify the biological range uncertainties of proton beams exploring various models for the evaluation of biological dose in about 100 patients treated at CCB. **The computational methods developed within this project are now applied in several proton therapy centres, as clinical routines for quality assurance of patient treatment, and for pre-clinical research** Front. Phys. (2020) 8:578605

Over the past few years, development of personalized medicine has attracted considerable attention. Within this approach in nuclear medicine, diagnostic techniques, such as non-invasive imaging by means of

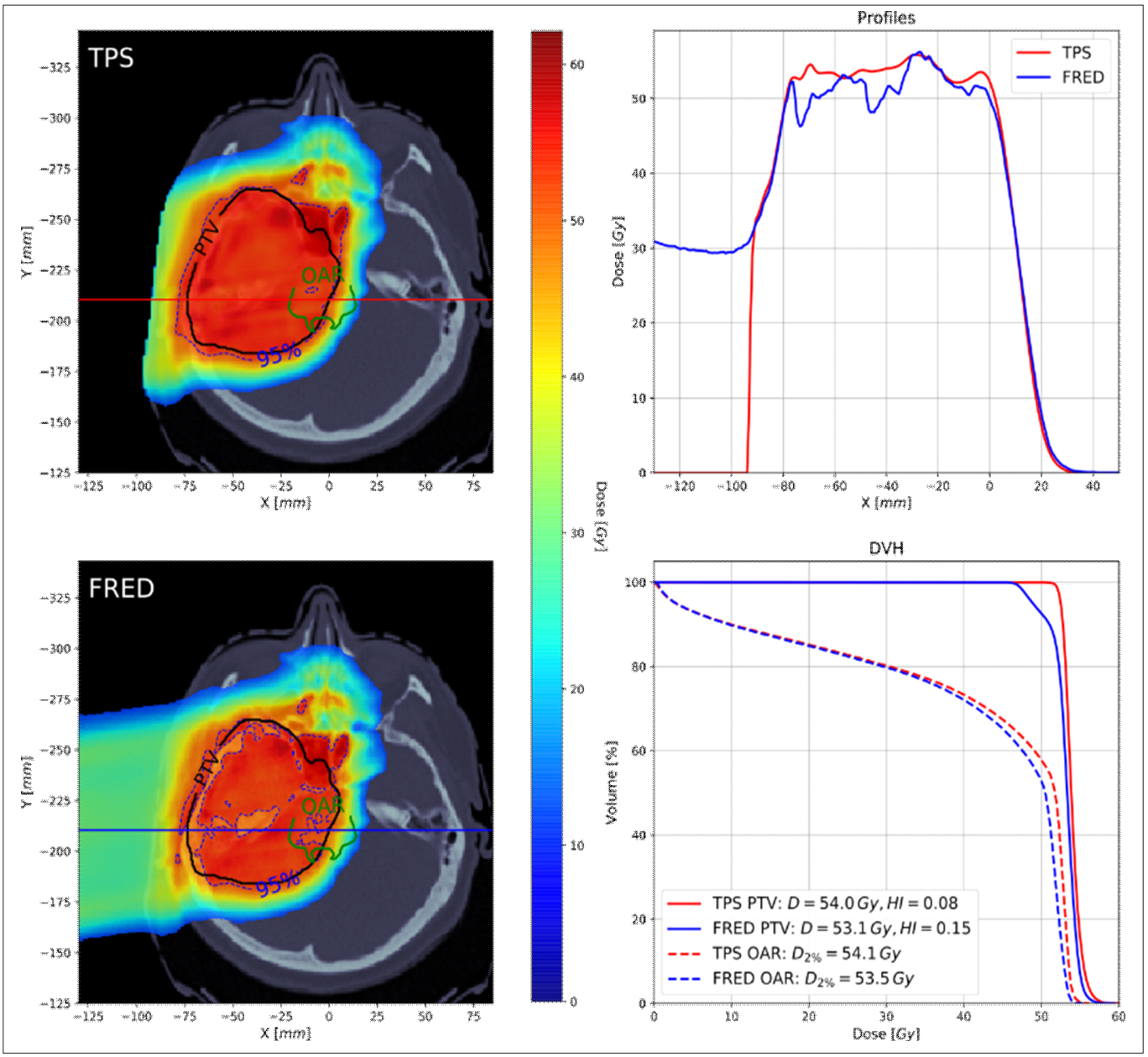

Fig. 6.17. Dose and DVH distributions obtained for a treatment plan of a patient treated at CCB calculated using a clinical treatment planning system (top−left panel) and the FRED Monte Carlo code (bottom−left panel). The respective dose and DVH distributions are shown in upper and lower right panels. Monte Carlo verification of the treatment plan may become a Quality Assurance procedure in patient treatment [adapted Front. Phys. (2020) 8:578605].

Positron Emission Tomography (PET) or Single Photon Emission Computed Tomography (SPECT), may be combined with individualized radiotherapy treatment. This combination, termed teranostics, exploits the same molecular targeting vectors labelled either with a diagnostic or with a therapeutic radionuclide. Only a limited number of matching radionuclides exhibit suitable decay characteristics for such an application. The radionuclides of scandium, ^{44}Sc/^{43}Sc and ^{47}Sc, are interesting teranostics candidates. Based on its physical and chemical characteristics, the − emitting ^{47}Sc is particularly interesting as a radionuclide therapy agent, while the decay characteristics of ^{44}Sc and ^{43}Sc are well-suited for diagnostic PET imaging. Due to its low-energy beta emissions, the ^{47}Sc isotope may be applied to preferentially treat small cell clusters, single tumour cells or micrometastases. At the same time, ^{47}Sc emits a 159 keV gamma line, enabling SPECT imaging to be performed concurrently with such radiotherapy. Proton bombardment of an enriched calcium target may produce ^{47}Sc [J. Radioanal. Nucl. Ch.,313(2017) 429] Together with IChTJ (Institute of Nuclear Chemistry and Technology, Warsaw), systematic studies of ^{47}Sc production in $^{nat}CaCO_3$(p,2n)^{47}Sc and $^{nat}CaCO_3$(p,pn)^{47}Ca reaction by protons over an energy range 60–0 MeV were performed using the AIC-144 cyclotron at IFJ PAN. **A maximum in the ^{47}Sc yield, of 143.95 ± 9.36 kBq/ Ah, at proton energies between 24 - 17**

MeV was stated, where the contribution of ^{48}Sc and ^{46}Sc impurities remained below 13% and 0.2%, respectively. Application of a consecutive indirect method (^{47}Ca/^{47}Sc generator) removes ^{47}Sc the ^{48}Sc or ^{46}Sc impurities. This separation process, based on the precipitation of $Sc(OH)_3$ and its separation on a 0.2 m filter is simple, rapid and efficient, so may be readily adopted in remote delivery of the ^{47}Sc radioisotope for teranostic applications.

IFJ PAN is among the few laboratories in Europe where in monitoring air radioactivity, apart from gamma emitters, the plutonium content in aerosols is also measured. Our data set for aerosol measurements commences in 1990, while the sum of wet and dry air precipitation has been measured regularly since mid-2005 [J.Environ. Radioact. 166 (217) 10]. If required, gaseous ^{131}I can be also evaluated using a charcoal trap situated inside the modified nozzle of the aerosol sampler below the standard filter. **These measurements are sensitive enough to have enabled observation of a five-fold increase in typical ^{137}Cs traces over the spring of 2020, due to spring fires at the Chernobyl zone.** Among nuclides of artificial origin, of particular interest is the appearance of ^{131}I, which occurs more frequently over colder periods than at summer time [Environ. Sci. Technol. 52 (2018) 8488].

During the first days of October of 2017 a mysterious ^{106}Ru air contamination was noted over large areas in Europe. A peak in the measured concentration exceeding 16 mBq/m^3 was observed in Kraków on October 2, 2017 - about three times higher than that of the ^{131}I maximum value we had observed as traces of the Fukushima cloud passed over Kraków in 2011. Our October 2017 investigation of traces of any other radionuclide revealed the presence of ^{103}Ru at a level of 1/3500 of that for ^{106}Ru. The presence of isotopes of only one element suggested that its release occurred as purified material was handled. Within an informal international collaboration lead by IRSN (Institut de Radioprotection et due Sûreté Nucléaire) and BSF (Bundesamt für Strahlenschutz), the release was found to be located in Russia [Proc. Natl. Acad. Sci. U. S. A. 116 (2019) 16750], [J. Environ. Radioact. 205-206 (2019) 79]. **Among the working hypotheses of this event are release from the Mayak nuclear reprocessing factory near Chelyabinsk, or release from a test related to the Russian nuclear jet engine project** [J. Environ. Radioact. 2014-215 (2020) 106151].

The Fukushima Dai-ichi Nuclear Power Plant (FDNPP) accident (2011) has caused a measurable radionuclide contamination of the environment worldwide. Despite the decade past this event, detailed knowledge of the pattern of fallout originating from

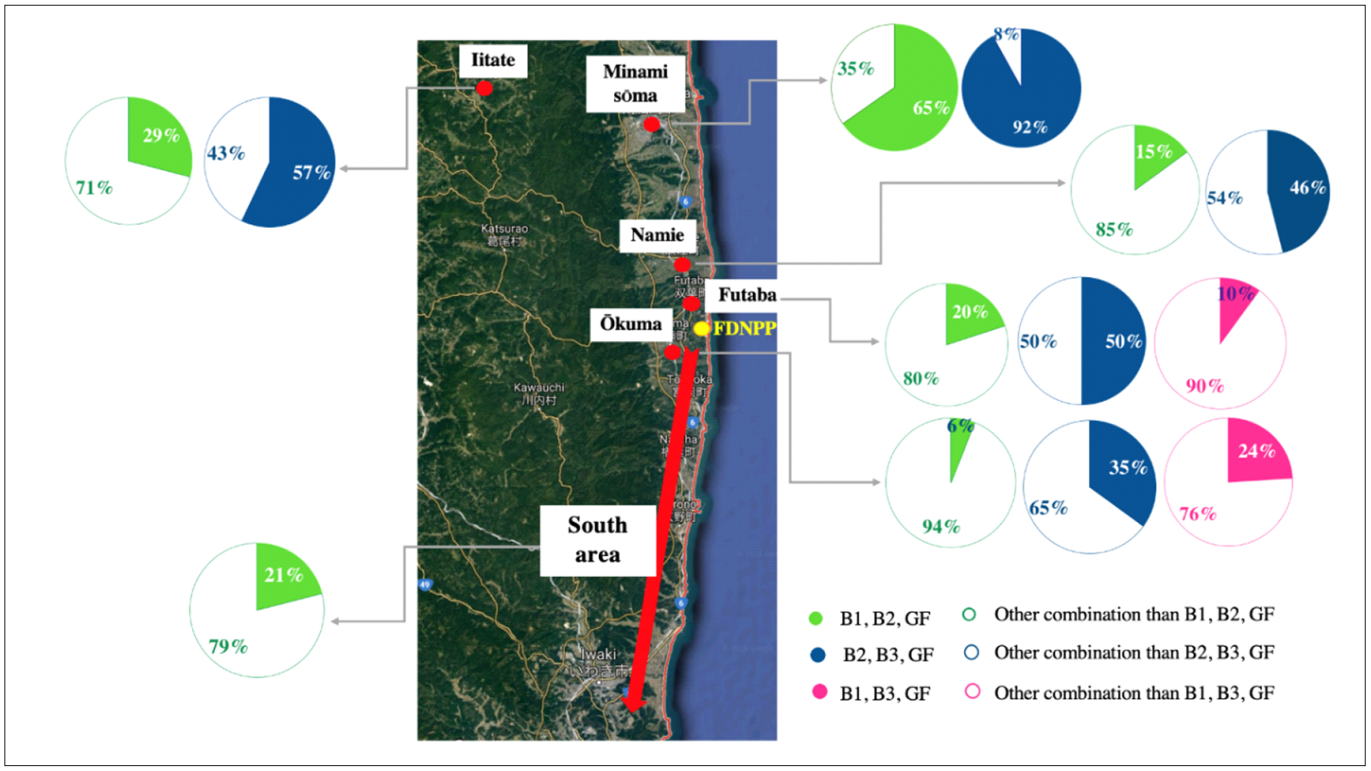

Fig. 6.18. Markers of specific Fukushima reactors and spatial occurrence of isotopic signatures for each reactor. By comparison, B1, B2, and B3 express the contributions arising from reactor units no.1, 2 and 3 of the FDNPP. GF represents global fallout [adopted from J. Environ. Radioact. 196 (2020) 133].

releases of each of the three damaged reactors still remained unknown. Analysis of archive environmental samples collected between 2011 and 2015 over the territory of the Fukushima Prefecture allowed us to evaluate the temporal dependences of activity concentrations of radioactive isotopes from massive releases (^{134}Cs, ^{137}Cs) and from trace releases (^{238}Pu, $^{(239+240)}$Pu, ^{241}Am, ^{244}Cm). It was then possible to identify, characterize and show the time evolution of the isotopic signatures (activity ratios of selected isotopes) in the FDNPP accident [J.Environ. Radaioact. 196 (2020) 133] using the **actinide isotopic ratios as fingerprints of fall-out from a given reactor**. The results combined with previously published data allowed us to prepare the first map of the spatial distribution of Pu isotope fingerprints (^{238}Pu/$^{(239+240)}$Pu) over the Fukushima Prefecture. It was possible to justify the coexistence of markers of specific FDNPP reactors and to determine the range of spatial occurrence of isotopic signatures individually for each reactor. (Fig. 6.18)

According to various prognoses, world glaciers are expected to lose some 80% of their volume by the end of 2100, while some are expected to completely disappear within decades if the current climatic conditions prevail. A key factor in the behaviour of contaminants on the surface of glaciers is cryoconite (Fig. 6.19) – an accumulation of dark-coloured material composed of mineral dust, organisms and organic matter.

A critical feature of cryoconite is its ability to accumulate contaminants. Given these properties, cryoconite is among the best candidates for monitoring the distribution of artificial radionuclides and of heavy metals in the environment.

Fig. 6.19 A cryoconite from the Werenskiold glacier (Svalbard).

We systematically studied the presence of artificial airborne radionuclides (^{137}Cs, ^{238,239,240}Pu, ^{241}Am and ^{90}Sr) in the glacial environment all over the world [The Cryosphere 14 (2020) 657 The Cryosphere 13 (2019) 2075 Sci. Rep. 8 (2018) 10802]. **Activity concentrations of ^{137}Cs, ^{241}Am and Pu isotopes in cryoconite samples from all over the world exceed activity concentrations in other components of the terrestrial environment and can reach high levels** (Fig. 6.20). The concentrations of artificial radionuclides found in cryoconite from different regions of the global cryosphere are among the highest ever observed on the Earth's surface outside of nuclear exclusion zones. All cryoconite samples presented in figure 6.20 were significantly enriched in fallout radionuclides, with activity concentrations comparable to those found in other cryoconite samples gathered in the northern hemisphere. Norway and

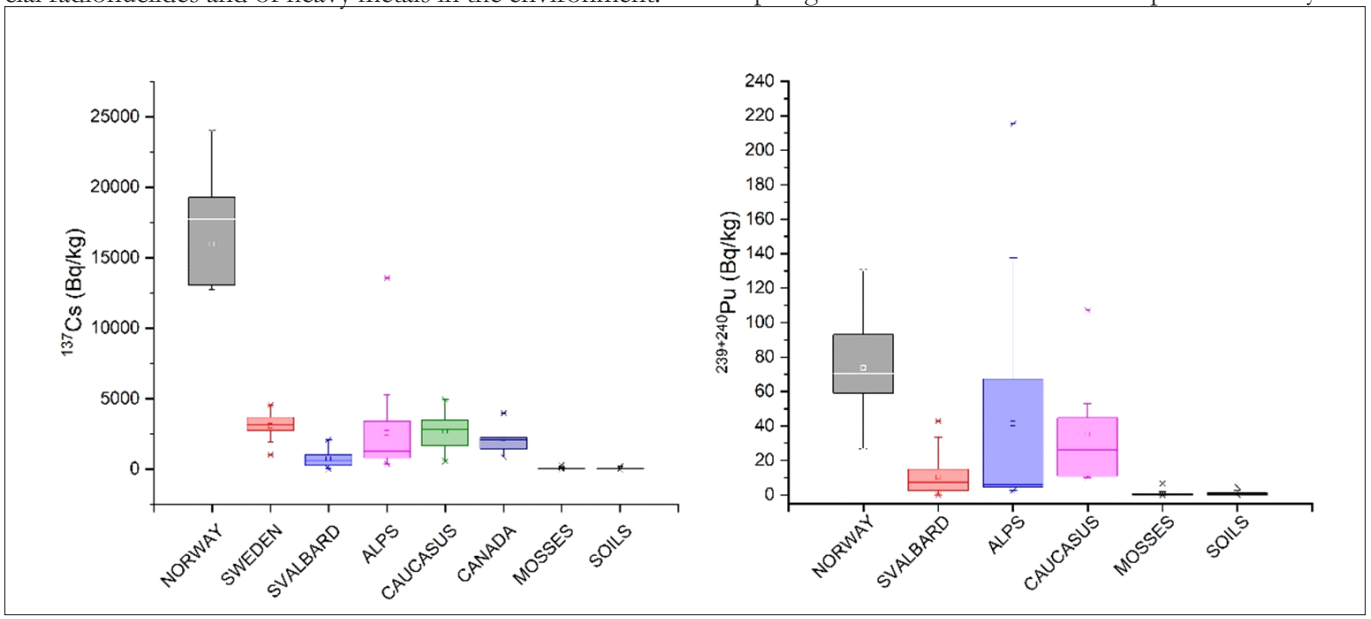

Fig. 6.20. Activity concentration of ^{137}Cs and $^{239+240}$Pu in cryoconite samples from the northern hemisphere.

the eastern Alps, were among the areas most affected by the Chernobyl fallout where ^{137}Cs was the dominant component. Activity concentrations of all anthropogenic radionuclides (^{137}Cs and Pu isotopes) obtained from moss samples gathered over the coastal zones of the Canadian Artic, Alaska, south-western Greenland and tundra soils from Svalbard, were all relatively low. **Among the radionuclides detected in cryoconite samples, we have identified ^{108m}Ag ($t_{1/2}$ 418 yr) in one of the Alpine glaciers (Morterasth-Ch). This artificial isotope has never before been observed in the terrestrial environment** [Catena 191 (2020) 104577]. It was produced in nuclear reactions involving silver components during test explosions in the 1960s.

Cryoconite holes connected with supraglacial channels are rich in cosmogenic ^{7}Be; in contrast, poorly hydraulically connected deposits are rich in artificial fallout radionuclides and elemental carbon. The ^{7}Be isotope is a cosmogenic nuclide produced in the high troposphere and in the low stratosphere. **The very different half-lives of ^{7}Be ($t_{1/2}$ 53.1 d) and those of artificial radionuclides allowed us to analyse our findings in relation to the age and maturity of cryoconite deposits, highlighting the potential use of radionuclides to investigate supraglacial hydrological and material cycling processes on the surface of glaciers.** These findings indicate the need to better understand the fate and impact of legacy contaminants within the cryosphere, particularly with respect to the potential for downstream impact on the quality of water and of the environment. In addition, cryoconite can be used to track environmental radioactivity sources. We have exploited atomic and activity ratios of artificial radionuclides to identify the sources of anthropogenic radioactivity accumulated in cryoconite samples (Fig. 6.21). The Pu signature of cryoconite from different Alpine glaciers is compatible with the stratospheric global fallout and with minor products of the Chernobyl accident. Differences are found when considering other geographic contexts. In the southern hemisphere, the intensity of global fallout was lower than that in the northern hemisphere, which is reflected by lower activities of $^{239+240}$Pu and higher activities of ^{238}Pu in the Antarctic cryoconite [Sci. Total Environ. 724 (2020) 138112]. The enrichment in ^{238}Pu is due to the high in total activity, but localized input of ^{238}Pu from the accidental re-entry of the SNAP 9A satellite over Madagascar in 1964.

Artificial radionuclides, such as ^{137}Cs, ^{90}Sr, ^{241}Am, ^{238,239,240}Pu as well as natural ones were the subject of study in biota of the Antarctic environment within a long-lasting collaboration between IFJ PAN and the Institute of Botany of the Jagiellonian University The activity concentration of those isotopes was determined in over a hundred samples collected in marine and terrestrial environments. Differences were discovered in the accumulation of ^{137}Cs between marine and terrestrial ecosystems. Furthermore, difference between mosses and lichens in their radio-caesium content was statistically confirmed. The internal dose rates assessment was prepared using the ERICA Tool. The dose rates were relatively low, never exceeding several dozen nGy/h, with the highest rate

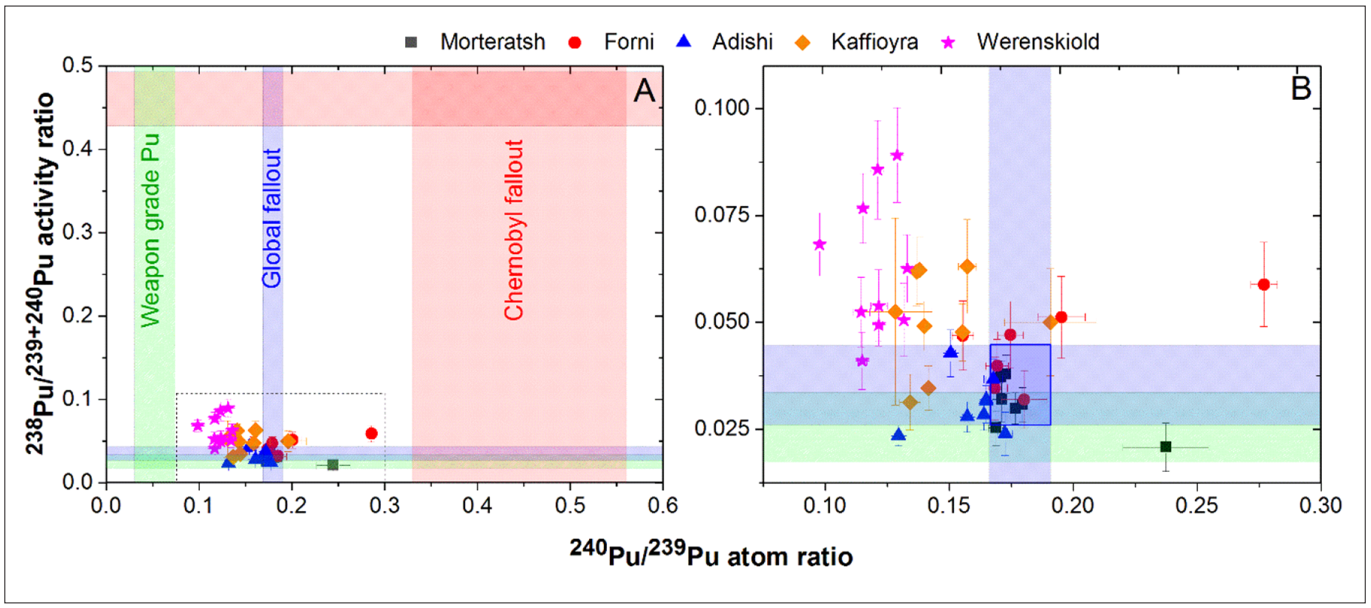

Fig. 6.21. Pu isotopic composition of cryoconite samples from the Alps (Morteratsh and Forni glaciers), Georgia (Adishi glacier) and Svalbard (Kaffioyra and Werenskiold glaciers) (panel B is an enlargement of panel A). ^{238}Pu/$^{239+240}$Pu is expressed as an activity ratio, ^{240}Pu to ^{239}Pu as an atomic ratio.

found for the petrel (Pagodroma nivea). [J. Environ. Radioact. 213 (2020) 106140, [Environ. Sci. Pollut. Res. 25 (12018) 436] The main finding was the diversification of plutonium sources in the natural environment of Antarctica. **Plutonium activity ratios and mass ratios were found to be different (in terms of statistical significance) between two groups of biological samples - terrestrial and marine.** [J. Radioanal. Nucl. Chem. 318 (2018) 1511]. Isotopic ratios for terrestrial samples were consistent with global fallout values, whereas those in marine samples were more diverse suggesting a varied content of Pu origin within these samples.

Earth's polar regions are considered to be most affected by climate change. In particular, such an impact may be reflected in triggering or enhancing the resuspension and subsequent redistribution of pollutants previously accumulated in various ecosystems of northern areas. The conducted polar research is aimed mostly at investigating the level, behaviour and transfer pathways of natural radionuclides (e.g., ^{40}K, ^{210}Pb, ^{226}Ra, ^{228,232}Th, ^{234,238}U) and of anthropogenic radionuclides (e.g., ^{90}Sr, ^{134,137}Cs, $^{238,239+240}$Pu, ^{241}Am), but mainly of the latter. The case study on the Western Arctic terrestrial environment (the Canadian Arctic, Alaska, SW Greenland) produced a rich and unique database on radioactive contamination. Overall, we noted a large diversity of radionuclide deposition, fate and provenance-coupled with the radioactive fallout pattern, local climatic conditions, organic matter content, radionuclide species and other factors. Investigation of the freshwater system of Canada's Arctic revealed the phenomena of sediment focusing and redeposition of contaminants for sediment records; the latter being perhaps initiated by global warming. Furthermore, **the tundra vegetation in Alaska was found to contain traces of ^{134,137}Cs from the Fukushima NPP accident** [Chemosphere 239 (2020) 124783]], and also post-Chernobyl ^{137}Cs, over the Canadian Arctic and Greenland shorelines [J. Environ. Radioact. 212 (2020) 106125]. These findings help to better understand and estimate the movement of radioactive clouds across the globe.

We experimentally confirmed the cases of internal radioactive contamination among medical personnel of nuclear medicine facilities [Radiat. Environ. Biophys. 56 (2017) 19 Radiat. Environ. Biophys. 57 2018) 77, Radiat. Environ. Biophys. 58 (2019) 469, Radiat. Prot. Dosim. 179 (2018) 275] Measurements of internal radioactive contamination by whole-body counters or biological samples require highly specialised equipment, are costly and time-consuming. Taking the above into consideration, a **method of passive in situ monitoring of radioactive air contamination based on active carbon** was developed and tested [J. Radioanal. Nucl. Chem. 318 (2018) 723]. This method is promising and after appropriate optimization could be broadly applied in nuclear medicine facilities.

❖

7. Division of the Cyclotron Centre Bronowice

The Cyclotron Centre Bronowice (in *Polish* – Centrum Cyklotronowe Bronowice, CCB) is a part of the Institute of Nuclear Physics Polish Academy of Sciences (IFJ PAN). CCB is a world-class proton radiotherapy center and a modern nuclear physics research laboratory. The activities of CCB are focused around two cyclotrons which now operate at IFJ PAN – the "old" in-house developed AIC-144 isochronous cyclotron (accelerating protons to the energy of 60 MeV), and the C 230 cyclotron with a proton beam of the energy of 230 MeV, installed in 2012 (Fig. 7.1).

Proton beams from the Proteus C-235 cyclotron with an energy up to 230 MeV are directed to the:

- nuclear research room
- proton radiotherapy station for ocular cancer
- two gantry rooms - therapeutic lines with a rotating arm.

CCB is the first proton therapy center in Poland. The treatment is carried out in close cooperation with medical partners of CCB. As part of the cooperation, CCB is responsible for the production of the beam, control of its parameters, and other activities related to the preparation and implementation of irradiation. In a constant process of increasing the staff's competences, in 2017 the first group of CCB physicists graduated from a 4-year long national training program in medical physics, receiving the title of Expert in Medical Physics.

Proton radiotherapy is one of the fastest growing forms of radiotherapy in the world. The introduction of scanning beam technology in the last decade and the growing number of proton therapy centers at universities and research

Fig. 7.1. The C 230 cyclotron − the main magnet and the beam line (quadrupoles and steering x y magnets). [Copyright K. Daniel]

institutes have resulted in a rapid increase in both clinical trials and research in medical physics and accelerator technology.

Our priority is to treat patients. Outside the clinical time, i.e. mainly in the evening, during nights and weekends, the beam is used for research purposes, mainly in the field of proton radiotherapy, nuclear physics, medical physics, dosimetry, microdosimetry, radiobiology, radiochemistry, and materials engineering. In addition, CCB conducts commercial activities by providing proton beams. CCB also offers proton beam operational tests to external clients.

In the field of medical physics, our work is focused on increasing the precision and safety of the therapy by improving the following methods: (i) verification of the proton beam range, (ii) patient positioning, (iii) radiotherapy of moving organs, and (iv) secondary and scattered radiation dosimetry. One of the main topics of our research is also the biological effectiveness of proton beams and its inclusion in treatment plans. The Institute of Nuclear Physics Polish Academy of Sciences takes part in all these research directions.

In addition, IFJ PAN conducts research in the field of biological effectiveness of protons in connection with the activity of chemotherapeutic agents, development of proton beam dosimetry methods, taking into account the measurements of ionization density (LET) of the beam, treatment planning procedures taking into account the biological effectiveness of protons, and methods of irradiating moving organs. The need to standardize treatment planning when introducing new scanning beam technology led to the formation of the IPACS group (Italy-Poland-Austria- Czech-Sweden) in 2014, which resulted in the standardization of planning protocols in these countries. This is crucial for compiling and comparing clinical results obtained in different centers.

March 2020 marked the outbreak of the SARS-COV-2 virus pandemic. During this uneasy time, the facility remained operational and ready to receive patients. We needed to change the organization of work in order to maintain the continuity of patient treatment. Despite the difficult situation related to the pandemic and thanks to the very positive and effective cooperation with our main clinical partner - the National Institute of Oncology (part in Krakow) - we continuously provided our services and even noted a significant increase in the number of patients.

The year 2021 is bringing the celebration of the 10th anniversary of the first proton therapy at IFJ PAN in Poland.

General Patient Statistics. By December 2020 over 400 patients had been successfully irradiated using proton scanning gantries, out of whom only 13 pediatric cases had been registered. The indications included, but were not limited to, chordomas, gliomas, astrocytomas, chondrosarcomas, oligodendrioglomas, esthesioneuroblastomas, sarcomas, and meduloblastomas. Adult patients were referred mainly from the National Institute of Oncology (NIO), Kraków Division (formerly known as the Center of Oncology – Institute, Kraków Division) but also from Radom Oncology Center (RCO) and Katowice Oncology Center (KCO). Pediatric patients were referred from the University Children's Hospital in Kraków

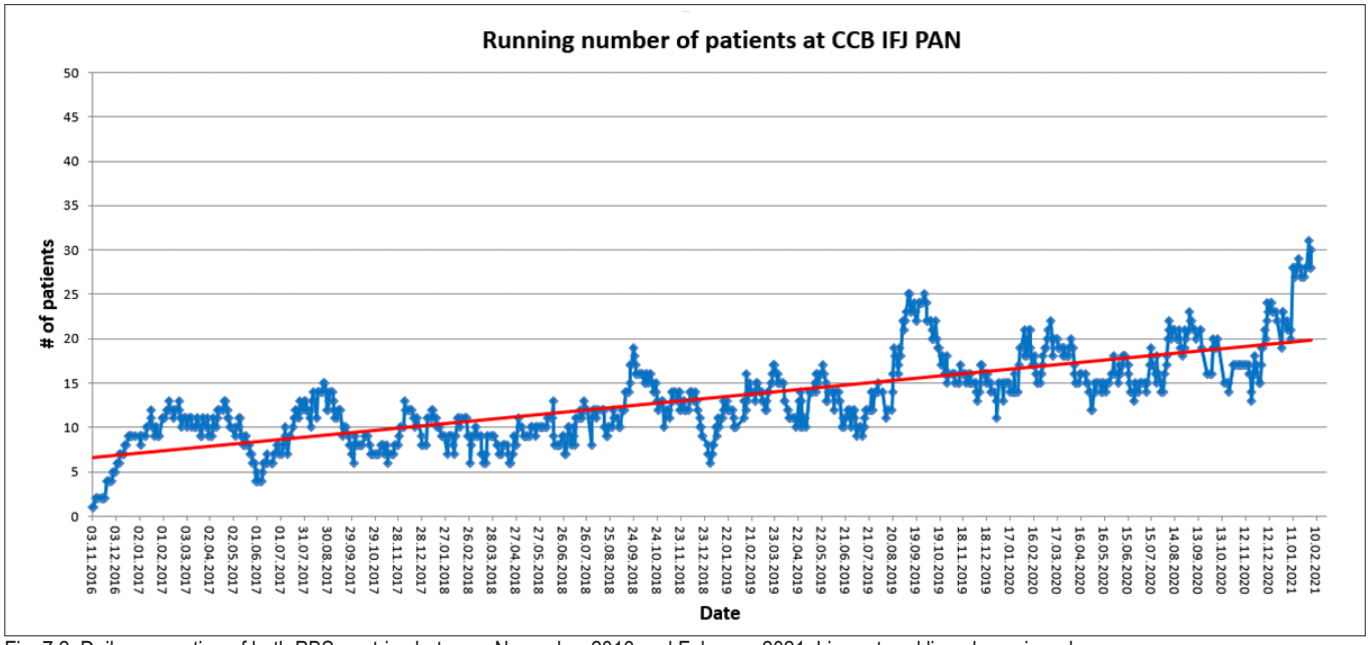

Fig. 7.2. Daily occupation of both PBS gantries between November 2016 and February 2021. Linear trend line shown in red.

(USDK) between January 2017 and April 2019. No pediatric patient has been treated since then.

The total number of patients treated daily on both PBS gantries had increased significantly from November 2016 by the time this report was created (February 2021), reaching recently over 50% percent of capacity (see Fig. 7.2).

A part of CCB is **the Cyclotron Proteus C-235 Group** which is responsible for service and maintenance of the Proteus 235 therapy system. The Cyclotron division consists of a team of engineers, trained by the system manufacturer IBA (Ion Beam Applications). CCB is one of a few centers in the world whose engineers are certified to inspect, maintain and supervise the proton therapy system during clinical and non-clinical workflow. Moreover, CCB has signed a service contract with IBA, which ensures undisturbed communication in order to reduce system downtimes. The agreement provides several benefits, such as access to IBA's professional expertise, extensive knowledge database, on-site troubleshooting and help with two cyclotron maintenances in year.

The Cyclotron Proteus C-235 Group main fields of activities:

- Employee training in acceleration techniques and accelerators technology.
- Supervision over the safety of employees and safe work with the accelerator.
- Maintaining Proteus 235 Therapy System ready for clinical and non-clinical uses.
- Cyclotron parameters supervision during patient irradiation and ion beam experiments.
- Performing scheduled preventive maintenance procedures and unplanned corrective activities.
- Development work on new proton beam parameters for clinical and non-clinical irradiations.
- Research and development on high intensity proton beam current for experimental uses.

The Cyclotron AIC-144 Group is responsible for service and maintenance of the Cyclotron AIC-144. The isochronal cyclotron AIC-144 shall be used to accelerate light ions (protons, deuterons, alpha particles).

The accelerated protons in the form of a focused beam have optimum parameters for this type of cyclotron:

- energy 60MeV;
- beam current 80nA;
- stability of the beam current 5%.

In the years 2011-2016 the AIC-144 cyclotron was used to irradiate patients with a cancer of the eyeball. Since 2016 the 60 MeV the fixed proton beam of the AIC-144 cyclotron has been used in dedicated research in dosimetry and medical physics.

Treatment Planning Group (Pracownia Planowania Leczenia). The basic aim of the Treatment Planning Group (PPL) is to coordinate patients' workflow processes with respect to proton radiotherapy performed at Cyclotron Centre Bronowice. The tasks of the Group are divided into three main categories: patient handling, computerized treatment planning, and IT system management which corresponds to three sections: radiation therapists (RTTs), physicists and IT specialists.

RTTs take responsibility for preparation of patient specific immobilization devices, CT scanning for treatment planning, patient positioning and position verification at gantry treatment rooms and fractional dose delivery. In addition, they conduct daily quality assurance procedures of the CT scanner, patient position verification devices and other medical applications. The coordination of patient scheduling and patient related information interchange is part of their daily routine.

Physicists prepare treatment plans based on clinical prescriptions for both gantry and eye treatment rooms, perform multistage plan verification before the deployment, and accomplish eye patient positioning verification. Quality assurance of treatment planning and patient positioning equipment and software, such as the CT scanner, surface imaging cameras and Treatment Planning System, is part of their duties. Moreover, they implement improvements and new technologies into treatment processes as well as prepare procedures for new clinical indications. They also participate in various local and international collaborations aiming at research and development in the areas of treatment planning, treatment delivery and quality assurance (such as the IPACS and EPTN working groups).

IT specialists are responsible for the management of treatment control systems, treatment planning systems, various patient positioning and position verification systems, and many general purpose IT systems, including document management system, bug and failure tracking system etc. Furthermore, they take care of video surveillance, access control, data archiving, network infrastructure, printers, personal computer devices, and many more. The development of new treatment related software is also within their scope of interest.

Proton Ocular Radiotherapy Group (Pracownia Terapii Oka). The activity of the group is primarily related to radiotherapy of ocular tumors. It covers operation, test and technical maintenance of dedicated treatment rooms at the C-235 Proteus and AIC-144 cyclotrons and development of related technical and quality assurance procedures. The staff conducts dosimetric verification of clinical treatment plans, designs and tests patient–specific accessories and operates the treatment room during patient irradiations. Non-clinical activities include application of proton beams for research purposes.

While clinical work is mostly done with the C-235 cyclotron, the AIC-144 cyclotron based unit hosts most of experimental activities, conducted in cooperation with the Division of Application of Physics IFJ PAN. These involve exposures of in-vitro cancer cells cultures, testing novel radiation detectors and investigating the effects of proton radiation on electronic devices.

Dosimetry and Quality Assurance Group (Pracownia Dozymetrii Kontroli Jakości). The mission of the group is to supervise the applications of ionizing radiation (especially the proton beam) in therapy and research. The aim of the quality control in radiotherapy is to ensure excellent patient care using advanced radiotherapeutic equipment. Quality assurance procedures and tests involve acceptance testing, characterization and commissioning and routine quality assurance of clinical radiotherapy systems' use. Novel testing and verification procedures are being developed to ensure reliable performance as well as accurate dose delivery.

A more detailed description of the responsibilities of the medical physicists group at CCB can be found below:

Quality Assurance of the therapy system – in accordance with applicable law, periodic tests have to be done in order to ensure the proper operation of therapeutic accelerators. In proton therapy the precision of beam delivery is crucial, therefore a lot of tests are performed using specialized measurement devices, such as ionization chambers, scintillation detectors, film detectors, etc.
CCB was selected as the leading facility for the dosimetric audit of Pencil Beam Scanning systems organized by European Radiation Dosimetry Group (EURADOS).

Dosimetric verification of Patient Plans – all patient irradiation plans need to be verified before the first therapeutic session. Using an array of ionization chambers, measurements in water tank are performed. The results of the measurements are compared with the calculations of the Treatment Planning System. Also new methods of verification are developed in cooperation with other researchers, such as the one described in paper: Monitoring Proton Therapy Through In-Beam PET: An Experimental Phantom Study [IEEE Transactions on Radiation and Plasma Medical Sciences Volume: 4, Issue: 2, March 2020]

Beam model configuration – the Treatment Planning System is a software application which allows one to calculate dose distributions for patients. However – the beam model needs to be configured properly. The configuration of measurements and their analysis are performed by specialists from the Dosimetry and QA Group. The staff also takes part in developing new methods of beam calculations (Commissioning of GPU–Accelerated Monte Carlo Code Fred for Clinical Applications in Proton Therapy [Front. Phys., 21 January 2021].

Calibration and test of measurement devices – precision is the most important factor in proton beam measurements, therefore periodic tests and calibrations of measurement devices need to be performed.

Experimental irradiations – preparing and performing. A lot of research requires irradiation using a proton beam. The specialists from the Dosimetry and QA Group cooperate with researchers in order to find the optimal way to irradiate samples (such as biological samples) and perform experiments according to researchers' needs. This cooperation may result in publications, such as:

- Influence of Therapeutic Proton Beam on Glioblastoma Multiforme Proliferation Index — A Preliminary Study [ACTA PHYSICA POLONICA A , Vol.137(2020), No.1]
- Fancy-Shaped Gold–Platinum Nanocauliflowers for Improved Proton Irradiation Effect on Colon Cancer Cells [Int. J. Mol. Sci.2020,21, 9610]

Tests with the beam for external customers – as tests with proton beams are highly needed also in industry, a lot of tests for external customers are performed at CCB. The irradiation of a wide range of samples is performed – starting with pollen and ending with electronic devices used in space industry.

As measurement devices and calculation algorithms in proton therapy need to be successively improved, it still attracts the attention of researchers. Therefore, the Dosimetry and QA Group members participate in a lot of research activities. Some of them are described in section Highlights.

The Quality Control Section (in Polish – Sekcja Kontroli Jakości, SKJ) is responsible for the implementation, management and improvement of the Quality System (QMS) based on PN/EN ISO 17025:2018. The mission of SKJ is to ensure the correct, efficient and effective process and procedure flow at CCB (See Fig. 7.3).

SKJ supervises CCB documentation and equipment, ensures the compliance of CCB activities with legal regulations in the field of radiotherapy and performs periodic quality assessments (audits and evaluations). Moreover, SKJ cooperates with CCB units and external organizations in the field of Quality Policy and prepares reports on the functioning of the QMS and the need for its improvement for CCB Management Board.

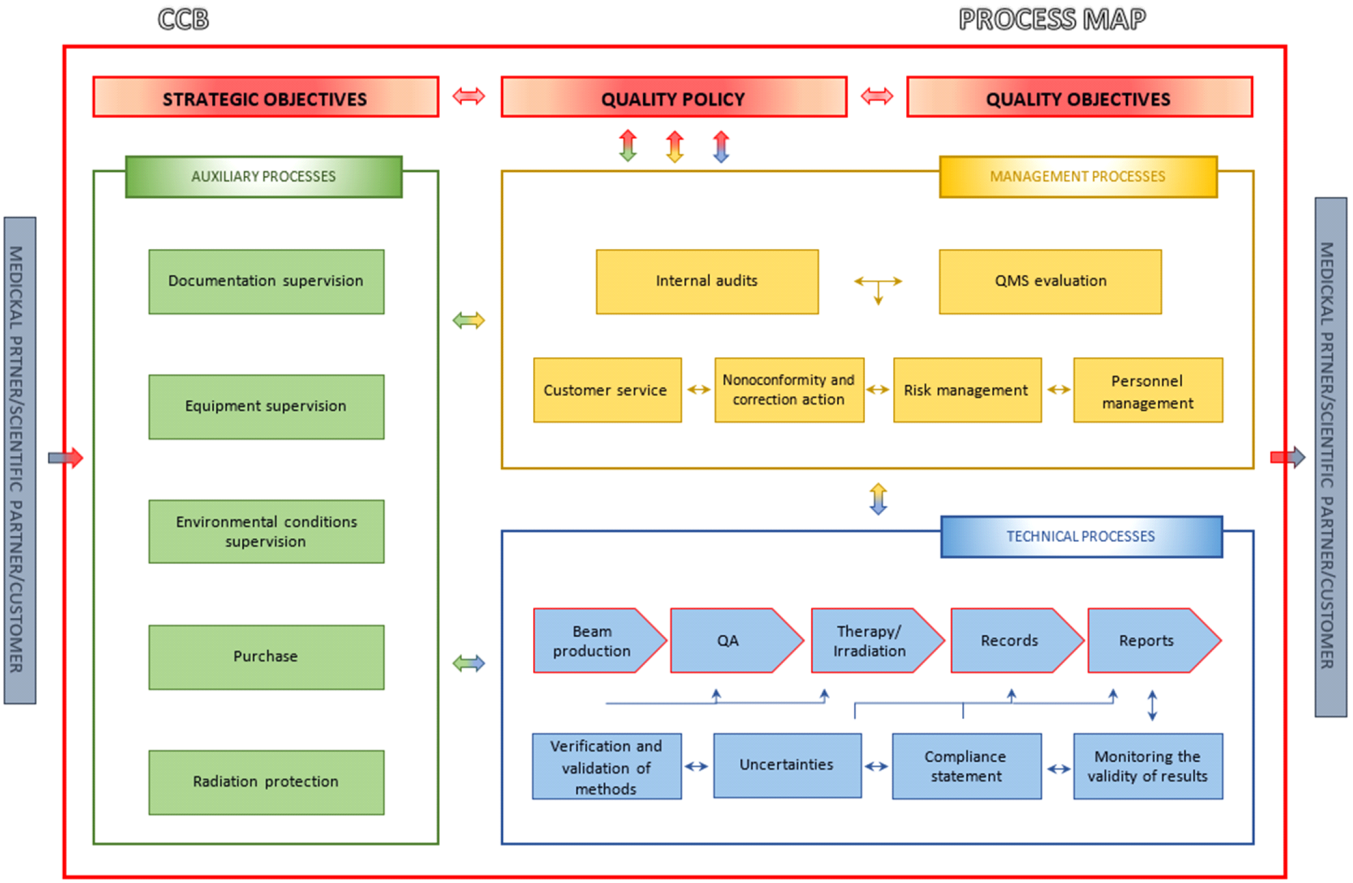

Fig. 7.3 Quality Policy – CCB process map.

Selected Highlights of the Division of Cyclotron Centre Bronowice

Proton radiotherapy has been conducted in Poland since 2011. In 2011-2015, 128 patients of the University Hospital in Krakow with melanoma of the eyeball were irradiated at the station built at IFJ PAN at the AIC-144 cyclotron. Since 2013, the procedure has been financed by the Polish National Health Fund. **CCB IFJ PAN fully covers the current demand for this type of therapy in Poland and offers irradiation to all patients referred for treatment.**

In February 2016, the clinical work was transferred to a new, dedicated therapeutic station at the Proteus C-235 cyclotron, using a proton beam with an initial energy of 70 MeV. Patients are positioned using a robotic therapeutic chair and a pair of X-ray tubes in an orthogonal system. The position meets the requirements and regulations of law and quality and safety standards for medical devices, which is confirmed by the CE Medical mark. The duration of a radiotherapy cycle is approximately 4-5 weeks. It begins

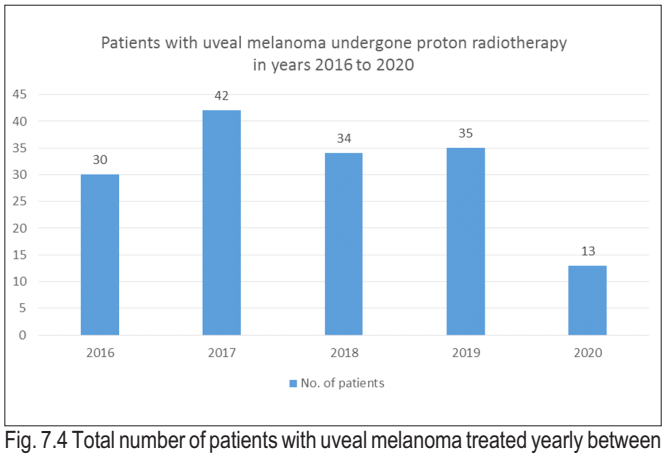

Fig. 7.4 Total number of patients with uveal melanoma treated yearly between 2016 and 2020.

with the preparation of a patient at the Clinical Department of Ophthalmology and Ophthalmic Oncology of the University Hospital in Krakow. From 4 to 5 tantalum markers are sewn onto the eyeball around the base of the tumor. Their task is to support the location of the tumor, which is invisible in X-ray imaging, and they also allow the patient to be positioned later at the radiotherapy station. The patient is then transferred to CCB IFJ PAN and during the next few visits medical physicists prepare a treatment plan, which is then approved by a radiotherapist. After its verification and preparation of individual beam-forming elements, a week of therapy follows, during which on four consecutive days a total of four fractional doses of 13.64 Gy each is delivered to the treatment volume. **Over the years 2016-2020, 154 patients under a contract with the Polish National Health Fund with eye tumors were irradiated at the C-235 cyclotron** (see Fig. 7.4).

Proton radiotherapy with the use of Pencil Beam Scanning (PBS) has been carried out at IFJ PAN since November 2016 at two gantry-type therapeutic stations that allow irradiation from any direction (0^0-360^0).

Both gantries are equipped with a dedicated snout that enables irradiation of fields up to 30 cm x 40 cm. Patient positioning is carried out by means of a robotic table, an orthogonal set of X-ray lamps and an optical system. At each station, it is possible to treat pediatric patients using anesthesia columns and kits installed there, designed in consultation with anesthesiologists from the University Children's Hospital in Krakow. Treatment planning is carried out with the use of Computed Tomography scans obtained from a CT. The center is equipped with dedicated equipment for dosimetry and quality control of therapeutic beams. The use of irradiation with a scanning beam allows therapists to obtain a fully three-dimensional intensity modulation. This translates into a very high conformity of the treatment plan, i.e. no dose in the distal areas and a lower dose in the proximal areas (in front of the target area) compared to analogous photon plans. CCB IFJ PAN is one of the first centers in Europe to have mastered this irradiation technique. Before the center was launched, the medical physicists of the Oncology Center in Warsaw had performed comparative measurements. Currently, the dosimetric consistency of the center is carried out by the Warsaw Oncology Center with the use of mailed dosimetry.

Radiotherapy in gantries started in November 2016, but only one patient was irradiated in that year. **Over the years 2017-2020 404 patients (mostly from our main clinical partner - the National Institute of Oncology, Krakow) were irradiated, including 13 children** (Fig. 7.5). **The number of patients is systematically growing. I**n 2019 it amounted to 107 adults and 5 children. In 2020 133 adult patients were irradiated in gantries. All patients referred for irradiation were admitted. The extension of the list of indications for reimbursement by the National Health Fund in 2019 only marginally contributed to the increase in the number of patients. Pediatric patients have not been referred for treatment at the center since April 2019. Having 10 years of experience in conducting proton radiotherapy, CCB IFJ PAN can irradiate annually about 400–500 patients (depending on indications and the number of fractions).

There is still little clinical evidence of proton therapy with respect to photons. To demonstrate the potential benefits of this emerging treatment modality, collaborative clinical trials need to be performed. In response to this problem, a PACS group was formed in late 2014. Initially it consisted of physicians and medical physicists from the Treatment Planning Group (PPL) of CCB IFJ PAN, the Cancer Center and Institute of Oncology in Kraków (currently the National Research Institute of Oncology in

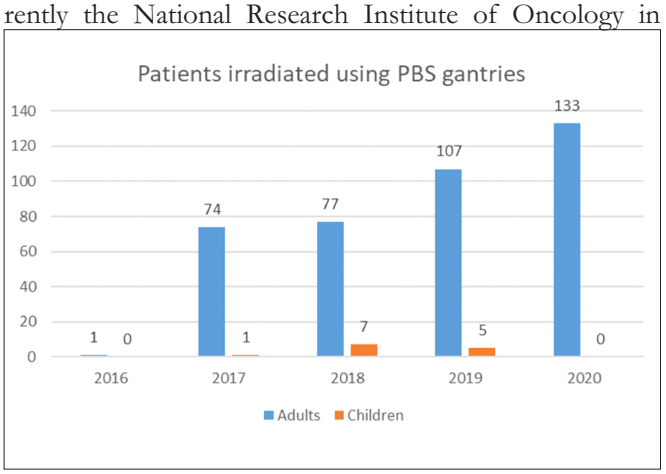

Fig. 7.5. Total number of adults and pediatric patients treated yearly between 2016 to 2020.

Kraków), and from three other centers in Austria, Czech Republic and Sweden. Later on a proton center from Italy joined the initiative. **The main goal of the IPACS (Italy, Poland, Austria, Czech, Sweden) group is to harmonize of treatment protocols in proton radiotherapy and to synchronize efforts in order to perform multicenter clinical trials. The first step of the collaboration was to harmonize proton treatment planning for selected indications and test patient cases.** As a result, common treatment planning guidelines for head and neck tumors were established to prioritize aims and objectives and to evaluate the planning results (see Table 1) [ACTA ONCOLOGICA 2019, VOL. 58, NO. 12, 1720–1730].

Table 1. Priority list for OAR and target structures dose objectives used for treatment planning of sinonasal cancer cases. The first four priority structures and the CTV need to meet also the constraints after robustness evaluation.

Priority	Structure	Objectives
1	Spinal cord	$D_{2\%}$ 50 Gy(RBE)
2	Brainstem	$D_{2\%}$ 54 Gy(RBE)
3	Chiasm	$D_{2\%}$ 54 Gy(RBE)
4	Optic nerve L/R	$D_{2\%}$ 54 Gy(RBE)
5	GTV, CTV, PTV	(described in the text)
6	Parotid gland L/R	D_{mean} 28 Gy(RBE)
7	Larynx	D_{mean} 40 Gy(RBE) $D_{2\%}$ 63 Gy(RBE)
8	Oral cavity	D_{mean} < 30 Gy(RBE)
9	Retina L/R	$D_{2\%}$ 54 Gy(RBE)
10	Cochlea L/R	D_{mean} 30 Gy(RBE)
11	Esophagus	$V_{50Gy(RBE)}$ 30%
12	Pharyngeal constrictor muscle	D_{mean} 41 Gy(RBE)
13	Temporomandibular joint L/R	D_{mean} 30 Gy(RBE)
14	Submandibular gland L/R	D_{mean} 28 Gy(RBE)
15	Thyroid	$V_{50Gy(RBE)}$ 30%
16	Lens L/R	$D_{2\%}$ 7 Gy(RBE)
17	Other	As low as possible
18	BODY−CTV	$D_{2\%}$ 107%

The clinical equipment and treatment planning systems vary at each of the participating centers, resulting in certain discrepancies of the outcomes (Fig. 7.6). Investigations have showed potential advantages of proton radiotherapy for treatment of H&N tumors by sparing critical organs at risk, such as spinal cord or brainstem.

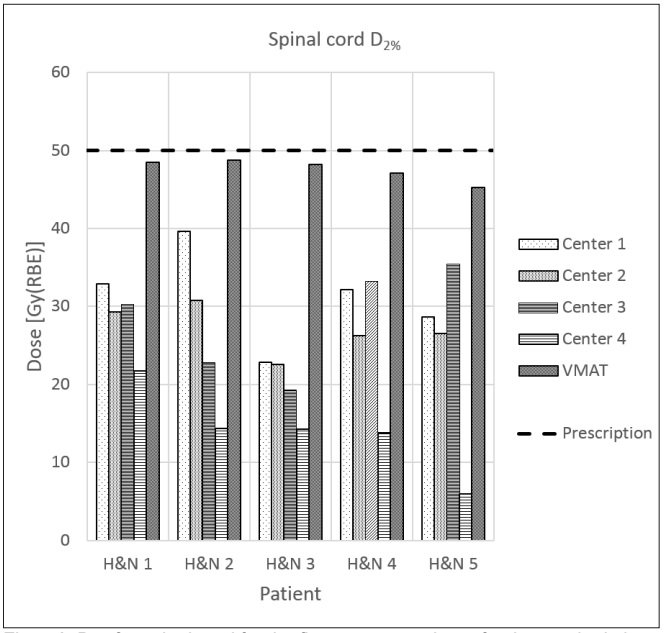

Fig. 7.6. $D_{2\%}$ for spinal cord for the first treatment phase for the nominal plans for all 5 head and neck cases from each center and the VMAT plan is shown. The dashed line shows the objective for the total treatment, i.e., for the sum of both treatment phases, which was $D_{2\%}$ 50 Gy(RBE) for the spinal cord.

Guidelines for further indications will be developed in the next years, starting from skull base tumors and following with breast cancer. The next milestones will be to harmonize plan quality assurance procedures and finally to create common treatment protocols in order to prepare for multicenter clinical trials.

The ESTRO society created a set of working package groups within EPTN. **The Treatment Planning Group (PPL) participates in the work of WP5 group, which concentrates its current activities on treatment planning related topics, such as collective TPS specifications, planning standards and case solutions, TPS commissioning and validation, alternatives to patient specific verifications, CT/HU calibration, robustness analysis, LET based planning and 4D planning.**

An example of the WP5 efforts is a comparative study of computed tomography scanners entitled *Inter-centre variability of CT-based stopping-power prediction in particle therapy: Survey-based evaluation* [Physics and Imaging in Radiation Oncology 6 (2018) 25–30]. The study shows large inter-center variability in the implementation of CT scans, image reconstruction and especially in specification of the CT to stopping power ratio (SPR) conversion, which implies the need for future standardization.

The Treatment Planning Group (PPL) invented and developed methods for achieving much higher plan conformity of proton pencil beam scanning treatments by applying patient specific 3D-printed or field specific compensators.

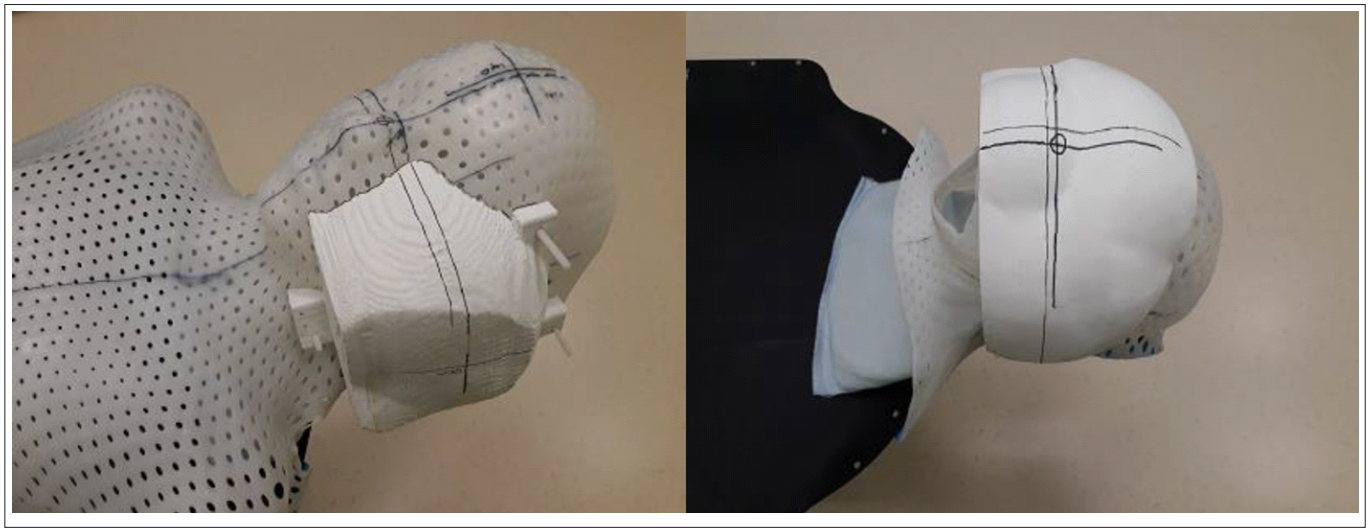

Fig. 7.7. Sample 3D printed compensators.

Pediatric patients are very demanding, not only because they usually require intensive immobilization including anesthesia, but also in terms of clinical prescriptions and critical organ sparing. The minimum proton energy obtained from modern cyclotrons using energy selection systems is usually higher than 70 MeV. In order to irradiate shallow tumors, one needs to apply a range shifter, which causes a huge degradation in spot lateral penumbra. To minimize this side effect, patient specific 3D-printed compensators (an example is shown in Fig. 7.7) were developed in April 2017 and applied clinically to several pediatric H&N patients. As a consequence, we observed a significant reduction of unwanted doses distributed to the normal tissue surrounding the target (Fig. 7.8).

Another group of pediatric patient specific indications is cranio-spinal irradiation (CSI) in the case of medulloblastoma (shown in Fig. 7.9). Again, in order to preserve best lateral properties of the proton scanning beam, a dedicated field specific compensator was designed and developed by the Treatment Planning Group (PPL), manufactured by the Division of Scientific Equipment and Infrastructure Construction (DAI), and applied clinically.

A second type of field specific compensators for treatment of sacrum and pelvic tumors is under construction and will be introduced clinically in 2021.

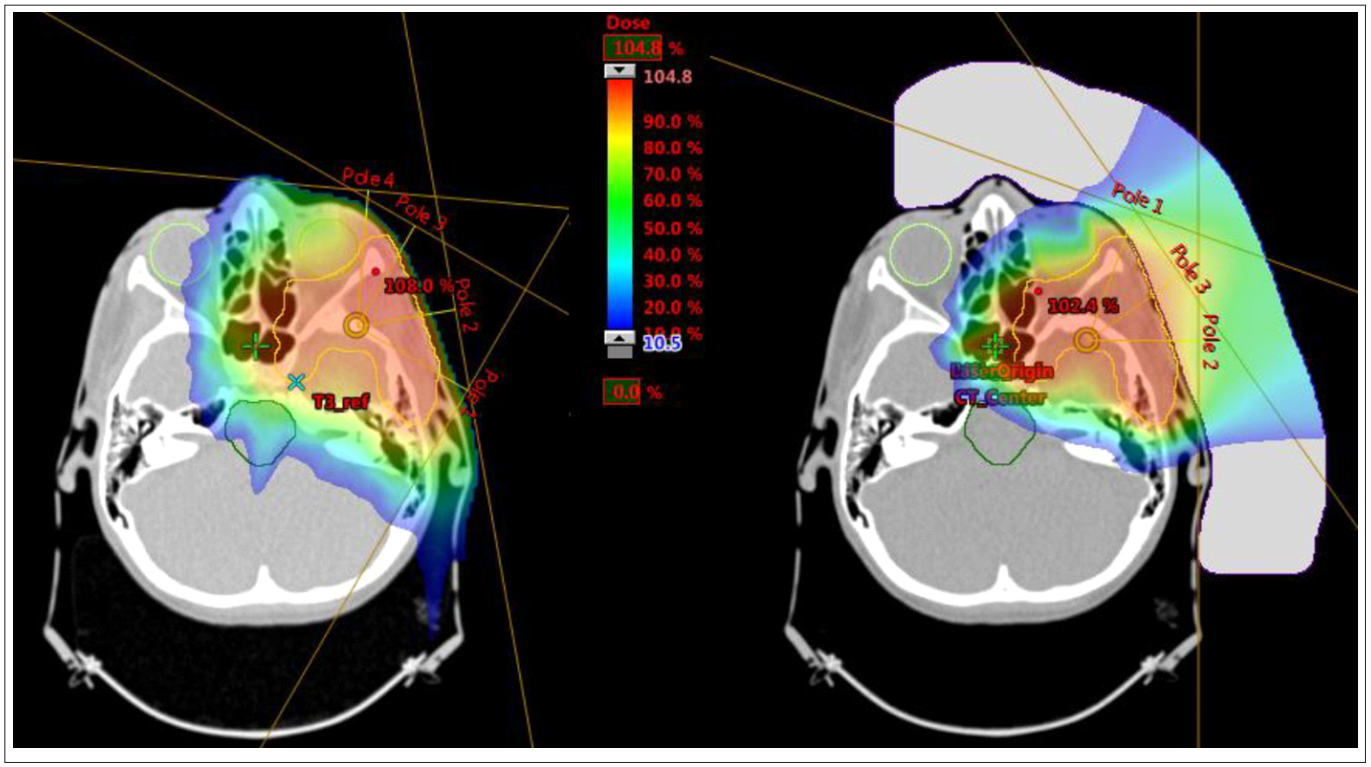

Fig. 7.8. Sample plan comparison. Standard plan (left) and plan with 3D printed compensator (right).

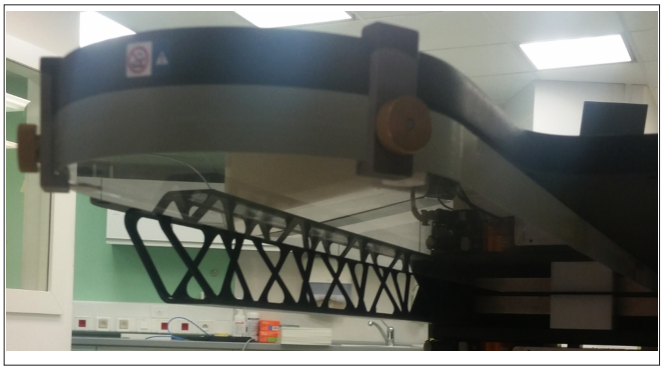

Fig. 7.9. CSI field specific compensator attached to the treatment table.

Dosimetric verification of PBS treatment plans requires 2D dosimeters because of the possible presence of hot and cold spots. Currently, the MatriXXPT (IBA Dosimetry) array of ionization chambers is applied at CCB to simultaneously measure the dose and evaluate the spatial dose distribution in PBS radiotherapy. However, the MatriXX spatial resolution is limited, which is due to the size of the chambers and the distance between them (4.5 and 7.6 mm, respectively). As an alternative, Gafchromic EBT3 films with spatial resolution below 1 mm can be applied for QA. The setup of the **dose spatial distribution measurements using Gafchromic films** is presented in Fig. 7.10.

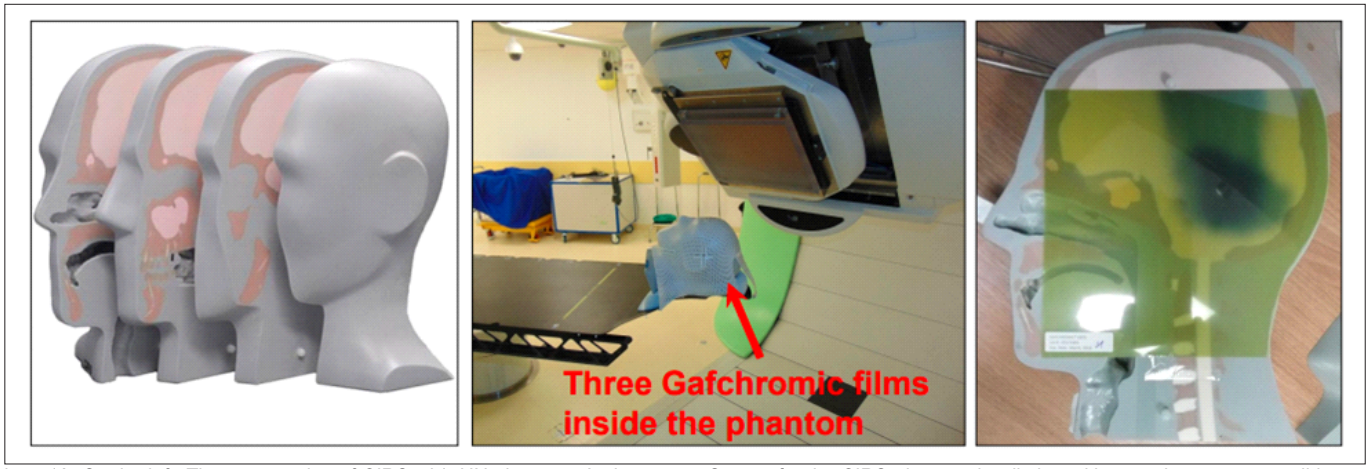

ig. 7.10. On the left: The construction of CIRS 731−HN phantom. At the center: Set−up for the CIRS phantom irradiation with scanning proton pencil beam treatment plan. On the right: Gafchromic film in the anthropomorphic phantom after irradiation.

Many studies have shown the critical impact of beam energy distribution (simplified as the dependence on linear energy transfer (LET)) on detector efficiency of the Gafchromic films. **The film can be digitized by scanning it with a flatbed color scanner. Therefore, in addition to EBT3 film calibration, the scanner uniformity and stability corrections have to be applied to increase the accuracy of the system** (Fig. 7.11).

The aim of the work was to develop a dosimetric system, composed of the EBT3 film, a scanner and a set of correction algorithms to recalculate the measured response into absorbed dose in water for clinical proton beams. Finally, **an advanced home-developed software tool, AnalyseGafchromic, was developed to facilitate the use of the films in clinical conditions.** [Radiation Protection Dosimetry (2018), Vol. 180, No. 1–4, pp. 324–328] .

For commissioning of a proton therapy unit, depth dose distributions must be determined and introduced into the Treatment Planning System. In the pencil beam scanning (PBS) technique, integral depth dose (IDD) acquisition should be performed. A detector should be large enough to detect the entire beam laterally broadened by scattered and secondary contributions. **A standard plane-parallel ionization chamber (IC) 4.08 cm in radius proved not to be large enough to register all protons and nuclear recoils from the proton pencil beam.** The measured and FLUKA calculated relative dose difference RDD(z) for the highest energy of 226.08 MeV is presented in Fig. 7.12 .

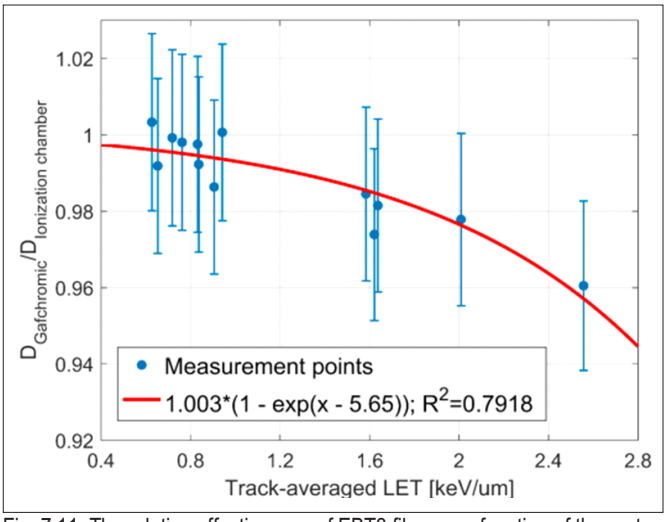

Fig. 7.11. The relative effectiveness of EBT3 films as a function of the proton beam LET. In order to determine the dependence, plans with different ranges and modulations have been measured with Gafchromic film and Markus type ionization chamber simultaneously. Track−averaged LET values have been simulated using the particle transport code SHIELD−HIT12A (v.0.6.0). The total uncertainty of film effectiveness consists of the uncertainty of absolute dose determination with Markus chamber and the film readouts reproducibility

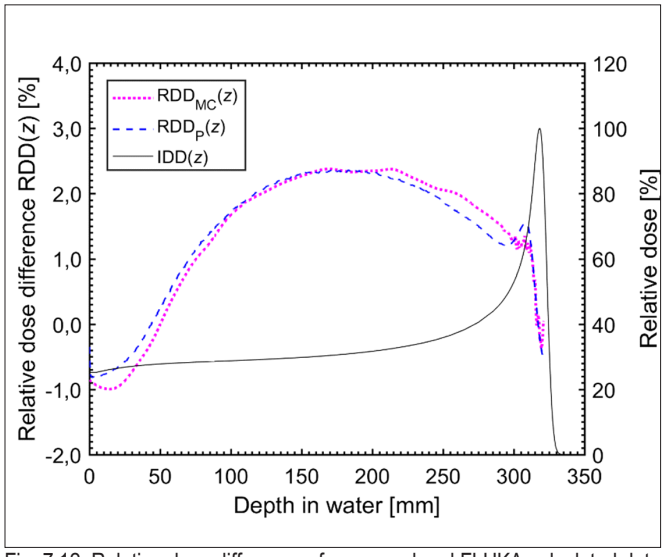

Fig. 7.12. Relative dose difference of measured and FLUKA calculated data for 226.08 MeV proton pencil beam (= 2.4 mm). RD(z) data was derived from MC calculations for IC−6cm.

In recent years a huge effort has been made to quantify the missing dose fraction, calculate energy and depth-dependent correction factors for the IC data, or modify analytical formulae of IDD(z). **The purpose of the work was to quantify, using measurements and Monte Carlo transport calculations, the ionization chamber's (IC) geometrical efficiency versus the chamber radius and proton beam energy.** The focus was put on the analysis of commercially available ICs of 4.08 and 6 cm radius in a clinically available proton energy range 70–226.08 MeV. The calculated geometrical efficiency for the proton energy range between 70 and 226.08 MeV at the mid-range depth for IC-4cm and IC-6cm is shown in Fig. 7.13.

The IDD(z) calculations were cross-checked with experimental data which allowed us to verify to what extent the construction of the chambers (the distance between the electrodes) affects their response [Radiation Protection Dosimetry (2018), Vol. 180, No. 1–4, pp. 334–337] .

Accurate determination of an absorbed dose is essential in radiation therapy. In the process of calibrating the beam output or when verifying the dose delivered to the patient, various correction factors need to be applied to the readout of an ionization chamber (IC) in order to achieve clinically relevant accuracy of measuring and determining the absorbed dose. The degree of saturation of the ionization current in ionization chambers exposed to radiation of different quality is related to several physical processes of which initial and volume recombinations are considered to be the most important. To correctly configure the beam model in TPS,

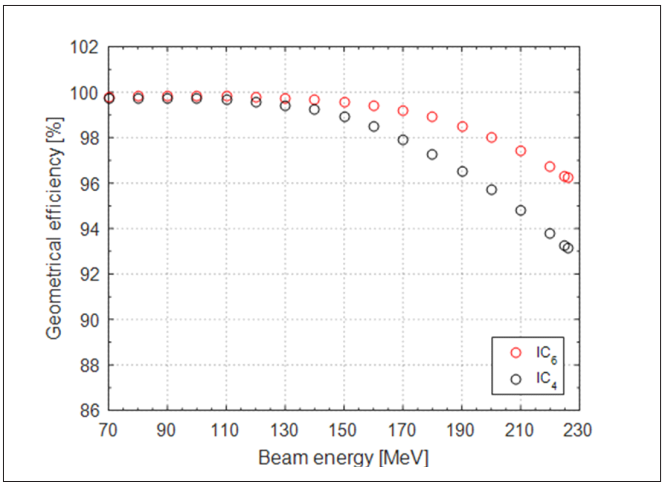

Fig. 7.13. MC calculated geometrical efficiencies for IC−4cm and IC−6cm as a function of energy obtained in the middle of R80

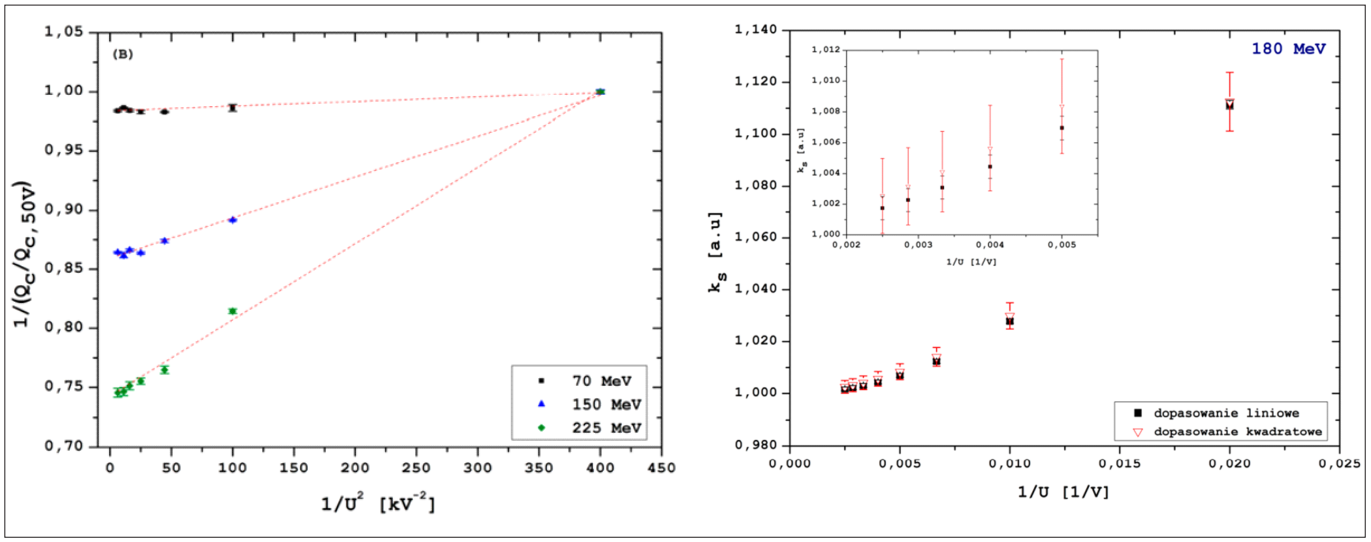

Fig. 7.14. Left: experimental data for the Markus TM23343 IC: inverse of the chamber readings (corrected charge) obtained for PBS of different energies at chamber voltages ranging between 50 and 400 V, normalized to the point at 50 V plotted against the 1/U2 with a linear fits over the full voltages range. Right: ks values as a function of 1/U, obtained using a Markus TM23343 IC exposed to scanning proton beam of energy 225 MeV.

the k_s correction factor should be experimentally verified over the whole range of clinically used energies of the PBS applied in the TPS. Measurements of the values of the ion recombination (k_s) and polarity (k_{pol}) correction factors in water, for a plane–parallel Markus TM23343 IC, using the cyclotron-based Proteus-235 therapy system with an active proton PBS of energies 30–230 MeV have been performed.

The PBS dose rates were estimated by combining direct IC measurements with the results of simulations performed using the FLUKA MC code. The values of k_s were also determined by the TVM ("two-voltage" method) for uniformly irradiated volumes over different ranges and modulation depths of the proton PBS, with or without a range shifter. **The comparison of the experimental results with those obtained from theoretical calculations was made and applied to QA protocols** [Med. Phys. 45 (1), January 2018 0094-2405/2018/45(1)/391/11].

A precise characterization of therapeutic proton pencil beams is essential for the commissioning of any treatment planning system (TPS). The procedure of dosimetric commissioning and validation is usually performed within commercially available active and/or passive dosimetry systems. However, the existing solutions do not offer a dynamic range, and the possibility to perform measurements in water with single quantum sensitivity using only one device has not been reported yet. The usefulness of diamond detectors, produced using Chemical Vapor Deposition method (CVD), for therapeutic proton beam profilometry and diagnostics was verified. Measurements of a single proton beam spot were performed in a gantry room using scanning technique (Fig. 7.15). **To ensure a sufficient spatial resolution and dynamic range for profile measurements, single-crystal CVD diamond (scCVDD) detectors with high charge collection efficiency were used.**

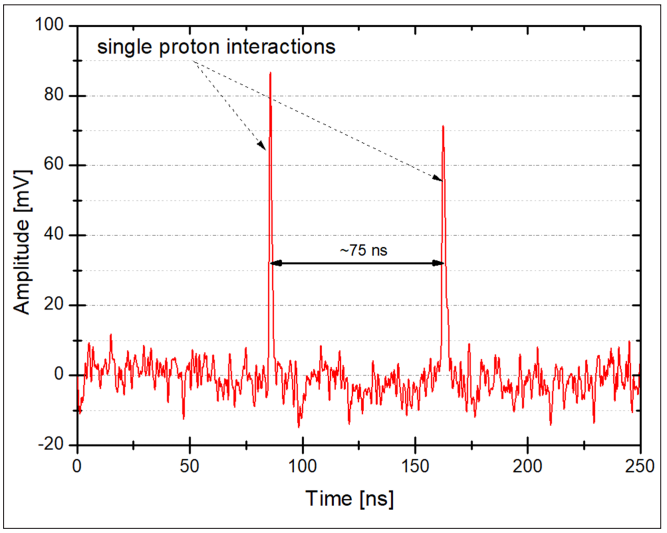

Fig. 7.15. Exemplary signals by 70 MeV protons at 100 um scCVD diamond, registered by the oscilloscope during measurements.

The scCVDD detector was placed in front of the gantry nozzle where the beam passes through perpendicularly to the detector surface. The proposed method, based on a diamond detector, gives results in a very wide dynamic range,

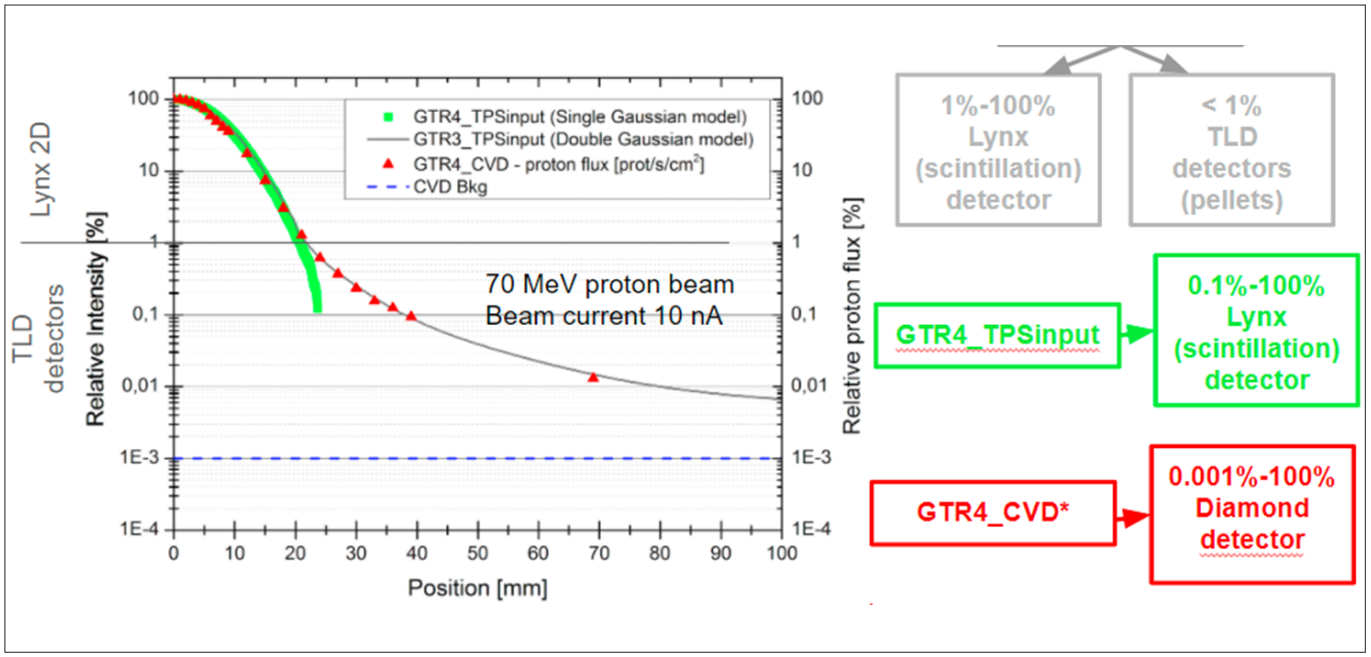

Fig. 7.16. Comparison of 70 MeV proton beam profiles obtained with different methods: GTR3_TPSinput profile (grey) was obtained with a commercially available 2D scintillation detector by IBA–Dosimetry (for core region of the beam 1–100%) and TLD pellet detectors placed in distance approx. 10mm (for low–intensity regions <1%); GTR4_TPSinput profile (green) was obtained with a commercially available 2D scintillation detector by IBA–Dosimetry; Red triangles represent relative proton flux measured with diamond detectors at GTR4. It is quite clear that the core region of the profile at GTR4 agrees well with the Lynx detector, but in the region <1% differences seem to be not negligible.

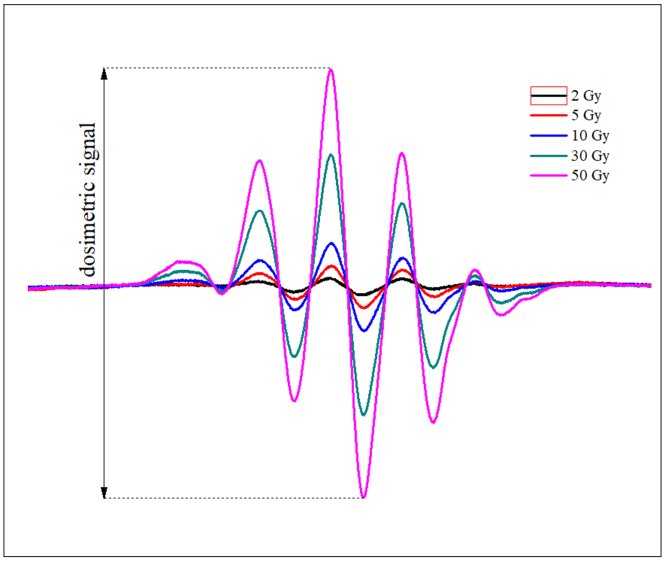

Fig. 7.17. EPR spectra of alanine irradiated with doses up to 50 Gy.

enables performing measurements in a single particle mode, and has better background control than commercially available detectors. The PBS beam profile comparison obtained with different methods is shown in Fig. 7.16. It is also evident that low dose regions have to be taken into account during TPS commissioning. The use of diamond detectors operating in a single particle mode results in reaching 5 orders of magnitude of the dynamic range, which can be potentially wider at higher beam currents (more protons in the beam core).

Moreover, the amplitude (integral) of the pulse may be used to determine the energy deposited by individual protons and possibly related to LET. Future work will focus on an experimental characterization of the beam profilometry, energy deposition and the LET spectra in mixed radiation fields produced by therapeutic proton beams in water. [Radiation Protection Dosimetry (2018), Vol. 180, No. 1–4, pp. 282–285]

This type of research is currently of great importance as it may prove to be the key to ensure the best patient care and reliable and accurate dose delivery.

The development of *a special in-vivo dosimetry system for proton ocular radiotherapy* based on EPR/alanine detectors in the years 2012-2016 proved the usefulness of this type of detectors in proton beams. In alanine exposed to ionizing radiation some stable free radicals are generated, the concentration of which can be evaluated by Electron Paramagnetic Resonance (EPR) spectrometry. This concentration of free radicals is proportional to the absorbed dose (see Fig. 7.17).

The main advantages of alanine as a dosimeter are tissue-equivalence, linear response over a large dose range (0.5-500 Gy), signal stability and its non-destructive EPR readout. These features make alanine also a promising detector for a dosimetry comparison of proton beams, both scanning and passively scattered. **In 2017 EPR/alanine dosimetry system was successfully used in the first international passive dosimetry intercomparison of ocular radiotherapy facilities (passive beams) carried out at IFJ PAN** (Fig. 7.18).

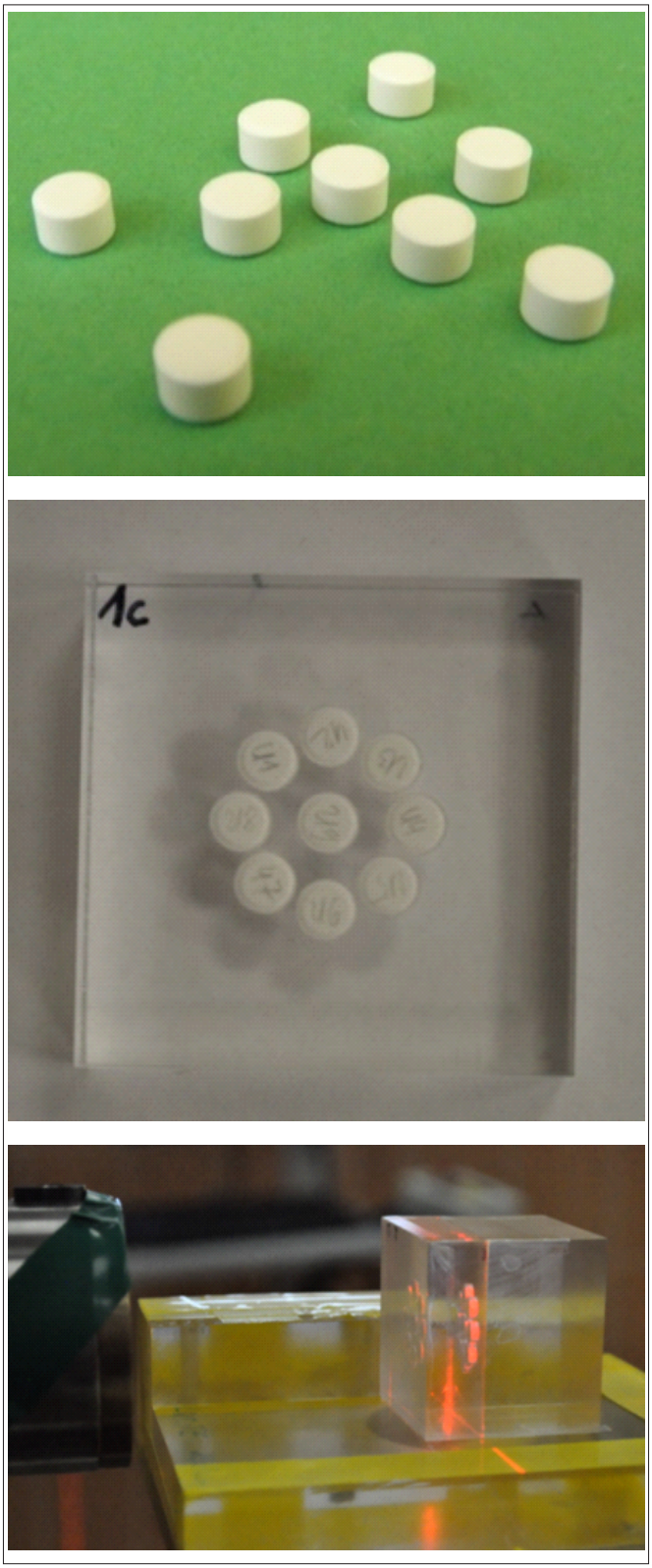

Fig. 7.18. Alanine pellets and fantoms dedicated to dosimetry intercomparison of ocular radiotherapy facilities.

Further investigation of alanine as a potential tool for mailed audits in proton pencil scanning beams, performed in collaboration with the European Radiation Dosimetry Group EURADOS, demonstrated low linear energy transfer (LET) dependence and an agreement between the measured and treatment planning system (TPS) dose below 1% [Physica Medica 82 (2021) 134–143]. Based on these studies, alanine was used for the evaluation of medulloblastoma planning and irradiation methods developed at CCB (Fig. 7.19). Craniospinal irradiation is challenging because of the involvement of large treatment volume, which is realized by junction of several radiation fields. In such a field configuration a potential undesired dose inhomogeneity at the junctions can appear . The experiment showed the compatibility of alanine doses (measured) and TPS doses (planned) in junction areas at the acceptable level of 1% [Abstracts / Physica Medica 52 (2018) 99–187].

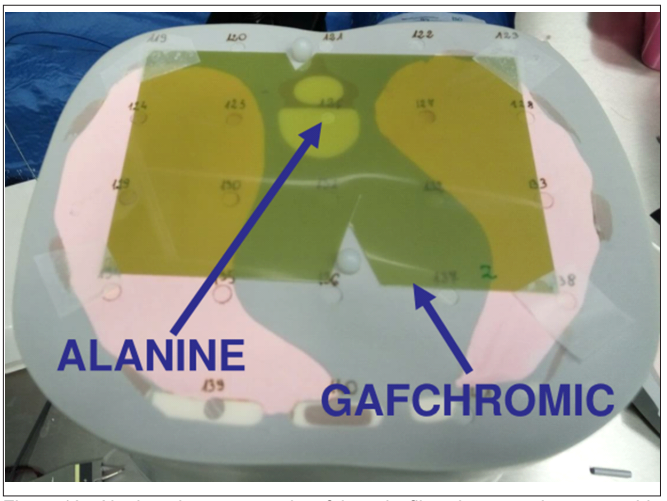

Fig. 7.19. Alanine detectors and gafchromic films in an anthropomorphic phantom of a 5−year−old child used for the examination of dose homogeneity in the junction area in medulloblastoma proton irradiation.

Currently, the EPR/alanine dosimetry is investigated as a routine tool for pencil scanning beam intercomparison. The aim of this work is to develop a reliable method for dosimetric audits in proton radiotherapy centers. The investigations are done in cooperation with the EURADOS Working Group 9 – Radiation dosimetry in radiotherapy.

❖

8. Division of Scientific Equipment and Infrastructure Construction

In between 2017-2020 the engineers and technicians from the Division of Scientific Equipment and Infrastructure Constraction (DAI) (about 60 staff members) continued their involvement in the realization of the Polish in-kind contribution to the European Spallation Source (ESS). IFJ PAN is responsible for the acceptance test of the RF cryomodules (together with ESS) and installation of the RFDS (Radio Frequency Distribution System) and power converters [Proc. SPIE, 11054 (2019) 110540A]. The team working at ESS in Lund consists of almost 20 people, who draw on their experience from similar activities carried out at the European XFEL construction [Proceedings of LINAC2014, Proceedings of IPAC2014]. In 2018 the DAI engineers started activities regarding Long Shutdown 2 of the Large Hadron Collider (LHC) and continued their involvement in the projects commencing before 2017, such as the International Thermonuclear Experimental Reactor (ITER). In 2018 and 2020 the international conferences devoted to superconductivity and particle accelerators (SPAS) were organized by IFJ PAN, at which DAI employees gave presentations and participated in discussions.

A team of engineers from IFJ PAN has been participating in testing the components of the linear proton accelerator, as a part of the ESS (European Spallation Source) facility, currently under construction in Lund, Sweden. The superconducting part of the accelerator consists of 30 RF cryomodules (9 medium beta + 21 high beta) composed of elliptical type cavities and 13 RF cryomodules with spoke type cavities. The DAI engineers have been involved in the site acceptance tests of the cryomodules equipped with elliptical type cavities which were performed in a dedicated facility called Test Stand 2 (TS2). The test starts in the preparation area where a cryomodule is checked at room temperature and the initial measurements are performed. Next, the cryomodule is moved to the radiation protection bunker where the SRF tests at 2K temperature are executed.

Commissioning of the test stand was the first important achievement and proof of good cooperation between the ESS and DAI groups. The installation work in the bunker and in the preparation area was performed. The components such as waveguides, cryogenic auxiliary lines elements, dedicated platforms were assembled and checked, followed by the installation of the prototype cryomodule

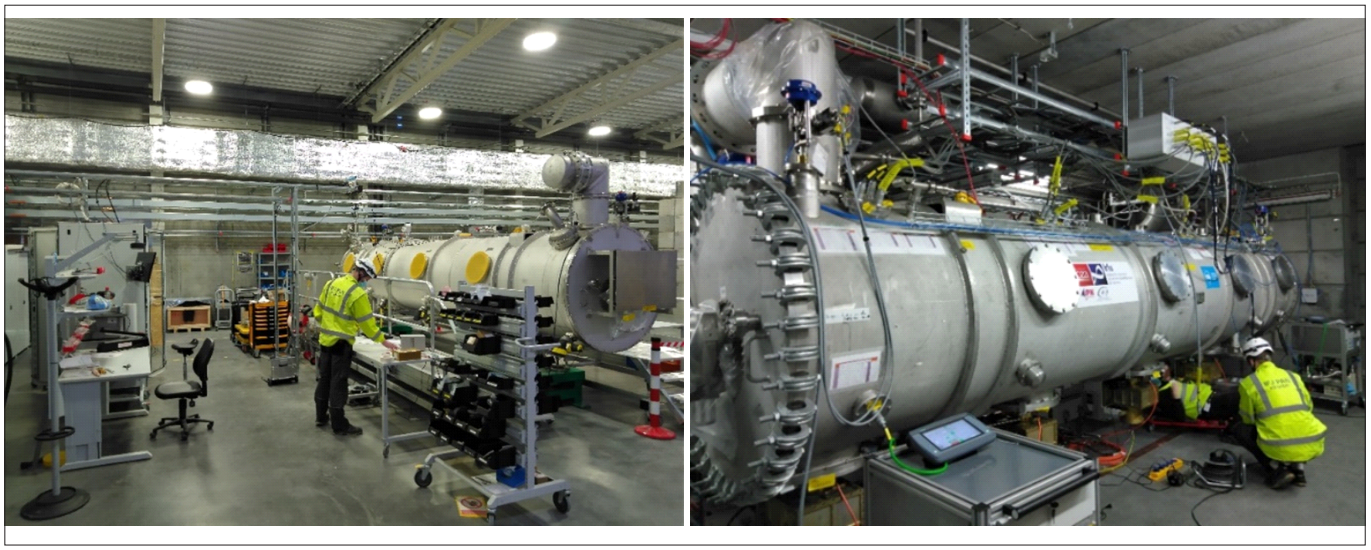

Fig. 8.1. First series cryomodule in TS2 preparation area (**left**). Prototype cryomodule installed in the test stand(**right**).

Fig. 8.2. DAI engineers working in ESS cryo control room.

(CM0). This important accomplishment took place in 2019 and paved the way for the next milestone, namely cooling down of the first cryomodule in the bunker. The operation and malfunctions of the test stand infrastructure and CM0 required continuous fixing work, thus the engagement of the DAI engineers and their expertise were essential. The installation and calibration of the test stand elements such as the helium level meters, temperature sensors, and helium flow meters were carried out and the first run of the test stand infrastructure was performed.

In 2020 two cool down "campaigns" were carried out for the cryomodule CM0. During the first run (February-March) the cryogenic operation and other infrastructure elements were checked.

It was very important for the people involved in this operation to learn how the whole system behaves. The lesson learned during the first run provided information on malfunctions and issues which were not possible to detect at room temperature and which had to be fixed before the second attempt could be made. A very important task was to measure the heat loads generated by the cryomodule and cryogenic system (e.g. transfer lines, valve box …) during cryo-operations. The second run (July-September 2020) allowed the engineers to check the results of the repairs and improvements applied between the campaigns. Based on the lessons learned during these runs, the optimization of processes was performed. Finally, crucial simulations focused on different malfunctions/accidents were performed and their influence on the system was examined.

The installation of the RFDS (Radio Frequency Distribution System) and Power converters for the ESS accelerator was another task in which IFJ PAN engineers and technicians were involved. These tasks took place in all three areas of the accelerator: in the gallery, in the stubs, and in the tunnel. So far, the IFJ PAN team has performed the installation of almost an entire waveguide system, including tuning of the waveguides, around 114 (162 in total) full lines, plus 48 reduced during value engineering in total. The waveguides consist of different elements: straight sections with different lengths, E-bends, H-bends, directional couplers, bellows, shutter switches, air cooling waveguides, coax bends, removable waveguides, coax straight sections (more than 5500 RF components plus related infrastructure). In total, around 4 km of RF distribution system components were inspected, installed, measured and tuned. The installation work was a very complex process that required a number of additional tasks to do, among others preparation of dedicated procedures and reports as well as initial trainings with mock-ups. Of great importance for the successful construction of the accelerator was also to inspect the site and perform acceptance tests as well as to implement RAMS

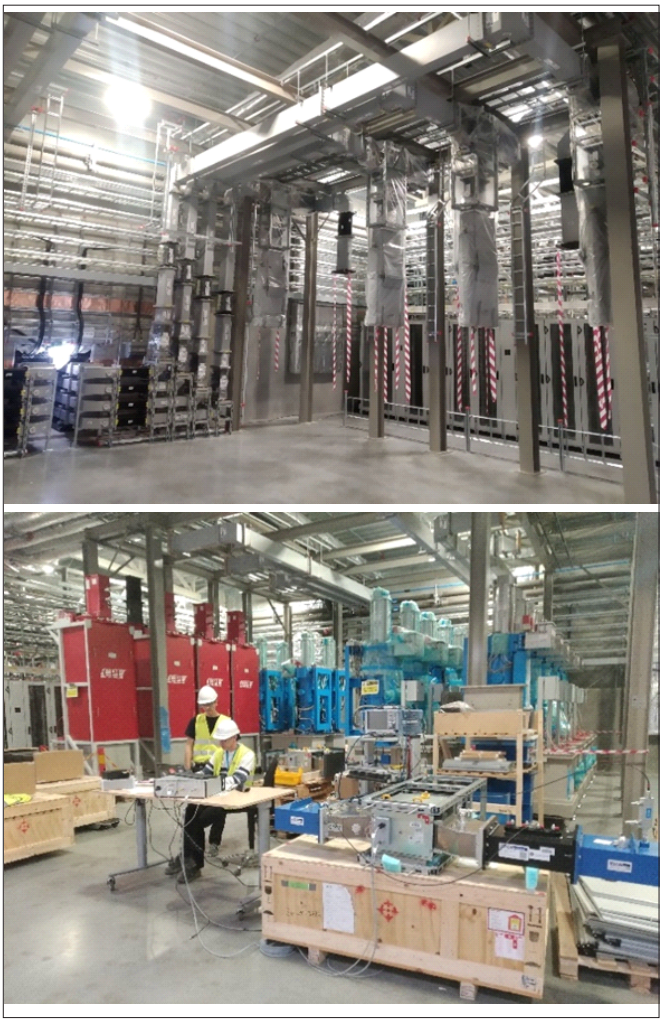

Fig. 8.3. Installed wave giudes (**top**). Installation and testing of the circulators (**bottom**).

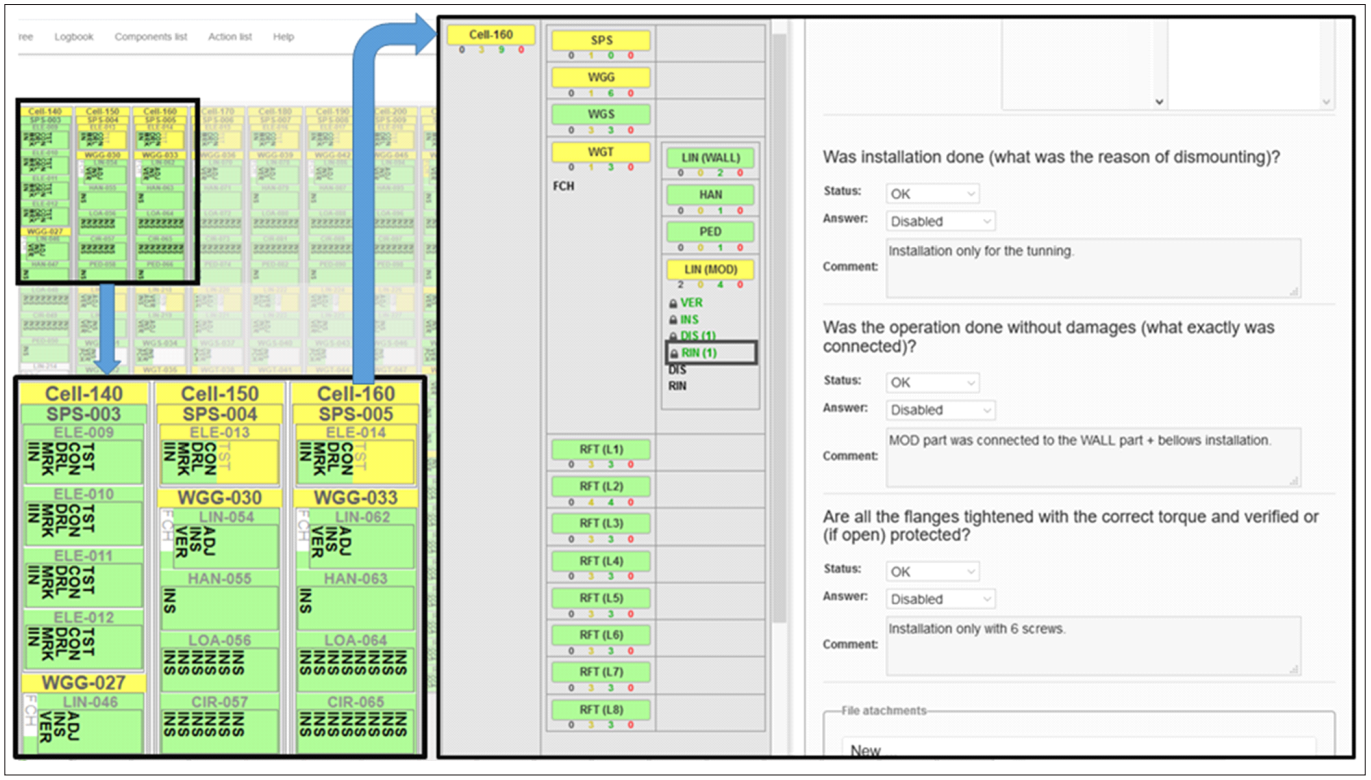

Fig. 8.4. Custom database application. A way from the main panel to the details window.

(Risk Assessment Method Statement) and other safety documentation, especially with respect to the quality control processes. In order to be able to keep these controls at a high level, the DAI engineers prepared and are currently developing a dedicated software to control all of the activities under the IFJ PAN team's responsibility at ESS.

Custom database application, progress monitoring and logbook functionality were developed for the quality control process and as first aid tools. Relevant data concerning installation works is stored in a dedicated database, enabling quality control and giving an overview of the work progress. (Fig. 8.4). The data is stored in the hierarchical structure of groups, forms and steps. A group can contain other groups or forms. A form is composed of steps. A logbook makes it possible to take note of some important information quickly and gives a possibility of tagging entries and attaching files. The application stores the full history of edits. The logbook entries are displayed in an inverse-chronological order and can be filtered by each of their parameters.

DAI engineers and technicians finalized projects related to the upgrade of test and measurement equipment as well as software upgrades needed for electrical quality assurance (ELQA) of superconducting circuits of the Large Hadron Collider (LHC) during the second break in operation called long shutdown (LS2). The work included the production of eleven multichannel high voltage insulation testers and four sets of remotely controlled multiplexers needed for the electrical verification of the LHC arc interconnections.

DAI also provided support to the ELQA team at CERN during the technical stops of the LHC run. This included investigations of the nonconformities in the superconducting circuits of the LHC and electrical tests related to the replacement of one of the main superconducting dipoles. (Fig. 8.6).

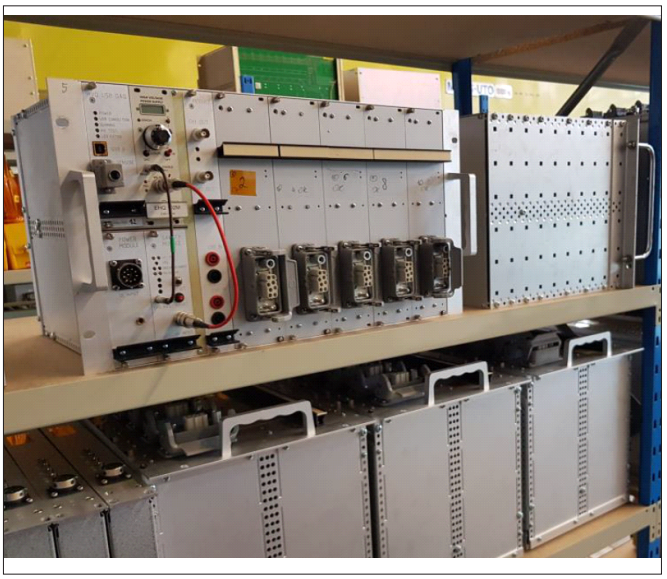

Fig. 8.5a. Complete multichannel high voltage testers ready to be used in the LHC tunnel. (Image copyright DAI).

Fig. 8.5b. Standard ELQA measurements in the LHC during Long Shutdown 2. (Image copyright DAI).

In 2018 the LS2-related activities started at CERN, which required the presence of up to 25 engineers and technicians from IFJ PAN on site in order to execute a series of extensive tasks:

- Standard measurements on more than 1600 LHC superconducting circuits and their instrumentation before and after the warm-up of the LHC.
- Software development, design and fabrication of four dedicated diode lead measurement systems.
- Four precise resistance measurements of all main dipole bypass protection diode leads located in 1232 cryo-assemblies, at different stages of the insulation consolidation.
- Measurements related to the replacements of twenty superconducting magnet cryo-assemblies.
- Standard measurements on all superconducting circuits and their instrumentation before and after the cool-down of the LHC.
- Installation and supervision of electrical insulation monitoring systems during the warm-ups and cool-downs of all LHC sectors.
- Maintenance of the ELQA equipment and software.

The last measurement campaign is scheduled to be finished in April 2021. During each campaign the IFJ PAN personnel was responsible for the investigation of the revealed nonconformities and proper reporting of the results.

DAI engineers have also started collaborating with IPP CAS. **The majority of their efforts were devoted to two topics: modeling of the Central Solenoid (CS) and dynamic analysis and design of the foundations for the tokamak.** At the end of 2020 a new line of work on the 3rd topic started – electromagnetic modeling of the forces on the vacuum vessel (VV) during Vertical Displacement Events (VDE). The initial work on the design of the Central Solenoid (Fig. 8.7a) started with 2D axisymmetric modeling (Fig. 8.7b) in order to determine the optimal size and shape of the conductor. Circular and elliptical geometries were considered, with the elliptical one found to be better due to smaller stress concentrations (Fig. 8.7c). A number of parametric studies were carried out for the insulation around the conductor and between the layers and the coils. The first results were presented at the WILGA 2019 Symposium [High-Energy Physics Experiments 2019]. The 2nd topic was related to the application of pre-stress, being of the order of several MN, because of a thermal contraction occurring when the Central Solenoid is cooled to 80 K. The preload was implemented via force applied on the top surface of the CS. This work was presented during the PCM-CMM 2019 conference in Krakow [AIP Conference Proceedings 2239, 020047 (2020)].

Fig. 8.6. Four sets of new AIV multiplexers. (Image copyright DAI)

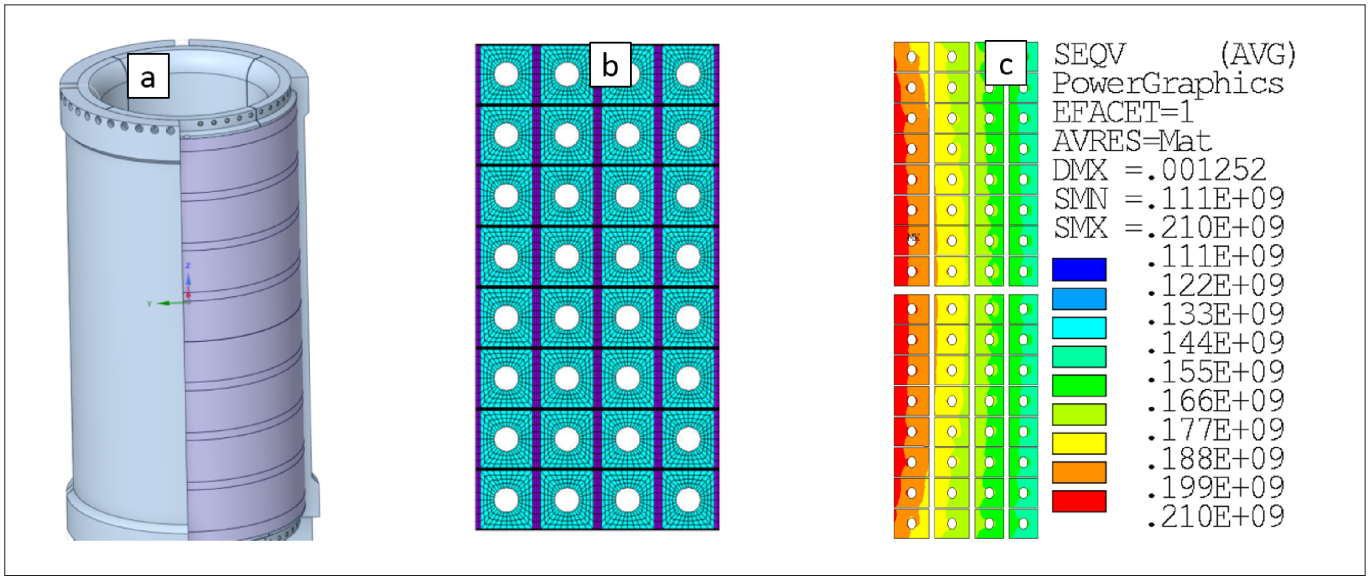

Fig. 8.7. a) Geometry of the CS; b) Mesh of one coil of the 2D model; c) Von Mises stress in [Pa] in the two middle coils of the CS for the case with 8x6.125mm elliptical holes and 4mm insulation thick in radial direction.

In the second half of 2020 the work on a periodic 3D slice started with the goal of studying the details of the pre-load system and the tie-tubes which were included in a simplified way in the 2D model. **The first analysis on the subject of the design of the foundations was related to finding the time profiles of the vertical reactions under the tokamak.** The first considered plasma disruption scenario was the Current Quench (CQ) – Fig. 8.8a. A 3D model of the tokamak structure was built in Ansys Workbench software and, based on the electromagnetic forces computed by IPP, the transient analysis was performed. The reactions from the supports were obtained as the forces acting on the foundations [High-Energy Physics Experiments 2019]. Later on, more severe plasma disruption scenarios than CQ were found – the Vertical Displacement Events (VDE) giving much larger electromagnetic forces [AIP Conference Proceedings 2239, 020036 (2020)]. In the final stage of the study, the geometry of the concrete foundations as well as the steel reinforcements, the supporting piles and a portion of the surrounding soil were added to the full 3D model of the tokamak (Fig. 8.8b) and the stresses and deformations (Fig. 8.8c) of the concrete slab were found. A number of parametric studies, including the thickness of the foundations, the position of the anchors, and the dimensions of the supporting columns, were carried out. Based on this study the final geometry of the foundations was chosen for the project.

A mechanical analysis of a 4-layer 2.5 Tm Canted-Cosine-Theta (CCT) dipole was carried out in order to verify the validity of the geometric design made in CERN. A number of FEM models were

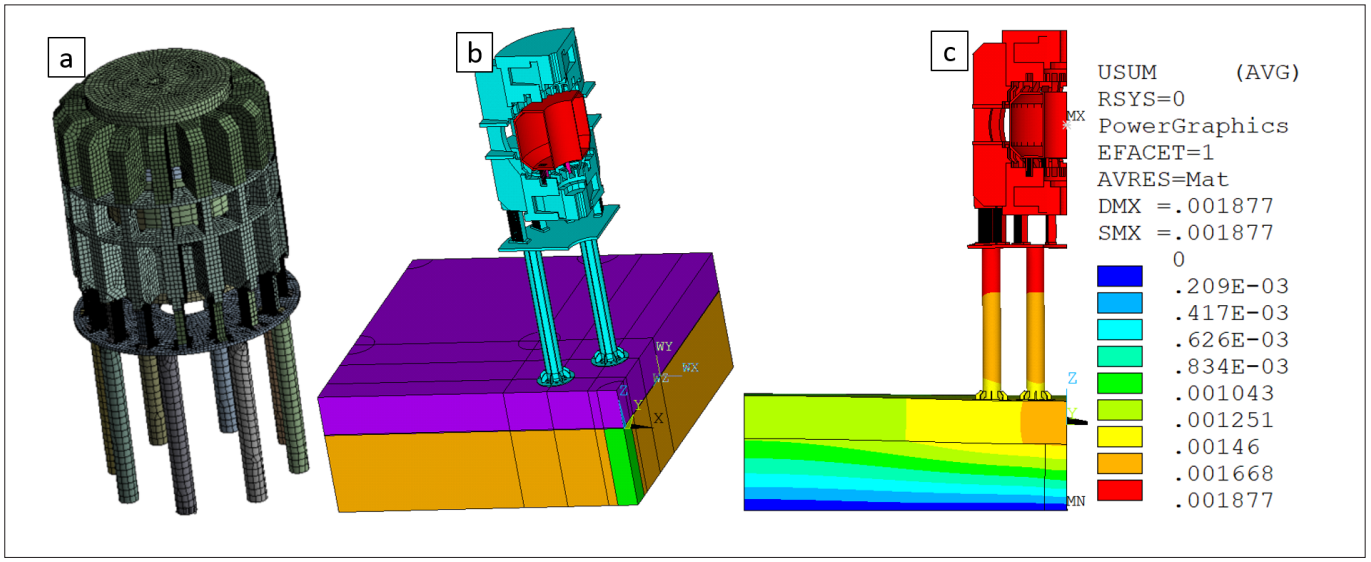

Fig. 8.8. a) Mesh of the 3D model for QC; b) Geometry of the model with foundations; c) Deformation of the foundations in [m] under self-weight

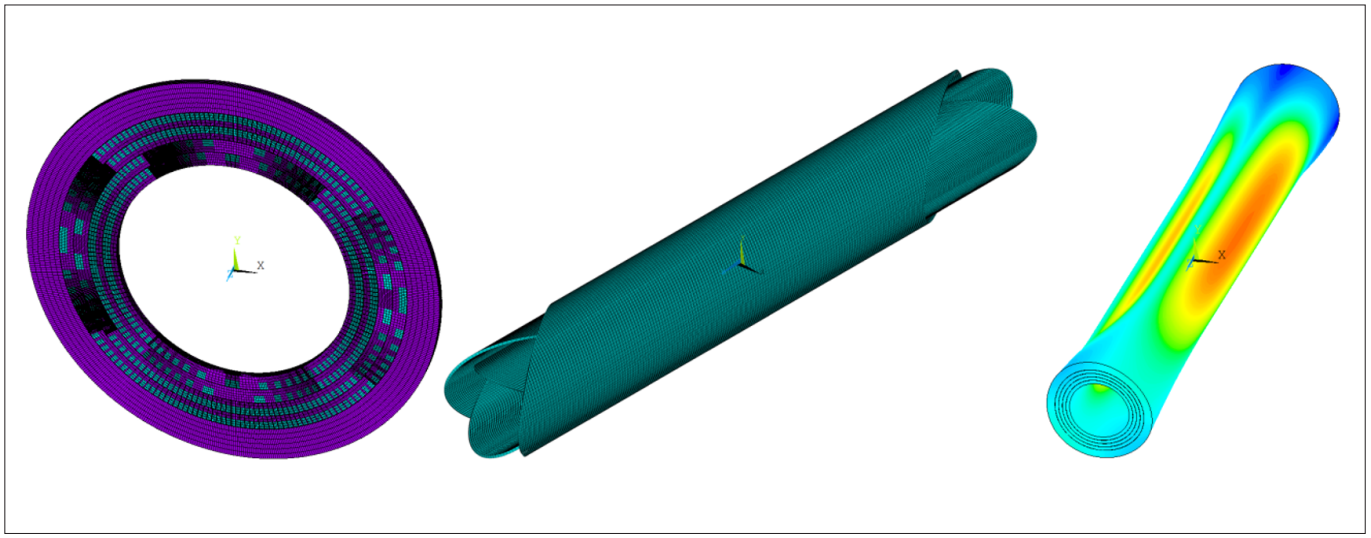

Fig. 8.9. Periodic 3D model (**left**); mesh of the coils in the full 3D model (**middle**); deformation of magnet in [m] due to Lorentz forces only (**right**)

developed, including 3 types of 2D models: a simplified 2D model with smeared anisotropic properties of the coils in the perpendicular plane, a simplified 2D model in the longitudinal plane, and a detailed 2D model including the exact geometrical features of the sliced coil. In order to develop the parametric 3D model, the mathematical description of the geometry of a multilayer CCT magnet was derived, as it was not available in literature [Cryogenics, Volume 107, April 2020]. This allowed us to develop a periodic 3D model which was implemented in the APDL language in the Ansys software. A new 16 CPU Dell workstation enabled full 3D modeling of the nested dipole opened, which was possible especially owing to the increased RAM capacity and RAID-0 array of fast SSD NVMe discs. A full 3D model was built and solved, followed by the conclusion that the bonding between the layers can break because of large torque resulting from Lorentz forces. These findings were presented at the Eucas 2019 conference [J. Phys.: Conf. Ser. 1559 012073]. In order to solve the problem of the large torque, castellated layers were proposed. A new full 3D model was built – this time it included the castellation as well as the plastic filler and a thin layer of solidified resin. The castellated design was shown to perform well by satisfying the stress limits in the formers and the coils. (Fig. 8.9).

Within its contribution to the T2K project, DAI is in charge of the design and production of two elements of the HA-TPC detector. In 2020 in DAI major progress was achieved in relation to the project. Both the Module frame and the micromegas stiffener underwent positive reviews and were authorized for production. (Fig. 8.10).

The Module frame is the component that connects the TPC chamber and the micromegas detectors. Four Module frames and 32 micromegas stiffeners are needed for the experiment. What is more, one Module frame is made for

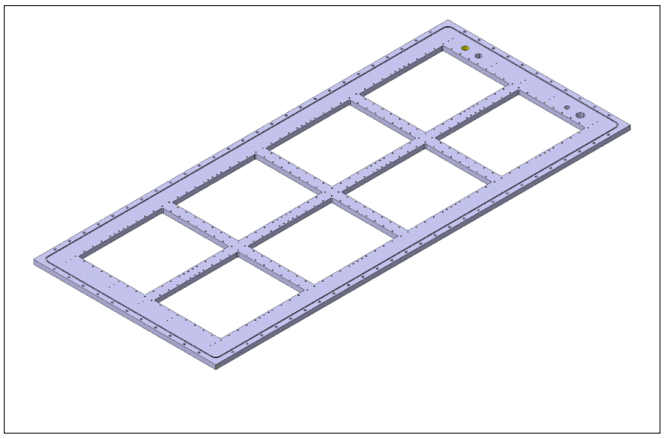

Fig. 8.10. Module frame for TPC chamber

the cable rooting and assembly tests. Four additional stiffeners will be produced as spare parts. In total, five Module frames and 36 micromegas stiffeners will be manufactured. Owing to the large dimensions of the Module frame, the drawing "good for realization" was made in DAI and the machining was performed in an external company in Krakow. (Fig 8.11). On the other hand, the micromegas stiffener production is a full responsibility of DAI. Considering the mechanical complexity of the micromegas stiffener, the machining process was optimized with respect to the tolerances, machining time and tooling. To conclude, at the end of 2020 both the production rate of the stiffeners and the manufacturing of the five Module frames were going according to the project schedule.

DAI was also involved in the International Thermonuclear Experimental Reactor (ITER). The objective of this activity was the diagnostics of

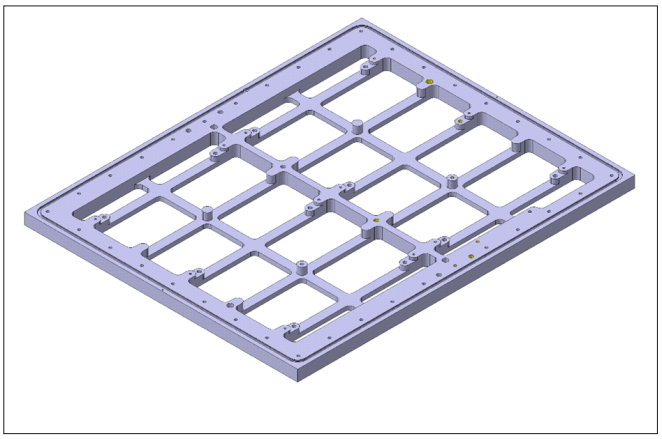

Fig 8.11. Micromegas stiffener

subcomponents of the Radial Neutron Detector (RNC). The RNC is one of the plasma diagnostic systems dedicated to ITER. It is planned to use diamond detectors as part of the RNC. The single-crystal Chemical Vapor-Deposited (sCVD) diamond detectors were validated at DAI for future ITER operations [Nucl. Instr. Meth. A, 936 (2019) 62-64]. **The thermal fatigue tests were carried out in order to verify the detector's performance in high temperature and during thermal cycling conditions.** The detectors were heated in two different schemes: Steady Temperature Test (STT) and Temperature Cycling Test (TCT). The sCVD detectors were heated to the baking temperature 240°C and then cooled to 100°C. At 100°C the detectors were irradiated by -sources, while spectrometric and dark current measurements were performed. Four diamond detectors of two different brands were subjected to STT and TCT simultaneously in the dedicated vacuum chambers.

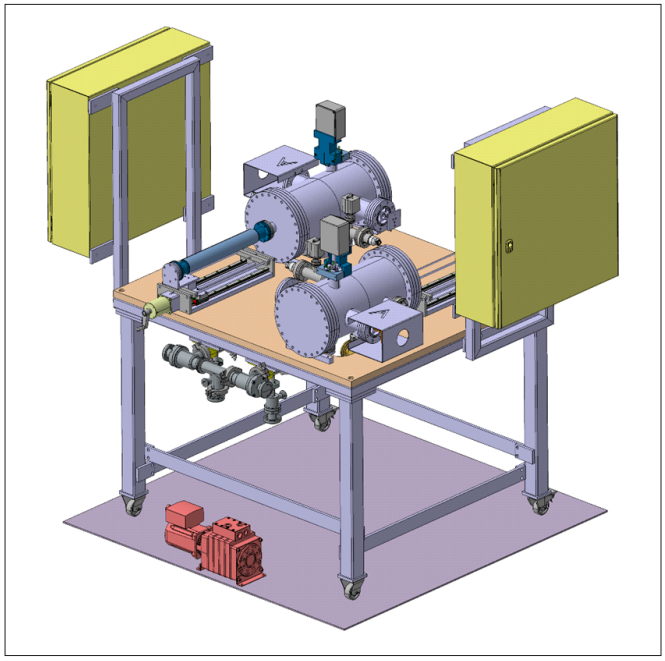

Fig. 8.12. Both vacuum chambers used for the ITER projects

Two identical chambers were designed at DAI to maintain 1 mbar inside. Both chambers were connected to the industrial PLC systems in order to control the thermal cycle conditions. In 2020, preparations for the continuation of thermal fatigue tests of a new type of detectors were started. These detectors are built of matrices of single crystal diamond. Moreover, the vacuum chambers were adopted for the other components to be tested for the ITER project. In this task the Electrical Feedthrough (EF) will be examined to withstand dedicated temperature cycling schemes in vacuum. In Fig. 8.12 the visualization of the vacuum chambers is shown.

At the beginning of 2017, **our Department established cooperation with the Superconductors and Superconducting Devices section (SCD) of the Magnets, Superconductors and Cryostat group (MSC) at the Technology Department (TE) of CERN** to deepen our knowledge necessary for the implementation of the test stand project. DAI employees worked with well-known specialists in the domain of applied superconductivity. For three years they gathered experience related to the electrical characterization of superconductors in the world-class laboratory. Three thousand samples were tested and all results analyzed. That translated into unique and broad expertise on samples test and its possible results and common problems. Nb_3Sn wires samples are about 1.5 m long. It the beginning they are wound on a titanium-alloy cylindrical sample holder. In the second step they are reacted in a furnace at a temperature above 600°C for one to two weeks. After the reaction, they are gently rewound for stabilization and soldered to copper terminals of the sample holder. Two samples are mounted on a cryostat insert and connected to voltage taps. The insert in the cryostat is cooled down to 4.2 or 1.9 K in about 6h.

Then four measurements at background field from 9 to 15 tesla are performed. Finally the samples are warmed up, inspected, and archived. During data analysis the critical current is found and its relation to magnetic field is determined. Moreover, samples are analyzed in relation to a tested pair, reaction batch, wire technology, diameter, reaction type, and designed magnet. After a year of work, the DAI engineers finished the third version of the specification. They defined the perspectives for the electrical characterization of superconductors, standards for tests of NbTi, Nb_3Sn, MgB_2 and 2G HTS samples at CERN and detailed specification of each subsystem of the complete system. At the end of 2019 the specification took its final form. The system was expected to provide at least 16 T background magnetic field at magnet temperature 4.2 K, sample current

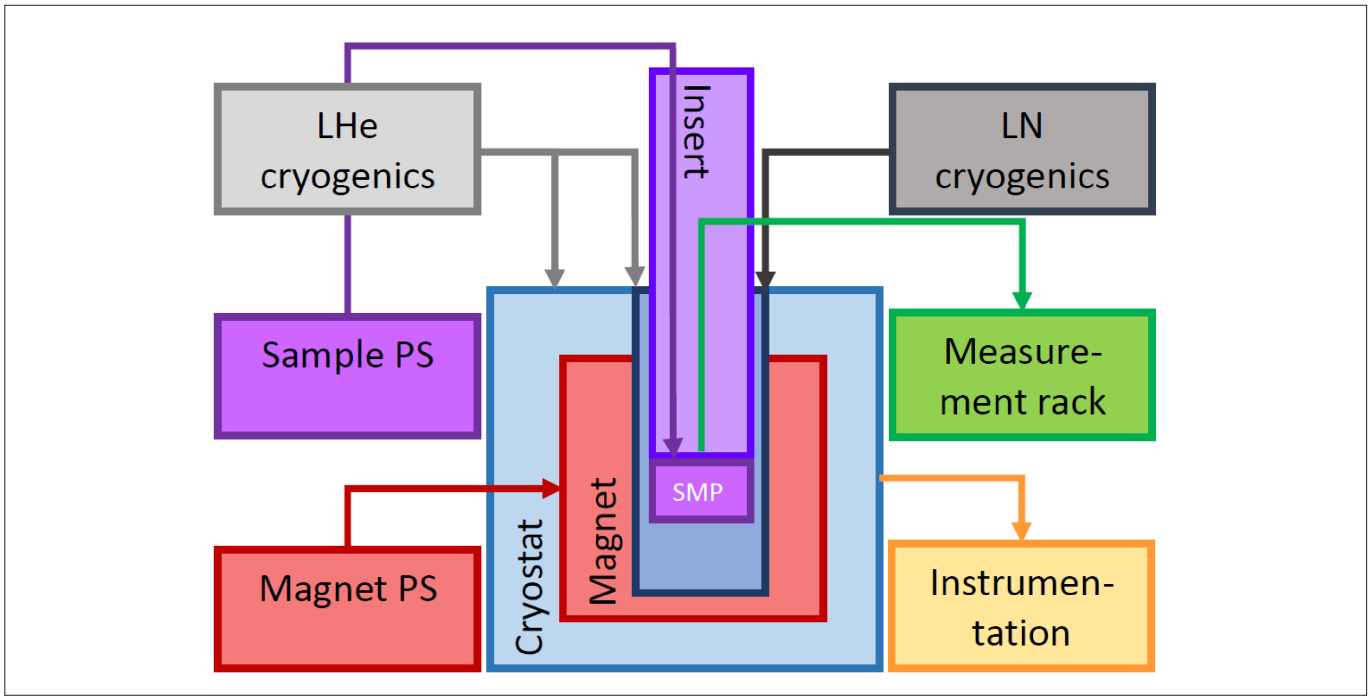

Fig. 8.13. Graph representing the main components of the test station.

of at least 1 kA, and sample temperature from 1.9 K to 150 K. In March 2020 the next milestone in the development of the system was achieved: the documentation for a public procurement contract for the supply of a system for the voltage-current characterization of superconductors at IFJ PAN was completed. The system to be purchased will enable electrical characterization of a variety of superconducting wires in high field, in a wide range of temperatures and with very high currents. It will be placed in the experimental hall in building 26. The system will contain:

- a liquid helium cryostat with instrumentation and safety equipment,
- a superconducting solenoid magnet operating at 16 T at 4.2 K,
- a magnet power supply with a magnet protection system,
- a variable temperature insert operating at a temperature of 1.9 K – 150 K,
- an insert with 1 kA current leads,
- a flexible vacuum insulated liquid helium transfer line,
- an auxiliary equipment necessary for safe operation.

DAI Engineers developed special tools which were then used to assemble the Surface Scintillator Detectors (SSD) for the Pierre Auger Observatory. **In 2018 DAI engineers and technicians started mounting the detectors and by 2019 they mounted 228 pieces of SSD.** (Fig. 8.14).

Following the assembling process, the detectors were tested in order to make sure that they were fully operational and could be shipped to their destination. The tests were performed on a dedicated test stand, designed and constructed by DAI employees.

The quality control was adapted to all the processes as well as special reports and databases were prepared to collect all the important information.

Fig. 8.14. SSD detectors on the wooden pallet ready for shipment.

New cryogenics and recovering infrastructures were installed. The general idea of the installed equipment and dependence is shown in Fig. 8.15. Warm gas coming from the labs is directed to two 15 m^3 helium balloons, then it gets to the suction part of a recovery compressor. The compressor is able to handle up to 70 m^3/h of warm gas and it compresses it up to 200 bar. From

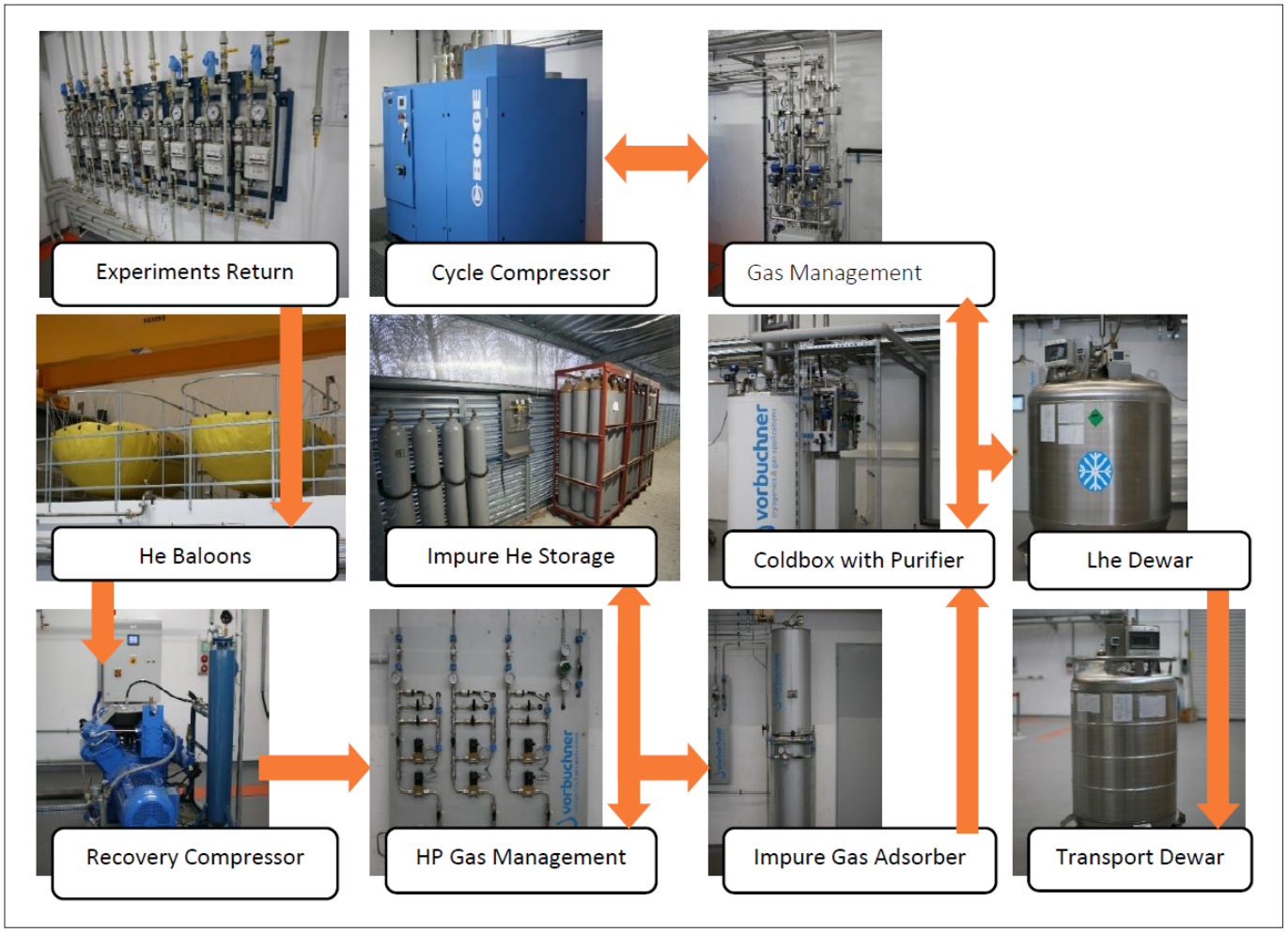

Fig. 8.15. Cryogenics and recovering installation at IFJ PAN DAI.

it the gas is further transferred through a high pressure management panel to a high pressure storage (containing 108 90l gas bottles operating at 200 bar) or to a cold box through an impure gas absorber. The cold box can handle helium contaminated by air up to 5% using a cold internal purifier. The nominal liquefaction rate is up to 35l/h with LN_2 precooling, or is reduced during operation without LN_2 precooling. The liquefier is a fully automated unit, working in the Claude refrigeration cycle. The liquefied helium gets to a 1000 litre storage tank and from this point can be delivered to labs and other experiments.

❖

9. Accredited Laboratories

Laboratory for Calibration of Dosimetry Instruments – NLW

www.wzorcowanie.ifj.edu.pl

This laboratory performs calibration of radiation survey meters in terms of air kerma rate and in terms of radiation protection units, using ^{137}Cs -rays. Calibration is also performed in terms of surface emission of particles (^{239}Pu and ^{241}Am -particles and ^{90}Sr/^{90}Y, ^{36}Cl and ^{14}C -particles). The laboratory is equipped with a gamma-ray irradiator containing three, remotely interchangeable ^{137}Cs sources, of activities 1.96 TBq, 25 GBq and 250 MBq. Using this irradiator and a 7 m-long calibration bench, it is possible to obtain calibrated dose rates ranging between 1 Gy/h and 1 Gy/h. In recent years the laboratory calibrated more than 1000 active dosimeters and dose-rate counters per year for customers from all regions of Poland. Besides active instruments, the laboratory calibrates also individual and environmental passive dosimeters in terms of kerma in air, H*(10), Hp(10), Hp(3) and Hp(0.07) for customers from Poland and other countries. The laboratory performs also calibrations for various research conducted at the IFJ PAN.

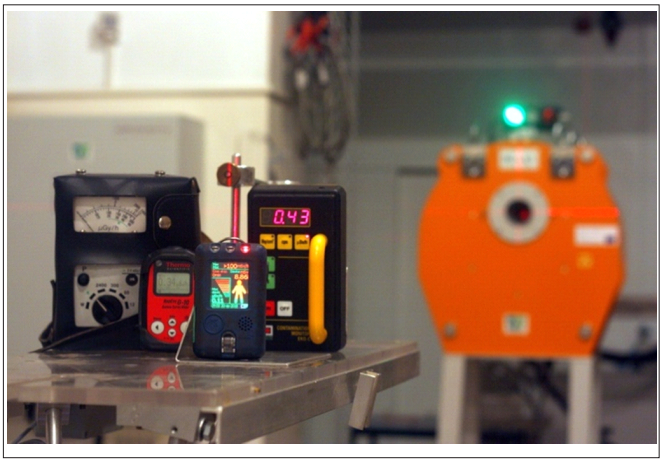

Fig. 9.1. Various radiation survey meters on Cs−137 calibration bench.

Laboratory of Radioactivity Analyses – NLP

lap.ifj.edu.pl

The expertise within the Laboratory of Radioactivity Analyses stems from several years of research on environmental radioactivity following the Chernobyl accident in 1986. In 2008 the Laboratory was accredited by PCA (No. AB 979) to conform with the ISO 17025 laboratory standard for measurements of gamma-ray emitters, among them ^{137}Cs, in different materials. In 2013 the PCA accreditation was extended to measurements of plutonium by means of alpha-ray spectrometry in radio-chemically prepared samples. The Laboratory is equipped with low-background HP germanium detector gamma-ray spectrometers and with alpha-ray spectrometers with semiconductor detectors. This accreditation assures the compatibility and high credibility of measurements within the Polish national monitoring system. Measurements of many different types of samples can also be performed for external customers.

Laboratory of Individual and Environmental Dosimetry – NLD

ladis.ifj.edu.pl

The Laboratory of Individual and Environmental Dosimetry (LADIS) is accredited by the Polish Centre for Accreditation in accordance with PN-EN ISO/IEC 17025:2018-02 and consists of two sections. The Section of Dose Control started its activities in 2002 using, as the first dosimetry service in Poland, LiF thermoluminescence dosemeters, developed at IFJ in the 60's of the past century and performs measurements of individual and environmental doses. Most of the 2017–2020 measurement services concern individual dosimetry of workers exposed to ionizing radiation (measurements of $H_p(10)$, $H_p(0.07)$, $H_p(3)$) and measurements of K_{air} in environmental monitoring. Currently, LADIS performs over 50.000 measurements yearly for more than 10.500 institutions in Poland. The other section of the LADIS laboratory offers Quality Assurance services by performing quality control tests of medical X-ray equipment for radiography, fluoroscopy, mammography, computed tomography, for intraoral and panoramic dental systems, digital mammography, digital radiography and dental CBCT systems.

Fig. 9.2. Physicist preparing extremity dosemeters for the client.

Laboratory of Radiometric Expertise IFJ PAN - NLR

radon.ifj.edu.pl

The Laboratory of Radiometric Expertise continues its research activities in the following general fields: physics of natural radioisotopes, high-sensitive, low-background measurements of gamma isotopes, investigation of indoor radon and of factors affecting the quality of indoor air (IAQ). During the years 2017-2020 three PhD theses have been defended that covered the following subjects:

- dependence of the effective dose due to radon and its short-lived progeny inhalation on indoor air parameters (2018);
- determination and investigation of thoron emanation coefficient;
- gamma radioactivity induced in the Proteus C-235 cyclotron environment.

The Laboratory offers a broad range of accredited methods of measuring radioactivity in the environment:

- measurements of concentration of natural gamma-ray isotopes (radium, thorium, potassium) in solid samples using low-background gamma spectroscopy,
- measurements of radon Rn-222 concentration in liquid samples using alpha-ray spectroscopy,
- measurements of radon Rn-222 concentration (indoor, outdoor and in soil gas) using alpha-ray spectroscopy and CR-39 track detectors.

Accredited activity is defined in the scope of Accreditation No AB 788 (Polish Centre for Accreditation) and meets requirements of the PN-EN ISO/IEC 17025:2018-02 standard.

The Laboratory has extended recently the accreditation to determine the annual average indoor radon concentration basing on the measurement with the use of SSNTD method. The value of annual average radon concentration is compliant with the requirements of radon legislation in EU.

A unique mobile laboratory (the CHIMERA Laboratory, sponsored by European Union funds), is able to measure environmental gamma-ray dose rates and to perform gamma-ray spectrometry in-situ, as well as to measure locally radon concentration in air and in water, which is of

potential application to the Polish nuclear power programme.

In May 2019 the Laboratory of Radiometric Expertise organized the III International Conference "Radon in the Environment 2019", in Kraków, Poland. This meeting gathered over 120 participants from 28 countries (including Australia, Equador, USA, Peru, China, India, Japan, Russia).

On 7th November (Maria Skłodowska-Curie birthday anniversary) each year the Laboratory of Radiometric Expertise continued the organization of the "European Radon Day" in Kraków, in the form of a research and training session to educate the public and local authorities on the issues of radon.

Over the years 2017-2020 the staff of the Laboratory published 15 research articles in international peer-reviewed scientific journals, published 3 other reports, and delivered 19 conference presentations. Two staff members of the Laboratory are co-authors of the first "European Atlas of Natural Radiation" that aims to provide reference values and harmonized data for scientific community and national competent authorities. The Atlas is free for download in pdf format: (https://remon.jrc.ec.europa.eu/About/Atlas-of-Natural-Radiation/Download-page)

Also, over 380 reports of measurements and radiometric expertises for ca. 80 customers were issued over that period.

Staff members of the Laboratory were invited to the expert group at the Main Sanitary Inspectorate which developed „National Radon Action Plan" according to the Polish Atomic Law requirements. They have also developed (in cooperation with other institutions) the procedure of intercomparison radon measurements that will be used by the Ministry of Health to implement „National Radon Action Plan".

The head of the Laboratory was appointed a National Contact Person for Poland to coordinate national data collection for the UNSCEAR Questionnaire on Public Exposure. He was also invited as an expert to Sungroup Radon for the UNSCEAR Public Exposure Project.

❖

10. Postgraduate Studies

The International PhD Studies and the Krakow School of Interdisciplinary PhD Studies

The doctoral studies at the Institute of Nuclear Physics (IFJ) were launched in 1984 and since that time PhD degree in physics was granted by the Scientific Council of IFJ to more than 250 of its alumni (>40 in the years 2017-2020). Many of our graduates are employed by scientific and commercial institutions all over the world. Up to date, 5 of them have been distinguished by earning the title of a full professor, and more than 45 have been awarded the post-doctoral degree of doctor habilitated (dr hab.) in physics (17 of our former PhD students obtained this degree in the years 2017-2020).

Within the implementation of the PhD program we cooperate closely with scientific institutions in Krakow and Lesser Poland Voivodeship. The institutional and formalized collaboration with the AGH University of Science and Technology and the Jerzy Haber Institute of Catalysis and Surface Chemistry of the Polish Academy of Sciences dates back to 2009 when, together with these two institutions, we launched a common interdisciplinary PhD project "Interdisciplinary PhD Studies: Advanced Materials for Modern Technology and Future Energy Production <ISD>" and won a national competition, thanks to which the project could be financed from the EU Operational Program Human's Capital. The project was successfully completed in the years 2009-2015 and within it 58 young scientists were awarded the degree in physics and chemistry, among them 15 students from our Institute.

The ISD project was the cornerstone of our further collaboration. In 2017 the ISD partners, acting as a consortium joined by the Jerzy Maj Institute of Pharmacology of the Polish Academy of Sciences, Collegium Medicum of the Jagiellonian University, Faculty of Chemistry of the Jagiellonian University and the Faculty of Material Engineering and Ceramics of AGH, successfully applied for two new interdisciplinary PhD programs named "Physics, Chemistry and Biophysics for New Materials and Technologies <FCB>" and "Interdisciplinary Research for Innovative Medicine <InterDokMed>". Our projects won a national competition and were qualified to be financially supported by the EU Operational Program "Knowledge-Education-Development" <PO WER>. During the academic year 2017/2018 125 PhD students (among them 17 were pursuing research at our Institute) were recruited to both projects that started in the autumn of 2017. The time scheduled for preparing theses is four years. Currently the PhD students enrolled in the projects are completing their theses and preparing for defenses. The first defenses of the PhD theses prepared under the FCB and InterDokMed projects are expected during the fourth quarter of this year.

On July 20, 2018 a new law on higher education and science, called the Constitution for Science, was introduced in Poland. The law significantly changed the rules of awarding a PhD degree. In particular, doctoral studies were replaced by doctoral schools which are obliged to provide interdisciplinary education in at least two disciplines of science and/or arts. The research institutes of the Polish Academy of Sciences located in Krakow: the Henryk Niewodniczański Institute of Nuclear Physics (IFJ PAN), the Jerzy Haber Institute of Catalysis and Surface Chemistry (IKiFP PAN), the Jerzy Maj Institute of Pharmacology (IF PAN), the Aleksander Krupkowski Institute of Metallurgy and Materials Engineering (IMIM PAN), acting jointly with the two faculties of the AGH University of Science and Technology: Faculty of Physics and Applied

Computer Science (WFiIS) and Faculty of Materials Engineering and Ceramic (WIMiC), decided in the late winter of 2019 to take advantage of their previous experience and to organize and run a new interinstitutional interdisciplinary doctoral school to train PhD students in the domain of basic science: physics and chemistry, in the domain of medical sciences with emphasis put on pharmacology and pharmaceutical sciences, as well as in technical sciences, namely materials engineering. A multilateral agreement to establish the doctoral school, acting under the name of Krakow School of Interdisciplinary PhD Studies, abbreviated as KISD, was signed on May 6, 2019 and this day is the official date of launching the school. The Institute of Nuclear Physics was appointed as the leader of KISD and coordinator of all its activities. Following the preparation and approval of the required documents by all partner institutions, the first enrollment at the School was carried out in September 2019 and 29 PhD students began their education.

At present, after two regular recruitments supplemented by special recruitments addressed to candidates whose studies and research are financed from external sources, we have in total 62 PhD students, including 9 people from abroad: 3 from Ukraine, 2 from India, and one person from each of the following countries: Canada, Iran, Lebanon and Czech Republic. The KISD partners are actively searching for external sources of financing, especially within the international scientific cooperation involving the PhD students, and their efforts have brought fruit in the forms of grants financed by the National Agency of Academic Exchange, such as the PROM programs awarded to IFJ, IKiFP and IF, and the STER program awarded to IFJ acting on behalf of KISD, as well as a special project focused on close cooperation between scientific institutions and industry called "Doktorat wdrożeniowy" (Industrial Doctoral Program), launched and financed by the Ministry of Science and Higher Education.

Prospective candidates to KISD are required to be university graduates with a MSc degree. To be enrolled in the PhD studies the candidates have to pass entrance exams, the scope of which depends on the profile of the unit in which the student will do research and prepare the thesis. Additionally, each candidate has to be accepted by a senior academic staff member (full or associate professor) who in the future will become the supervisor of the candidate's thesis. KISD is open to foreign students and is well prepared for their recruitment - as mentioned, currently we have 9 foreigners, in their vast majority eager to obtain the degree in physics, but also in chemistry. The educational offer of KISD, which includes proposed subjects of theses related to the research done in partner institutions as well as subjects of future lectures and classes, is published yearly. In the first year of training our syllabuses cover three moduli: the general one devoted to competences needed for any scientist and future university teacher, such as didactics, elements of statistics, data processing and modern programming languages; the so-called interdisciplinary modulus within which problems of various branches of modern science are presented to non-specialists; and the modulus of soft skills - methodology of scientific research, intellectual properties, preparation of scientific publications and grant applications. The second year is devoted to much more specialized education, conducted in small groups and related to the theses' subjects. The remaining two years of PhD studies are focused on individual work with supervisors, collecting and processing results and, finally, preparing the thesis.

Like it was in the past, we put emphasis on research conducted by our students within international cooperation or, more generally, on facilitating their access to the international scientific community. We promote internships in foreign research centers, participation in conferences and preparation of theses in international cooperation. An illustrative example of the latter is the PhD program entitled "Copernicus Doctorate in Physics", approved and signed in 2014 by our Institute and the University of Ferrara in Italy. Its aim is to pursue research supervised by two tutors and leading to the PhD degree awarded by both institutions. In the years 2017 and 2018 three of our PhD students completed this program and were awarded the double degree.

During 2017-2020 48 PhD students completed and defended their theses being awarded the degree in physics, one of them was specially recognized by the very prestigious Prime Minister Award. Our PhD students were also awarded grants addressed solely to young researchers preparing their theses like the PRELUDIUM and ETIUDA grants.

❖

11. Outreach Activities – Promotion and Education in Science

Over the past years 2017-2020, the Institute of Nuclear Physics Polish Academy of Sciences (IFJ PAN) continued its efforts to promote science and education among the general public as well as primary and secondary school students.

The main objectives of these activities were:

- to familiarize the public with science, not only in the field of physics, but also related disciplines, including radiobiology, radiotherapy, dosimetry, radiochemistry, medical physics, biophysics, engineering, and interdisciplinary research,
- to promote research carried out at our Institute in collaboration with top-class foreign and domestic research institutions,
- to stimulate and develop young people's interest in physics.

IFJ PAN is actively involved in popularizing science through participation in public outreach events, which are regularly organized on a large scale in our country. Some of these events are held annually in collaboration with other research centers from Małopolska and other regions of Poland. Within the discussed period of time, our Institute took part in quite a few important annual outreach projects:

The Małopolska Researchers' Night is the largest annual event dedicated to the promotion of science in which our Institute participates. On that particular night several tents are put up on the green premises of our Institute. Inside them, our staff present achievements and activities of all six scientific divisions of IFJ PAN, including experiments and shows performed in front of a live audience. All our guests are also invited to take a tour around the Institute, during which they can visit our most interesting laboratories along the trail *In the Labyrinth of Science*. Within the framework of the "Science Cinema" we present a series of popular-science movies, such as: *The Mysterious World of Atomic Nuclei*, *Unraveling the Secrets of DNA* (Golden

Fig. 11.1. Małopolska Researcher's Night, 2019 *(photo: L. Grin)*.

Copernicus award at the Festival of Films for Education 2010, Warsaw), and *Bronowice Chronicle*, produced at the Institute by dr hab. Jerzy Gręboszz, as well as the film *Moving the Horizon*, directed by Wiktor Niedzicki. Each year the Night is accompanied by other interesting events: *The Tricks of Physics* – a show of experiments which reveal some secrets of Nature, *Physics for Adults* – a show of R-rated experiments, *Phycisist's sofa: ask a physicist* – a place where anyone

Fig. 11.2. Małopolska Researcher's Night 2020, conducted on-line *(photo: A. Czarny)*.

can ask a physicist a question about physics, or the so-called *Lamusownia* (*The Junk Room*) – a trip into the past of IFJ PAN in the form of an exhibition of old experimental instruments showing how physics was once practiced. Each year on this particular day the Institute is visited by over a thousand science enthusiasts of all ages.

In 2020, because of the COVID-19 pandemic, the 14th edition of the Małopolska Researchers' Night was of a special nature. The entire program of the Night organized at IFJ PAN was carried out on-line. It included live broadcasts on physical shows, interactive lectures or meetings with scientists, as well as video projections prepared especially for this occasion.

The Cracow Science and Art Festival is just another event at which we can present our scientific achievements to the broad public. It is organized annually by Krakow's universities and research institutes. Our program is wide and attractive: we invite the participants of the Festival to a "journey to the beginnings of the Universe", reveal the secrets of gravitational waves, dark matter and black holes, demonstrate the advantages of proton radiotherapy, explain how the cyclotron works and how cancer treatment is carried out using the proton beam at Cyclotron Centre Bronowice (CCB) IFJ PAN. The program also features the CREDO project, an idea born at IFJ PAN devoted to the detection of cosmic rays with the use of smartphones.

Fig. 11.3. The Cracow Science and Art Festival, 2017 *(photo: M. Perzanowski)*

The Science Picnic of Polish Radio and the Copernicus Science Center is yet another annual event dedicated to popularizing science – it is held annually at the National Stadium in Warsaw. Science popularizers representing our Institute hosted such shows as: *Ionizing radiation and its propagation in the environment, Transport of contaminants in the environment, Accelerate a particle in a particle accelerator, A scientific breakthrough? Now it's your turn – use your smartphone to probe the Universe!* The picnic attendees could also take part in a quiz about searching for invisible radiation, examine masks used in proton radiotherapy at the Cyclotron Centre Bronowice, learn about the therapeutic application of magnets, or expand their knowledge on radiation and its impact on our health.

Fig. 11.4. M. Gałązka is presenting the visual model of an interrogation room and the functioning of a one−way mirror during the Science Picnic of Polish Radio and the Copernicus Science Center, 2019 *(photo: W. Zając)*

Also worth mentioning are several very important events aiming to popularize research and organized exclusively by our Institute:

The musical spectacle *At the intersection of two infinities*, the concept of which came from prof. Adam Maj, with music by Józef Skrzek, film narration by dr hab. Jerzy Gręboszand directed by prof. Adam Maj, was one of such events. The spectacle was prepared specially to celebrate the 45th Congress of Polish Physicists and was a special item on the Open Day Program of the Congress. Musical compositions developed specially for the show had their premieres there.

The show, painted with music and film, is an artistic vision of the history of our Universe. It leads the spectator from singularity just before the Big Bang (Bubble Universe), through the Big Bang, the production of the hydrogen element, the formation of stars and light elements (from helium to iron) during stellar nucleosynthesis, and finally to Supernova explosions, allowing elements heavier than iron to form and to scatter all these elements into the vastness of the Universe, thus creating life. The climactic piece of music refers to the fact that we are children of the Universe.

The show ends with a vision of a possible scenario for the end of our Universe, e.g. as a result of the Big Rip, and finally a vision of the possibility of creating a new singularity (and perhaps a New Universe).

Fig. 11.5. Musical spectacle "At the intersection of two infinities", 2019 *(photo: Ł. Pawlikowski).*

The Institute also hosted **popular science shows, which were greatly appreciated by primary and secondary school students**. They were conducted by Wiktor Niedzicki – a well-known physics promoter, and dr Dominika Kuźma from IFJ PAN. These events were attended with great applause by nearly a thousand primary and secondary school students from Krakow and its vicinity. The lecturers proved that science is not confined to a laboratory – we encounter its phenomena and use it in everyday life.

On the occasion of the series of popular science shows, in 2018 the Institute published a booklet describing and illustrating selected simple physical experiences for children, entitled *The Fourth Wiktor's Laboratory*.

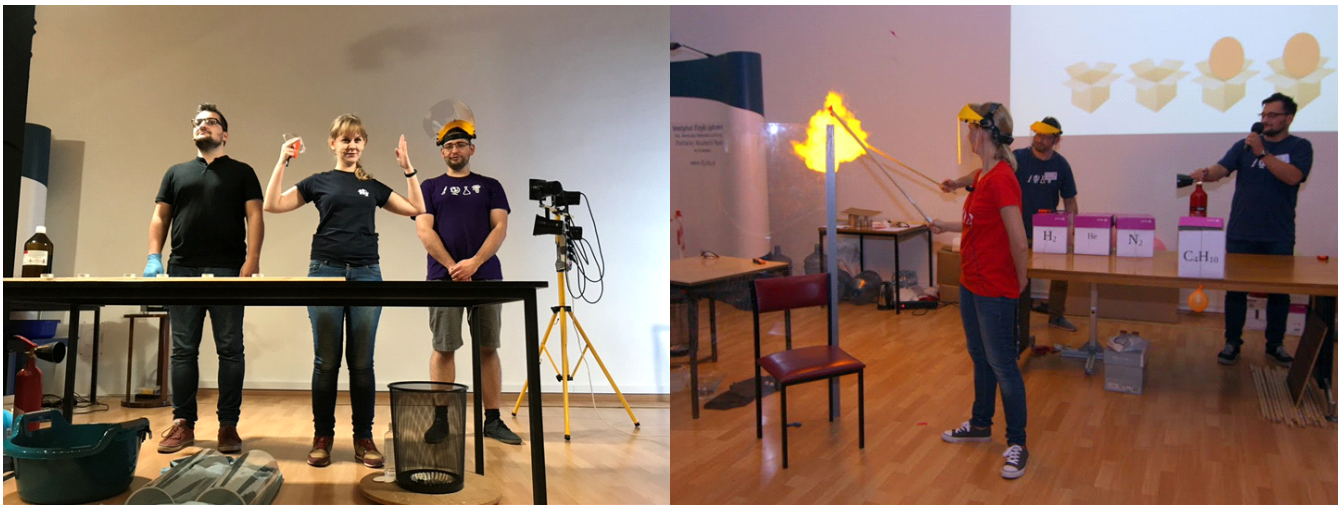

Fig. 11.6. D. Kuźma, M. Kiełbowicz, and S. Bysiak are attracting the attention of their audience during Physics Tricks *(photo: A. Bystrzycka – left, L. Grin – right)*.

Fig. 11.7. Wiktor Niedzicki is signing The Fourth Wiktor's Laboratory, 2018 *(photo: B. Różewicz)*.

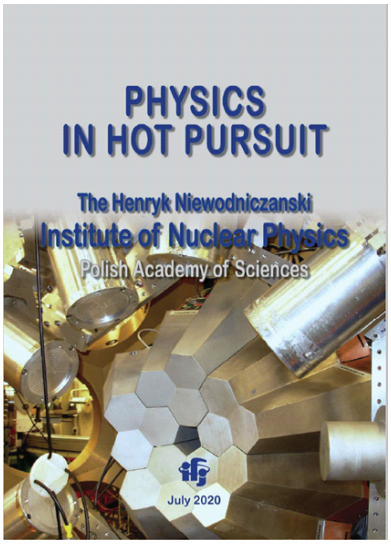

Fig. 11.8. The front cover of the popular science brochure "Physics in hot pursuit", 2020.

The Senate of the Republic of Poland proclaimed 2020 the Year of Physics to honor Polish physicists and their achievements and to appreciate the importance of this field of science for civilization. To draw attention to the up-to-date achievements of scientists from IFJ PAN, on the initiative of prof. Tadeusz Lesiak, **a brochure entitled** *Physics in hot pursuit* **was published**. The materials included in the publication were selected on the basis of scientific achievements disseminated in the form of press releases to the media, which were presented on the Eurek Alert! in previous years. The content of the book is divided into six main chapters, arranged thematically in such a way as to increase its readability. The highlights of our research achievements are presented in an accessible and concise form. The book was published by IFJ PAN in Polish and English.

In cooperation with the International Particle Physics Outreach Group (IPPOG) and CERN, our researchers organize the **International Particle Physics Workshops for high school students** (as part of the *International Masterclasses – Hands on Particle Physics*) – an annual event. Our offer also includes student internships – Particle Physics Laboratory – **IFJ PAN Particle Physics Summer Student Program held** annually. These events are intended to encourage students of physics and related sciences to become involved in particle physics research by giving them an opportunity to independently analyze latest experimental data from the ATLAS, ALICE, Belle, LHCb, NA61 / SHINE and T2K experiments.

In recent years, an **Open Day for university students** and **Childrens' Day** were organized at IFJ PAN, both on an annual basis. The Open Day is an event dedicated to students to give them the opportunity to talk to our

Fig. 11.9. IFJ PAN workshops are attracting a growing number of high school students. *International Particle Physics Workshops, 2019 (photo: R. Staszewski)*.

researchers and read the current offers of student internships and bachelor's, master's and doctoral theses. Moreover, the aim of the Open Day is to introduce interested parties to various research techniques – both experimental and theoretical – and to demonstrate methods of sample preparation as well as experimental equipment tuning. While touring the studios/laboratories (in organized groups), the visitors can have individual discussions with potential internship and/or diploma supervisors, inquire about details, and plan further cooperation with IFJ PAN. The Children's Day program, on the other hand, includes:

- a show of surprising physical experiments – *Physics Tricks on Bis*,
- workshops on building models of molecules,
- a series of mini-presentations, during which children's questions on everyday life are answered, e.g. what is sound?, what is the origin of colors?, what can you learn by counting words in a book?

A series of presentations was organized to **promote the didactic offer of IFJ PAN among students of European universities**. Research opportunities at IFJ PAN were presented in the form of 11 seminars to students of

Fig. 11.10. Foreign students are attending a seminar as part of the didactic offer of IFJ PAN *(photo: L. Grin)*.

physics and related sciences from Serbia, Macedonia, Hungary, Ukraine, Bulgaria, Portugal, and Germany. Each seminar was followed by discussions on topics related to physics, details about the IFJ PAN summer school, the possibility of undertaking doctoral studies in Poland, and further possible cooperation.

Cosmic Ray Extremely Distributed Observatory (CREDO) project is an initiative aiming to build a global

Fig. 11.11. The CREDO Detector application transforms your smartphone into an important element of the largest particle detector in history.

system of cosmic ray detectors with the participation of scientific and educational institutions as well as individual enthusiasts from almost all continents [PoS (Asterics2019) 2019, 034]. Under the separate agreements the project currently involves 42 entities from 19 countries on five continents [Symmetry 2020, 12(11), 1835], supported by a growing number of amateurs using their own smartphones to detect cosmic ray particles through the mobile application called CREDO Detector, designed and developed at IFJ PAN in 2018 [Symmetry 2020, 12(11), 1802]. The application serves to detect secondary cosmic radiation using mobile devices, and it currently operates on more than 7,000 devices located in approx. 150 countries around the world, providing data (approx. 10 million detections to date) which are both the subject of scientific analysis and the goal of educational and social activity [Appl. Sci. 2021, 11(3), 1185]. The latter includes e.g. the international competition "Particle Hunters" organized by IFJ PAN since 2018 (mentioned further below).

The project "Physics as the key to understanding the world" implemented as part of the Social Responsibility of Science program – Excellent Science and co-financed by the Ministry of Science and Higher Education, is another popularizing activity to be hosted by IFJ PAN in the years 2020-2022. The aim of the project is to reach a wide audience of all ages to arouse curiosity in physics. The project consists of four weekly series of popular science shows: *Fascinating Physics, CREDO and cosmic rays, Surprising Physics, Particle Accelerators.*

The events are scheduled to take place in the IFJ PAN auditorium, which provides approximately 150 seats. Each cycle will include 12 presentations for different age groups: primary and secondary school students and other individuals. The project coordinator is dr. Dominika Kuźma. More information about the project is available on the website.

Other forms of instilling interest in science included various types of **physics competitions for school students** organized by the Institute. One such activity was the annual QuickPhysX competition. Here, doctoral students and employees of IFJ PAN gave short, easy to understand popular science presentations on any topic related to physics. Other initiatives included the contests: for a washable tattoo design entitled "Tattoo with physics in the background", and the "Particle Hunter" competition which involved team detection of secondary cosmic radiation particles and local radioactivity using smartphones equipped with the CREDO Detector application. The aim of the "Particle Hunter" is to create a network of users of the CREDO Detector application to promote the idea of co-creating science by amateur researchers, and to enable children and adolescents to participate in scientific research and even become co-authors of scientific discoveries. Several hundred students from several dozen schools in the country have been involved in this campaign.

The Institute also participated in the organization of the Lesser Poland Physics and Astronomy Competition for primary and secondary school students and the national competition "Chain of experiments", organized on the initiative of students of the Faculty of Physics, Astronomy and Applied Computer Science of the Jagiellonian University in Krakow.

Every year, the Institute issues **notes on major scientific achievements attained with significant participation of researchers from IFJ PAN**, published on the global scientific press service EurekAlert!, which is run by the American Association for the Advancement of Science. These press reports, based on articles published in renowned journals, have from several to several thousand openings per month.

The Institute is also active on **Facebook**, **Twitter** and **YouTube** – posting information and videos on its activities and ongoing outreach events.

Last but not least, IFJ PAN scientists are often invited by various scientific and cultural institutions to deliver popular-science lectures, participate in discussion panels, and conduct laboratory exercises. They also collaborate with the media by publishing their articles on popular science blogs, or appear on television and in radio broadcasts.

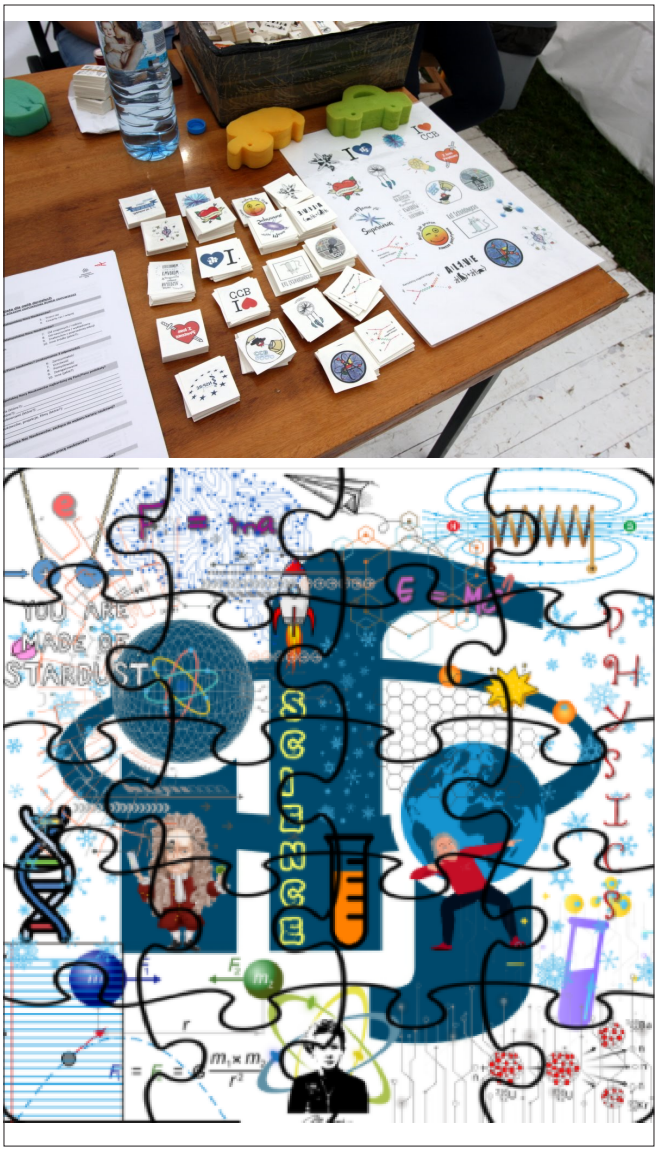

Fig. 11.12. Physics competitions for school students *(photo: L. Grin – top, H. Sharma – bottom)*.

❖

List of Authors

René Ángeles Martínez
Sergii Antropov
Szymon Bacher
Piotr Bednarczyk
Jakub Bielecki
Paweł Bilski
Etienne Blanco
Wojciech Błachucki
Barbara Błasiak
Paweł Błasiak
Dariusz Bocian
Ewa Borsuk
Renaud Boussarie
Andrzej Bożek
Rafał Broda
Wojciech Broniowski
Kamil Brudecki
Paweł Brückman
Maciej Bury
Ada Bystrzycka
Sabrina Casanova
Janusz Chwastowski
Michał Ciemała
Izabela Ciepał
Natalia Cieplicka-Oryńczak
Joanna Czapla-Masztafiak
Anna Czarny
Arpan Das
Nikolaos Davis
Michal Deák
Joanna Depciuch
Aleksandra Deptuch
Agnieszka Dołęga
Stanisław Drożdż
Ewa Dryzek
Jerzy Dryzek
Anna Drzewicz
Magdalena Fitta
Wojciech Florkowski
Bogdan Fornal
Wawrzyniec Gaj
Jan Gajewski
Mirosław Gałązka
Alessandro Giachino
Wojciech Gieszczyk
Tomoki Goda
Krzysztof Golec-Biernat
Krzysztof Gorzkiewicz
Dariusz Góra
Katarzyna Górska
Jerzy Grębosz
Lidia Grin
Leszek Grzanka
Konrad Guguła
Nadine Hammound
Piotr Homola
Tomasz Horwacik
Andrzej Horzela
Łukasz Iskra
Stanisław Jadach
Yannen Jaganathen
Axel Jardin
Marek Jeżabek
Paweł Jochym
Ewa Juszyńska-Gałązka
Anna Kaczmarska
Tomasz Kajdrowicz
Robert Kamiński
Karol Kasprzak
Małgorzata Kąc
Renata Kierepko
Janusz Kisiel
Mariola Kłusek-Gawenda
Maria Kmiecik
Piotr Konieczny
Renata Kopeć
Piotr Kotko
Marek Kowalski
Rafał Kowalski
Krzysztof Kozak
Adam Kozela
Artur Krawczyk
Michał Krupiński
Dawid Krzempek
Agnieszka Kulińska
Avdhesh Kumar
Aleksander Kusina
Krzysztof Kutak
Dominika Kuźma
Jarosław Kwapień
Wojcich M. Kwiatek
Łukasz Laskowski
Ambra Lattanzi
Piotr Lebiedowicz
Małgorzata Lekka
Janusz Lekki
Tadeusz Lesiak
Jaromir Ludwin
Zbigniew Łodziana

Edyta Łokas
Natalia Łopuszyńska
Jerzy Łukasik
Waldemar Maciocha
Rafał Maciuła
Adam Maj
Antoni Marcinek
Barbara Marczewska
Magdalena Matejska-Minda
Adam Matyja
Katarzyna Mazurek
Barbara Michalec
Jerzy W. Mietelski
Izabela Milcewicz-Mika
Ryszard Misiak
Beata Murzyn
Krzysztof Myalski
Vahabeddin Nazari
Jacek Niemiec
Barbara Obryk
Jacek Okołowicz
Paweł Olko
Rafał Ortwein
Natalia Osiecka-Drewniak
Paweł Oświęcimka
Jacek Otwinowski
Vitalii Ozvenchuk
Czesława Paluszkiewicz
Magdalena Parlińska-Wojtan
Wiktor Parol
Łukasz Pawlikowski
Piotr Pawłowski
Robert Pełka

Marcin Perzanowski
Jan Pękala
Przemysław Piekarz
Natalia Piergies
Ewa Pięta
Henry Przybilski
Andrzej Ptok
Krzysztof Pysz
Martin Rohrmoser
Maciej Roman
Beata Różewicz
Antoni Ruciński
Andrzej Rybicki
Radosław Ryblewski
Marzena Rydygier
Sebastian Sapeta
Anna Sas-Bieniarz
Michał Sądel
Wolfgang Schäfer
Mirko Serino
Himanshu Sharma
Michał Sienkiewicz
Rajeev Singh
Andrzej Siódmok
Konrad Skowron
Maciej Skrzypek
Paweł Sobieszczyk
Gabriel Sophys
Bogdan Sowicki
Iwona Sputowska
Ewa Stanecka
Tomasz Stanisz
Rafał Staszewski

Tomasz Stebel
Małgorzata Sternik
Sławomir Stuglik
Jan Swakoń
Antoni Szczurek
Adrian Szeliga
Jakub Szlachetko
Iwona Świerblewska
Jacek Świerblewski
Maciej Trzebiński
Adam Trzupek
Andreas van Hameren
Anna Wach
Michael Waligórski
Barbara Wasilewska
Przemysław Wąchal
Zbigniew Wąs
Marcin Wątorek
Władysław Węglarz
Urszula Wiącek
Henryk Wilczyński
Mariusz Witek
Marta Wolny-Marszałek
Krzysztof Woźniak
Jacek Wrzesiński
Wojciech Zając
Jakub Zaremba
Joanna Zemła
Beata Ziaja-Motyka
Piotr Zieliński
Mirosław Zięblíński
Agnieszka Zwoźniak

❖

ISSN: 1425-3763 *(printed version)*
ISSN: 2544-5162 *(electronic version)*